Catalytic Supercritical Water Oxidation of Nitrogen-containing Organic Compounds

by

Mauricio Julio Angeles Hernández

A thesis submitted to
The University of Birmingham
for the degree of
DOCTOR OF PHILOSOPHY

Supercritical Fluids Technology
Research Group
School of Chemical Engineering
The University of Birmingham
January 2010

Abstract

The results of the catalytic oxidation in supercritical water of two non-biodegradable and highly toxic nitrogen-containing organic compounds (DBU and quinoline) are presented. The reactions were studied in a tubular fixed-bed reactor over three catalysts: Pt/Al_2O_3, CuO/Al_2O_3 and MnO_2/CuO. The effect of operating conditions, namely temperature, pressure, oxygen concentration and initial concentration of the organic compounds were studied to evaluate their influence on its removal. Reaction rates were calculated from the experimental data collected. In addition, the selectivities and stabilities of the catalysts were investigated.

Before conducting the experimental study the isothermal and isobaric operation of the reactor was verified together with the complete decomposition of hydrogen peroxide to oxygen and water in the preheating section and the reproducibility of experimental data was verified. Absence of external concentration gradients was determined experimentally for each reaction. The results showed that temperature was the main controlling variable of the catalytic oxidation. On the contrary, the effect of pressure depended on the catalyst used. Increasing the concentration of the organic compound did not affect their oxidation. Meanwhile, oxygen concentration above a stoichiometric ratio of two did not considerably improve the reaction.

A power-law kinetic model was proposed to quantify the oxidation reaction. Three Langmuir-Hinshelwood-Hougen-Watson reaction rates were also explored to fit the experimental data. In the absence of a specific reaction mechanism the kinetic data were best represented by the power-law kinetic model.

CO_2 was the main carbon product of the reaction with small amounts of inorganic carbon species dissolved in the liquid effluent. Meanwhile, NH_4^+, NO_3^- and NO_2^- ions were the only nitrogen species detected in the liquid effluent.

Pt/Al_2O_3 proved to be the most effective catalyst because it promoted faster reactions rates, had higher selectivity towards CO_2 and produced lower nitrogen species.

Surface analysis of the spent catalysts identified that the loss of activity was due to the

reduction of surface area. Leaching of active metals and chemical changes on the surface of the active metals and support of the catalyst were found for CuO/Al_2O_3 and MnO_2/CuO.

To conclude, it was demonstrated that catalytic supercritical water oxidation is a feasible and effective alternative for the destruction of contaminants in water. The thesis also includes suggestions for further research to continue the development of this technology and consolidate the process at industrial scale.

To my parents

and

Enrique, Carolina, Alejandra and Milan

Acknowledgements

This work has been the product of not only one person, but the kind contribution of a group of institutions and persons, to whom I am deeply grateful.

Firstly, I would like to thank the Consejo Nacional de Ciencia y Tecnología (CONACYT), México (Studentship No. 204623) for the opportunity of studying abroad and the financial support provided for this research and Secretaría de Educación Pública (SEP) through its Dirección General de Relaciones Internacionales for the financial support provided for this research.

I am especially grateful for my always understanding supervisors Dr. Regina Santos and Dr. Gary Leeke. I appreciate your objective suggestions, our discussions, your experience and your infinite patience but above everything, I treasure the opportunity of working together. Dear Regina, you always supported and believed in me and who was there for me all the time. Dear Gary, I could not be more grateful because you lent me a hand when I needed it the most. To both of you again thank you very much.

I would also like to thank Prof. William Zimmerman, Dr. Buddhika N. Hewakandamby and Dr. Laurent F.C. Jeanmeure from the Department of Chemical and Process Engineering of the University of Sheffield for their useful discussions on the modelling of the heterogeneous catalytic reactions.

I would to like to thank Dr. Serafim Bakalis and Prof. Michael Winterbottom for their useful discussions and suggestions on reaction rate mechanisms and the fitting of the experimental data.

I am also grateful to Dr. Rachel Bridson, Dr. Idoko Ochuma and Mr. Graham Burns from the School of Chemistry, for their technical assistance in developing analytical methods.

My gratitude to Dr. Teijun Lu, who always found time for helping me.

I would like to thank the office staff especially to Mrs. Lynn Draper for all her help through these years and the workshop for its assistance.

I am grateful to Dr. Jorge Ancheyta who is an example to me and who has showed me this path. I also would like to thank to Dr. Miguel Valenzuela whose support and counsel have

guided me through this journey.

There is a group of people that is also important to me and in one way or another have helped me through this effort, Dr. Karin Mehauden, Mr. Olgun Ural, Mr. Ponmile Osibo, Dr. Fabian Peña, Dr. Rene Bruckner, Miss. Naeema Aldarmaki, Miss. Zoë Brown, Mr. Peter Bath and Dr. Linda Tuck.

My family and friends who made me feel as I was never gone and gave me the force to continue. Miss. Elisa Navaro because while one thinks in what is left behind, one can not see that what is coming to you might change you forever. And to those who I have forgotten, to all of them, thank you, this work belongs to you and I could not have done it without each of you.

Contents

List of Figures

List of Tables

Abbreviations

BET: Brunauer, Emmet and Teller

BVP: Boundary value problem

CSCWO: Catalytic supercritical water oxidation

CSTR: Continuous stirred tank reactor

CWR: Cool wall reactor

DBU: 1,8-diazabiciclo(5.4.0)undec-7-ene

DVS: Dynamic vapour sorption

EoS: Equation of state

GC: Gas chromatography

GC-MS: Gas chromatograph coupled to a mass detector

HPLC: High performance liquid chromatography

IAWPS: International Association for the Properties of Water and Steam

IVP: Initial value problem

IC: Inorganic carbon

ICP: Inductively coupled argon plasma

ICP-OES: Inductively coupled argon plasma - optical emission spectrometer

i.d.: inside diameter

LHHW: Langmuir-Hinshelwood-Hougen-Watson

MOL: Method of lines

NDIR: Non-dispersive infrared

NO_X: Nitrogen oxides

o.d.: outside diameter

SCF: Supercritical Fluid

SCW: Supercritical water

SCWO: Supercritical water oxidation

SR: Stoichiometric ratio

SS: Stainless steel

TC: Total carbon

TFA: Trifluoroacetic acid

TOC: Total organic carbon content

TR: Tubular reactor

TWR: Transpiring wall reactor

XRD: X-ray diffraction

WAO: Wet air oxidation

WHSV: Weight hourly space velocity, which is defined as $WHSV = \frac{\rho F_{i_0}}{W}$

Chapter 1

Supercritical Fluids Technology and Reactions

The critical point of a pure chemical substance or a mixture of them, is the point of highest temperature and pressure at which its vapor and liquid coexists in equilibrium (Figure 1.1). Above this point there is no noticeable difference between the phases. At pressure and temperature conditions higher than the critical point, a fluid becomes supercritical. Although, this seems to be the most accepted definition, it is rather incomplete. According to Jessop and Leitner [1], a more general definition should also include the boundary until where the supercritical region is extended, that is determined by the sublimation curve at enough high pressure that the fluid condenses to a solid. A supercritical fluid (SCF) is another state of matter with physicochemical properties ranging between gases and liquids. SCF's solvation power is perhaps the most exploited property. Many fluids change their chemical and physical properties upon reaching the supercritical state, factors that change their solvation power completely. Some substances that are dissolved in a solvent at ambient conditions can become less soluble at supercritical conditions. The common case is water, most salts are soluble in water at room temperature and pressure (around 100 g/L) but at supercritical conditions the solubility of salts decreases considerably (1-100 ppm) [2]. The properties of water at ambient conditions are due mainly to hydrogen bonding, which causes water to support ionization of salts and to dissolve poorly organic substances. Because hydrogen bonding is an exothermic process, the equilibrium constant decreases with temperature and thus the dielectric constant as well. However, supercritical water (SCW) becomes an excellent solvent for gases and organic compounds. This change in solvent polarity has been the corner stone of the development of SCF's technology.

Supercritical fluids have received much attention for their many applications to complex process separations in chemical industry. For example, supercritical carbon dioxide (CO_2) has been

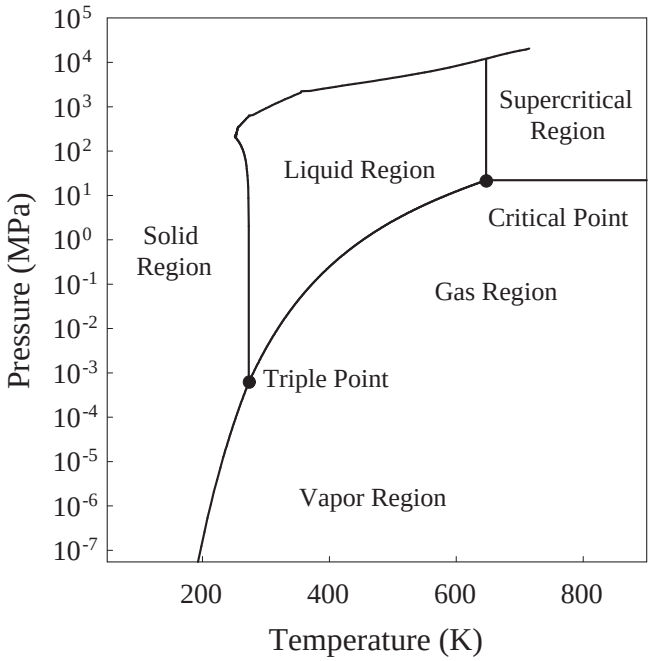

Figure 1.1: Phase Diagram of Pure Water [3]

used extensively as a media for extraction processes like: decaffeinating of coffee, denicotinisation of tobacco and extraction of spices and pigments [4]. The separation of the solute from the solvent occurs with a slight change of pressure or temperature. These processes are well-established technologies and have been widely used and applied in many other fields through the years. Nonetheless, their application has been limited to small volume and high value products [5, 6]. Besides their solvation power, the diffusivity and viscosity of supercritical fluids, which are closer to gases, play also a key role during the separation. Consequently, processes limited by diffusion effects in the liquid phase are improved when they are carried out at supercritical conditions. For this reason, SCF extraction has been increasingly applied at industrial scale and research, and now it has been adopted as a topic into chemical engineering separation books [7]. Besides all their advantageous properties, as pointed out by Brennecke and Eckert [8], SCF extraction should not be the first separation process tried but rather the last. This relies on the fact that operation at supercritical conditions involves high pressure and sometimes high temperature and thus it becomes an energy costing and hazardous operation. Nevertheless, their continuous development obeys more to environmental and government regulations that conventional processes cannot meet all the time. SCF processes are known as green technologies mainly

because they base their operation on the utilization of non-hazardous chemicals. Most of the processes use either carbon dioxide or water, which are non-toxic compared with the traditional organic solvents used in processes like organic synthesis [9]. Reverchon and De Marco [10] have extensively reviewed the SCF extraction process, where they present the recent developments and future trends.

Moreover, SCF's have been applied in fields like particle production and chemical reactions. In the former, SCF's have been applied to nanotechnology for the production of nanoparticles and nanostructure materials. Nanoparticle production covers a wide range of applications from explosives production, polymers, biopolymers, ceramics or pharmaceuticals compounds [11]. For example, controlling the size of the particle of pharmaceutical compounds, the products can be engineered to enhance their activity in the body or modification of the the delivery routes. Reactions at supercritical conditions, on the other hand, has been a field that has received a lot of attention in research and it will be discussed in the next section.

The success of the SCF technology exploitation depends on the understanding of the physicochemical and thermodynamic properties and how they are related to the supercritical phenomena itself. Hauntal [12] have summarized the technical information of the recent advances in several branches of supercritical fluids application in order to widen the knowledge of their phenomena.

Perhaps, SCF's processes have not been completely accepted as fully alternative solutions for high-volume chemical manufacture process because of their high capital costs. However, as it was rightly pointed out by Teja and Eckert [13], "Although we would welcome such applications, it seems more likely that the niche markets described in this commentary will make up a significant fraction of the manufacturing sector in the future. Supercritical fluids have already made inroads into these markets, and their contributions are likely to continue to increase. The variety of these niche applications and the increasing amount of research devoted to understanding the mechanisms of supercritical processes attest to the maturing of this technology and to the increasing likelihood that it will be a significant contributor to manufacturing in the future".

1.1 Reactions at Supercritical Conditions

The burst of research activity on the field of chemical reactions at supercritical conditions is a consequence of their physicochemical and transport properties. One example is solvation power;

supercritical fluids have been used advantageously as a media for chemical reactions that involve compounds immiscible at ambient conditions. Moreover, applications of SCF's to chemical reactions is a result of their ability to change reaction rates, yields, selectivity and mass transfer effects in heterogeneous reactions by tuning their solution properties with thermodynamic conditions or the addition of a cosolvent [14]. Diffusivity and viscosity of supercritical fluids are closer to gases (Table 1.1) and consequently, reactions limited by diffusion effects in liquid-phase are improved when they are carried out at supercritical conditions. Density which is strongly dependent on temperature and pressure near the critical point, can be used to control the dielectric constant and hence reactions kinetics. Thus, small pressure or temperature changes above the critical point can improve dramatically the selectivity of reactions at supercritical conditions.

Table 1.1: Diffusivity and viscosity of water

Property	Liquid	SCF	Gas
Diffusivity, cm^2/s	2.6 x 10^{-6} - 2 x 10^{-5}	7 x 10^{-4} - 1.4 x 10^{-3}	0.1 - 0.4
Viscosity, Pa s	0.2 - 0.3	0.01 - 0.03	0.01 - 0.3

Subramaniam and McHugh [15] and Savage et al. [16] have presented two excellent reviews on the general applications of SCF's in chemical reactions and more recently Jessop and Leitner [1] focused their attention into chemical synthesis. Some other reviews have been specifically devoted to the application of SCF's to catalytic reactions [17, 18]. These reviews demonstrate the potential and flexibility of SCF's to perform a great number of reactions like hydrogenations, isomerizations, oxidations, enzymatic, polymerizations, free radical, Diels-Alder synthesis, Fisher-Tropsch synthesis, esterifications, hydrolysis or hydrotreatment. The selection of a solvent for certain reaction is extremely important for the success of a reaction. Solvents play an important role in the reaction as they can accelerate the reaction rate up to several orders of magnitude. Although the selection of supercritical fluids as solvent relies on the chemical reaction studied, carbon dioxide (CO_2) and water (H_2O) are preferred. CO_2 is best in food and pharmaceutical applications because its critical point (304.2 K and 7.383 MPa) is closer to ambient conditions and it preserves the integrity of labile materials. On the other hand, water (647.1 K and 22.055 MPa) is the most common chemical used in industry and it is the reason

why it is also has also been exploited. The next paragraphs will give an overview on the research undertaken on chemical reactions involving supercritical water.

1.2 Reactions in Supercritical Water (SCW)

Water is a cheap and non-toxic solvent and it is neither combustible nor explosive and is environmentally friendly. Water could be used as a substitute for some other solvents in chemical reactions and thus contributes to waste-avoidance and natural resources conservation. Consequently, applications involving water as a mean to perform chemical reactions has recently grown. It was pointed out by Kruse and Dinjus [19] that the application of SCW to reactions is a consequence of its transport and physicochemical properties, which they grouped into two categories:

- Macroscopic point of view
  - Miscibility
  - Dielectric constant
  - Ionic product
  - Transport Properties: Diffusion and viscosity
- Microscopic point of view
  - Collision frequencies
  - Dipole moment
  - Hydrogen bonds
  - Solutions (Interaction of water with ions and molecules causing local density variations)
  - Effect on chemical reactions (values of local dielectric constant or change in reaction mechanism)

When a reaction occurs at supercritical conditions it is likely that a sum of the above properties affect the reaction. Water participates actively as a solvent, collision partner or catalyst and

each of these properties are important for the development of chemical reactions, especially in the boundary of the critical point of water where they change sharply due to small changes in pressure and temperature. Figure 1.2 shows the density, viscosity, ion product and relative permittivity of water at 23.0 MPa. All properties suffer abrupt changes in the proximity of the critical point of water; exceeding this point water properties remain without noticeable changes. Reactions that occur close to the critical point of water may follow different pathways than those performed in the supercritical or subcritical region. For example, the ionic product of water could influence a reaction to follow an ionic mechanism because water acts as an acid-base catalyst instead of a free-radical mechanism [20]. The use of water to substitute conventional solvents for environmentally benign chemical process and the ability to manipulate its properties has opened the opportunity to explore as a media for chemical reactions.

The understanding of how water influence chemical reactions has become the standpoint in the development of reactions in SCW. The contribution of water in reactions as merely a solvent is a forgotten misconception because water plays a key role. Akiya and Savage et al. [24] have elucidated the importance of water in chemical reactions at high-temperature and they have summarized how water participates in chemical reactions. The first one is its participation as a reactant/product in bond-breaking reactions like hydrolysis, as a supplier of hydrogen atoms and its interaction in elementary steps such as those that occur in supercritical water oxidation. Secondly, its influence to catalyze reactions; water when it dissociates produces a high concentration of H^+ and OH^- ions which rapidly influence acid- or base-catalyzed reactions (see Figure 1.2c), although this effect is by far more noticeable at ambient conditions. Besides, it also facilitates reactions when it catalytically influences the formation of a geometrically less hindered transition state; by releasing protons, water facilitates the formation and cleavage of bonds. And finally, the solvation effects due to inhomogeneities in the vicinity of the solute molecules and the bulk, and the physical effect of water on solute molecules in absence of solvent-solute interactions (third bodies collisions).

Table 1.2 illustrates the influence of SCW in chemical reactions. From the formation of alternative lower-energy transition states by hydrogen-bonding interactions to its dissociation power to promote acid-base catalyzed reactions or its participation as reactant in free radical mechanisms to its cage effects around the solute due to density inhomogeneity, the roles of water

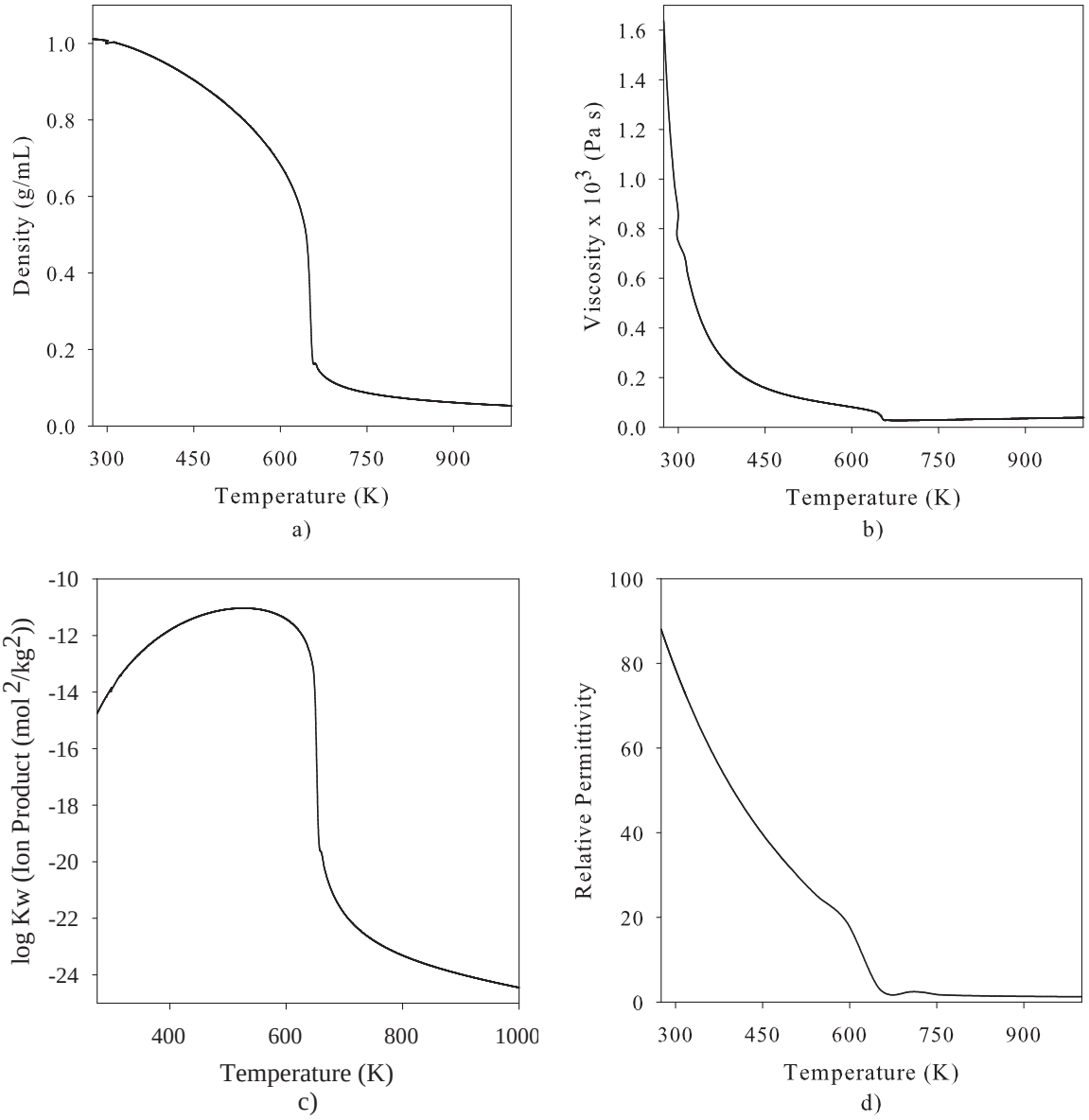

Figure 1.2: Isobaric Properties of Water at 23 MPa [3, 21, 22, 23]

in chemical reactions are complex and it is likely that contributions of some of them could affect the development of a reaction.

Reactions in supercritical water can be cataloged depending upon their purpose as synthesis or degradation reactions [19, 25]. Degradation in SCW is perhaps the most important reaction; it involves complete oxidation and thus efficient elimination of aqueous wastes effluents by a process known supercritical water oxidation [26]. Some other important degradation reactions involves the gasification of biomass for the production of alternative fuels or hydrous pyrolysis for organic

Table 1.2: Roles of High Temperature Water in Chemical Reactions
(Adapted from [24])

Role of Water	Affected Reactions
Reactant/Product	Reactions in which water acts as reactant (e.g., hydrolysis, hydration, hydrogen abstraction)
Catalyst	Proton-transfer reactions in which water interacts with reactant(s), typically via hydrogen bonding
Acid/Base catalyst precursor	Acid/base-catalyzed reactions
Preferential solvation/desolvation of transition state	Reactions with change in solute-solvent interactions (e.g. hydrogen bonding, electrostatic, etc.) between the reactant(s) and transition state
Solvent dynamics	Very fast reactions (faster than solvent reorganization)
Density inhomogeneities	Any reaction can be affected by the local composition differing from the bulk composition
Energy transfer	Nominally unimolecular elementary reactions
Cage effects	Bimolecular reactions (reversible and irreversible)

synthesis. The field of organic synthesis is relatively new because in many synthesis reactions that involved hot compressed water (e.g. condensations, Diels-Alder, dehydration, etc.) occur at liquid-like densities of water at subcritical and near-critical conditions [27, 28, 29]. Nonetheless, organic synthesis involving SCW have grown in applications because the variability of mainly dielectric constant and ionic product with pressure and temperature. The next sections will be focused on the applications of SCW in the field of chemical reactions.

1.2.1 Dehydration, Diels-Alder, Rearrangement and Hydrogenation Reactions

When reactions occurs in SCW, water plays an important role in the process as a consequence of its physicochemical properties. The synthesis of products using SCW has been explored for a great number of reactions. Such synthesis is the dehydration reaction, Krammer et al. [30] studied the dehydration of 1,4-butanediol and glycerin for the production of tetrahydrofuran and acrolein, respectively. SCW demonstrated that both reactions proceeded selectively to the desired products without any other byproduct. Some other reactions investigated were the dehydration of alcohols [31, 32, 33], cyclic hydrocarbons [34], acetaldehyde [35] and lactic acid [36]. Diels-Alder reactions constitute another important reaction in SCW; a comparison of the mechanism followed by the reaction at ambient conditions proved that the physicochemical properties of water affected the selectivity of the reaction [37]. SCW could catalyze reactions that in other cases are carried out under the presence of strong monoacids. The rearrangement conversion of pinacol to pinacolone proved to proceed faster and completely selective to pinacolone than the conventional reaction (usually carried out in the presence of concentrated acids such as sulphuric acid) when SCW acted as an acid catalyst for the reaction [38]. Another example is the non-catalytic Beckman rearrangement reaction of cyclohexanone oxime [39].

Water has also been used in the hydrodesulfurization reaction for the removal of sulfur from diesel fuels [40]. In the reaction the the water-gas shift reaction in SCW produced species that hydrogenate the dibenzothiophene (a model sulphur compound present in diesel). Some other applications include the hydrogenation of carbazole and naphthalene [41].

1.2.2 Hydrolysis and Biomass Conversion

Hydrolysis and gasification share an important characteristic which is the cleavage of the $C-C$ bond. Hydrolysis is mainly used for organic synthesis and gasification is intended for production of hydrogen and fuel gases. Bühler et al. [20] have elucidated the reaction mechanisms of hydrolysis of glycerol in SCW. The main products were methanol, ethanol, formaldehyde, carbon monoxide, carbon dioxide and hydrogen. The importance of their study relied on the elucidation of mechanisms through the reaction products. Based on their study, the hydrolysis of glycerol proceeded by free radical and ionic pathways. The predominance of either reaction mechanism

depended on reaction conditions. Ionic pathway was preferred at higher pressure and/or lower temperatures meanwhile free radical mechanism dominated at lower pressures and/or higher temperature. Consequently, tuning pressure and temperature lead to changes in product distribution. Other studies have involved the hydrolysis of tert-butylbenzene, hexadecane, polyethylene, ethyl acetate, acetonitrile, acetamide, glucose, cellulose and lignin [25, 30, 42, 43, 44].

1.2.2.1 Gasification of Glycerol - A Preliminary Experimental Study

Biomass conversion has become very important to reduce the depletion of carbon dioxide into the atmosphere and to minimize the concern for disposal of wastes and their conversion to fuel gases. Wet biomass represents a large portion of the biomass produced and thus its conversion has become attractive; one example is the gasification reaction of glycerol. Glycerol has become a major concern especially because it is one of the byproducts in the production of biodiesel. Biodiesel is a renewable fuel product of the hydrolysis of vegetable oils and can be effectively used when it is blended with fossil diesel [45]. The production of biodiesel generates large amounts of glycerol, which could also be converted to produce alternative fuels. When gasification of glycerol occurs it decomposes in contact with water to produce hydrogen that can be used to generate energy according to the idealized reaction [46]:

$$C_3H_8O_3 + 3H_2O \longrightarrow 3CO_2 + 7H_2 \tag{1.1}$$

Nonetheless some other side reactions, like reforming, water-gas shift and methanation can produce methane or carbon monoxide according to:

$$C_3H_8O_3 \longrightarrow 3CO + 4H_2 \tag{1.2}$$

$$CO + H_2O \longleftrightarrow 3CO_2 + 7H_2 \tag{1.3}$$

$$CO + 3H_2 \longrightarrow CH_4 + H_2O \tag{1.4}$$

To demonstrate the feasibility of using glycerol a preliminary experimental study of five experiments were carried out in the laboratory rig at temperature of 673 to 873 K and pressure

of 23.0 and 25.0 MPa in a tubular reactor. The reactor was a 3 m coiled tubing section of stainless steel with i.d. of 2.11 mm and o.d. of 6.35 mm. A stream of constant concentration of glycerol of 0.02 mol/L was fed to the tubular reactor. The concentration of glycerol dissolved at ambient conditions in water varied from 16.82 to 34.39 g/L. The gaseous outlet stream was sampled and analyzed by a gas chromatograph equipped with a thermal conductivity detector. Figure 1.3 depicts the findings of the glycerol gasification in SCW. The products identified in the gas stream comprised hydrogen, methane, carbon monoxide, carbon dioxide and some unidentified light hydrocarbons. The gaseous products obtained agreed with gasification of glucose in SCW [42]; however, only hydrogen and methane were considered. Figure 1.3a shows the product distribution as a function of temperature. Hydrogen and methane production were not favored at temperatures of 673 K. Hydrogen mol fraction was not affected by temperatures above 773 K. On the contrary, the production of methane was largely favored at high temperatures. These results agreed with previous findings by Xu et al. [47], where they proved that hydrogen and methane production were increased with temperature. Pressure on the contrary did not have an appreciable effect in the reaction. Almost same product distributions were found at 23.0 and 25.0 MPa (see Figure 1.3b). Remaining glycerol in the liquid effluent was not detected, nonetheless the presence of small carbonaceous particles were found. The appearance of resultant tars and particulate matter is a major limitation in biomass gasification. These particles could potentially damage downstream process equipment or become an environmental issue and therefore limit the development of the technology. However, some other alternatives like catalytic gasification can be also considered to suppress the intermediate production and increased hydrogen selectivity [48, 49]. Coal, plastics or petroleum can also be gasified to produce hydrogen [50]. Consequently, gasification in SCW may contribute considerably to ease the growing energy demand in the future and avoid the concern regarding a glycerol market saturation.

1.2.3 Oxidation Reactions

Oxidations in SCW have been studied for two purposes: partial and complete oxidation. Partial oxidation in SCW has been used for organic synthesis. This selective oxidation can lead to the production of higher value products or intermediates for the synthesis of other valuable materials e.g. oxidation of methanol to formaldehyde [51], methane to methanol [52], olefins

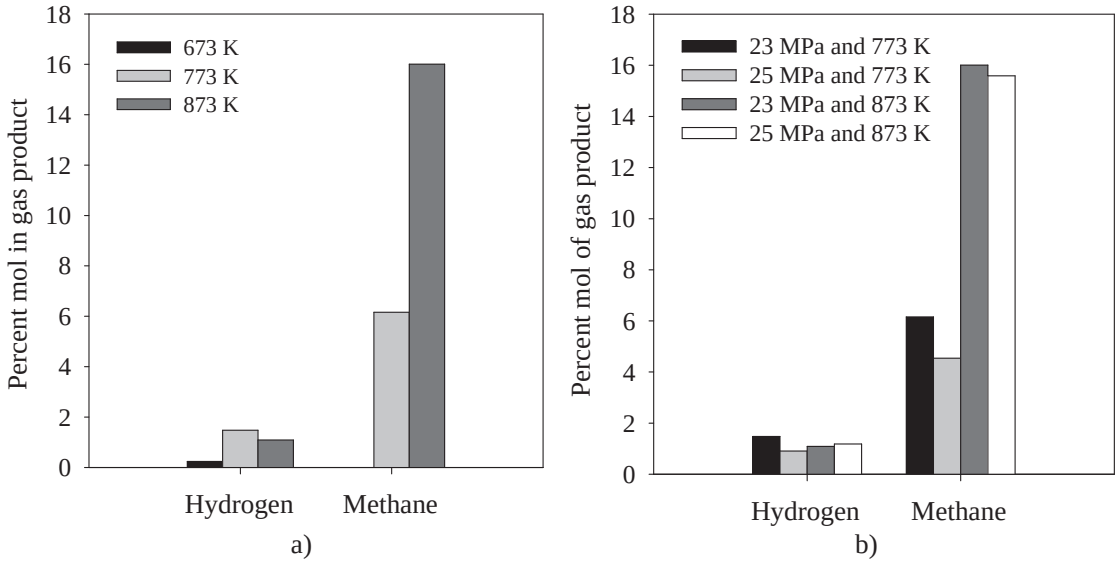

Figure 1.3: Gasification of Glycerol in SCW

for the production of glycol [53], cyclohexane to cyclohexanone [54], the selective oxidation of *p*-xylene for the production of terephthalic acid, which is very important for the production of polyethylene terephthalate [55] or catalytic desulfurization and denitrogenation of hydrocarbons [56, 57].

One interesting application of partial oxidation is the production of hydrogen. SCW partial oxidation is carried out for gasification of low-grade fuels such as biomass, solid wastes and coal. In the process the oxidation is performed using sub-stoichiometric quantities of oxygen (non-catalytic reaction). The presence of oxygen in aqueous media rapidly oxidises the feed avoiding the formation of char and increases the yield of hydrogen [58, 59]. During the reaction water acts as reactant via the water-gas shift reaction (see Equation 1.3) and the carbon-steam gasification, which may produce higher amounts of hydrogen that the present in the feed:

$$C + H_2O \longrightarrow CO + H_2 \tag{1.5}$$

Some other compounds being oxidised in SCW investigated were isobutene [60], cyclohexane [61], n-hexadecane [62] and lignin [62].

Complete oxidation is applied to the destruction of organic matter in aqueous wastes in a process known supercritical water oxidation. The process has met the highest environmental

constrains achieving the destruction of contaminants of 99.99%. Since the early 80's the research and development of the process have made it in an efficient alternative for the treatment of a wide range of toxics and hazardous streams [26, 63]. The next chapter is devoted to reviewing the supercritical water oxidation process.

Chapter 2

Supercritical Water Oxidation

Nowadays the solutions for disposal of organic, hazardous and toxic wastes have become a priority and a common concern [64, 65]. Furthermore, stricter environmental regulations have targeted destruction of some compounds found in the wastes up to 99.99% [66]. Organic compounds total concentration in waste water streams must accomplish a maximum of 125 mg/L of chemical oxygen demand while in the case of total nitrogen, European Union legislation have established a maximum limit concentration of 15 mg/L and where also nitrates concentration in the streams is also a major concern [67]. Conventional technologies like chemical and biological oxidation, activated carbon adsorption, land-base, and incineration might sometimes be very specific to the type of streams they treat and all have operational drawbacks. As a consequence, new technologies must be explored in order to propose novel solutions to deal with the waste-disposal problem we are currently facing. One of these technologies is the supercritical water oxidation (SCWO) process which offers several advantages over the conventional technologies.

SCWO attains the primary goal of the destruction of the organic matter, which land-based alternatives like land-filling, deep-well injection and lagooning does not address and they are likely to contaminate surrounding groundwater and soil. In addition, it will result in air pollution by the volatile organic compounds. On the other hand, biological treatment and activated carbon oxidation are economically attractive for content of organics lower than 1%. Incineration becomes competitive when the concentration of organic matter in the inlet stream is higher than 20 to 25%; thus the heat required for the high temperature operation is provided by the waste (see Table 2.1) [68]. However, incineration's main drawbacks are the emissions of gas which might contain gases such nitrogen oxides (NO_x) or sulphur oxides (SO_x). Furthermore, pre-treatments are required to control the amount of water fed into the reactor and there is special disposal of the

ash generated. In the remaining range of concentration (1 - 20%) wet air oxidation (WAO) and SCWO are by far more economically attractive than incineration. WAO have been extensively used to treat sludge, waste water or industrial wastes [24, 69]. Nonetheless, WAO requires further treatment of the products because of the production of some refractory intermediates. Moreover, achieving higher elimination values in shorter time has also motivated to look for alternatives that successfully accomplish these aims; it is when SCWO was envisioned. SCWO can be seen as a logical extension of the WAO in terms of the operating conditions, however in spite of sharing some operational characteristics with WAO, the unconventional behaviour of supercritical water contributes to the enhancement of the process efficiency.

Table 2.1: Operating conditions of SCWO, WAO and Incineration

Operating Condition	SCWO	WAO	Incineration
Temperature, K	723 - 873	395 - 623	1173 - 1373
Pressure, MPa	25	0.5 - 20	0.1

Undoubtedly, the use of higher pressures and temperatures greater than WAO or incineration (see Table 2.1) might lead to a high energy demanding process, and as a consequence high operational costs, integration of heat recovery and its high efficiency make SCWO a competitive technology for the degradation of waste [70, 71]. A cost comparison has shown that operation of incineration can be up to 500% higher than SCWO [72].

If the use of technologies like SCWO is targeted to give minimal contaminant eradication, it is important also to evaluate the process operation from an environmental point of view. Recently, Svanström et al. [73, 74] have presented two environmental assessments of SCWO for the oxidation of sewage sludge using the life cycle assessment and compared SCWO technology with conventional methods like incineration, co-incineration with municipal solid waste, spreading on agricultural land and fractionation. The evaluation combines environmental aspects and energy consumption indicators. From the handling options assessed only spreading on agricultural land did not result in savings of natural resources consumed. In addition, all systems exhibited savings in greenhouse gas emissions, although the study pointed out the importance of integration of energy recovery steps. To conclude, the evaluation showed that SCWO were among the best

alternatives for the task and also left the door open for future improvements of the process to make it more environmentally efficient.

2.1 The SCWO process

SCWO is used to oxidise completely the organic matter present in aqueous streams at temperatures and pressures above the critical point of water (647.1 K and 22.055 MPa). During the SCWO process, the organic compounds react completely with oxygen to form mainly carbon dioxide and water. Heteroatoms present such as chlorine, sulphur or phosphorus are transformed into their corresponding mineral acids such as hydrochloric, sulphuric and phosphoric. When nitrogen is present in the structure of the organic compound, it is converted principally to molecular nitrogen (N_2), or if the reaction is incomplete, it leads to the formation of ammonia (NH_3), nitrous oxide (N_2O), hydrazine (N_2H_4), nitrous acid (HNO_2) and nitric acid (HNO_3) [75]. Nitric oxide (NO) and nitrogen dioxide (NO_2) are not formed because at the temperature at which the process is normally carried out does not favor their formations pathways. In addition, NO_2 that could be formed is rapidly converted to nitrate or nitrite [2]. Meanwhile, metals are oxidised to their maximum oxidation state.

Since the appearance of the SCWO process patent in 1981 [76] and an early review by Joshi et al. [77] on the treatment of aqueous waste streams suggesting further research on the field, the SCWO processes has been successfully applied for destruction of a wide range of wastes. Some applications involving the SCWO process includes the destruction of pharmaceutical and biopharmaceutical wastes [78], different types of sludge [72, 79, 80], nuclear fuels [81], ashes produced by incineration processes [82], waste water from coke plants [83], hazardous and toxic wastes [84, 85], waste plastic from recycling plants [86], hydrocarbons [87], water-soluble polymers [88], human waste [89] and foodstuff [90]. Novel SCWO processes have been design to perform two stage operations for oxidation of organic matter and recovery of inorganic materials [80, 91, 92] and precious metals [93, 94] or pyrolysis and oxidation [95].

The conventional process diagram of a commercial SCWO unit is shown in Figure 2.1. The waste water is pumped from the reservoir by a high pressure pump that delivers the feed to 250 bar (25.0 MPa). The feed is preheated in a heat exchanger using the reactor outlet stream. If the stream does not reach the desired temperature (400°C) additional heating is provided by a

gas fired heater. The waste line is mixed with pressurised oxygen at the reactor inlet. Once the reaction starts the temperature rises to 600°C. The outlet stream is cooled down by exchanging heat in the economizer, then a water tank where it generates steam and a cooler before it is finally depressurised. Two streams are obtained in the gas separator tank. The gas stream is rich in CO_2, unreacted O_2 and N_2. The liquid on the other hand contains the residue of the process.

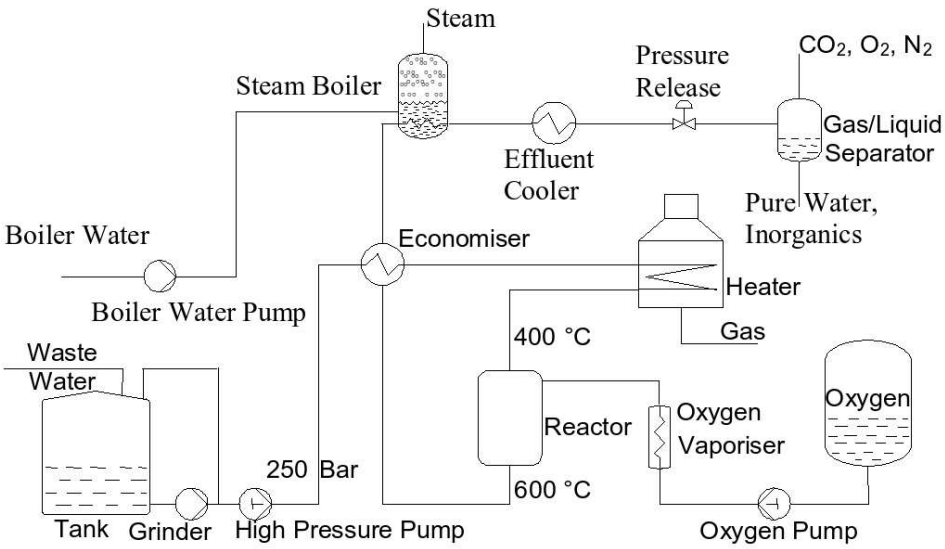

Figure 2.1: AquaCritox® Process Diagram [94]

Around the world there are several companies that have built or they are licensed to build SCWO commercial units. Some of them are General Atomics (USA), Chematur Engineering AB (Sweden) now licensed to Supercritical Fluids International (Ireland), Foster-Wheeler (USA), Eco Waste Technologies (USA) (rights acquired in 1999 by Chematur Eng. AB), SRI International (USA), HydroProcessing (USA), Organo KK (Japan), Mitsubishi Heavy Industries (Japan), Komatsu MFG Co. Ltd. (Japan) and Kurita Water Industries Ltd. (Japan). The companies have built SCWO plants in their country locations [96, 97]. The use of SCWO technology as alternative for waste treatment has not extended as many companies expected because of some inherent operations problems; however efforts done among researchers around the world have allowed that SCWO reaches a better commercial development. Figure 2.2 shows a demonstration plant of the AquaCritox® process designed by Chematur Engineering AB and recently licensed

to Supercritical Fluids International for its commercial exploitation.

Figure 2.2: AquaCritox® Demonstration Plant

2.1.1 Design Considerations

Although, the process has been successfully proven to eliminate a wide range of wastes based on the research over the last 25 years, it has however not reached its full potential use in industry. The reasons for this unexpected trend are basically due to the unwillingness of industries to acquire state of the art technology for waste treatment [91] or the operational problems in some steps of the process. In general, the SCWO process involves four main stages: feed preparation and pressurization, reaction, salt separation, and heat recovery and depressurization. The major problems related with SCWO are salt deposition and corrosion. Research has been done to alleviate this two major problems of the process. Bermejo and Cocero [96] have thoroughly reviewed the technical aspects of the industrial process stressing that understanding the corrosion and salt deposition phenomena, together with thermodynamic, transport and physicochemical properties of SCW will produce more efficient SCWO plants that lead to a better acceptance of the process.

2.1.1.1 Corrosion

The SCWO process is a very intensive process in terms of the mechanical and thermal stress at which the operating equipment is subjected when it operates above the critical point of water. The design of the equipment should be done in terms of the mechanical and thermal stress and the corrosion generated by the operation itself. Chemical corrosion originated from byproducts formed during the reaction and the oxygen present in the reacting mixture should also be considered. Consequently, the reactor is where the corrosion problems are constantly found. Typically during the oxidation a variety of mineral acids are formed depending on the heteroatoms in the waste streams. Halogen heteroatoms are the most dangerous to the material process, because their mineral acids accentuate the corrosion of the equipment especially at high temperatures. The selection of the construction material for the process will vary depending upon the type of the waste treated. Stainless steel 316 is preferred for streams containing non-halogenated heteroatoms in continuous operation at laboratory scale (tubular reactors). It offers some advantages: its construction is relatively simple and cheap and it can be periodically replaced. For laboratory batch reactors and larger scale operations high nickel content alloys are preferred because they are corrosion-resistant. Two types of high nickel content alloys have been continuously used in the SCWO: Inconel® 625 and Hastelloy® C-276. Both alloys have performed very well and resist chemical and thermal corrosion, although they are by far more expensive than stainless steel. Their use is also not recommended for halogen-containing wastes, and consequently special nickel based alloys have been developed to deal with halogen wastes [98]. Another solution is the use of titanium, although the price of the unit will be high and thus unattractive. The inclusion of special ceramic coating on the reactor has also been suggested as a possible alternative [99]. However, the best approach to avoid corrosion has been to implement new reactor designs.

2.1.1.2 Salt Deposition

As it mentioned earlier, the solubility of common salts in supercritical water is drastically limited to a few milligrams per litre. Thus the presence of precipitated solids is commonly encountered in SCWO reaction units. The presence of solids can lead to erosion, plugging or fouling in the unit. The presence of salts is inherent to waste streams and some of them are formed during the

reaction and surprisingly it is one of the main reasons why the process has not reached a better commercial development [100]. The common approach to avoid the problem is desalination of the water streams or to increase the density of the reacting mixture and thus enhance the solubility of salts [2]. The latter obviously addresses an increment in operating costs and mechanical stress within the equipment. Some reactor designs have been implemented to cope with the solids deposition. Reactors have been envisaged to alternate feed and flushing streams [101], use a salt dissolution promoting agent with after salt discharge [102], allow injection of hydrogen peroxide at different points in the reactor to cool down and promote the reaction [103], allow the suspension of solids [104] or add scrapers and injection of water to quench the reaction products and solubilise the salts [105]. In order to deal with the salt deposition problem more research has to be carried out in order to have a better understanding of the water-salt phase behavior, heat and mass transfer to control and/or avoid the precipitation of salts in the reactor [106].

2.1.1.3 Reactor Designs

Generally at laboratory scale when kinetics studies are being undertaken batch and continuous reactors are preferred. However, batch reactor is the most common type of reactor encountered in the laboratory. They are versatile and its operation is not complicated. Continuous stirred tank reactors (CSTR) are perhaps the best for kinetic studies purposes because their design equation is mathematically simpler than batch or tubular reactors; and thus the reaction kinetics parameters of the reactions are easier to obtain. The only drawback is that reaching the adequate operating conditions for a reactor to behave as a CSTR are sometimes not an easy task. Tubular reactors have very important advantages over tank reactors; the construction of a tubular reactor (TR) is relatively simple and cheap and it can be adapted to perform heterogeneous catalytic studies; here again reaching ideal operation is not easy and the derived design equation might become very complex.

On the other hand, in industry continuous reactors avoid the need of depressurisation to feed reactants or recover products. The most important characteristic of continuous reactors, especially when operated at supercritical conditions, is the operation variables like pressure, temperature and residence time can be varied almost individually. This tuning of operation conditions can be used to optimize the reaction [107].

For the specific case of SCWO the reactor should consider the two other factors previously discussed, corrosion and salt precipitation, which have driven the design of reactors for SCWO reactions.

2.1.1.3.1 Cool Wall Reactor (CWR). The CWR is divided in two zones the reaction and the pressure shell that allows the isolation of thermal and mechanical effects within the reactor (see Figure 2.3). The reaction shell is built from a special material capable of resisting the oxidative atmosphere where temperatures can rise up to 1073 K. This section is enclosed in a pressure vessel; the system is maintained under the reaction pressure of around 25 MPa. During operation, the pressure chamber wall is kept cooled at 673 K that leads to lower thermal stress and enhancement the solubility of solids formed. As well as its successful operation the reactor possesses a second important operation characteristic, it has been designed to maximise heat recovery from the reaction [108]. One modification that comprises the creation of a turbulent flow zone of the ignited reaction mixture allowing reduction of the reactor size was proposed by McBrayer et al. [109]. While, Miyabashi [110] has proposed a variation of CWR that removes the overheating using several cooled chambers located along the reactor.

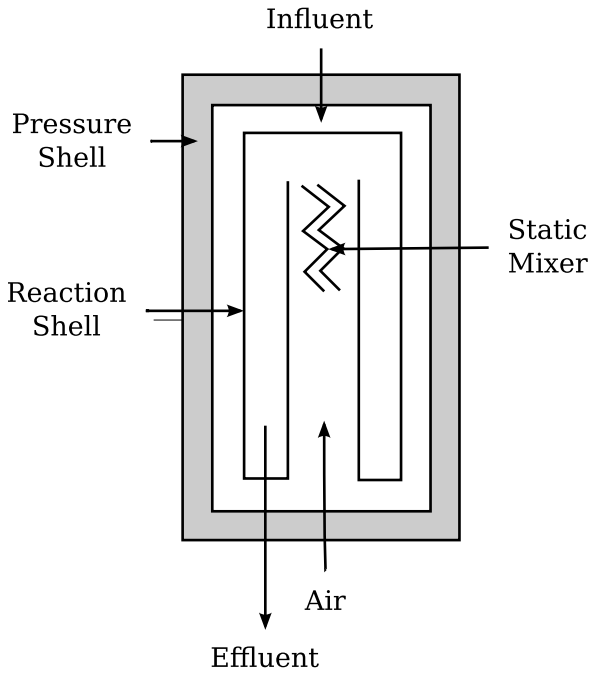

Figure 2.3: Cool Wall Reactor [96]

2.1.1.3.2 Transpiring Wall Reactor (TWR). The TWR has been successfully introduced as a suitable alternative for dealing with corrosion and salt deposition. The reactor principle of operation is to create a protective thin layer of solute-free water. The reactor is divided in two sections: the pressure chamber and an inside porous liner (see Figure 2.4). Water is fed outside the porous liner which then goes through the liner creating an inner water layer that protects the outer chamber from salt deposition and corrosive species from the reaction. Two temperature regions are created, around the liner the temperature is lower because of the water to cool the unit, and in the centre of the reactor where the reaction temperature is higher [97, 111]. Crooker et al. [85] have successfully treated halogenated waste with a TWR. In their study they showed that the reactor can reach elimination of 99.99% and that interior inspections did not reveal either corrosion or salt deposition. Another study has revealed that TWR performed successfully at lower temperatures than the critical temperature of water, that led to an energy-saving operation [100]. Mueggenburg et al. [112] provided a modification of the TWR that include a wall of lining of laminated platelets. The array of superimposed platelets forms a perforated wall capable of controlling the water fluid forming a protective water film. Following the same principle Naufflete et al. [113] have proposed a TWR where the liner is coated with a high corrosion resistant material such as ceramic or diamond-like material.

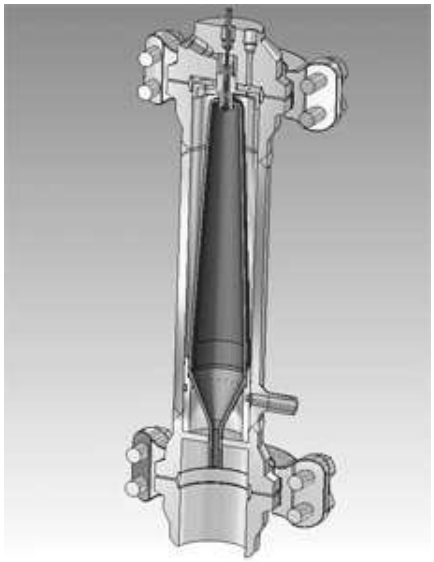

Figure 2.4: Transpiring Wall Reactor [114]

2.1.1.3.3 Reverse Flow Tank Reactor with Brine Pool. Hong et al. [115] have proposed a reactor with two temperature zones. In the reactor, the solids formed from the reaction and the salt precipitated are solubilised by injecting cool water at the lower part of the reactor. The water washes away the solid from the reaction. The upper part of the reactor is maintained at a reaction temperature (873 K), while the lower zone operates at 573 K [97]. Another modification of the reverse flow reactor reactor is provided by Li and Glyona [116]. In their design cold water is mixed with a part of the effluent that is recirculated to the reactor. Pilz et al. [104] suggested a reactor where the water is fed at the bottom of the reactor. The flow is kept at a velocity that maintains the solids in suspension in a turbulent zone. Water and dissolved solids are discharged in the boundary of the turbulent zone.

2.1.1.3.4 Other Reactor Designs. Here a summary of other reactor designs that do not directly fall into the categories already described are provided, however they may share some technical characteristics. For example Stenmark et al. [117] have designed a variation of a tubular reactor. The reactor is divided into a vertical and horizontal section. Other tubular reactors have been implemented with injection ports of water along the reactor in order to quench the reacting mixture and solubilise the deposited solids and thus enhance the reactor life-time [103, 118]. Another modification includes a static mixer inside the reactor [119] or a system that allows the overhead quenching of the effluent [120].

Some other designs deal with heterogeneous catalytic reactions. The inclusion of catalyst can be beneficial for higher oxidation rates at shorter times and milder operating conditions. Yamamoto et al. [121] and Gupta and Muthukumaran [122] have design a reactor that uses an in situ catalyst. A precursor catalyst which is an alkali metal or an alkali earth metal is added. Once the reaction takes place the precursor material is then transformed to a metal acidic salt. The catalyst formed accelerates the reaction and at the same time neutralizes the acidified products. Anikeev et al. [123] designed a heterogeneous catalytic unit where the waste feed and oxidant are passed through mixers and catalyst packets where the mixture is partially oxidised. Then it is brought into contact with fresh feed and mixed before it enters the reactor.

Other reactors maximise the heat recovery of the process, for example Cho et al. [124] have designed a unit that increased the use of the heat generated by the reaction. In their design the product stream discharged is cooled down by using it to pre-heat the waste. Minor modifications

have been also done like better mixing devices for reactants to make the process more efficient [125]. The research therefore on the field of reactor designs have been fruitful in providing options to deal with the common problems of solids deposition and corrosion that will lead in the future a full commercial development of the SCWO technology.

2.1.1.4 Thermodynamic, Transport and Physicochemical Properties of Water

The calculation of thermodynamics, transport and physicochemical properties of water becomes very important for understanding the phenomenon of SCWO, and consequently, for designing or modelling new or existing units. With reliable data it might be possible to prevent the salt deposition or the corrosion within the reactor. For this reason, it is vital to obtain very accurate predictions of water properties because they will lead to better equipment designs. For the case of SCWO where water is the primary component of the reacting mixture, the reliable prediction of its properties has become the key for designing more efficient equipment. At near-critical and supercritical conditions the calculations of properties are a challenging task because the non-idealities of the substances at these conditions. Care must be taken in the selection of the appropriate means to evaluate the thermodynamic, transport and physicochemical properties of water.

For calculation of thermodynamic properties of pure substances or mixtures of them, cubic equations of state are always preferred because the prediction of thermodynamic properties is simpler than more complex formulations [126]. In the literature, there are guidelines to carefully select the appropriate equation of state (EoS) depending on the substances interacting and the conditions of pressure and temperature [127, 128]. Regardless, for scientific use the International Association for the Properties of Water and Steam (IAPWS) formulation 1995 is recommended for the calculation of thermodynamic properties of water [3]. This water EoS has replaced the old formulation proposed by Haar et al. [129] and it should be used instead for all thermodynamic calculations involving water. The IAPWS 1995 is a complex equation that involves several constants in a polynomial mathematical equation, nevertheless it becomes very important if operation near the critical point is performed. Figure 2.5 shows a comparison of the volumetric prediction of ideal gas EoS, Peng-Robinson EoS [130], Soave-Redlich-Kwong EoS [131] and the IAPWS formulation 1995 EoS. For prediction close to the critical point of water only the IAPWS

was able to accurately predict the steep change of density of water in the boundary of its critical point. Meanwhile, the cubic EoS had errors of at least 28% in their prediction. At 675 K the difference between their predictions is small and above 700 K the curves overlap; at this conditions water behaves almost like an ideal gas and thus a better prediction of cubic EoS is obtained.

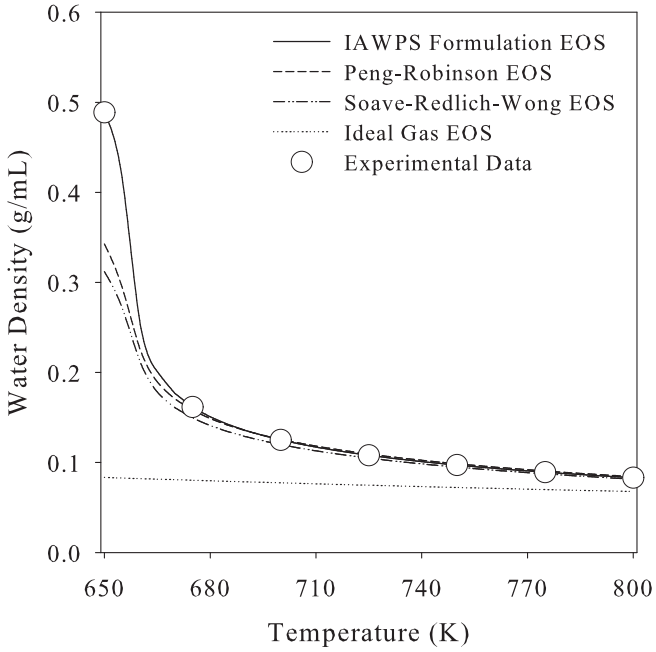

Figure 2.5: Comparison of Equations of State

The simplicity of cubic EoS does not necessarily mean that they should be completely discarded or unable to account for complex interactions that occur at supercritical conditions. In fact, for mixtures given the appropriate interactions parameters used in the mixing rules the Soave-Redlich-Kwong EoS was able to increase its accuracy of phase calculations behavior at near-critical and supercritical conditions [132]. Nonetheless, those interaction parameters are not usually available for all systems. Recently, Bermejo et al. [133] have compared the Peng-Robinson and Anderko–Pitzer EoS to calculate phase equilibrium data of air-water mixtures. They have shown that the Anderko-Pitzer EoS was able to predict the volumetric properties of the mixture, however they found discrepancies in the prediction of the heat capacity by the Peng-Robinson EoS. The heat capacity is often overlooked, however their prediction is very important especially for designing heat exchanger units. In many of the laboratory units and at industrial

scale (see Figure 2.1) the heating of the feed occurs at isobaric conditions. Like density, the heat capacity at constant pressure (Cp) of water reaches a maximum value near the critical point (see Figure 2.6). If a cubic EoS rather than IAPWS 1995 formulation was chosen to predict the Cp of water, the error in the prediction of Cp would lead to inefficient heat exchanger designs. Thus the selection of the a suitable EoS is one of the key factors in the design.

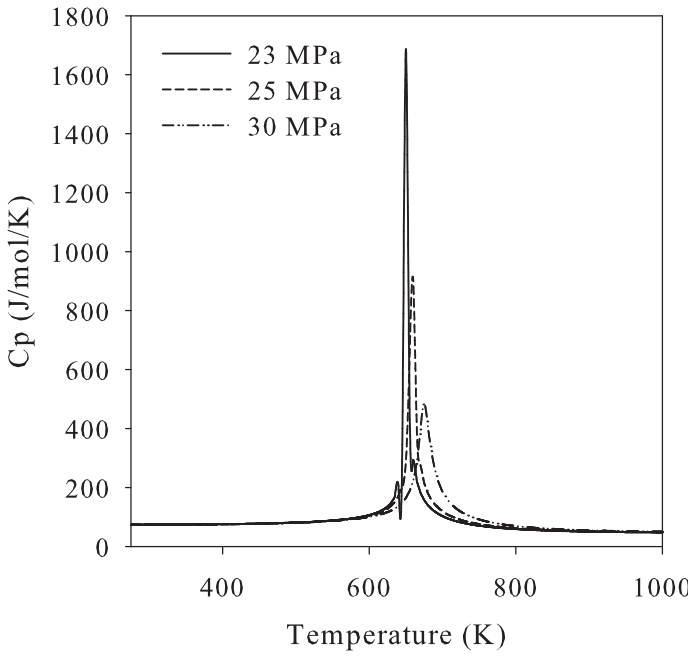

Figure 2.6: Heat Capacity at Constant Pressure of Pure Water [134]

In specialised literature, there are appropriate formulations for the predictions of transport and physicochemical properties of water. Regarding transport properties, Senger and Kamgar-Parsi [21] have proposed an equation to predict the viscosity of water. Diffusivity is a physicochemical quantity difficult to predict especially when mixtures are involved; Lamb et al. [135] have published an equation able to predict the self-diffusion coefficient of water in compressed and supercritical water which provides a good estimate when no data of diffusion coefficients of mixtures are available. Woerlee [136] has proposed a practical equation for the prediction of viscosity and diffusivity applicable for supercritical fluids that can be alternatively used.

Physicochemical properties can be successfully predicted using specific equations for water; Fernandez et al. [23] have provided the equation for the static permittivity (static dielectric constant) of water. This equation is useful to predict changes in the solvent properties of water

and to give a better understanding of the solute-solvent interaction during the reaction. For the case of ionic reaction mechanisms, especially those at subcritical conditions where acid-base catalyzed reactions are likely to happen, it is important to know how water participates in the reaction. Marshall and Franck [137] have developed an equation for the prediction of the ionic product of water over a wide range of pressure and temperature.

2.2 Kinetics of the SCWO

The complexity of the prediction of reaction rates at supercritical conditions arises from the fact to produce reliable equilibrium data of the chemical species involved and their interaction with the solvent in which the reaction takes place [8]. For example, near the critical point the compressibility of supercritical fluids is high and small changes in pressure leads to large density variations, which is intimately related to their solvation power. The liquid-like density gives supercritical fluids a high capacity for solutes. Consequently, solubility grows exponentially as a consequence of density, which is often overlooked in reactions at supercritical conditions. The changes of density as a consequence of the addition of an inert solvent has affected the reaction rate of a high-pressure gas-phase reaction [22, 138, 139].

In an effort to describe the course of SCWO reactions three different approaches have been followed:

- Empirical kinetic rate models
- Mechanisms based on elementary reactions
- Transition state theory

The empirical rate models are very useful to screen and evaluate the performance of the reaction. They provide a powerful tool to understand the global reaction and the effect of variables like temperature or reactants concentration. Catalytic and non-catalytic SCWO reactions have been mainly represented by power-law kinetic models and thus they will be discussed in detailed in the following section. Perhaps, the two possible drawbacks are that sometimes they lack the provision to further information about the reaction mechanism details and the effect of external variables like pressure. The last two approaches are truly an insight into the reaction and provide a

comprehensive knowledge of the reaction. By no means both theories can be thoroughly detailed here and further information can be found elsewhere [140, 141, 142].

2.2.1 Empirical Reaction Rate Models

In general oxidation reactions of organic compounds at supercritical conditions follow the stoichiometry:

$$\nu_C C + \nu_{O_2} O_2 \longrightarrow \nu_{CO_2} CO_2 + \nu_{H_2O} H_2O \tag{2.1}$$

Where C denotes the compound to be studied and ν_C, ν_{O_2}, ν_{CO_2} and ν_{H_2O} are the stoichiometric coefficients of the carbon, oxygen required for the reaction, carbon dioxide and water, respectively. The form of the stoichiometric equation could change if any heteroatom forms part of the compound. For simplicity, it is assumed that the reaction is bimolecular and thus Equation 2.1 gives:

$$\nu_A A + \nu_B B \longrightarrow Products \tag{2.2}$$

Both A and B are the reactants of the reaction; for our case A represents the compound to be studied and B the oxygen. When the precise mechanism is unknown (which is in most of the cases is the rule rather than the exception) and for convenience, it is valid to assume that empirical models like the power-law are able to represent the stoichiometry of the reaction. For a bimolecular reaction the reaction rate in terms of the power-law is represented as:

$$-\mathscr{R}_A = k\, C_A^a\, C_B^b \tag{2.3}$$

Where k represents the kinetic constant of the reaction and a and b are the reaction orders of A and B. C_A and C_B refer to the concentration of reactants at any given time in batch reactors or space for continuous reactors. In a few cases, it is presumed that water participates in the reaction and the the reaction rate could include the concentration effect of water and Equation 2.3 takes the form:

$$-\mathscr{R}_A = k\, C_A^a\, C_B^b\, C_{H_2O}^c \tag{2.4}$$

In which c is the reaction order of water. If the kinetic constant dependency on temperature follows the Arrhenius equation a new form of Equation 2.4 is derived

$$-\mathscr{R}_A = A \ \exp^{\left(-\frac{E_A}{RT}\right)} \ C_A^a \ C_B^b \ C_{H_2O}^c \tag{2.5}$$

Where A is the pre-exponential or frequency factor and E_A is the activation energy (generally given in kJ/mol). Equation 2.5 represents the general case in how the reaction rates are expressed; however in order to develop a kinetic study different concentration of reactants are used and the concentration is measured over time or space.

2.2.1.1 Non-catalytic SCWO

As mentioned earlier, SCWO (see Section 2.1) is very flexible for the treatment of different wastes. In order to understand the process itself it is important to understand how individual compounds are oxidised under supercritical conditions. The research in SCWO have been focused on gases and organic compounds, nonetheless the co-oxidation effects of mixtures have been also studied. Tables 2.2-2.4 present a summary of the research done in non-catalytic SCWO.

Table 2.2 illustrates the research carried out on gases and relatively simple organic molecules. Ammonia and acetic acid have been the focus of many studies because they represent two highly refractory compounds that are commonly produced in the reaction. For example, ammonia was hardly oxidised at temperatures lower than 873 K [143, 144], and this is the reason that drove the SCWO research into these compounds. Simple organic molecules and gases exhibited a reaction order dependency of one with respect to their concentration in the feedstream, and null or weak dependency respect to oxygen concentration. Even different studies using the same compound have not drawn a clear conclusion of the effect of oxygen in the reaction [144, 145, 146, 147]. Where initial concentration of the compound and operating conditions used during the experimentation might have some influence on the parameters obtained. When larger amounts of oxygen than the stoichiometric value are added to the reaction, the concentration of oxygen remains constant and could be lumped into the kinetic constant (a common practice in chemical kinetics), showing a reaction order with respect to oxygen of 0. However, the trend of fractional values obtained cannot be easily explained and it is likely to happen because of the nature of the reaction.

Table 2.2: Kinetic Parameters for the SCWO of Gases and Simple Compounds

Compound	Reference	Reactor	E_A, (kJ/mol)	$a^\star$	$b^\star$
Carbon monoxide	[148], [149]	TR	120	1.01	0.03
Ammonia	[145]	Batch	139	1	0
Ammonia	[144]	TR	157	1	0
Ammonia	[146]	TR	144.74	0.74	0
Ammonia	[150]	TR	347.5	1	0.44
Methanol	[151]	TR	178	1	0
Methanol	[152]	TR	178-194	1-1.6	0
Methanol	[153]	TR	85.9	N/K	N/K
Methanol	[154]	TR	328	1	0
Ethanol	[155]	TR	213.9	1.34	0.55
Ethanol	[143]	TR	340	1	0
Acetic Acid	[156]	TR	172.2	0.89	$0.2^\dagger$
Acetic Acid	[153]	TR	208	N/K	N/K
Acetic Acid	[157]	TR	205	1	0
Acetic Acid	[157]	TR	180	1.01	0.16
Acetic Acid	[158]	Batch	73.6	1.0	0.6
Acetic Acid	[159]	TR	217	1	0
Acetic Acid	[159]	TR	168	0.72	0.27
Methylethyl ketone	[153]	TR	230	N/K	N/K
Methylene chloride	[153]	TR	45.6	N/K	N/K
Ethylene glycol	[153]	TR	171	N/K	N/K

TR: Tubular Reactor

N/K: Not known

* Where a and b are the reaction orders according to: $-\mathscr{R}_A = k\, C_A^a\, C_B^b$

† Given in terms of hydrogen peroxide concentration

Phenol has become the centre of many research studies mainly because it is a very stable molecule and it represents a model compound for understanding the oxidation of aromatics in SCW. Phenol studies have been carried out by many research teams and a summary of the kinetics studies are given in Table 2.3. Phenol exhibits a reaction order of one in most of the cases, however its dependency on oxygen varies from 0 to a very high value for reaction order of 2.75. Not even the values of activation energy agree; values as small as 39.2 and as high as 124.8 were obtained, although the reaction orders for phenol were equal to 1.

Table 2.3: Kinetic Parameters for the SCWO of Phenol

Reference	Reactor	E_A, (kJ/mol)	$a^\star$	$b^\star$	$c^\star$
[160], [161]	CSTR, TR	124.766	1.041	0.381	0
[162]	TR	94.62	1	N/K	0
[163]	TR	39.2	1	0	0
[153]	TR	108	N/K	N/K	N/K
[164]	TR	99.6	1	2.75	1.38
[157]	TR	45.1	1	0	0
[157]	TR	51.8	1	0.5	0.7
[165]	TR	63.8	1.09	1.23	-0.05
[166]	TR	N/K	0.5-1.0	>0	>0

CSTR: Continuous Stirred Tank Reactor

TR: Tubular Reactor

N/K: Not known

* Where a, b and c are the reaction orders according to: $-\mathscr{R}_A = k\, C_A^a\, C_B^b\, C_{H_2O}^c$

Table 2.4 reviews the research done in molecules containing nitrogen, chlorine, phosphorus and other aromatics. According to the results (even) isomers could present very similar reaction orders (e.g. cresols) or exhibit different values (e.g. hydroxybenzaldehyde). Moreover, the isomers could exhibit the same dependence on the reaction orders and a complete different dependence on oxygen concentration (e.g DCB). These facts confirm that is not likely to establish a generalised equation for dealing with organic compounds and there are still some phenomena that require more research to be able to understand the SCWO process. Regardless, it also proves

the wide variety of contaminants that can be successfully treated via SCWO and supports the reason of the continuous development of the process.

Other compounds that have been studied under SCWO, however their kinetics were not suited to be included in the tables; these are high molecular weight carboxylic acids [180, 181], nitrogen compounds in 2-propanol mixtures [182], methanol-ammonia mixtures [183], (methanol alone which was useful in the evaluation of the effects of mixing of the streams in the development of the reaction [184],) decachlorobiphenyl [185], 2,4,6-trinitrotoluene [186], polychlorinated biphenyls [187], ammonium sulfide [188] and 4-chlorobiphenyl [189].

A comparison of different oxidants in the reaction has also been studied, for example 2,4-dichlorophenol with hydrogen peroxide and oxygen [190], acetic acid with potassium permanganate as oxidant [191], phenol, 2,3-dichlorophenol, m-cresol using potassium persulfate and hydrogen peroxide [192]. The results show that hydrogen peroxide indeed accelerates the reaction compared to oxygen which is a consequence of free radicals generated once the hydrogen peroxide was thermally decomposed. Nevertheless, it did not perform better than potassium persulfate, however for convenience of its preparation, to avoid any deposition of potassium salts in the experimental setup and for safety reasons when compared to oxygen, hydrogen peroxide is a better alternative.

2.2.1.2 Catalytic SCWO

Although SCWO can achieve eliminations of organic compounds over 99% percent, waste sometimes includes very stable organic compounds, which are partially oxidised or lead to the formation of refractory byproducts, such as carboxylic acids or ammonia. These are resistant to complete oxidation and require more severe operating conditions. Consequently, research in SCWO has been also conducted in homogeneous and heterogeneous catalytic systems. The addition of a catalyst aims to improve the elimination of the contaminants in shorter reaction time, promote the selectivity towards complete oxidation products (mainly CO_2 and H_2O) and enhance the process economics by reducing the reactor size and the severity of operating conditions [55].

Several studies have been carried out to verify the feasibility of the inclusion of a catalyst in the supercritical water oxidation process. It has been proven that the addition of catalyst

Table 2.4: Kinetic Parameters for the SCWO of Heteroatoms Compounds

Compound	Reference	Reactor	E_A, (kJ/mol)	$a^\star$	$b^\star$	$c^\star$
DBU	[167]	TR	145	0.9	0.4	0
Nitrates-Ammonia Salts	[168]	TR	224.6-278.2	1	1	0
Nitrobenzene	[169]	TR	36.6	1.04	0.49	0.07
Isopropylamine	[170]	TR	64.12	1.13†	0.24	0
Thiodiglycol	[171]	TR	41.53	1.02†	0.10	0
Quinoline	[147]	TR	226	0.8	0.3	0
o-cresol	[172]	TR	141.1	0.54	0.35	1.46
m-cresol	[172]	TR	N/K	0.655	0.61	0
p-cresol	[172]	TR	N/K	0.603	0.537	0
o-hydroxybenzaldehyde	[173]	TR	N/K	0.47	0.57	0
m-hydroxybenzaldehyde	[173]	TR	N/K	0.98	-0.33	0
p-hydroxybenzaldehyde	[173]	TR	N/K	0.77	-0.02	0
EDTA	[174]	TR	47-53.72	2.048‡	0.357§	0
Methyl amine	[175]	TR	255.4	1	0	0
Benzene	[176]	TR	270	0.4	0.17	1.4
1,3-DCB	[177]	TR	29.7	1	1	0
1,4-DCB	[178]	Batch	65.8	1	0	0
Methylphosphonic acid	[179]	TR	228	1	0.3	1.17

TR: Tubular reactor

DBU: 1,8-diazabicyclo[5.4.0]undec-7-ene

EDTA: ethylenediaminetetracetic acid

DCB: dichlorobenzene

N/K: Not known

* Where a, b and c are the reaction orders according to: $-\mathscr{R}_A = k\, C_A^a\, C_B^b\, C_{H_2O}^c$

† Given in terms of total organic carbon concentration

‡ Given in terms of chemical oxygen demand

§ Given in terms of hydrogen peroxide concentration

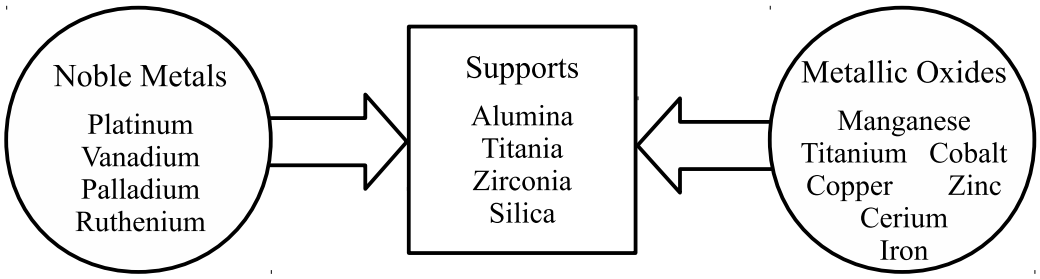

Figure 2.7: Catalyst and Supports for SCWO

substantially increased the reaction rate with a higher degree of conversion attained at shorter residence times when compared to non-catalytic oxidation [193]. An additional advantage is that by reducing the reaction temperature and pressure, it consequently could lessen the corrosion problems. The use of catalyst for the complete oxidation of organics is not new, on the contrary it is an intensively studied area, however their application to SCWO is relatively new and it has been the main topic in many research studies. Spivey [194] have carefully reviewed the complete heterogeneous catalytic oxidation of volatile organics, which has set the basis for the selection of appropriate catalyst for SCWO. Later Ding et al. [157] published a review devoted to catalytic supercritical water oxidation (CSCWO). A more detailed fundamental description of the catalytic oxidation process can be found elsewhere [195]. Figure 2.7 condenses the findings of the reviews in volatile organics and CSCWO into a basic guide of the active noble and metal oxides together with the supports that could theoretically produce a catalyst with excellent properties for the complete oxidation of organic compounds in supercritical water.

In their paper Ding et al. [157] considered also topics like the roles of water in the reaction, the catalyst preparation and two other important factors: the activity and stability of the catalyst, which become very important at the operating conditions of the process. The selection of the catalyst is not easy because it depends on many factors that occur during the reaction. The catalyst could be active for the reaction but not selective or in the worse case loose its activity within a short period of operation. Consequently, the selection of the appropriate noble metal (which for waste water treatment on a large scale should be avoided) or metal oxide relies on three important aspects, namely activity, selectivity and stability. The latter being the most difficult to achieve at the operating conditions of the process where an oxidant atmosphere, the presence of mineral acids at high pressure and temperature are always present. Some metals might change

from an active phase to another and loose their activity at the operating temperature in the presence of oxygen. A clear example is MnO_2, which can be reduced to Mn_2O_3 and therefore be inactive phase for oxidation. Such transformations are very common in SCWO and so they should be considered for any catalyst design. Two other important aspects that should be considered for a catalyst are its activity for a particular reaction and its product selectivity towards complete oxidation products.

The following two sections comprises a review of the kinetics of the catalytic oxidation of organic compounds in supercritical water and when it was possible the kinetics was presented as Equation 2.5.

2.2.1.2.1 Homogeneous Catalytic Reactions. The key step in homogeneous catalysis is the separation of the catalyst from the unreacted material and products. At supercritical conditions the separation could be done by small changes in pressure and temperature that lead to a tuning in the properties of water which opens the opportunity to develop more research in homogeneous catalytic oxidation. However, homogeneous catalytic reactions for the complete oxidation of organic compounds have not been studied in depth.

An early study done by Lin et al. [196] for the oxidation of 2-chlorophenol proved the ability of salts of lithium to improve the reaction. They calculated an activation energy of 44 kJ/mol and the reaction orders of 0.95, 0.56 and 0.45 for 2-chlorophenol, oxygen and water, respectively. Qi et al. [197] carried out the oxidation of aniline over metallic salts of iron (Fe), manganese (Mn) and copper (Cu) and vanadium pentoxide. They demonstrated that salts of copper and manganese were the most effective for the destruction of aniline. Gizir et al. [198] also showed that among several salts used, copper sulfate ($CuSO_4$) gave the best eliminations of phenol and chlorophenols. Some other catalysts have been shown to enhance the oxidation reaction such as heteropolyacids ($H_4SiW_{12}O_{40}$) [199].

However, there is one issue remaining; is it truly an homogeneous process? Were salts and reacting mixture co-existing in a single phase? The solubility of salts is poor in supercritical water and thus it is important to verify the complete dissolution of the catalyst. At this stage the importance of the phase equilibrium for understanding the reaction becomes vital in the development of the research in this field.

Table 2.5: Kinetic Parameters for the CSCWO of Phenol

Reference	Catalyst	Reactor	E_A, (kJ/mol)	$a^\star$	$b^\star$	$c^\star$
[193]	$CuO - MnO_2/Al_2O_3$	FBTR	N/K	0.94	0.29	0
[204]	CuO/Al_2O_3	FBTR	78	0.86	0.22	0
[205]	TiO	FBTR	135	0.69	0.22	0
[206]	MnO_2	FBTR	48.3	0.83	0.36	0
[207]	MnO_2	FBTR	N/K	1	0.74	-1.98

FBTR: Fixed-bed tubular reactor

N/K: Not known

* Where a, b and c are the reaction orders according to: $-\mathscr{R}_A = k\, C_A^a\, C_B^b\, C_{H_2O}^c$

2.2.1.2.2 Heterogeneous Catalytic Reactions. Phenol is undoubtedly the most studied compound in both SCWO and CSCWO because it is a model compound of heterocyclic molecules, and understanding its catalytic oxidation researchers have hoped to extend their findings to some other aromatic compounds. Table 2.5 shows a summary of the catalytic research done on phenol oxidation. Generally, phenol shows a reaction order close to unity which is comparable to the non-catalytic route, however the reaction order respect to oxygen in almost all cases smaller than 0.4. The table shows that the catalytic phenomenon seemed to depend less on the concentration of oxygen. Also catalytic oxidation of phenol have been studied over V_2O_5 and CuO [200] and activated carbon [201, 202, 203], nonetheless the kinetic data provided were not suitable to be included.

Savage [208] has presented a study of three catalysts for the oxidation of phenol and compared the results to non-catalytic oxidation reactions. The catalytic materials compared were TiO_2, MnO_2 and mix of MnO_2/CuO. The study revealed important results of the oxidation in terms of selectivity towards the production of CO_2. As was expected, the catalyst accelerated the destruction of phenol, and among them the MnO_2/CuO mix provided the fastest elimination of phenol. However, in terms of CO_2 selectivity only the catalytic mix MnO_2/CuO performed better than the non-catalytic route; MnO_2 alone provided lower selectivity than the non-catalytic route. The finding suggests that mixtures of active metals perhaps help to reach the two key roles of the catalyst in the reaction faster reaction and higher selectivity.

Table 2.6: Kinetic Parameters for the CSCWO of Phenol

Compound	Reference	Catalyst	Reactor	E_A, (kJ/mol)	$a^\star$	$b^\star$
1,4-DCB	[213]	V_2O_5	Batch	55.1	1	1
Pyridine	[214]	Pt/Al_2O_3	FBTR	343.91	2.05	0.44
Pyridine	[215]	$\alpha - Al_2O_3$	FBTR	227.61	0.42	0.73
Pyridine	[215]	$MnO_2/\gamma - Al_2O_3$	FBTR	190.85	1	1
Pyridine	[215]	$Pt/\gamma - Al_2O_3$	FBTR	287.26	2.25	0.43
Pyridine	[215]	$MnO_2 - CeO_2/Al_2O_3$	FBTR	196.42	1.12	1.14
Ammonia	[216]	$MnO_2 - CeO_2/Al_2O_3$	FBTR	189	0.63	0.71
Ammonia	[157]	Inconel beads (nickel-chromium alloy)	FBTR	29.7	1	0
Acetic Acid	[217]	$Cu - Zn - Co$ oxides	FBTR	109.7	0.689	0.473

FBTR: Fixed bed tubular reactor

DCB: dichlorobenzene

* Where a and b are the reaction orders according to: $-\mathscr{R}_A = k\, C_A^a\, C_B^b$

Table 2.6 shows the catalytic oxidation of various compounds and the different catalysts used. The work has been almost concentrated on nitrogen- and chlorine-containing organic compounds. Other research has been conducted to evaluate the catalytic oxidation of 2-propanol, tert-butanol, 1-methyl-2-pyrrolidone, acetic acid and benzoic acid over a mix of Cu and Zn oxides [209] and to assess the catalytic properties of CrO_3 [210], $CuO/Zeolites$ [211] or even the catalytic influence of salts [185, 212], nonetheless kinetic parameters were not provided in the form of Equation 2.5 to be included.

Also studies have identified a simultaneous participation of the catalytic and non-catalytic route [178]. When the reaction orders are not integers like those observed, they might also depend on both the temperature and concentration and it is therefore preferable to express the reaction rate in forms that include a more detailed approach to the heterogeneous phenomenon. These reaction rate models are named the Langmuir-Hinshelwood-Hougen-Watson (LHHW) rate expressions. Some reaction rates have been given in this form, for example phenol [218] and

ammonia [216] or by a more specific oxidation reaction model named Mars-van Krevelen [195] that involves the participation of the metal into the reaction [204]; however, they do not agree on the type of mechanism that the CSCWO follows.

2.2.2 Transition State Theory

It has been demonstrated experimentally that reactions which occur near the thermodynamic critical point of the reaction mixture show an abnormal behaviour of their reaction rates. An explanation for this phenomena is given in terms of the transition state theory [219]. The transition state theory relates the molecular changes due to rupture and formation of bonds and the solvent effect in the reaction. The ability of transition state theory to include the effect of the solvent make it a useful tool for the prediction of reactions rates.

Although transition state theory has been applied to represent reactions in solution, it can be extended to gaseous, catalytic and supercritical reactions [220]. The rate of a chemical reaction is a complex function of the thermodynamic state of the system, which is influenced by temperature, pressure, concentration of the reactants, the catalyst and the solvent effect or the inert species present during the reaction [221]. For example for a bimolecular reaction, there is a transition state (M) between reactants and products such as [222]:

$$A + B \leftrightarrow M \rightarrow Products \tag{2.6}$$

According to the transition state theory a quasi-equilibrium is assumed between the reactants A and B [223, 224]. The reaction rate is determined by the rate at which the transition states moves along the reaction coordinate[1]. It depends on the transition state equilibrium constant of formation $\left(K^{\ddagger}\right)$ which can be accessed by $\Delta G^{\ddagger} = -RT \ln K^{\ddagger}$ and this provides a useful relationship of the rate constant in terms of the thermodynamic quantities of the transition state.

$$\left(\frac{\partial lnk}{\partial P}\right)_T = \frac{1}{RT}\left(\frac{\partial \Delta G^{\ddagger}}{\partial P}\right) = -\frac{\Delta \nu^{\ddagger}}{RT} \tag{2.7}$$

Where $\Delta \nu^{\ddagger}$ is denominated the activation volume. While the activation energy (E_A) is used to represent the effect of temperature, the activation volume accounts for the effect of pressure

[1]The reaction coordinate represents the course of the reaction, since reactants move along it to reach the transition state and then to products.

in the reaction rate. Because volume is a function of the system pressure, the reaction constant should be expressed in pressure-independent concentration units or a correction for this fact has to be made. The activation volume is given by the difference of the partial molar volumes between the transition state and the reactants as follows:

$$\Delta\nu^{\ddagger} = \overline{\nu}_M - \overline{\nu}_A - \overline{\nu}_B \tag{2.8}$$

The transition state volume could give information about the structure and properties of the transition state, however they cannot be directly elucidated from the activation volume. One very useful approach is to treat the activation volume as the sum of two other quantities:

$$\Delta\nu^{\ddagger} = \Delta\nu_1^{\ddagger} + \Delta\nu_2^{\ddagger} \tag{2.9}$$

Where the structural contribution $\Delta\nu_1^{\ddagger}$ represents an intrinsic size or difference in molecular size between reactants and transition state, due to any change in the transition state due to bond breakage or formation, and is useful in mechanistic interpretation and in elucidation of internal interactions. The solvent dependent part $\Delta\nu_2^{\ddagger}$ comprises any variation of the solvent shell surrounding the reactants as they move along the reaction coordinate [225]. It is difficult to interpret the activation volume data because it could represent the result of several unaccountable effects, nevertheless some efforts have been made to use $\Delta\nu_1^{\ddagger}$ to predict the effect of pressure in the reaction. Once the transformation is established the reaction problem is reduce to an equilibrium, or thermodynamic problem. The advantage is that thermodynamics are far better understood than rate processes [221, 226].

Anikeev et al. [227] have calculated the activation volumes for the oxidation of aliphatic nitro compounds in supercritical water and successfully correlated the pressure effect on the reaction rate. The values of the activation volumes reported were in a range of -702 to -764 cm^3/mol. If these values are compared with those from reactions in the liquid phase carried out in organic solvents where the activation volumes were in the order of -50 to $+50$ cm^3/mol [228], the enhancement in the activation volume is appreciable and produced by the clustering of the supercritical water around the molecules of solute [229].

2.2.3 Mechanisms Based on Elementary Reactions

At this point, it is common to formulate a valid question about the reaction: what could be the mechanism of SCWO? Until now the reaction rate has been considered as the summary of a more complex process and not just a reaction where: $A + B \rightarrow Products$. If we look closely at stoichiometry of some of the reactions, they involve a large number of molecules that participate in the reaction. This fact is unlikely to happen because the probability that the number of molecules indicated by the stoichiometric equation would share at the same time, the same spatial an electronic configurations such that bonds could be broken and atoms could be rearranged in a single step is almost null. The stoichiometry purely reflects the reactants consumption and product yields, however they are not able to represent the changes at atomic and molecular level that occur when the reaction proceeds [230]. Moreover, stoichiometric equations should be seen as the summary of all those changes. Furthermore, the values of the reaction orders in many of the rate expressions cited earlier are not integers and differ from the stoichiometric values. This relates to the mechanism of the reaction itself. The mechanistic equation cannot be related to the stoichiometry of the reaction, because the molecularity of the reaction has a theoretical context, meanwhile the stoichiometry and reaction orders are completely empirical values. Empirical models cannot explicitly indicate the mechanism of a reaction and when the reaction gradually proceeds many side reactions became immersed into a global reaction which is then represented by a power law kinetic model. However, the chemistry of the reaction is hidden and only the final outputs of the reaction are obtained.

The chemistry of SCWO reactions have found a parallel with combustion reactions. Essentially, both produce complete oxidation of a fuel in the case of combustion or oxidisable organic matter for SCWO and have mainly water and carbon dioxide (this depends on whether any heteroatoms are present) as final products. However, the two reactions differ basically in the high water concentration and the unusual physicochemical properties exhibited by SCW. Extensive research of combustion reactions have been possible through the use and modelling of the unimolecular and recombination reactions, and it has been established that their reaction mechanism is comprised within a complex network of free radical reactions. An example of a unimolecular process is the dissociation of ethane:

$$C_2H_6 \longrightarrow 2CH_3\bullet \tag{2.10}$$

and for the recombination process it is the reverse process; the reaction between two methyl radicals to produce ethane:

$$CH_3\bullet + CH_3\bullet \longrightarrow C_2H_6 \tag{2.11}$$

The approximate description of the dynamics of the process is given by the Rice-Ramsperger-Kassel-Marcus (RRKM) or quasi-equilibrium theory, which in essence applies the transition state theory to a set of excited reactant molecules. The main distinction between the two theories is while the transition state theory assumes a quasi-equilibrium between reactants and the activated complex, the RRKM theory establishes a "non-return" configuration once this state has been reached [141].

The models applied to oxidation in supercritical water have been derived of those already available for combustion and adapted to lower temperatures (around 773 to 873 K) and higher pressures (25 - 28 MPa) where SCWO takes place. At these operating conditions the reacting mixture, which is mainly water, behaves as an ideal gas and therefore interactions other than collisions between water and other molecules are overlooked. In addition, it was also assumed that SCWO reactions proceed via free radicals and some reactions have been also added to the combustion mechanisms to account for other chemical processes that occur at supercritical conditions.

The intricate reaction network can be modelled using specialised software capable of building such a complex mechanism like CHEMKIN® [231], CHEMACT or CHEMDIS [232, 233]. Such computer software allows the investigation of hundreds of possible reaction combinations in order to understand comprehensively a particular reaction. The software was originally conceived to be applied to gas-phase combustion reactions and has been adapted to model SCWO reactions due mainly to the similarities of the set of reactions mechanisms that occur SCWO.

Although, relatively simple molecules have been modelled using elementary reactions like carbon monoxide [234, 235, 236], hydrogen [234, 235, 236, 237, 238], methane [236, 239] and methanol [154, 236, 237, 240], recent efforts have been made on modelling the oxidation of heavier molecules such as methylamine [241] or benzene [233] and to model the co-oxidation

effect of binary mixtures of methanol and ethanol [242] and methylphosphonic acid and ethanol [243, 244].

In general, the predictions provided by the models agreed reasonably well with the experimental data and the mechanisms have been useful to identify the importance of some radicals like the hydroperoxy radical ($HO_2\bullet$) for the reaction or the induction times in the reaction. On the other hand, the oxidation mechanisms were less accurate predicting the oxidation of, for example methanol and CO and rather more complex molecules like benzene where the model underpredicted the production of CO and CO_2 [233]. Although the mechanism can be complex by the large number of reactions involved, they can be simplified if the key reactions are identified and a new reduced mechanism can be elucidated [240].

Perhaps, the lack of prediction of the oxidation mechanisms is because it does not consider some essential phenomena that occur in SCWO. Firstly, the role of water as a solvent and its interaction with the solute molecules rather than just be considered as a collision partner. Secondly, the consideration that the mechanism only proceeds via free radicals might not completely true. Bühler et al. [20] have carried out the pyrolysis of glycerol in supercritical water and identified the reaction products to distinguish whether the reaction follows a free radical or ionic mechanism. Although it is a different reaction, they proved a non-Arrhenius behaviour of the reaction. Moreover, what could be the most important observation is based on the product distribution; the ionic reaction pathway was the only explanation of how some of the products were produced and that both ionic and free radicals mechanisms were happening in the process. Hayashi et al. [245] have also supported the importance of ionic reactions in supercritical water. Finally, the reactions modelled have been conducted in an operating condition region where supercritical fluids resemble an ideal gas. However, the mechanisms have not yet been able to predict reactions near the water critical point where interactions between solvent and solute are stronger and large changes on the physicochemical properties of water are a consequence of small changes in pressure and temperature.

Chapter 3

Experimental Section

3.1 Thermodynamic and Physicochemical Properties of Reagents

Both 1,8-diazabicyclo(5.4.0)undec-7-ene (DBU) and quinoline critical properties were estimated using the Joback modification of Lydersen's group contribution method and acentric factors using the Lee-Kesler vapor pressure relations [246]. Critical properties of water were taken from IAWPS Formulation 1995 [3] while critical properties of oxygen appeared in Sandler [247] (critical properties are shown in Table 3.1). The densities of DBU, quinoline and oxygen were calculated from a modified version of the Benedict-Webb-Rubin equation of state (EoS) [248] by Edmister et al. [249]. Water density was calculated by the IAWPS Formulation 1995 [3]. The Lee-Kesler mixing rules were used to obtained the pseudocritical properties of the mixture and the acentric factor.

A *Fortran 95* computer code was written to perform the calculation of the flow rate and reagent concentrations. The reaction conditions are first defined and the program provides a backward calculation of the concentration of reactants and flow rates at ambient conditions to accomplish the selected reaction conditions. The program integrates as subroutines the IAWPS 1995 formulation for calculation of water density and the Benedict-Webb-Rubin EoS for the computation of the density of oxygen, DBU and quinoline. Whenever the properties of DBU and quinoline were not available the estimation of the property of mixture was done assuming a solution at infinite dilution.

3.1.1 Mixture Properties at Infinite Dilution

The thermodynamic property of a mixture given in terms of partial molar properties at certain system pressure (P) and temperature (T) is given by [247] :

Table 3.1: Properties of Reagents

Property	Water	Oxygen	DBU	Quinoline
Chemical Formula	H_2O	O_2	$C_9H_{16}N_2$	C_9H_7N
MW, g/mol	18.015	31.999	152.24	129.61
Critical Temperature, K	647.096	154.6	571.454	782.15
Critical Pressure, MPa	22.064	5.046	3.74538	4.66
Critical Volume, cm^3/mol	55.948	73.4	501.5	469.0
Acentric Factor	0.344	0.025	0.431	0.329

$$\underline{\theta} = \sum_{i=1}^{n} x_i \overline{\theta}_i(T, P, \underline{x}) \tag{3.1}$$

where the partial molar property is written as

$$\overline{\theta}_i = \overline{\theta}_i(T, P, \underline{x}) = \frac{\partial(N\underline{\theta})}{\partial N_i} \mid_{T,P,N_{j\neq i}} \tag{3.2}$$

N is the number of mol of the i species. In a ternary system any thermodynamic property is given by

$$\underline{\theta}(T, P, \underline{x}) = N_1\overline{\theta}_1(T, P, \underline{x}) + N_2\overline{\theta}_2(T, P, \underline{x}) + N_3\overline{\theta}_3(T, P, \underline{x}) \tag{3.3}$$

At reaction conditions the concentration of water in the reacting mixture accounts for at least 0.99 of the composition, consequently it is assumed an infinite dilute solution. Now consider the case where N_2 and N_3 are equal to 1, at infinite dilution $N_1 \gg N_2$ and $N_1 \gg N_3$ thus $x_1 \sim 1$, $x_2 \sim 0$ and $x_3 \sim 0$ and the following expression is obtained:

$$\underline{\theta}(T, P, \underline{x}) = N_1\bar{\theta}_1(T, P, x_1 \sim 1) + \bar{\theta}_2(T, P, x_2 \sim 0) + \bar{\theta}_3(T, P, x_3 \sim 0) \tag{3.4}$$

At infinite dilution it is assumed that the thermodynamic properties of the mixture are those of water when no other available data are given.

3.2 Design of the Catalytic Reactor

One of the aims of moving to a catalytic process is to reduce the severity of the process by decreasing mainly the pressure and temperature; which means that operation can be close to the critical point of water. In the vicinity of the critical point, water density is the most important factor of design because it varies sharply near its thermodynamic critical point (Figure 3.1). The reaction rate ($\mathscr{R}$) is a complex function of the temperature, pressure, reactants concentrations and the space time or its reciprocal space velocity for continuous steady state operations. In the case of heterogeneous catalytic reactions the space velocity has a different connotation than in homogeneous systems given by:

$$WHSV = \frac{\rho\, F_{i_0}}{W} \tag{3.5}$$

Where $WHSV$ is the weight hourly space velocity, ρ is the reacting mixture density, F_{i_0} is the initial volumetric flow rate of i and W is the weight of the catalyst (active metal plus support). If $\mathscr{R}_i = \mathscr{R}_i(T, P, C_i, WHSV)$ once T, P and C_i are fixed, $WHSV$ is the only degree of freedom in the process and by varying it, the mass flow rate of reagents or the catalyst weight, the space velocity will control the degree of conversion in the reactor.

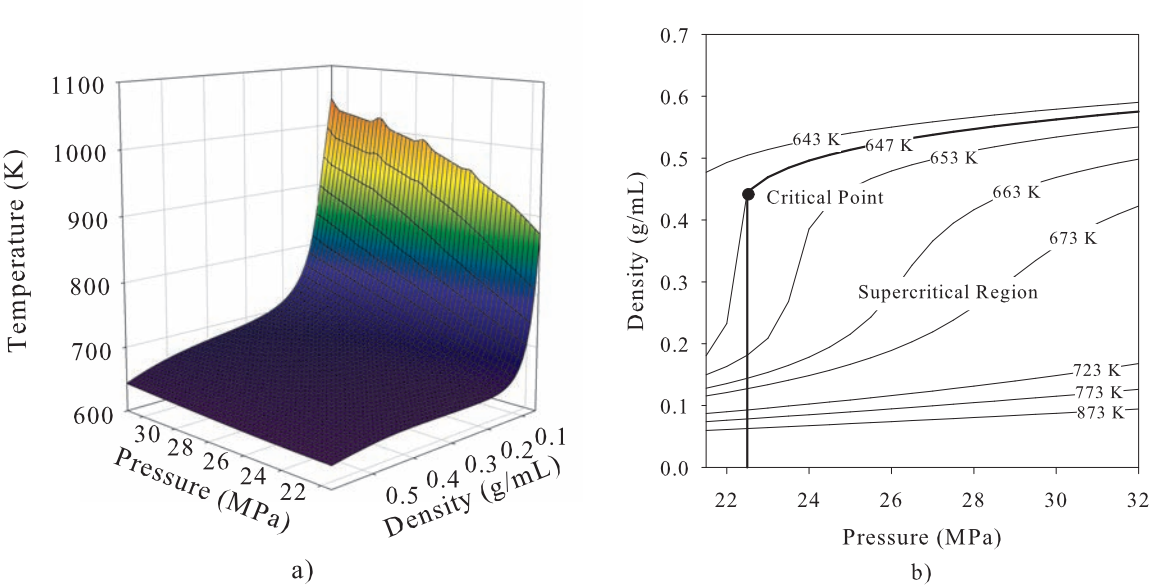

Figure 3.1: Water Density near Critical and Supercritical Conditions

However, in fixed-bed tubular reactors the flow rate of the reacting mixture is linked to the

hydrodynamics of the operation. To be conveniently considered as an ideal reactor (which largely simplifies the equation design and thus the treatment of kinetic data) the tubular reactor must operate in a region where the flow rate assures a plug flow operation. As a preliminary design consideration there are two conditions that a fixed-tubular tubular reactor must fulfill [250]:

$$\frac{d_R}{d_p} > 10 \tag{3.6}$$

$$\frac{L}{d_p} > 50 \tag{3.7}$$

Where d_R is the reactor diameter, d_p is the particle diameter and L is the length of catalytic bed. It is important to keep in mind that small particle diameters might result in non-isobaric operation and thus it will produce changes in the axial concentration of the reactants. For estimating the pressure drop in the reactor due to the catalytic particles the Ergun equation provides useful information [230, 251]:

$$\left(\frac{[\mathscr{P}_0 - \mathscr{P}_L]\,\rho}{G^2}\right)\left(\frac{d_p^*}{L}\right)\left(\frac{\varepsilon_B^3}{1-\varepsilon_B}\right) = \frac{150\,(1-\varepsilon_B)}{\left(d_p^* G/\mu\right)} + 1.75 \tag{3.8}$$

where the term $[\mathscr{P}_0 - \mathscr{P}_L]$ is the pressure drop along the packed bed, ρ and μ are the density and viscosity of the reacting mixture, L is the length of the packed column, G is the mass velocity, ε_B is the porosity bed and d_p^* is the equivalent particle diameter that is obtained from $d_p^* = 6/a_v$ in which a_v is the area per unit volume of an individual particle.

3.3 Catalytic Supercritical Water Oxidation Rig

A schematic diagram of the laboratory scale Catalytic Supercritical Water Oxidation (CSCWO) rig is shown in Figure 3.2. The rig is comprised of three sections:

- Delivery and preparation
- Reaction
- Depressurization, cooling and sampling

The delivery section accounts for the pressurization, heating and premixing of the reagent streams. It consists of three streams: oxidant solution, water and organic compound solution

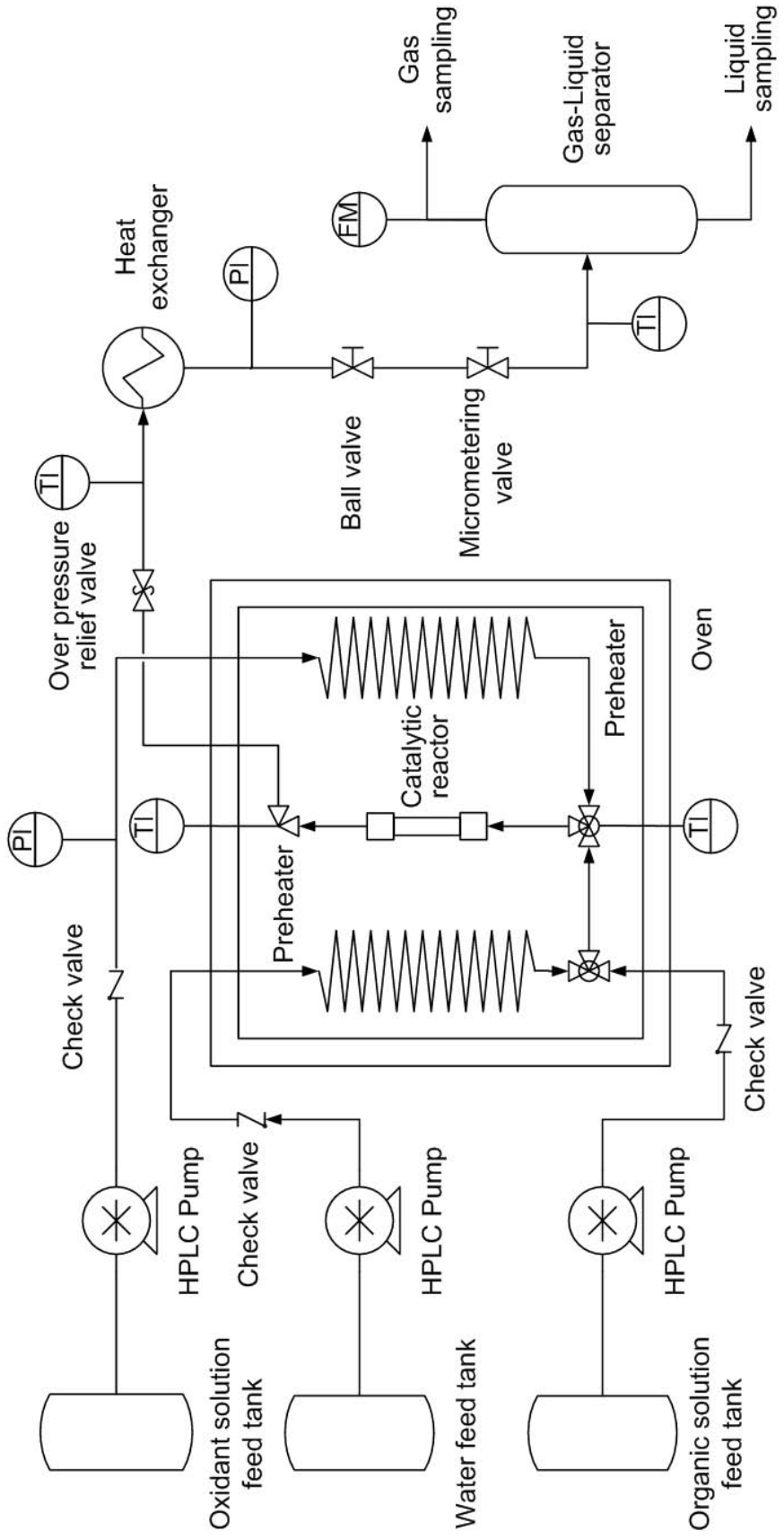

Figure 3.2: CSCWO Rig

stream, which were delivered by two Gilson 305 and one Jasco PU-1586 liquid chromatography pumps, respectively. The maximum flows delivered by the pumps were 10 mL/min for the two Gilson 305 and 20 mL/min for the Jasco PU-1586 at a maximum pressure of 60.0 MPa. The pumps pumped the three streams until the desired operating pressure. The heating of the streams was carried out isobarically within an air heated electric furnace (AEW, Hampshire). The oxidant solution and water stream were preheated in two coiled sections each having a length of 7 m made of stainless steel (SS) 316 tubing with 6.25 mm o.d. and 2.1 mm i.d. Meanwhile the concentrated solution of the organic compound was fed into 1.2 m tubing section made of SS with 6.25 mm o.d. and 2.1 mm i.d and then it was mixed with supercritical water at a short distance (70 mm) to the inlet of the reactor, so hydrous pyrolysis of the organic compound is reduced. The mixing of the streams occurs in the pipe line after the two tees and the 10 μm sintered filter (see Figure 3.3). Complete mixing is assured once the reacting mixture went through the stainless steel porous disc when it entered the reactor. The turbulence created in the microchannels of the disc assures a high quality mixing of the streams.

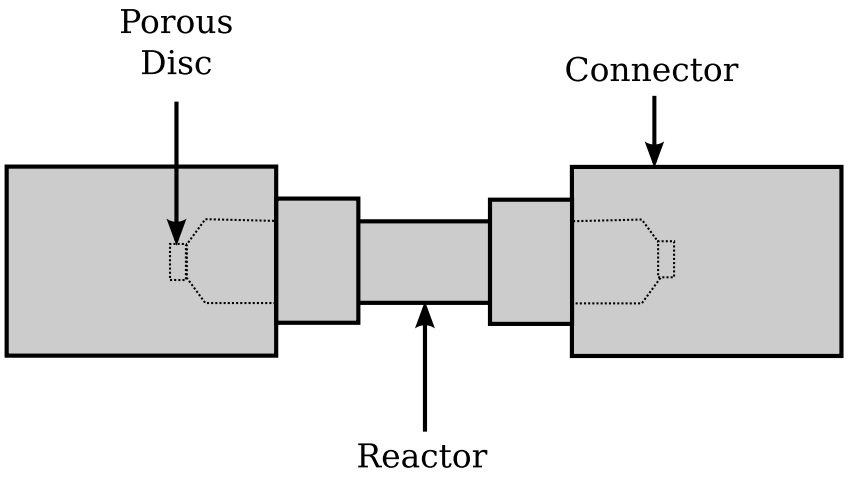

Figure 3.3: Assembly of the Catalytic Reactor

The catalytic reactor is a SS 316 tubing section; it has dimensions of 100 mm length, 14.28 mm o.d. and 4.76 mm i.d. (see Figure 3.4). Porous SS discs (10 μm sintered filter; Mott Corporation) were place at both ends of the reactor to confine the catalyst within the reactor. After intensive operation under supercritical conditions SS can be corroded causing operational problems. As a consequence, the equipment should be periodically inspected or replaced. At these operating conditions nickel base alloys (i.e. Hastelloy C-276 or Inconel 625) are preferred

as a construction materials. The selection of SS was based on internal safety regulations. For this specific process (oxidant and corrosive atmosphere under high pressure and temperature) and independently of the construction material, the lifetime of the rig was limited (2 years of operation or 1000 operation cycles) and parts of the rig must be totally replaced and thus SS was cheaper for the construction. The selection of a specific material could influence the reaction paths because metal or metallic oxides in the alloy have been identified to act as catalyst. Segond et al. [146] reported that the SCWO of ammonia occurs via a parallel homogeneous and heterogeneous mechanism in the wall of the reactor. They have concluded that the reaction in the wall catalyzed by the stainless steel reactor was significant. Meanwhile, Webley et al. [144] pointed out that in the case of Inconel 625, the contribution of the wall reaction was lower than the homogeneous reaction. However, this effect has not been studied for the oxidation of the organic compounds. The preheating system and the reactor were enclosed within the air heated electric furnace.

Figure 3.4: Catalytic Supercritical Water Oxidation Reactor

Once the reacting mixture left the furnace, it was cooled by passing through a heat exchanger then expanded through a ball and micrometering valves to ambient pressure. After the expansion the mixture passed through a gas-liquid separator where liquid samples were taken to be analyzed. After the separator, in the gas stream an ADM 2000 online gas flow meter (Agilent Technologies)

was set to record electronically the volumetric flow data of gases produced during the reaction via a data port. A gas sampling port situated in the top part of the separator allowed gas samples to be taken for further analysis (samples were analyzed as they were collected).

The temperature along the experimental rig was measured by four thermocouples, located at the mixing point of the solutions just before the reactor inlet, at the reactor outlet, before entering the heat exchanger and after the set of two valves, respectively. Pressure was monitored at the inlet of the oxidant feed stream and after the heat exchanger.

3.3.1 Operation of the CSCWO Rig

The CSCWO rig has been designed to carry out oxidations reactions above the critical point of water. Nonetheless the maximum operation conditions allowed due to safety regulations was 30.0 MPa at 873 K. The operation procedure is as follows:

1. Because the catalytic reactor was removed and placed for each experimental run, it was good practice to evaluate if system was hermetic. For this purpose the ball valve (after the second pressure indicator and before the separator) was closed and the chromatography pumps were switch on at flow rates of 3 mL/min for the two Gilson 305 and 2 mL/min for the Jasco PU-1586. By doing this the rig was pressurized until the pressure reached 30.0 MPa, failure to do so indicate that there might be a leak present in the rig. The pumps were switched off again and the ball valve opened.

2. The set point on the oven control panel was programmed to reaction temperature.

3. The start button was pressed on the oven control panel to initiate the heating. The vent compartment on the top of the oven was closed.

4. The oven temperature reset button was pressed on the oven control panel.

5. The timer reset button on the oven control panel was pressed.

6. The cooling system was switch on to a temperature of 263 K (-10°C).

7. The HPLC pumps were held in stand-by mode until the oven reached a temperature of 20 degrees below of reaction temperature.

8. The oxidant solution pump was switched on, primed, the flow rate programmed and started.

9. The water pump was switched on, primed, the flow rate programmed and started.

10. The micrometering valve was closed to pressurize the rig; this should not be completely closed, over tightening would lead to damage of the needle valve. (After here, the pressure was constantly monitored; the pressure was released by slightly open the micrometering valve and viceversa). Only the micrometering valve was used for controlling the pressure. It is worth to point out that the response time was slow. It is also important to mention that sudden increments of the system pressure can be present at any time.

11. At this point the rig was maintained with the actual settings until the oven reached the reaction temperature.

12. The organic solution pump was switched on, primed, the flow rate programmed and started.

13. After a while the rig reached steady state operating conditions (this took around 10 to 30 min).

14. The pressure was adjusted by opening or closing the micrometering valve.

3.3.2 Shutdown Procedure of the CSCWO Rig

The increment of pressure is basically a consequence of the flow rate delivered to the rig. Two safety features were included in the design. The Jasco PU-1586 has an integrated pressure sensor that will stop the fluid being pumped once the system reaches 31.0 MPa. Secondly, in case of overpressure (above 32.0 MPa) a relief valve will open releasing the overpressure in the system. In the event of overpressure it is recommended to follow the procedure below for shutting down the rig or after an experimental run:

1. The organic solution pump was switched off.

2. The oxidant solution pump was switched off.

3. The water pump was switched off.

4. The micrometering valve was opened by turning slowly the handle anticlockwise.

5. The furnace was switched off by pressing the stop button.

6. All lines were flushed by pumping water at a flow rate of 1 mL/min in each pump for 1 h.

3.4 Reagents Preparation

The preparation of the organic compound solution and the hydrogen peroxide solution will be describe in this section.

3.4.1 DBU and Quinoline Solution

The solutions of DBU (Fluka >99%) and quinoline (Acros Organics 99%) were prepared by weighing the appropriate amount of the organic compound and then dissolving it with distilled deionized water (Milli-RO Plus 30, Millipore water purification system) in a 250 mL measuring flask and homogenized. DBU and quinoline were used as received.

3.4.2 Hydrogen Peroxide (H_2O_2) Solution

Although, oxygen [190], potassium permanganate [191] and potassium persulfate [192] have been considered as oxidants in previous research, hydrogen peroxide was selected because it is safer and the solutions can be delivered without the need of extra safety considerations in the design of the rig. The solution of H_2O_2 is thermally decomposed according to:

$$2H_2O_2 \longrightarrow 2H_2O + O_2 \tag{3.9}$$

The solution was prepared by diluting a concentrated solution of hydrogen peroxide (50% wt Sigma-Aldrich) with deionized water to the concentration required for the experimental run. The solution of hydrogen peroxide was kept on ice to avoid any H_2O_2 decomposition. The concentration of hydrogen peroxide was determined by titration with potassium permanganate (described later in the analytical techniques in Section 3.5.1).

3.5 Analytical Techniques

Table 3.2 resumes the analytical techniques used during the research project. They were used to measure concentration of reagents and gas and liquid products and catalyst properties.

Table 3.2: Summary of Analytical Techniques

Analytical Technique	Analysis or Species Quantified
Titration with Potassium Permanganate	Hydrogen Peroxide
Total Organic Carbon Analysis	Total, inorganic and organic carbon
High Performance Liquid Chromatography	DBU and Quinoline
Gas Chromatography	Carbon monoxide, carbon dioxide, methane, nitrogen, oxygen and nitrogen oxides
Inorganic Nitrogen Speciation	Ammonium, nitrates and nitrite ions
Inductively Coupled Plasma	Metals
Dynamic Vapour Sorption	Catalyst surface analysis
pH meter	pH

3.5.1 Determination of Hydrogen Peroxide (H_2O_2)

The method for determining the concentration of hydrogen peroxide is based on a British Standard method [252]. This determination is carried out via a titration method using a standard solution of 0.1 N potassium permanganate ($KMnO_4$). The following reaction occurs when potassium permanganate (Merck KGaA $\geqslant$99%) is added to a hydrogen peroxide solution acidified with dilute sulphuric acid (H_2SO_4):

$$2KMnO_4 + 3H_2SO_4 + 5H_2O_2 \longrightarrow K_2SO_4 + 2MnSO_4 + 8H_2O + 5O_2 \tag{3.10}$$

As the titration proceeds, the potassium and manganese sulphates give colourless solutions. As soon as potassium permanganate is in excess, the solution becomes pink and therefore the potassium permanganate acts as its own indicator. The end-point of the reaction is the first permanent pink colouration (a short lasting pink colouration is expected).

Of the three mineral acids: sulfuric acid (H_2SO_4), nitric acid (HNO_3) and hydrochloric acid (HCl), solely H_2SO_4 is suitable for use with potassium permanganate, HNO_3 is itself

an oxidising agent and it can interfere with the oxidant action of potassium permanganate. Furthermore, potassium permanganate reacts with hydrochloric acid (HCl) as follows:

$$2KMnO_4 + 16HCl \longrightarrow 2KCl + 2MnCl_2 + 8H_2O + 5Cl_2 \tag{3.11}$$

3.5.1.1 Titration Procedure for Hydrogen Peroxide

The equivalent weight (EW) of an oxidizing or reducing agent is simply defined as that weight of the reagent which reacts with or contains 1.008 g of available hydrogen or 8 g of available oxygen. By available it is meant being capable of being utilized for oxidation or reduction reactions. The amount of available oxygen may be indicated by writing the following hypothetical equations, for hydrogen peroxide:

$$H_2O_2 \longrightarrow H_2O + O \tag{3.12}$$

and potassium permanganate:

$$2KMnO_4 \longrightarrow K_2O + 2MnO + 5O \tag{3.13}$$

The latter equation is often written in the form:

$$2KMnO_4 + 3H_2SO_4 \longrightarrow K_2SO_4 + 2MnSO_4 + 3H_2O + 5O \tag{3.14}$$

Based on the above equations the equivalent weight for H_2O_2 and $KMnO_4$ is given by:

$$\text{EW } H_2O_2 = \frac{\text{MW } H_2O_2}{2} = 17.01 \text{ geq} \tag{3.15}$$

and

$$\text{EW } KMnO_4 = \frac{(2)(\text{MW } KMnO_4)}{10} = 31.6 \text{ geq} \tag{3.16}$$

In alkaline solution, two molecules of potassium permanganate yield three atoms of oxygen, together with a manganese dioxide as a brown precipitate. Considering these facts, potassium permanganate is always used to titrate solutions sufficiently acidic to avoid the formation of manganese oxide.

Titration Method:

1. Take 1 mL of the H_2O_2 solution into a 250 mL conical flask.
2. Add 5 mL of H_2SO_4 2 N (Fisher Scientific volumetric solution) and 5 mL of distillate water and shake.
3. Titrate with the standard solution of potassium permanganate until the first permanent pink coloration.
4. Repeat twice.

Then the concentration of hydrogen peroxide is given by:

$$N_{H_2O_2} = \frac{(\text{Average mL } KMnO_4)(\text{N}_{KMnO_4})}{\text{mL } H_2O_2} \tag{3.17}$$

And finally:

$$\frac{\text{g } H_2O_2}{\text{mL}} = \frac{(N_{H_2O_2})(17.01)}{1000} \tag{3.18}$$

Details about the standardization and storage of the potassium permanganate solution are given in Appendix A.

3.5.2 Total Organic Carbon (TOC) Analysis

The instrument used was a Shimadzu TOC-5050 Analyzer with autosampler. The TOC measured by the instrument is performed indirectly by subtracting the inorganic carbon (IC) from the total carbon (TC) in the sample. The TC is measured by a catalytic oxidation carried out at 953 K. The reaction takes place in a quartz combustion tube packed with a platinum catalyst, which is contained in an oven that is maintained at the reaction temperature. The oxidant material for the reaction is a high purity air, which is continuously saturated with water and introduced into the combustion tube. The air is also used as a carrier gas. When the sample is injected into the combustion vessel the carbon in the sample is converted to CO_2. The gas then carries the oxidation products into an IC reactor vessel, after which the products are cooled and dried. The gas sample is sent into a halogen scrubber and then to a cell where the CO_2 is quantified

by a non-dispersive infrared (NDIR) gas analyzer based on the area of the signal produced by the sample.

The measurement of IC is performed by introducing the sample into the IC reactor vessel where the carrier gas flows as tiny bubbles through the IC reagent (phosphoric acid solution at 20% wt). Only IC is decomposed to CO_2 which is then taken to the NDIR detector. The concentration of the IC in the solution is calculated following the same principle as the TC content [253].

3.5.3 High Performance Liquid Chromatography (HPLC) Analysis

HPLC analyses were carried out using an Agilent Technologies 1100 Series high performance chromatograph equipped with an ultraviolet detector. The mobile phase for the identification was water (Fisher Scientific HPLC grade), acetonitrile (Fisher Scientific HPLC grade) and trifluoroacetic acid (TFA) (Fisher Scientific HPLC grade).

3.5.3.1 DBU HPLC Analysis

The analysis parameters of DBU were as follows:

Solvent A: Water and 0.05% TFA

Solvent B: Acetonitrile and 0.05 % TFA

Column: Phenomenex Luna C18(2), 5 μm and 150 x 4.6 mm

Analysis Time: 12 min

Post Analysis Time: 3 min

Injection Volume: 5 μL

Temperature: 323 K

Wavelength: 230 nm

Gradient Method: See Table 3.3

The gradient method used a system of two HPLC pumps, where each pump delivered an specific solvent (water or acetonitrile). The binary system allowed to vary dynamically the proportion of solvents in the mobile phase at a constant flow rate. In the analytical method presented in Table 3.3, the mobile phase consisted of only water (0% of solvent B) at the beginning of the analysis (time 0 min.) and then the proportion of solvent B was gradually increased

until it reached 95% in the stream over a period of time of 8 min. Then the ratio of solvents was maintained for two minutes until the ratio was again changed to a mobile phase that only contained water at 10.01 min. The system continues delivering water until the end of the analysis.

Table 3.3: HPLC Gradient Method for DBU Analysis

Time, min	% Solvent B	Flow, ml/min
0.00	0	1
8.00	95	1
10.00	95	1
10.01	0	1
12.00	0	1

3.5.3.2 Quinoline HPLC Analysis

The quantification of quinoline was performed using the following HPLC method:

Solvent A: Water and 0.05% TFA

Solvent B: Acetonitrile and 0.05 % TFA

Column: Phenomenex Luna C18(2), 5 μm and 150 x 4.6 mm

Analysis Time: 12 min

Post Analysis Time: 3 min

Injection Volume: 5 μL

Temperature: 323 K

Wavelength: 230 nm

Gradient Method: Refer to Table 3.4

3.5.4 Gas Chromatography

The gas analysis of nitrogen oxides was performed in an Agilent Technologies 6850 gas chromatograph equipped with a thermal conductivity detector (TCD). An Alltech Porapak Q column was used to performed the gas separation. The specification of the column is 80/100, 12 ft long, 0.125 inches of o.d. and 0.085 inches wall thickness. The gas sample was introduced by a pneumatic sampling valve with a loop of 0.25 mL. The identification method is shown in Table 3.5. The

Table 3.4: HPLC Gradient Method for DBU Analysis

Time, min	% Solvent B	Flow, ml/min
0.00	0	1
8.00	95	1
10.00	95	1
10.01	0	1
12.00	0	1

nitric oxide standard gas and nitrous oxide had a concentration of 100 ppm in helium (Scientific and Technical Gases Ltd.). Higher concentrations of nitrogen oxides standards are not supplied due to safety reasons.

Table 3.5: Nitrogen Oxides Identification

Parameter of Analysis	Gas	Flow Rate
Carrier gas	Helium	
Carrier Flow Rate, mL/min		18
Reference Gas	Helium	
Reference Gas Flow Rate, mL/min		18
Makeup Gas	Helium	
Makeup Gas Flow Rate, mL/min		2
Sampling Loop, mL		0.25
Temperature of the oven, K		305
Temperature of the detector, K		523
Time of analysis, min		25

The gas analysis of carbon dioxide (CO_2), carbon monoxide (CO), oxygen (O_2), nitrogen (N_2) and methane (CH_4) was accomplished in an Agilent Technologies 6890N gas chromatograph equipped with a TCD detector and an Alltech CTR I column. The CTR I is a concentric column with two fixed phases. The outer column is 6 ft long and 0.25 inches o.d., meanwhile the inner

column is 6 ft long and 0.125 inches o.d. The identification method is shown in Table 3.6. The gas cromatograph was calibrated with a low and high concentration standard. The low concentration standard (Scientific and Technical Gases Ltd.) was a mixture of 0.994% CO_2, 1.01% CO, 1.00% O_2, 0.996% N_2, 1.00% H_2 and 1.01% CH_4 with balance in helium, whereas the high concentration (Alltech) was a mixture of 15.0% CO_2, 7.0% CO, 7.0% O_2 and 4.5% CH_4 with balance in nitrogen.

Table 3.6: Gases Identification

Parameter of Analysis	Gas	Flow Rate
Carrier gas	Helium	
Carrier Total Flow Rate, mL/min		65
Reference Gas	Helium	
Reference Gas Flow Rate, mL/min		65
Makeup Gas	Helium	
Makeup Gas Flow Rate, mL/min		2.0
Sampling Loop, mL		1.0
Temperature of the oven, K		305
Temperature of the detector, K		523
Time of analysis, min		15

3.5.5 Inorganic Nitrogen Speciation in Liquid Samples

Nitrogen oxidation products in the liquid samples were analyzed by photometry using a Merck Spectroquant Nova 60. The Spectroquant Nova 60 was used to identify three ions that could be present as a result of the reaction: nitrogen, ammonium, nitrate and nitrite. The photometer uses test kits that react with the ions present in the sample to form colourful chemical complexes which can be used to perform their quantification.

3.5.5.1 Ammonium (NH_4^+) Cell Test

The ammonium nitrogen ($NH_4 - N$) occurs partially in the form of ammonium salts and partially as a ammonia. A equilibrium dependency on pH occurs between the forms. In strongly alkaline solution, ammonium nitrogen is present almost entirely as ammonia, which reacts with hypochlorite ions to form monochloramine. This reacts with a substituted phenol to form a blue indophenol derivative which is determined photometrically. The method is analogous to EPA 350.1, US Standard methods 4500-NH_3 D and ISO 7150/1 [254].

3.5.5.2 Nitrate (NO_3^-) Cell Test

In sulphuric and phosphoric acid solution, nitrate ions react with 2,6-dimethylphenol (DMP) to form 4-nitro-2,6-dimethylphenol which is determined photometrically. The method is analogous to ISO 7890/1 [254].

3.5.5.3 Nitrite (NO_2^-) Cell Test

In acidic solution nitrite ions react with sulphuric acid and an aromatic amine to form a diazonium salt, which in turn reacts with N-(1-naphthyl)ethylenediamine dihydrochloride to form a red-violet azo dye which is determined photometrically. The method is analogous to EPA 354.1, US Standard Methods 4500-NO_2^-B and EN 26 777 [254].

3.5.6 Dynamic Vapour Sorption (DVS) Method

The DVS method was used to investigate the interactions between water and catalytic particles and to measure the catalyst surface areas. The analysis was performed on a DVS Advantage automated gravimetric vapour sorption analyzer (Surface Measurement Systems Ltd.). The DVS Advantage measures the uptake and loss of vapour gravimetrically using a Cahn D200 recording ultra-microbalance with a mass resolution of ± 0.1 μg. The relative concentration around the sample was controlled by mixing saturated and dry carrier gas (high purity nitrogen) streams using mass flow controllers. The measurement temperature was maintained constant at 298.0 K, ± 0.1 K, by enclosing the entire system in a temperature-controlled incubator.

3.5.6.1 Water Sorption-Desorption Method

Interactions between catalyst and water vapour provides valuable information in the change of catalyst properties. During the analysis, the amount of water adsorbed and desorbed by the catalyst was measured isothermally. The water intake of the catalyst was used to produce adsorption and desorption curves. The shape of the sorption curves depends on the solid-vapour interactions and leads to conclusions about the interaction mechanism [255, 256]. Ideally, adsorption and desorption are reversible processes that occur when their isotherms overlap. If they do not overlap, the difference between both processes is known as hysteresis or hysteresis gap [257]. Hysteresis is a complex process which can be caused by the combination of interaction types between adsorbate and solid.

Fresh and spent catalyst samples were analyzed by DVS water sorption in order to identify any change on the surface of the catalyts by comparing their sorption isotherms. The method of analysis is shown in Table 3.7.

Table 3.7: DVS Water Sorption Method

Parameter	Value
Solvent	Water
Temperature, K	298
Range of partial pressure studied, %	0-90
Increments on partial pressure, %	10
Equilibrium constrain, %/min	0.02
Drying of sample, h	4
Number of cycles	2

3.5.6.2 Surface Area Measurements

The surface area measurements are based on the theory proposed by Brunauer, Emmet and Teller (BET) [258]. The BET method is used to measure the area available for adsorption of a gas molecule. The novelty of the DVS application is the use of a gravimetric method and an organic solvent (n-octane) instead of the traditional methods that are based on volumetric

analysis and use a gas as adsorbate. The DVS process offers two important advantages; it takes place at atmospheric pressure and room temperature and the amount of sample necessary for the analysis is smaller [256]. The BET method assumes no interaction between adsorbate-adsorbate molecules and it assumes a simple adsorption mechanism where the surface of the solid is occupied homogeneously by the adsorbate forming a monolayer around it [259]. The results are used to fit the BET equation and calculate the surface area of the solid. The method developed for surface measurement by DVS is shown in Table 3.8.

Table 3.8: DVS Organic Sorption Solvent Method

Parameter	Value
Solvent	n-octane
Temperature, K	298
Range of partial pressure studied, %	0-51
Increments on partial pressure, %	3
Equilibrium constrain, %/min	0.002
Drying of sample, h	4
Number of cycles	3

3.5.7 Inductively Coupled Plasma - Optical Emission Spectrometer (ICP-OES)

The ICP-OES was used to identify traces of metals in the outlet stream samples that may have leached from the catalyst surface. The instrument used was a Fisons/ARL 3410+, which operates in sequential mode with analytical wavelength range between 180 and 800 nm. The wavelength of analysis of each metal and their lower detection limits of the instrument are shown in Table 3.9.

3.5.8 X-ray Diffraction (XRD)

X-ray diffraction was used to identify the crystalline structure (if there is any) and chemical composition of the catalysts. Analyses were performed on fresh and spent (after reaction) catalysts

Table 3.9: Metals Wavelength and Lower Detection Limits

Metal	Detection Wavelength, nm	Lower Detection Limit, ppm
Copper	324.754	0.005
Manganese	257.610	0.005
Platinum	265.945	0.10

in order to account for any changes on the catalyst surface due to the chemical reaction. The phase analysis was performed in an Enraf Nonius PSD120 diffractometer with a monochromatic CuK source operated at 40 kV and 30 mA.

3.5.9 pH Measurement

The pH of the organic compound solutions and liquid effluent were measured using a Seven Multi Mettler Toledo pH meter. The change in pH was used to investigate the possible influence of ions, such as CO_3^{2-}, HCO_3^-, NO_3^- and NH_4^+ as being responsible for changes in the solution pH.

3.6 Catalysts

Supercritical water oxidation has become a promising alternative for the complete oxidation of organic matter in water. The process has proven to be effective for a wide range of organic and inorganic compounds and industrial wastes, however there is still some concern about production of intermediates. Their stability causes operational problems due to the severe operating conditions required, which limits the commercial uptake of the process. Among these stable intermediate compounds are carboxylic acids or ammonia. Though their production depends on the composition of the feed stream and the severity of the process, their stability is higher than the precursor compounds. Stability of carboxylic acids and ammonia have opened the opportunity for a more efficient treatment via catalytic oxidation [216, 217]. Catalytic supercritical water oxidation pursues not only a more efficient oxidation, but also a less energy consuming process and a reduction in the stress and corrosion in the equipment [96].

3.6.1 Selection of the Catalysts

In Chapter 2 a thorough review of the catalytic oxidation research was presented. Part of the survey dealt with suitable catalysts for CSCWO process. Research has been mainly focused on transition metals oxides, such as manganese and copper [177, 193, 200, 204, 206, 216]. In the case of nitrogen-containing organic compounds pioneering work over Pt, MnO_2 and MnO_2/CeO_2 [214, 215] and transition metal salts of iron, copper and manganese and V_2O_5 have been reported [197] with promising results.

Previous work by our research group has focused on SCWO of nitrogen-containing organic compounds. They demonstrated the presence of ammonium ions and some other nitrogen-oxidation products, such as nitrate and nitrite ions [167, 260]. Benjamin and Savage [175] have also confirmed the production of ammonia as a product of the non-catalytic oxidation of methylamine. Aki and Abraham [215] found differences in the product distribution of inorganic nitrogen species with different catalyst ($\alpha - Al_2O_3$, $MnO_2/\gamma - Al_2O_3$, $Pt/\gamma - Al_2O_3$ and $MnO_2 - CeO_2/Al_2O_3$). The mechanism of organic-nitrogen oxidation to molecular nitrogen in supercritical water is unknown, albeit it is suggested that ammonia is formed as an intermediate during the transformation. Ammonia is a very stable compound and it requires a high operating temperature for its oxidation under supercritical water [143]. A better understanding of the ammonia oxidation could overcome the presence of such intermediates.

An insight might lie in the industrial application of ammonia oxidation. Ammonia oxidation is a well-known process for the production of nitric acid that is carried out over a platinum catalyst. The overall reaction is given by:

$$NH_3 + 2O_2 \longrightarrow HNO_3 + H_2O \tag{3.19}$$

Although it may comprise several other reactions the process could be simplified into three reactions:

$$4NH_3 + 5O_2 \longrightarrow 4NO + 6H_2O \tag{3.20}$$

$$2NO \longrightarrow N_2O_4 \tag{3.21}$$

$$2N_2O_4 + 2H_2O + O_2 \longrightarrow 4HNO_3 \tag{3.22}$$

Equation 3.20 is the desired reaction of the process; however, an undesirable side reaction is also favoured:

$$4NH_3 + 6NO \longrightarrow 5N_2 + 6H_2O \tag{3.23}$$

Whilst both reactions happen in the process, Equation 3.23 is strongly favoured by the system pressure [261]. Thus the selection of an appropriate catalyst for CSCWO of nitrogen-containing organic compounds must consist of two important features: it should be active for the complete oxidation of both the organic carbon and the nitrogen attached to the organic molecule. At industrial scale, ammonia oxidation is carried out over Pt and for this reason, Pt accomplishes both features [214, 261]. However, exploring other active materials besides platinum would also become of interest. Gang [262] have studied the catalytic oxidation of ammonia to nitrogen and have proposed suitable catalytic materials for this specific purpose. According to his research, a copper based catalyst contributed to the complete oxidation of ammonia. Copper oxide was found to be suitable for CSCWO and it was also selected for this purpose. Mixed manganese and copper oxides have been demonstrated to be effective for the catalytic oxidation of phenol [193]. Mixing the catalytic properties of both transition metal oxides was envisage to contribute to a better performance of the reaction. Table 3.10 shows the catalysts selected for the SCWO of DBU and Quinoline.

Table 3.10: Catalysts for CSCWO of DBU and Quinoline

Active Metal	Support	Loading	Shape	Size, mm	Supplier
Pt	Al_2O_3	0.5%	Cylindrical	3.0	Johnson Matthey
CuO	Al_2O_3	13%	Sphere	0.84−1.19	Sigma-Aldrich
MnO_2/CuO	Unsupported	Pure	Irregular	0.84−1.41	Carus Chemical Co.

3.6.2 Catalyst Preparation

Because the particle sizes of the commercial catalyst are not suitable for the fixed-bed microreactor, the catalysts were crushed and sieved to smaller particle sizes. The reduction in the particle sizes aimed to increase the flow distribution allowing the assumption of the plug flow idealization, and to facilitate the transport of the reactants and products by avoiding the presence of concentration gradients between the fluid and the fixed phase and from the catalyst surface to the active site. In this way, operation under a pure chemical kinetic control was sought.

3.6.3 Packing of the Catalysts

The packing of the catalyst was done with a slight variation of the method proposed by Al-Dahhan et al., [263] and was extended from the packing of a trickle-bed catalytic reactor. Their method reduces the variation of the experimental data as consequence of the packing of the fixed bed reactor. The packing material used during the research was silica (SiO_2, Acros Organics 99%) with a particle size between 212-250 μm. Because catalytic particles are smaller than the silica packing material, the required amount of catalyst and packing material was mixed before it was loaded into the reactor. The mixing prevents the agglomeration of the catalytic particles in a section of the tubing and assures an homogeneous distribution. The use of an inert material in the reactor mainly prevented pressure drops no greater than 0.35 MPa. Moreover, the dilution of the catalyst assures an even distribution of the temperature along the reactor and avoids the presence of hot-spots in the catalytic bed, which becomes important in the case of highly exothermic reactions such as oxidation [250].

Chapter 4

CSCWO of DBU

4.1 Preliminary Considerations

Before studying the catalytic supercritical water oxidation (CSCWO) a series of experiments were performed to verify the decomposition of the hydrogen peroxide in the preheating section and the effect of the packing material (SiO_2) on the reaction. Furthermore, a series of experimental considerations are given in order to establish a kinetic controlled catalytic reaction. Once, the hydrogen peroxide was thermally decomposed produced the oxygen required for the reaction.

4.1.1 Experimental verification of the H_2O_2 decomposition

In the process, it was assumed that the thermal decomposition of hydrogen peroxide takes place in the preheating section according to:

$$2H_2O_2 \longrightarrow O_2 + 2H_2O \tag{4.1}$$

In order to verify the complete decomposition of hydrogen peroxide in the preheating section, 4 experiments in absence of any catalyst were carried out at the operating conditions shown in Table 4.1. In the experiments only a solution of H_2O_2 was fed to the reactor (however the assumption of the presence of the organic compound was made to calculate the appropriate flow rates and concentration ranges) and the decomposition of hydrogen peroxide was measured by titration of the outlet stream with $KMnO_4$ (as described in Chapter 3). The experimental conditions were chosen to cover all the the maximum and minimum values of hydrogen peroxide solution concentrations, operating conditions and reacting mixture flow rates used in the research.

Once the sample was taken it was kept on ice to prevent any further decomposition. Analysis of the samples showed that none of the samples contained any residue of hydrogen peroxide and it confirmed that it was completely decomposed.

Table 4.1: Operating Conditions for Verification of H_2O_2 Thermal Decomposition

Parameter	Experiment 1	Experiment 2	Experiment 3	Experiment 4
Pressure, MPa	23.0	23.0	23.0	23.0
Temperature, K	653.15	653.15	773.15	773.15
Space Velocity, s	0.333	25.0	0.333	25.0
SR	3.0	0.5	3.0	0.5
H_2O_2 Solution, %W	0.135	3.2	0.35	8.3
Flow rate, mL/min	18.018	2.401	18.008	2.366

4.1.2 The Effect of Packing on the Removal of TOC

The evaluation of the catalytic properties of the silica and alumina were studied and compared with the non-catalytic SCWO reaction. Three experiments were conducted at 673 K and 23.0 MPa. The reactor of a volume of 1.781 cm^3 was packed with alumina and silica particles of 300-355 μm. DBU was used as the organic compound to be oxidised with an initial concentration of 0.3 mmol/L while the oxygen concentration was 7.8 mmol/L at the reaction conditions. The residence time was varied from 0.5 to 12 s. The removal of DBU was followed in terms of TOC and the results of the experiments are depicted in Figure 4.1. The experiments showed that the catalytic activity of both packing materials were not better than the non-catalytic reaction[1]. The addition of both solids affected the hydrodynamics of the reactor and consequently, the reaction conversion. The addition of the packing material was sought to increase appreciably the reaction rate compared with the non-catalytic route, and thus it was confirmed the poor catalytic properties of both packing materials. In addition, the oxidation over alumina was higher than on SiO_2 which showed better catalytic properties of the alumina. Silica was preferred because minimized the pressure drop in the reactor. This results agreed with Aki and Abraham [215] where they have also assessed and confirmed the poor catalytic activity of Al_2O_3. Nevertheless, its activity could also depend on the compound being oxidised [264].

[1] In the instertices the reacting mixture moves faster than in the hollow tube.

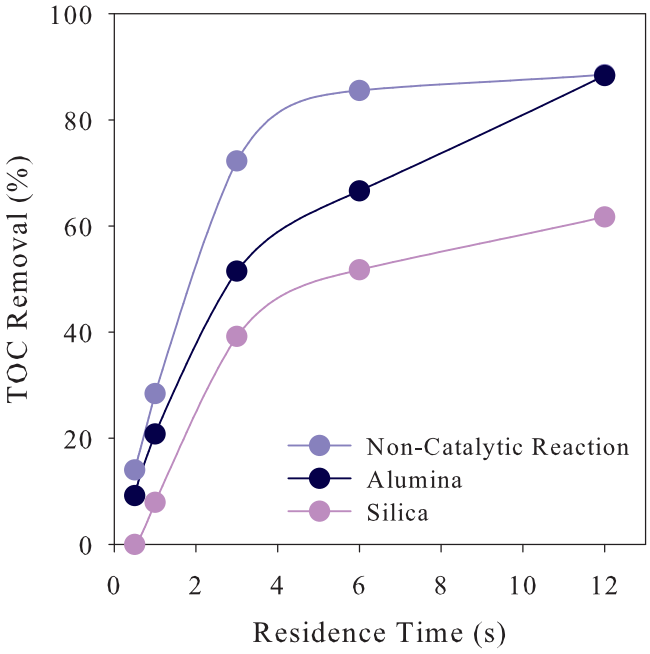

Figure 4.1: Effect of Packing Material

4.1.3 Evaluation of the Reactor Performance for the Acquisition of Reliable Kinetic Data

Packed-bed tubular reactors are perhaps the most common type of reactor for gas-solid reactions and consequently they are very common for kinetic studies. However, before any kinetic study is carried out in a tubular reactor some aspects regarding its operation should be investigated to obtain reliable experimental data [250].

4.1.3.1 Assessment of the Isobaric and Isothermal Operation of the Reactor

The first aspect to be addressed is the isobaric operation of the tubular reactor. The flowing of the reacting mixture through the catalytic bed generates a pressure gradient. In order to assure that isobaric operation is reached the particle size should be carefully selected. The smaller the particle size, the higher the pressure drop generated. This fact becomes important when fluids are compressible as in the case of supercritical fluids. Fluctuations of pressure lead undoubtedly to changes in the concentration of the reacting mixture.

The next step is to evaluate the isothermal operation of the reactor. Catalytic oxidation

reactions are highly exothermic and the amount of heat generated could lead to the presence of hot spots along the fixed-bed. The hot spots are a consequence of an unpredictable temperature increment in the axial position and therefore leads to operation of the reactor in a runaway condition [265]. Chemical reactions depend on temperature and the presence of fluctuations in this parameter could affect the reactor performance and mask the kinetics of the reaction. In an integral operation, it is very common to find temperature gradients, however there are some experimental practices that can be used to avoid them. There are three methods to prevent the presence of hot spots in the bed; the first is to consider a reactor modification by reducing the reactor diameter, which is sometimes difficult to accomplish if the reactor has already been designed. The next practice is the dilution of the feed concentration, which is usually done by injecting an inert material with the reagents. By diluting the concentration of reagents, the reaction generates less heat which is removed from the system by the inerts. And finally, the catalyst can be diluted with inert solid particles (generally SiO_2), which reduces the likelihood of local hot spot formation by improving the temperature distribution in the catalytic bed.

4.1.3.2 Evaluation of External and Internal Concentration Gradients

Once the effects of pressure and temperature that influence the reactor performance have been assessed and discarded, it is compulsory to evaluate whether the catalytic reaction undergoes in pure chemical kinetic control. Heterogeneous catalytic reactions comprise several steps other than the pure chemical reaction, which for a gas-solid reaction can be summarised as [266]:

1. Transport of the reactants from the bulk to the catalyst surface
2. Diffusion of reactants from the surface to the catalyst pores
3. Adsorption of reagents
4. Chemical reaction
5. Desorption of products
6. Diffusion of reagents and products from the pore to the catalytic surface
7. Transport of reagents and products from the surface of the catalyst to the bulk

Stages 1, 2, 6 and 7 are called interphase or external transport and 3 and 5 are denominated intraphase or internal transport (refer to Figure 4.2). External and internal transport processes are present in catalytic reactions and compete for the rate limiting step of the catalytic process. If any of the steps other than the reaction dominates the process, then the kinetic parameters calculated corresponds to apparent values. In a pure chemical kinetic control reaction steps 1, 2, 3, 5, 6 and 7 in Figure 4.2 occur rapidly compared to the chemical reaction. At this point only the reaction controls the catalytic process and the kinetic data obtained truly represent the reaction. At laboratory scale there are two common procedures which rely on evaluation of the conversion dependency on the superficial velocity and particle size [230, 250, 267].

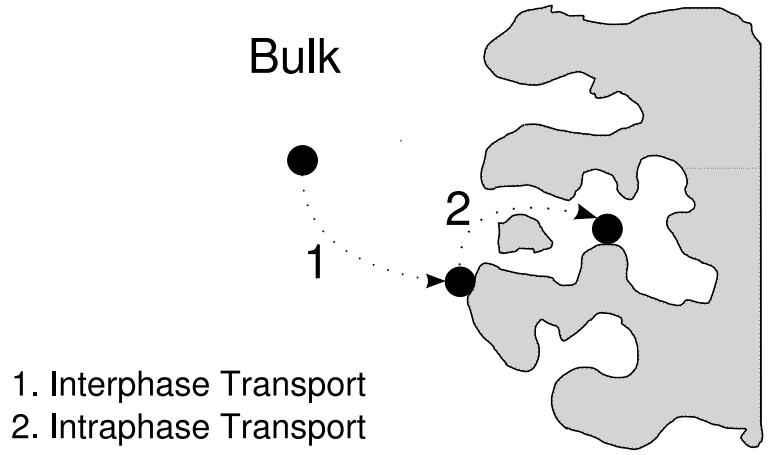

Figure 4.2: Interphase and Intraphase Transport in Chemical Reactions

4.1.3.2.1 External or Interphase Concentration Gradients. Assuming an isothermic operation of the reactor for a gas-solid reaction, it is common to find concentration gradients between the bulk and catalyst surface. If the reaction is limited by the transport of reagents from the gas to the solid phase then interphase concentration gradients are the limiting step. In order to avoid the presence of these interphase concentration gradients the conversion ought to be independent of the superficial velocity of the reacting mixture. During the test (refer to Figure 4.3), a series of experimental runs are planned where the weight of catalyst (W) and the flow rate of the reacting mixture (F_{i_0}) are varied proportionally to keep the same space velocity ($WHSV$) every time ($WHSV$ relates the flow rate to weight of the catalyst according

to $WHSV = \rho\ F_{i_0}/W$). In a reaction that is not limited by external concentration gradients the conversion of reactants does not change with the ratio of flow rate to the amount of catalyst. In the example the $WHSV$ was varied up to 5 times the initial conditions, however the number of experiments can be reduced if there is no variation in the conversion with the flow rate. Another way to evaluate the presence of interphase concentration gradients is by determining the activation energy. Reactions limited by external transport show activation energies $\leq$ 20 kJ/mol [268].

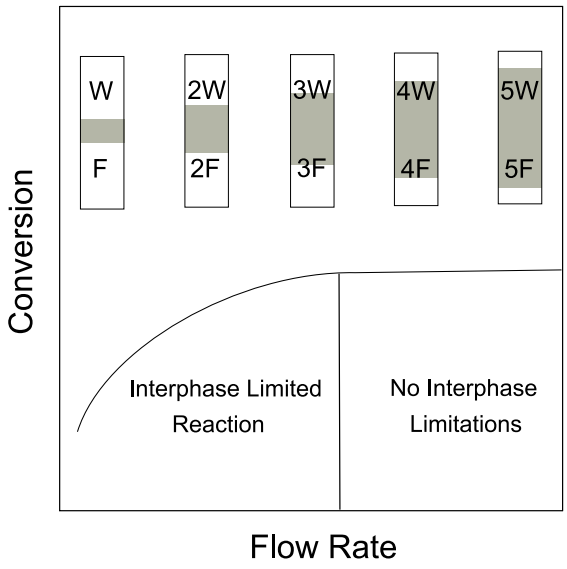

Figure 4.3: Evaluation of Interphase Concentration Gradients

4.1.3.2.2 Internal or Intraphase Concentration Gradients The most effective procedure to eliminate the internal concentration gradients is by reducing the size of the catalytic particle. The smallest particle size allowable is determined by the pressure drop generated in the catalytic reactor. The diagnostic is performed by quantifying the conversion of the reactants at different particle sizes. If the conversion varies by decreasing the particle size the reaction is limited by intraparticle concentration gradients. On the other hand, if conversion remains constant the system is under chemical kinetic control (Figure 4.4).

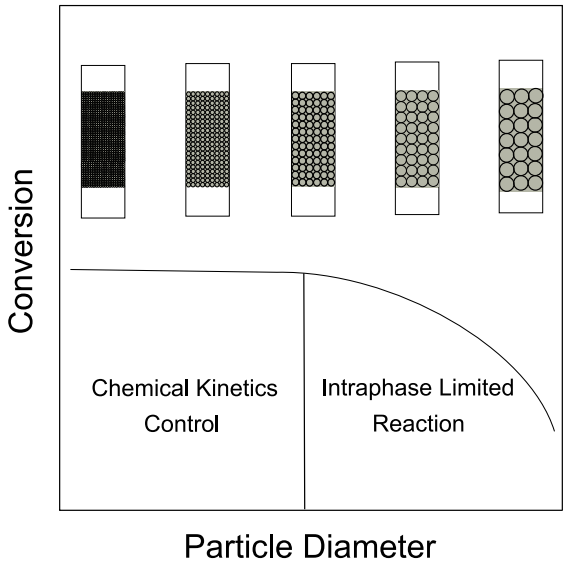

Figure 4.4: Evaluation of Intraphase Concentration Gradients

4.2 CSCWO of DBU over Pt/Al_2O_3 Catalyst

In this study a series of experiments were performed to evaluate the catalytic oxidation of 1,8-diazabiciclo(5.4.0)undec-7-ene (DBU) (Figure 4.5) using a platinum catalyst. DBU has been used for the synthesis of new drugs in the pharmaceutical industry. Furthermore, this amidine base is commonly used for dehydrohalogenation reactions [269] and also as catalyst for the polyurethane production [270]. The interest for the complete destruction of DBU arises from the fact that it is corrosive and a very toxic compound especially to aquatic organisms.

The stoichiometric reaction for the complete oxidation of DBU is given by

$$C_9H_{16}N_2 + 13O_2 \longrightarrow 9CO_2 + 8H_2O + N_2 \tag{4.2}$$

From this equation the stoichiometric ratio (SR) of DBU to oxygen is obtained to calculate the required oxygen concentration as a function of the initial organic concentration as follows:

$$\text{SR} = \frac{\nu_{DBU} C_{O_2 0}}{\nu_{O_2} C_{DBU_0}} \tag{4.3}$$

Where ν_i and C_{i_0} are referred to the stoichiometric coefficients and the initial concentration of the reagents. A SR of one is the minimum amount of oxygen required to completely oxidise

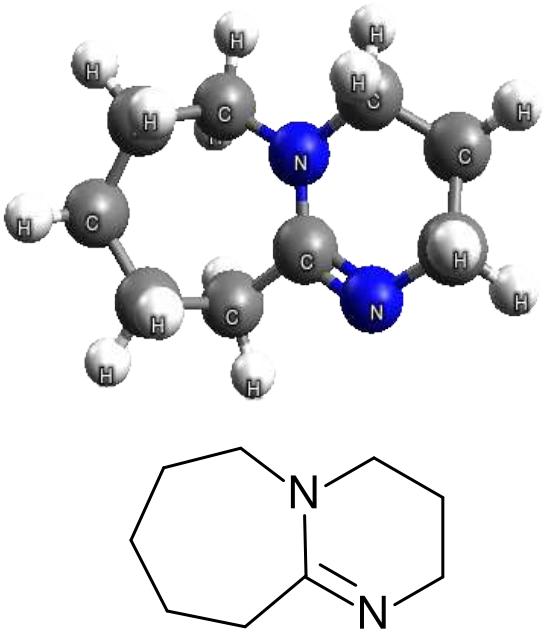

Figure 4.5: Chemical Structure of 1,8-diazabiciclo(5.4.0)undec-7-ene

a molecule of DBU. The oxidation of the organic compound could be followed in terms of the remaining total organic carbon or DBU content of the outlet stream which are defined as:

$$Removal_{TOC} = \frac{C_{TOC_0} - C_{TOC}}{C_{TOC_0}}(100) \tag{4.4}$$

$$Removal_{DBU} = \frac{C_{DBU_0} - C_{DBU}}{C_{DBU_0}}(100) \tag{4.5}$$

4.2.1 Evaluation of External and Internal Concentration Gradients

The evaluation of the concentration gradients was done by following the experimental procedures described previously (see Sections 4.1.3.2.1 and 4.1.3.2.2). The dilution of the catalytic bed with inert material and a very diluted feed solution avoids the presence of temperature gradients within the reactor. The inert particles also prevented high pressure gradients. During the experiments a maximum pressure drop of 0.3 MPa and pressure variation of ±0.35 MPa was recorded and can therefore be assumed as being in isobaric operation. Isothermal operation was considered because the temperature only varied within ±2 K.

4.2.1.1 Interphase Concentration Gradients

The evaluation of the presence of external concentration gradients was carried out at 673 K and 23.0 MPa. The removal of TOC was followed to evaluate the intraphase concentrations gradients. The initial concentration of the organic compound was 2.7 mmol of TOC/L, which corresponds to a 0.3 mmol of DBU/L, and oxygen was fed to give a SR of 0.5 at the reaction conditions. In the reactor the catalyst (355-425 μm) was diluted and packed with SiO_2 that had a particle size of 250-300 μm. The catalyst masses used were 0.04, 0.08, 0.12, 0.16 and 0.20 g and the space velocity ($WHSV$) varied from 0.5 to 3.0 s^{-1} (only results of 0.5, 2.5 and 3.0 s^{-1} at different catalyst weights were plotted). The results showed that TOC removal was constant for the catalyst weights equal to/or higher than 0.08 g (Figure 4.6). From this, it can be concluded that external gradients were not present if amounts of catalyst higher than 0.04 g were used.

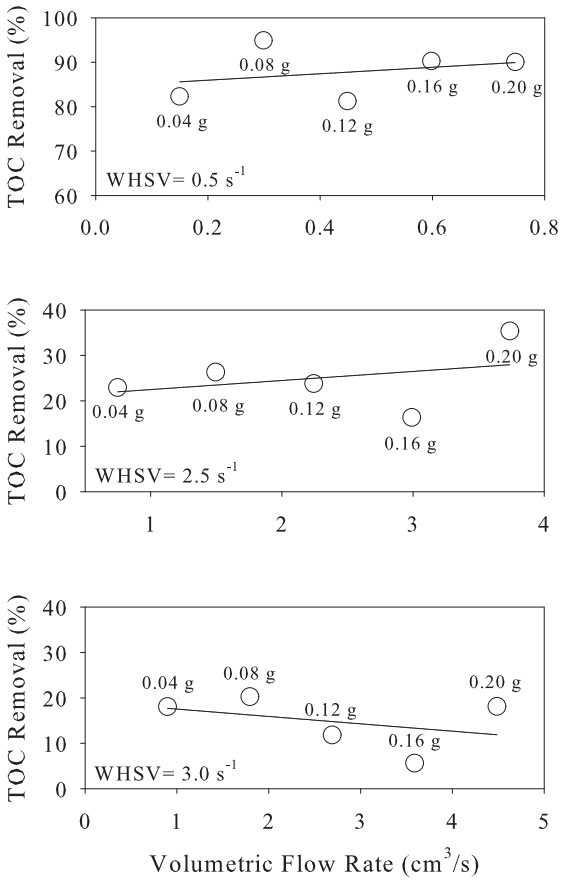

Figure 4.6: External Concentration Gradients of DBU on Pt

4.2.1.2 Intraphase Concentration Gradients

Absence of intraparticle concentration gradients were proved based on the assumption that in isothermal operation the conversion is independent of the particle sizes with which the reaction is being performed. In these tests, the operating conditions were 23.0 MPa and 673 K, whereas the reagent concentrations were of 0.3 mmol DBU/L and oxygen was supplied at a SR equal to 0.5. The amount of catalyst was 0.25 g and the particles sizes investigated appear in Table 4.2. Space velocities were varied from 0.3 to 1.2 s^{-1}, the selection of different $WHSV$ values was made to find out if the variation of conversion depended on the space velocity selected and thus avoid those operating conditions. The results of the conversion against particle sizes at a fixed space velocity are plotted in Figure 4.7. The conversion increased to a maximum when the particle size was reduced to 90-106 μm and decreased for the smallest particle size, which it is an unexpected behaviour of the reaction. Therefore, the reaction rate might be influenced by the intraparticle gradients. According to Aki and Abraham [214] effectiveness factors (calculated at relative the same operating conditions) greater than 0.96 were obtained using particles sizes of 90 μm. Consequently, smaller particle sizes were assumed to work with a minimum influence of concentration gradients. At this point it is assumed that the reaction was not affected by internal concentration gradients. This point will be taken up again to assess their presence in the reaction by a different approach (see Section 4.2.3.2).

Table 4.2: Particle sizes for Evaluation of Internal Concentration Gradients

Experiment	Particle Size Range, μm	Average Particle Size, μm
1	350−425	387.5
2	250−300	275.0
3	90−106	98.0
4	45−63	54.0

4.2.2 Reproducibility Tests and the Effect of Key Operating Conditions

Unreacted DBU was not identified in the effluent of the reactor, which indicates that it was rapidly converted into other compounds; hence TOC content in the effluent was used to follow

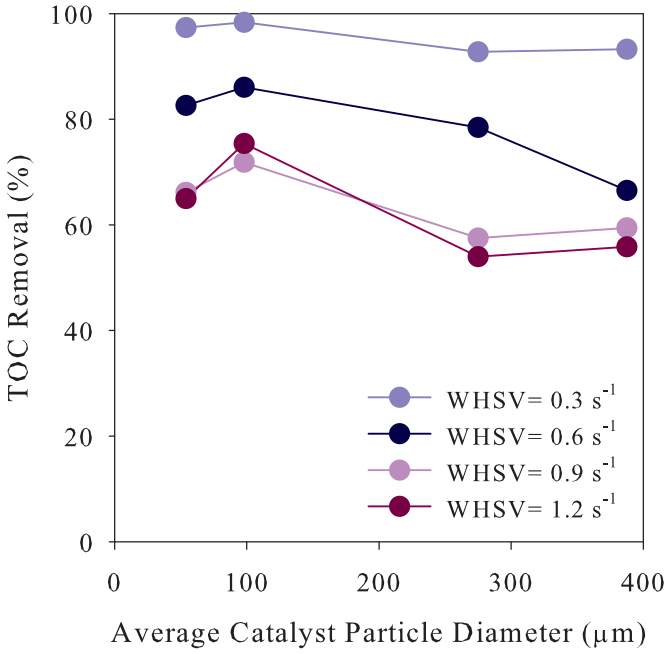

Figure 4.7: Internal Concentration Gradients of DBU on *Pt*

the oxidation reaction. Table 4.3 summarizes the experimental conditions explored in CSCWO of DBU over *Pt* and provides information about the catalytic bed.

4.2.2.1 Reproducibility Tests

The aim of the reproducibility test was to evaluate the experimental error of the CSCWO of DBU over *Pt*. A series of 5 tests were performed at 673 K and 23.0 MPa with an initial DBU concentration of 0.3 mmol/L and a SR equal to 1. The average of the TOC removal and its standard deviation are shown in Table 4.4. Figure 4.8 depicts the average TOC removal plotted with error bars of ± 1 of the standard deviation of the experimental data at each point. The maximum deviation occurred at lower space velocities. As $WHSV$ is inversely proportional to the flow rate of the reacting mixture (F_{i_0}); the error increased towards high flow rates. The control of the flow becomes less accurate and a maximum deviation of 8.6% was presented. These tests provide evidence of the uncertainty over the experimental data range.

Table 4.3: Experimental Conditions of CSCWO of DBU over *Pt*

Parameter	Interval Studied
Temperature Range, K	653-773
Pressure Range, MPa	23.0-30.0
Initial DBU Concentration Range, mmol/L	0.1-0.9
Initial Concentration of Oxygen Range (SR)	0.5-12
Catalyst weight, g	0.1±0.0001
Catalyst particle size, μm	45-63
SiO_2 particle size, μm	212-250
Bed length, cm	9.2±0.1
Dilution factor catalyst to SiO_2, v:v	1:7

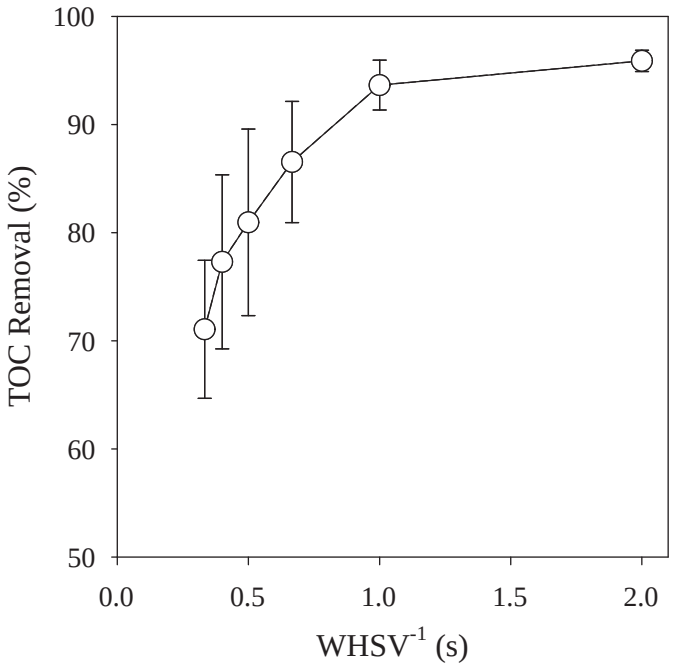

Figure 4.8: Reproducibility Tests of CSCWO of DBU over *Pt*

Table 4.4: Reproducibility Tests of CSCWO of DBU over Pt

$WHSV$, s^{-1}	Average TOC Removal, %	Std. Dev. of TOC Removal, %
0.5	95.88	0.98
1.0	93.64	2.30
1.5	86.53	5.60
2.0	80.95	8.63
2.5	77.30	8.06
3.0	71.06	6.38

4.2.2.2 Effect of Temperature on the CSCWO of DBU over Pt

DBU is partially hydrolysed (approximately 52%) at temperatures of 673 K and completely hydrolysed at 873 K, which reflects the instability of the organic compound at the operating conditions. Nevertheless, TOC has been found to remain almost constant without a significant change at temperatures below 873 K [167]. Solely, DBU hydrolysis produces a considerable amount of by-products that are not affected by the thermal decomposition in supercritical water. For this study, CSCWO of DBU was conducted at 23.0 MPa using an initial concentration of 0.3 mmol DBU/L which is equivalent to 2.7 mmol of TOC/L and a stoichiometric ratio of oxygen to DBU of 1. Figure 4.9 shows the effect of temperature on the removal of the total organic carbon content. Although, the reaction was influenced by temperature, the removal of TOC was markedly stronger when the temperature increased from 653 to 673 K, at higher temperatures the effect became smaller and finally at 773 K the change of the TOC removal at different space velocities became almost unnoticed. Elimination of TOC around 92.0% was reached at moderately low space velocities (0.5 s^{-1}) at a temperature of 673 K, and almost complete TOC removal (99.0 %) was reached at 773 K. The effect of temperature was minimized by the use of the catalyst and as a result DBU and TOC were efficiently removed from the stream at milder temperature, in comparison with the results provided by Ashraf [167].

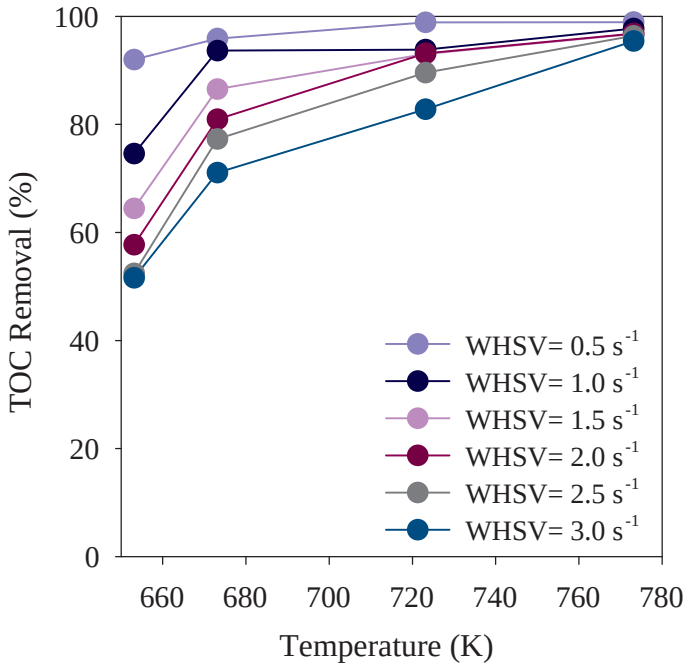

Figure 4.9: Effect of Temperature in the CSCWO of DBU over Pt

4.2.2.3 Effect of Pressure in the CSCWO of DBU over Pt

TOC removal was investigated over the pressure range of 23.0 to 30.0 MPa, at a fixed temperature of 673 K. The concentration of the reactants at reaction conditions were 0.3 mmol of DBU/L and oxygen was supplied to meet a SR of 1. The highest values of TOC removal during the experiment were reached at 23.0 MPa (see Figure 4.10), these results are contradictory to the effect observed in non-catalytic reactions. Previous studies on non-catalytic oxidation reactions of organic compounds [176, 197] have proved that an enhancement of the density of the reacting mixture promoted the reaction and supported the evidence that pressure affects positively the SCWO reaction.

Yu and Savage [204, 205, 206] have explored the effect of pressure (or water concentration) for the CSCWO of phenol. They have proved that this effect was almost unnoticeable for CuO and MnO_2, although there was slight improvement of conversion of phenol when the reaction took place over TiO_2. On the other hand, Segond et al. [146] have proved that there is a slight retardation of catalytic oxidation of ammonia as pressure was increased, which agrees with the results observed in Figure 4.10. This complex behaviour could be explained in terms of the

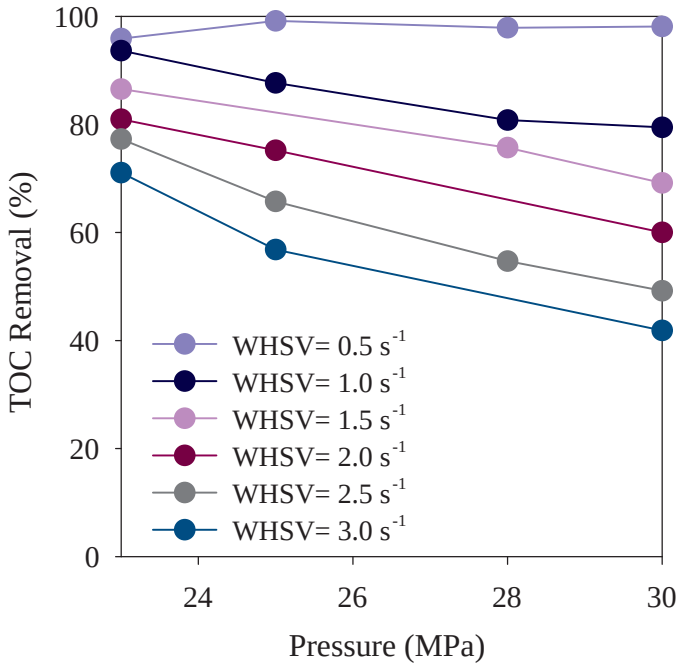

Figure 4.10: Effect of Pressure in the CSCWO of DBU over *Pt*

transport properties of the supercritical fluid. When pressure increased at constant temperature, the diffusivity drops and viscosity rises [271]. This effect slows down the transport of the substances in and out of the catalyst and thus reduces the reaction rate. Moreover, supercritical fluids exhibit exceptionally small kinematic viscosities; as a consequence their small viscosities and high densities exceptionally stress the effect of natural convection [272]. Another plausible explanation could be given in terms of the intermediates formed during the oxidation and that their side oxidation reactions were hindered by the increment of the system pressure. The results suggests that the pressure dependency on the catalytic reaction is evidently more complex than the non-catalytic reaction which only depends on changes of system density to proceed faster. This finding would open the possibility of studying the effect of pressure over a wider temperature interval to understand better its effect in catalytic reactions.

4.2.2.4 Effect of Initial DBU Concentration on the CSCWO over *Pt*

Experiments were performed at fixed operating conditions of 23.0 MPa and 673 K while oxygen was present at a SR of 1. The effect of initial concentration of DBU on the TOC removal is

illustrated on Figure 4.11. Although DBU removal was complete during the reaction, the TOC analysis revealed that the reaction was slightly affected by the concentration of DBU in the feed stream at space velocities higher than 0.5 s^{-1}. The effect of the initial concentration of the organic compound in a fixed bed reactor has been previously studied by Krajnc and Levec [217]. They reported that the concentration of the acetic acid did not affect its removal, nevertheless the results presented here only agree for the case of DBU removal, which was completely destroyed in the reaction. It was clear that initial DBU concentration affected the elimination of TOC. The reaction proceeded faster at higher concentration, which allows the use of CSCWO to be extended over a wider concentration of the organic compound without affecting the performance of the reaction.

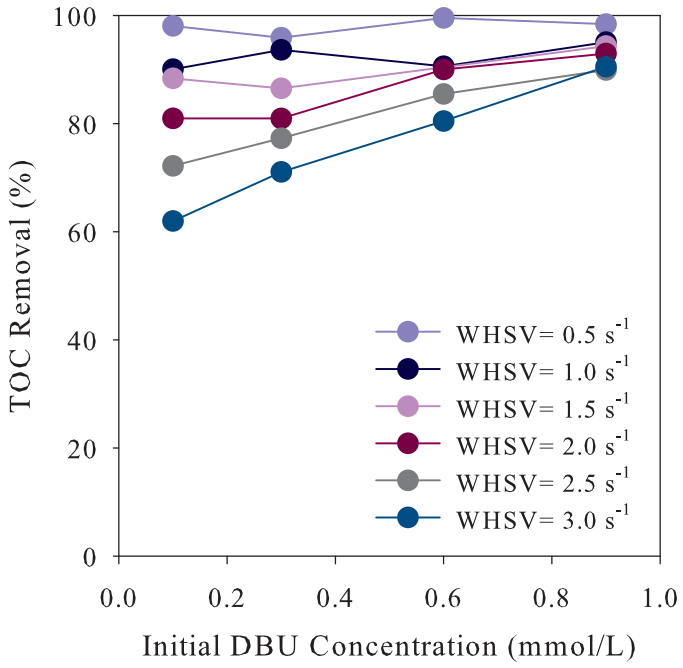

Figure 4.11: Effect of Initial DBU Concentration in the CSCWO over *Pt*

4.2.2.5 Effect of Initial Oxygen Concentration on the CSCWO of DBU over *Pt*

The effect of oxygen concentration on the TOC removal was investigated at 23.0 MPa, 673 K and an initial DBU concentration of 0.3 mmol/L. The initial concentration of oxygen promoted the disappearance of the TOC content. The effect is only appreciable at $WHSV$ higher than 0.5 s^{-1} because the reaction approaches completion at this point (see Figure 4.12). However the

effect of the oxygen on TOC removal becomes less obvious at a SR above 2. The findings of Yu and Savage [206] also proved that increasing the concentration of oxygen in the catalytic reaction promoted the oxidation of phenol. In their study oxygen concentrations above the stoichiometric value were used and phenol oxidation improved at higher oxygen concentrations. Nonetheless, the addition of high amounts of oxygen did not appreciably affect the removal of the organic compound. Oxygen evidently can be used to accelerate the reaction, however its improvement is limited to a certain range of concentrations.

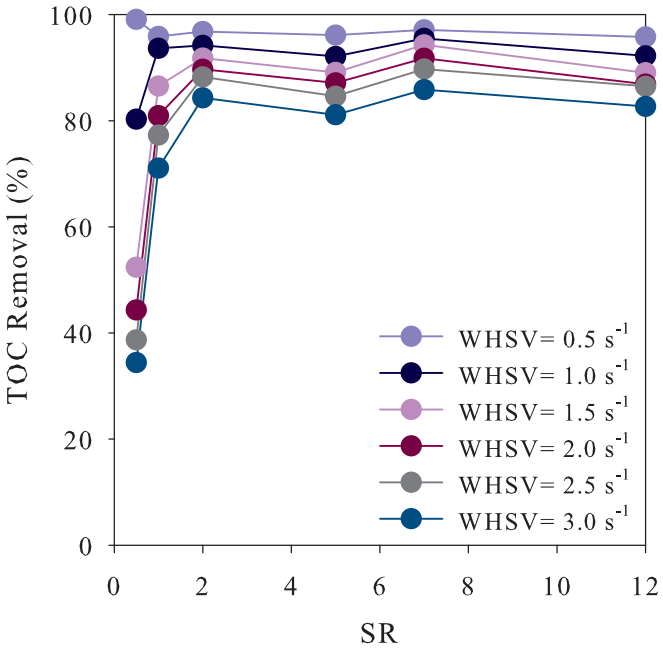

Figure 4.12: Effect of Initial Oxygen Concentration in the CSCWO of DBU over Pt

4.2.3 Kinetics of the Reaction

The kinetics of the reaction were obtained by the use of the integral method of analysis as proposed by Froment and Hosten [273]. During the kinetic analysis, the ideal tubular reactor continuity equation was used to fit the experimental data according to:

$$\frac{dX_i}{d(W/F_{i_0})} = -\mathscr{R}_i \tag{4.6}$$

X_i is the conversion of the i species in the reaction, W is the weight of the catalyst and F_{i_0} is the initial flow rate. $\mathscr{R}_i$ is the reaction rate of i that will be assumed to represent best the

catalytic reaction (the sign convention to identify the rate in terms of reactant or a product should be adopted). This ordinary differential equation is subjected to the following initial condition:

$$X_i(0) = X_{i_0} \qquad \text{when} \qquad W/F_{i_0} = 0 \tag{4.7}$$

Because DBU was not found during the reaction, the TOC was taken as the parameter to be followed during the reaction. Moreover, the power-law kinetic model was adopted to represent the reaction. Consequently the reactor continuity equation takes the following expression:

$$\frac{dX_{TOC}}{d(W/F_{TOC_0})} = kC_{TOC}^{a}C_{O_2}^{b} \tag{4.8}$$

Where the kinetic constant (k) and the reaction orders with respect to TOC and oxygen (a and b) will be fitted into the ordinary differential equation. For the fitting of the experimental data four numerical routines were implemented in *Python* [274]. The algorithms implemented were downhill simplex or Nelder-Mead, Powell, simulated annealing and Levenberg-Marquardt. The routines are part of *Python*'s scientific library *SciPy* [275] (a detailed discussion of the fitting of the experimental data is given in the Appendix B). During the fitting of the experimental data, Equation 4.8 is integrated numerically for each experimental data (a description of the solver for ordinary differential equation is given in Appendix C) [276]. Experimental data at 673 K and 23.0 MPa were fitted into a pseudo-homogeneous[2] tubular reactor. A plot that shows the difference between the experimental fraction converted and that predicted by the model is given in Figure 4.13. The best fitting values that were found with a confidence level of 95% are shown in the following equation:

$$-\mathscr{R}_{TOC} = 27.0064 \pm 5.6709\ C_{TOC}^{1.3150\pm0.1233}\ C_{O_2}^{0.0605\pm0.0806} \tag{4.9}$$

4.2.3.1 The Criterion of External Concentration Gradients

In addition, the interphase gradients were corroborated based on a comparison of the experimental values with a criterion proposed by Mears [277]:

[2]The term pseudo-homogeneous is commonly used to identify reactors in which the reaction takes place along the reactor volume (in our case the volume of the reactor was modified by the inclusion of the density of the catalyst), and not on the catalyst surface.

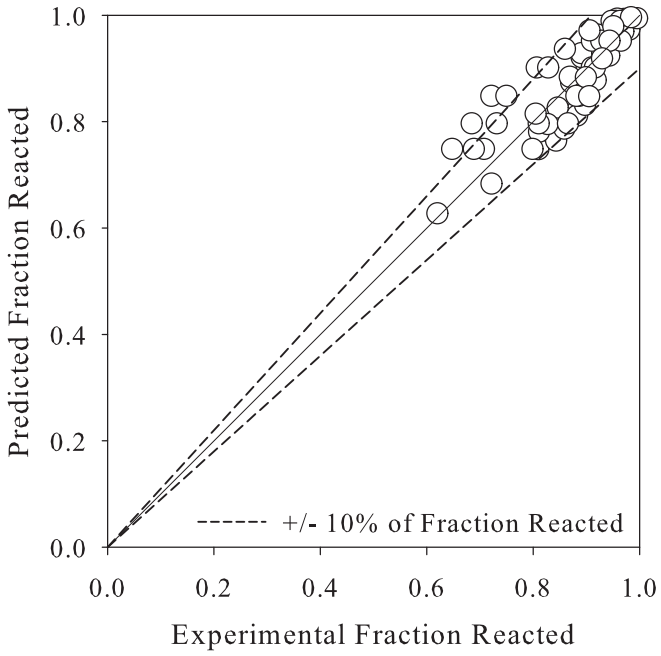

Figure 4.13: Comparison of Predicted and Experimental Fraction of TOC Reacted over Pt

$$\frac{-\mathscr{R}_{i_{Obs}} d_p}{2C_{i_B} k_c} < \frac{0.15}{n} \tag{4.10}$$

Where $\mathscr{R}_{i_{Obs}}$ is the observed reaction rate of i, d_p is the particle diameter, C_{i_B} is the concentration of i in the bulk, k_c is the mass transfer coefficient and n is the reaction order. If the condition in Equation 4.10 is satisfied then interphase gradients can be discarded. The mass transfer coefficient was determined from the Sherwood number (N_{Sh}) as shown in Equation 4.11. Molecular diffusivity ($\mathscr{D}_{i_m}$) of DBU in water was estimated to be 1.2745 x 10^{-3} cm^2/s using an expression suggested by Woerlee [136] which is applicable for supercritical fluids.

$$N_{Sh} = \frac{k_c d_p}{\mathscr{D}_{i_m}} \tag{4.11}$$

N_{Sh} was estimated using a correlation in terms of Schmidt and Reynolds numbers (N_{Sh} and N_{Re}) proposed by Wakao and Kaguei [278].

$$N_{Sh} = 2 + 1.1 N_{Sc}^{0.33} N_{Re}^{0.6} \tag{4.12}$$

The Reynolds and Schmidt numbers are defined by Equation 4.13 and 4.14 respectively. The

density (ρ) and viscosity (μ) used are those for water at the reaction conditions 0.1337 g/cm^3 and 2.745 x 10^{-4} g/cm s [3, 21], respectively.

$$N_{Re} = \frac{\rho u_S d_p}{\mu} \tag{4.13}$$

$$N_{Sc} = \frac{\mu}{\rho \mathscr{D}_{i_m}} \tag{4.14}$$

where u_S is the superficial velocity of the reacting mixture. The results of the criterion for the interphase gradient evaluation appear in Table 4.5. The reaction rate is given in terms of the TOC content. A reaction order observed previously for a similar oxidation reaction (n=2.68) [215] led to the smallest value (0.056) on the right side of the Equation 4.10, which means that values smaller than these would satisfy the Mears criterion. The $\mathscr{R}_{i_{Obs}}$ was calculated from the reaction rate previously obtained (see Equation 4.9). By evaluating and comparing the results, the experimental conditions satisfied the Mears criterion and thus the external mass gradients were confidently discarded.

Table 4.5: Mears Criterion for the CSCWO of DBU on *Pt* Catalyst

$WHSV$, s^{-1}	N_{Re}	k_c,cm/s	$-\mathscr{R}_{TOC_{Obs}}$, mmol/L s	$\frac{-\mathscr{R}_{TOC_{Obs}} d_p}{2C_{i_B} k_c}$
0.5	2.21	0.529	0.41	0.00027
3.0	13.25	0.575	2.21	0.01679
0.5	11.04	0.568	0.14	0.00025
3.0	66.27	0.688	9.65	0.01402

4.2.3.2 The Criterion of Pore Diffusion in Chemical Reactions

Weisz and Prater [279] proposed a criterion to determine whether there is influence of internal diffusion during the chemical reaction that is based on measurable experimental data applicable to CSCWO reactions [214]. However, it is limited to first order power-law reaction rate expressions which has hindered its applicability. An extension of the Weisz and Prater criterion to different reaction rate models is given by Bischoff [280]. The criterion is also given in terms of measurable data which is given by:

$$\frac{\mathscr{R}_{i_{Obs}} d_p^2 g(C_{i_{Obs}})}{2\int_{C_{i_{Eq}}}^{C_{i_{Obs}}} \mathscr{D}_{i_{Eff}}(C_i) g(C_i) dC_i} < 1 \tag{4.15}$$

Where $C_{i_{Eq}}$ is the equilibrium concentration found at the end of an infinite pore, which for non reversible reactions can be taken as zero. The $g(C_i)$ is an expression similar to the reaction rate ($\mathscr{R}_i$) without the inclusion of the kinetic constant. If the effective diffusivity ($\mathscr{D}_{i_{Eff}}$) is concentration independent, it is assumed as a constant during the reaction. The $\mathscr{D}_{i_{Eff}}$ is calculated from the catalyst properties from [281]:

$$\mathscr{D}_{i_{Eff}} = \frac{\epsilon}{\tau} \mathscr{D}_{i_m} \tag{4.16}$$

Where ϵ is the voidage of the catalytic bed and τ is the tortuosity factor. For the experiments $\epsilon = 0.38$[3] and because there is no information about the tortuosity factor, it is safe to assume in the worst case a value of 6 [281]. The value of $\mathscr{D}_{i_m}$ = 1.2745 x 10^{-7} m^2/s obtained previously was use to evaluate $\mathscr{D}_{i_{Eff}}$ = 8.0721 x 10^{-9} m^2/s. For convenience the integral in Equation 4.15 was expressed in terms of conversion by changing the integration variable to:

$$\frac{\mathscr{R}_{i_{Obs}} d_p^2 g(C_{i_{Obs}})}{2\mathscr{D}_{i_{Eff}} C_{i_0} \int_{X_{i_{Obs}}}^{1} g(X_i) dX_i} < 1 \tag{4.17}$$

Because the term $g(X_i)$ in the integral depends on the reaction rate proposed and to avoid having specific analytical solutions, the integral and the criterion were evaluated numerically by a computer program written in *Python* using the scientific library *SciPy*. The values of the criteria found were between 2.85 and 11.87, which indicate that diffusion phenomena was occurring during the reaction. Although, small particle sizes facilitated the transport of reagents and products, the reaction over the platinum catalyst is fast enough that the diffusion process prevailed.

When a reaction is influenced by diffusion, it is necessary to account for it through the evaluation of the effectiveness factor. The definition of the effectiveness factor (η) is given in terms of the reaction rate influenced by diffusion ($\mathscr{R}_{i_{Obs}}$) to that in a pure chemical kinetic control ($\mathscr{R}_i$) according to:

[3] This value was taken from Aki and Abraham [215] for a very similar particle size and shape.

$$\eta = \frac{\mathscr{R}_{i_{Obs}}}{\mathscr{R}_i} \tag{4.18}$$

Effectiveness factor values close to unity indicate that the reaction takes place without any diffusion process prevailing. The factor is calculated through the evaluation of the Thiele modulus which relates the kinetic and diffusive potentials [282]. The Thiele modulus has a simple and concentration independent mathematical expression for reaction orders of 1. Although, other expressions of the Thiele modulus can be derived for different reaction rates models, they produce a complex expression of the effectiveness factor. Strictly speaking, the Thiele modulus, and consequently, the effectiveness factor should be evaluated depending on the reaction rate proposed, however Bischoff [283] has simplified the calculation through the use of a generalized Thiele modulus:

$$\phi_L = \frac{L_p \mathscr{R}(C_{i_S})}{\sqrt{2}} \left[\int_0^{C_{i_S}} \mathscr{D}_{i_{Eff}}(C_i) \mathscr{R}(C_i) dC_i \right]^{-\frac{1}{2}} \tag{4.19}$$

Where ϕ_L is the Thiele modulus considering the geometry of the catalyst as a flat plate, L_p is the length of the plate and $\mathscr{R}(C_{i_S})$ is the reaction rate at the surface of the catalyst. What it is very useful about this treatment is that if a power-law kinetic model is assumed, and using the general modulus definition, the curves of the effectiveness factors as a function of the Thiele modulus were narrowed into a region where they are almost independent of the reaction order proposed. Consequently, by assuming a reaction order of one, this will not have an appreciable effect in the calculation of η (mainly in the presence of a strong diffusive process) and avoids the need to obtain an specific expression of the effectiveness factor for different reaction rate orders. As the treatment assumed that the catalyst particles were flat plates it is also necessary to considered the change of the geometry of the catalyst. Aris [284] has demonstrated that by choosing the appropriate characteristic lengths other geometries can be easily accessible. If a sphere geometry is considered, its Thiele modulus would be as $\phi_S = 3\phi_L$ [281]. Therefore, the effectiveness factor expression for a flat plate could be used for a spherical geometry by modifying its Thiele modulus to:

$$\eta = \frac{\tanh(3\phi_L)}{3\phi_L} = \frac{\tanh\phi_S}{\phi_S} \tag{4.20}$$

Because the reaction was limited by pore diffusion, it was necessary to modify the reaction rate and consequently the reactor model to account for this effect, hence Equation 4.8 was modified for this purpose. Essentially the ordinary differential equation could be properly arranged to give a similar reactor equation where the superficial velocity (u_S) and length of the reactor (L) replaced the term W/F_{i_0}. Thus the equation is given by [230]:

$$\frac{d(u_S C_i)}{dx} = -\mathscr{R}_{i_{Obs}} \tag{4.21}$$

By assuming u_S as constant and incorporating the effectiveness factor the equation is then transformed to:

$$u_S \frac{dC_i}{dx} = -\eta \mathscr{R}_i \tag{4.22}$$

The equation is conveniently expressed in dimensionless units when the characteristic length across the longitudinal axis (x) and the concentration (C_i) are scaled by using the initial concentration (C_{i_0}) and the length of the reactor (L) according to:

$$v_i = \frac{C_i}{C_{i_0}} \qquad \text{and} \qquad z = \frac{x}{L} \tag{4.23}$$

Where v_i and z are the new dimensionless variables. Then Equation 4.22 is then rearranged

$$\frac{dv_i}{dz} = -\frac{\eta \mathscr{R}_i L}{u_S C_{i_0}} \tag{4.24}$$

If data of conversion are given instead of concentration Equation 4.24 can be transformed by making $dv_i = d(C_i/C_{i_0}) = -dX_i$ where X_i is the conversion of the reactant and finally the resultant equation is given by:

$$\frac{dv_i}{dz} = \frac{\eta \mathscr{R}_i L}{u_S C_{i_0}} \tag{4.25}$$

Notice that the change in the sign in the Equation 4.25 is a consequence of the change of the variable of integration. Which subjected to the following initial condition:

$$X_i(0) = X_{i_0} \qquad \text{or} \qquad v_i(0) = v_{i_0} \qquad \text{when} \qquad z = 0 \tag{4.26}$$

If it is assumed that the reaction model is the power law then Equation 4.25 given in terms of the C_{TOC} and C_{O_2} is:

$$\frac{dv_{TOC}}{dz} = \frac{\eta\, k\, C_{TOC}^{a}\, C_{O_2}^{b} L}{u_S C_{TOC_0}} \tag{4.27}$$

This equation was used to obtain the kinetic parameters by fitting the experimental data into the continuity equation. As mentioned previously the Thiele modulus expression adopted a simple form for the case where the reaction order is 1. To simplify the problem some assumptions were made for the treatment of the experimental data. Firstly, because the SR was calculated based on the initial concentration of DBU, oxygen was in excess at all times, according to the theoretical reaction $C+O_2 \longrightarrow CO_2$; an equal amount of oxygen to carbon is required, thus it was assumed that the oxygen concentration was constant. Moreover, by using the definition of the generalized Thiele modulus the difference in the calculation of effectiveness factor by proposing a reaction order of one is negligible. Equation 4.9 can be rewritten as:

$$\mathscr{R}_{TOC} = k\, C_{TOC}^{a}\, C_{O_2}^{b} = (k\, C_{TOC}^{a-1}\, C_{O_2}^{b}) C_{TOC} = k'' C_{TOC} \tag{4.28}$$

Where $a \neq 1$. For expression as in Equation 4.28 the general Thiele modulus is given by:

$$\phi_L = L_p \sqrt{(n+1)\frac{k C_{i_S}^{n-1}}{2\mathscr{D}_{Eff}}} = L_p \sqrt{\frac{k}{\mathscr{D}_{Eff}}} \tag{4.29}$$

and thus the expression for the effectiveness factor is given as in Equation 4.20. Because the Thiele modulus, and consequently, the effectiveness factor are $f(C_{TOC})$; then the approach taken was to divide the reactor into small sections along the axial axis to solve Equation 4.27 and incorporate its solution into the routines for the fitting of the experimental data. This is explained in more detailed in Appendix B.

The experimental data at 673 K and 23.0 MPa were again analyzed by this approach and the reaction rate fitted was:

$$\mathscr{R}_{TOC} = 13.3626 \pm 1.4537\; C_{TOC}^{1.3730 \pm 0.1414}\; C_{O_2}^{0.1544 \pm 0.0632} \tag{4.30}$$

By comparing Equations 4.9 and 4.30, it is found that by incorporating the effectiveness factor, the value of the kinetic constant and the reaction order with respect to oxygen had

changed. The inclusion of the effectiveness factor to account for the effect of pore diffusion reduced the value of the kinetic constant and augmented the reaction order with respect to oxygen. By adopting this step in the calculation, it is now assured that the reaction proceeds in a pure chemical control and the kinetic parameters calculated were not influenced by internal concentration gradients.

It is well known that reactions at supercritical conditions show anomalous behavior due to mainly the change in density of the reacting mixture which is appreciable as the operating conditions approach the critical point of the reaction mixture. The change in density is responsible for changing the solute-solvent interactions during the reaction [14, 219]; however, because this effect is difficult to assess, it is usually assumed that the reaction dependency on temperature can be described by the the Arrhenius equation as:

$$k = A \exp\left(-\frac{E_a}{RT}\right) \tag{4.31}$$

Where A is the pre-exponential factor or frequency factor, E_a is the activation energy and R is the ideal gas constant. The constants A and E_a are termed Arrhenius parameters. To estimate the Arrhenius parameters, it is necessary to have experimental data at least for two different temperatures. The parameters were calculated from the kinetic constants at different temperatures and fitting k and T into Equation 4.31. It is important to point out that at every temperature, the procedure that involved the calculation of the Thiele modulus and effectiveness factor was performed to account for the influence of internal concentration gradients, this is important as the reaction proceeds faster at high temperatures. By adding the Arrhenius parameters, another expression which incorporate the influence of temperature can be obtained:

$$\mathscr{R}_{TOC} = 3.1022\text{x}10^{9} \pm 1.5452\text{x}10^{10} \exp\left(-\frac{109.5381 \pm 31.7854}{RT}\right) C_{TOC}^{1.3730\pm0.1414} C_{O_2}^{0.1544\pm0.0632} \tag{4.32}$$

In the previous equation all parameters fitted were estimated within confidence limits of 95%. In the equation, the activation energy is given in kJ/mol, while the frequency factor has the same units that those of the kinetic constant. The reaction rate is expressed in terms of the volumetric properties.

4.2.4 Product Identification

A series of experiments were carried out to identify the main products of the reaction. Experiments were carried out at isobaric conditions (23.0 MPa) and the reaction temperature was varied from 673 to 773 K. An initial concentration of 1.1 mmol of DBU/L and a SR of 1 were used in each experiment. Liquid and gas samples were taken at space velocities of 0.5, 1.75 and 3.0 s^{-1}. Although, efforts were carried out to identify the organic products by gas chromatography coupled to a mass detector (GC-MS), however due to their low concentration these products could not be identified. Nitrogen oxides were not detected, although their concentration could have been below the lower detection limit of the instrument (100 ppm). Figure 4.14 depicts the distribution of carbon and nitrogen found in the gas and liquid streams as a fraction of the initial amount at $WHSV = 1.75$ s^{-1}. Platinum promoted a fast oxidation of the organic carbon and a low production of inorganic carbon. The main product obtained was carbon dioxide, whose production was increased as the temperature rose. At 773 K the CO_2 constituted almost the only product of the reaction, although traces of CO and CH_4 were detected. Production of methane was favoured only at 773 K, its formation was not detected at lower temperatures.

On the other hand, because of the low content of nitrogen in the molecule and high conversion of TOC, the amount of nitrogen attached to any organic carbon was discarded. The nitrogen products found were inorganic species such as N_2, NH_4^+, NO_3^- and NO_2^- ions but only chemical species in the liquid phase were included in Figure 4.14b. This is because the reaction took place in an aqueous phase where ions are formed as intermediate products before they are finally oxidised to nitrogen. Their presence is in part responsible for the pH change of the solution. The initial pH of the solution was 10.7-11.9, which dropped to the acidic range of 2.2-5.9 after the reaction. NO_2^- and NO_3^- are products of the dissociation of nitric acid (HNO_3) and nitrous acid (HNO_2) which were responsible for the acidic pH of the solution. The presence of ammonium ion was as a consequence of acidic pH of the solution which favoured its presence [285]. Webley et al. [144] have suggested that ammonium cation can appear in the form of ammonium carbonate, after they have identified it as the product of the outlet stream of the SCWO of ammonia-methanol mixtures. This type of salt was present because the parallel mechanism which produce carbonate and ammonium ions during the incomplete oxidation of the nitrogen-containing organic molecules. However, this salt does not represent any particular

operational problem because it is soluble in SCW through an unusual mechanism in which ammonium salts decomposes to ammonia [286, 287]. The initial pH of the solution was 10.7-11.9, which dropped to the acidic range of 2.2-5.9 after the reaction. *Pt* was selected as its catalytic properties promote the oxidation of ammonia, which is one of the main refractory products. The concentration of ammonia in the form of ammonium ion was lowered at 673 K, ammonia production shifted at high temperatures. The catalyst also prevented the formation of a high concentration of nitrite and nitrate ions; the former being favoured at a temperature of 773 K.

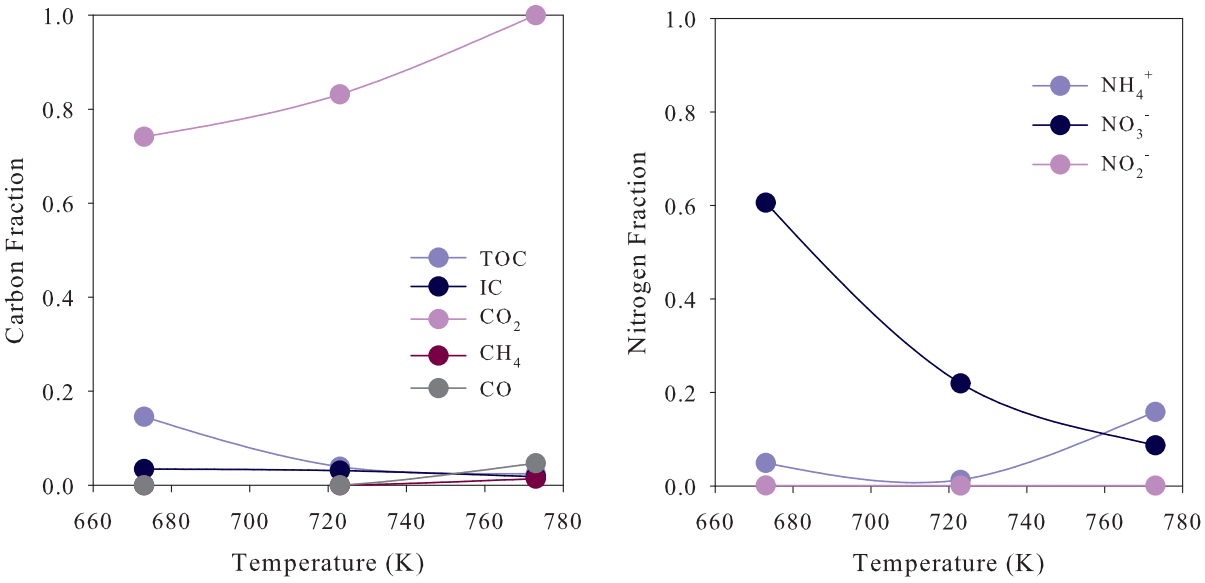

a) Distribution of Products Containing Carbon

b) Distribution of Products Containing Nitrogen

Figure 4.14: Carbon and Nitrogen Fraction for the CSCWO of DBU over *Pt*

4.2.5 Catalyst Activity

Catalyst stability can change specially at the operating at which SCWO takes place. The assessment of the catalyst stability was evaluated at 23.0 MPa and 673 K with an initial concentration of DBU of 0.3 mmol/L and a SR of oxygen of 1. During the test, samples were taken for TOC analysis. The catalyst activity slightly decreased towards the end of the activity test as measured in terms of the removal of the TOC content in the effluent as it is shown in Figure 4.15. Aki and Abraham [215] have previously confirmed the stability of *Pt* catalyst in the CSCWO process, nevertheless the activity of the catalyst was measured in terms of the removal of pyridine. If

the catalytic activity is only measured in terms of the organic compound, the catalyst would not lose its activity because DBU was not detected in the outlet stream. However, the results of this work suggest that chemical or physical changes to the catalyst were affecting the elimination of the intermediates produced in the reaction. Samples of the effluent were analysed by ICP-OES and confirmed that *Pt* was not leaching from the reactor (the lower detection limit of the instrument is 0.1 ppm). Consequently, another phenomenon is contributing to the deactivation of the catalyst.

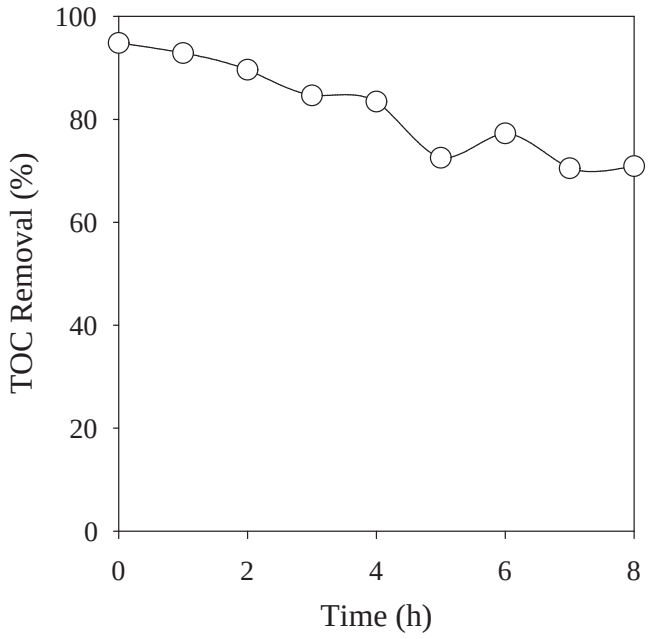

Figure 4.15: Catalyst Stability under CSCWO of DBU over *Pt*

Surface analysis by DVS of the catalyst before and after the reaction demonstrated a significant reduction of the surface area from 122.2 to about 59.1 m^2/g. This reduction in surface area would have also contributed to the loss of activity of the catalyst. In addition, the adsorption and desorption curves would imply that there were significant changes in the catalyst structure (see Appendix D for more information). The catalyst presented a hysteresis which reflected a difference between the adsorption-desorption curves, nevertheless the process was reversible. The shape of the curves for the fresh and spent catalyst showed a similar adsorption-desorption mechanism, but during the calculation of the isotherms the water intake revealed that a change to the surface of the catalyst used in the reaction had occurred.

Other researchers have established that Al_2O_3 is not a stable phase at supercritical conditions and is transformed to bohemite ($AlO(OH)$), which is more stable in the process [288, 289]. However, the XRD analysis of the catalyst did not show evidence of such structure (see Appendix E). Some evidence of a crystalline structure is shown but it is due to the presence of SiO_2 in the sample analysed. No platinum crystalline structures were identified. The spent catalyst chemistry had changed slightly in comparison to the fresh sample, but for both catalysts only amorphous structures were found.

4.3 CSCWO of DBU over CuO/Al_2O_3 Catalyst

Copper oxides either alone or mixed with some other catalyst have demonstrated to improve the elimination of organic compounds under supercritical conditions [204, 217, 218]. Since CuO catalysts have successfully performed under CSCWO for molecules containing heteroatoms like oxygen, its use could be extended for the treatment of nitrogen-organic compounds. One of the common reactions from aqueous oxidation of organic compounds that contain nitrogen is the tendency to produce ammonia during the reaction. Consequently, a catalytic material that is able to accomplish a dual functionality is desirable. CuO has been found to achieve ammonia oxidation, and consequently, in theory, it could destroy the organic compound and avoid the formation of ammonia during the reaction [290].

4.3.1 Evaluation of External and Internal Concentration Gradients

The evaluation of concentration gradients was performed following the procedure described previously (Section 4.1.3.2). A maximum pressure drop of 0.35 MPa and a pressure variation of $\pm$0.35 MPa assured isobaric operation and a temperature variation of $\pm$2 K satisfied the assumption of isothermal operation.

4.3.1.1 Interphase Concentration Gradients

The conversion based on the remaining TOC was used to evaluate the interphase concentration gradients. An initial concentration of 0.3 mmol DBU/L which was equivalent to an initial TOC concentration of 2.7 mmol/L was used during each experiment and the oxygen supplied met a SR of 1. The operating conditions were held constant at 673 K and 23.0 MPa. The catalyst

particle size was 212-250 μm and the masses of catalyst studied were 0.1, 0.2, 0.4 and 0.5 g. The catalyst was diluted with SiO_2 to avoid any hot spots during the operation. During the study the space velocity ($WHSV$) was varied from 0.2 to 0.6 s^{-1}. Figure 4.16 shows the findings of the experimentation for space velocities of 0.2, 0.5 and 0.6 s^{-1}. The results show that there was not an increment in TOC removal as the reacting mixture flow rate and the catalyst weight was increased, and consequently, the reaction proceeds without any influence of external concentration gradients.

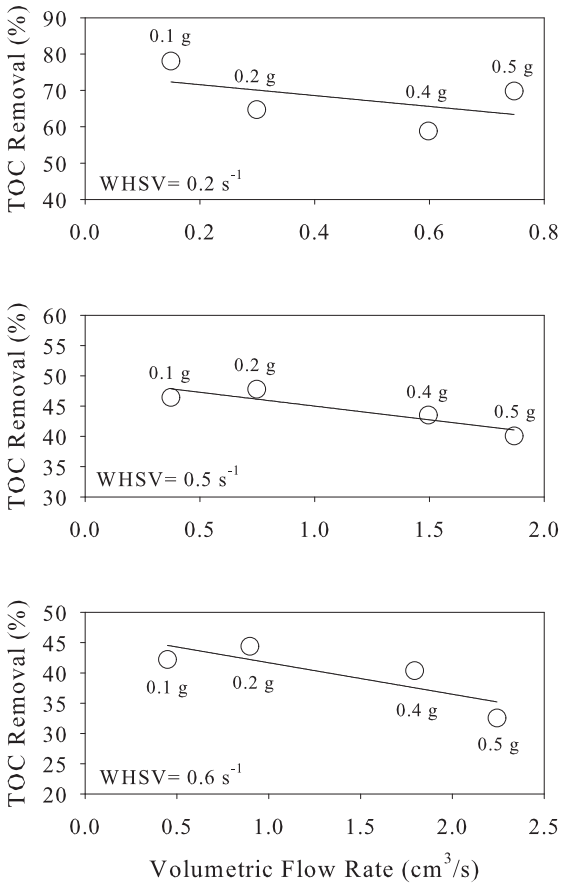

Figure 4.16: External Concentration Gradients of DBU over CuO

4.3.1.2 Intraphase Concentration Gradients

Internal gradients concentration were investigated by reducing the particle size of the catalyst and evaluating the change on the TOC removal for the reaction. The catalytic particles sizes studied are summarised in Table 4.6. The tests were performed at 673 K and 23.0 MPa with

a initial concentration of 2.7 mmol/L of TOC and oxygen was supplied to give a SR of 1. Experiments were performed at space velocities of 0.2 to 0.6 s^{-1}. Figure 4.17 shows the results from the experiments used to investigate the intraphase concentration gradients. The conversion increased slightly as the particle size was reduced from 212−250 to 150−212 μm. Smaller particles sizes than 150−212 μm resulted in no change in conversion at $WHSV = 0.2$ s^{-1} and a maximum improvement of TOC removal of 4% at higher space velocities. This assumes a minimum influence of intraphase concentration gradients which can be discarded. A more conclusive test to assure the absence of internal concentration gradients is given in Section 4.3.4.

Table 4.6: Particle sizes for Evaluation of Internal Concentration Gradients

Experiment	Particle Size Range, μm	Average Particle Size, μm
1	212−250	231.0
2	150−212	181.0
3	90−106	98.0
4	45−63	54.0

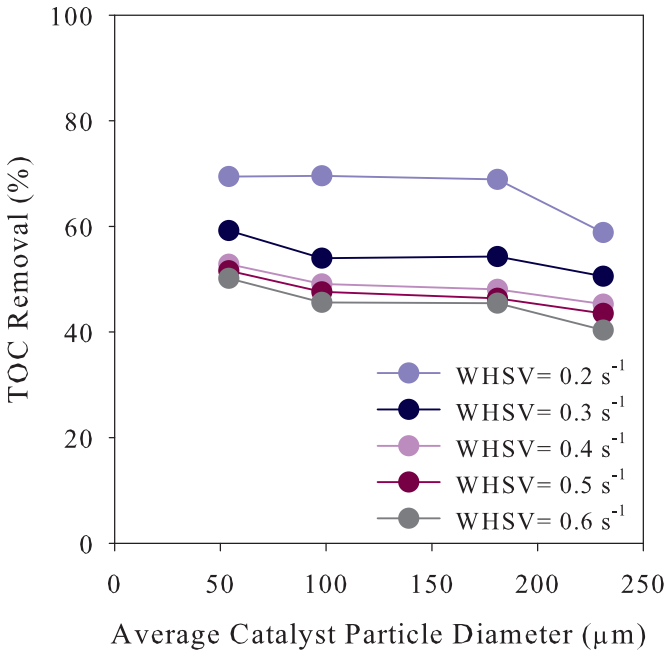

Figure 4.17: Internal Concentration Gradients of DBU over CuO

The absence of external and internal mass transfer concentration gradients will allow the convenient selection of the amount of catalyst and particle size to investigate the effect of the operating conditions and kinetics of the reaction.

4.3.2 Reproducibility Tests and the Effect of Key Operating Conditions

DBU was completely oxidised and only traces of it ($<$ 4 ppm) were detected in a few samples, and consequently, the TOC content in the effluent was used to study the extent of the oxidation reaction. An outline of the operating conditions studied and details of the catalytic bed used during the CSCWO of DBU over CuO is displayed in Table 4.7.

Table 4.7: Experimental Conditions of CSCWO of DBU over CuO

Parameter	Interval Studied
Temperature Range, K	653-773
Pressure Range, MPa	23.0-30.0
Initial DBU Concentration Range, mmol/L	0.1-1.1
Initial Concentration of Oxygen Range (SR)	0.5-12
Catalyst weight, g	0.4±0.0001
Catalyst particle size, μm	45-63
SiO_2 particle size, μm	212-250
Bed length, cm	8.1±0.1
Dilution factor catalyst to SiO_2, v:v	1:3

4.3.3 Reproducibility Tests

Reproducibility tests were carried out to estimate the experimental error in the CSCWO of DBU over CuO. For this purpose 5 experiments were conducted at 673 K and 23.0 MPa with an initial DBU concentration of 0.3 mmol/L and a SR of oxygen of 1. Samples were taken at space velocities of 0.1, 0.2, 0.3, 0.4, 0.5 and 0.6 s^{-1}. The average values of TOC removal and their standard deviation were calculated and are shown in Table 4.8 and are plotted in Figure 4.18 with their standard deviations presented in the form of error bars. The maximum experimental

error close to 7% was obtained at space velocity of 0.6 s^{-1}, although also a value close to 6% error was found at the lowest flow rates. The tests show the reliability of the data obtained during the present study.

Table 4.8: Reproducibility Tests of CSCWO of DBU over *CuO*

$WHSV$, s^{-1}	Average TOC Removal, %	Std. Dev. of TOC Removal, %
0.1	77.24	6.18
0.2	64.69	2.80
0.3	56.44	2.38
0.4	52.06	3.30
0.5	50.31	4.19
0.6	48.40	6.72

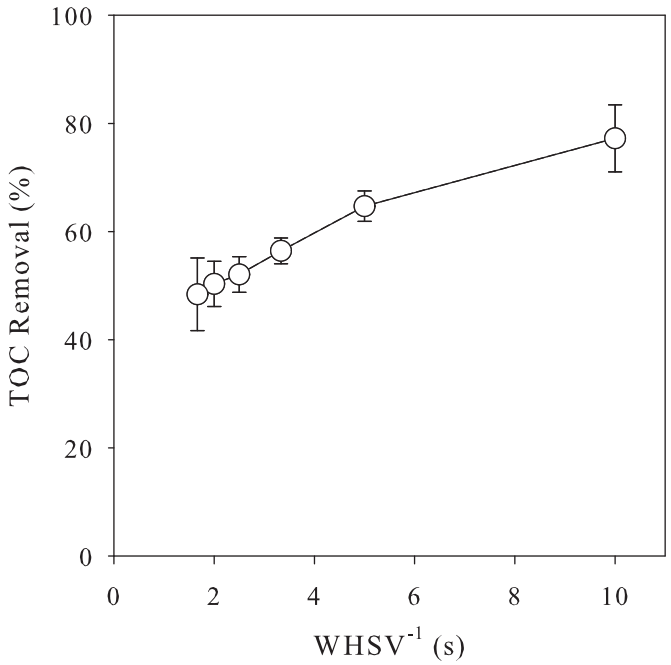

Figure 4.18: Reproducibility Tests of CSCWO of DBU over *CuO*

4.3.3.1 Effect of Temperature on the CSCWO of DBU over *CuO*

The effect of temperature on the CSCWO of DBU over *CuO* catalyst was studied in the range of 653 to 773 K at constant pressure of 23.0 MPa. An initial DBU concentration of 0.3 mmol/L was used for all the experiments, while the initial concentration of oxygen met a SR of 1. The effect of the temperature is shown in Figure 4.19 at space velocity intervals ranging from 0.1−0.6 s^{-1}. The temperature rapidly improved the removal of TOC at any space velocity and the TOC content was reduced to 98% at a temperature of 773 K and $WHSV = 0.1\ s^{-1}$. If this reaction is compared to the non-catalytic reaction the catalyst enhanced the removal of the DBU in terms of the TOC, allowing a reduction in the operation temperature and improving its effectiveness [167]. Nevertheless, in terms of TOC content the reaction was not particularly efficient since at 653 K only a 24% was removed at $WHSV$ =0.6 s^{-1}. Consequently, higher operating conditions or lower space velocities are required to reach complete elimination.

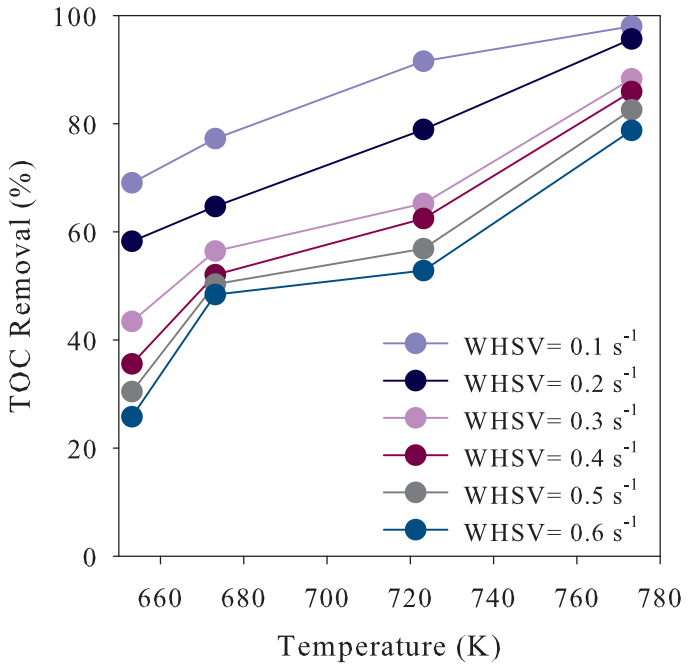

Figure 4.19: Effect of Temperature on the CSCWO of DBU over *CuO*

4.3.3.2 Effect of Pressure on the CSCWO of DBU over *CuO*

The pressure influence on the oxidation of DBU was studied at 673 K. For these experiments the initial concentration of DBU and oxygen were held constant at 0.3 mmol/L and a SR of 1, respectively. The pressure influence on the reaction is shown in Figure 4.20. Although, its effect was small the pressure increased the removal of the TOC. Pressure has been demonstrated by Yu and Savage [204] to have no effect in the elimination of phenol, however TOC removal was not studied. The effect of system pressure has been studied in a range where the density of water varied from 133.8 kg/m^3 at 23.0 MPa to 357.1 kg/m^3 at 30.0 MPa, which might not be sufficient to demonstrate the effect of pressure in the reaction. Transition state theory is often used to explain the contribution of pressure at supercritical conditions, however depending on the range of operating conditions, the effect of pressure could be a minor consideration [291]. Pressure influence on catalytic reactions is complex owing to the fact that it alters the kinetic constant through a change in both the solvent properties and transport properties of the species involved during the reaction.

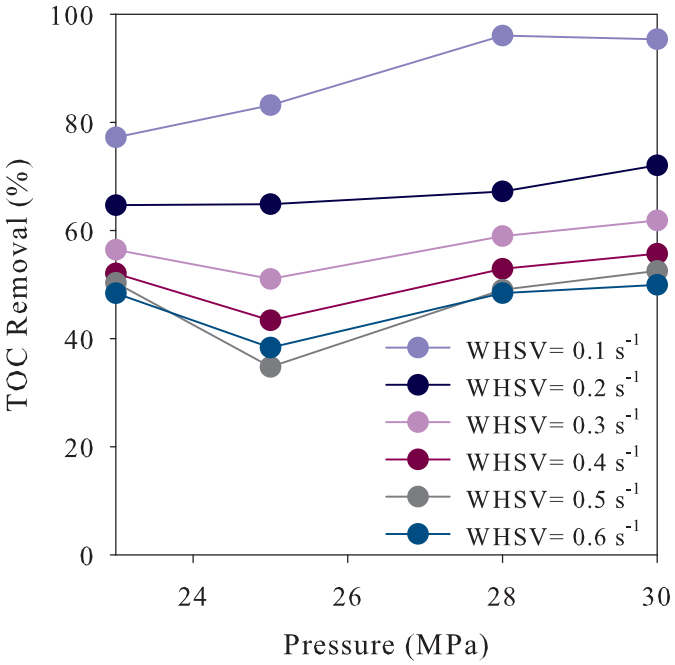

Figure 4.20: Effect of Pressure in the CSCWO of DBU over *CuO*

4.3.3.3 Effect of Initial DBU Concentration on the CSCWO over *CuO*

The effect of the initial concentration of DBU was studied in a range of 0.1 to 1.1 mmol/L. During each experiment the concentration of oxygen was maintained constant at a SR of 1, while the temperature and pressure were 673 K and 23.0 MPa. The results of the study are presented in Figure 4.21. The experiments showed that the concentration of DBU enhanced the elimination of the TOC content. This fact has been demonstrated previously during the CSCWO of phenol over the same catalyst, which showed that an increment of reactant concentration favoured the oxidation reaction [204]. This means that, higher concentrations of DBU can be efficiently treated without affecting the performance of the reaction.

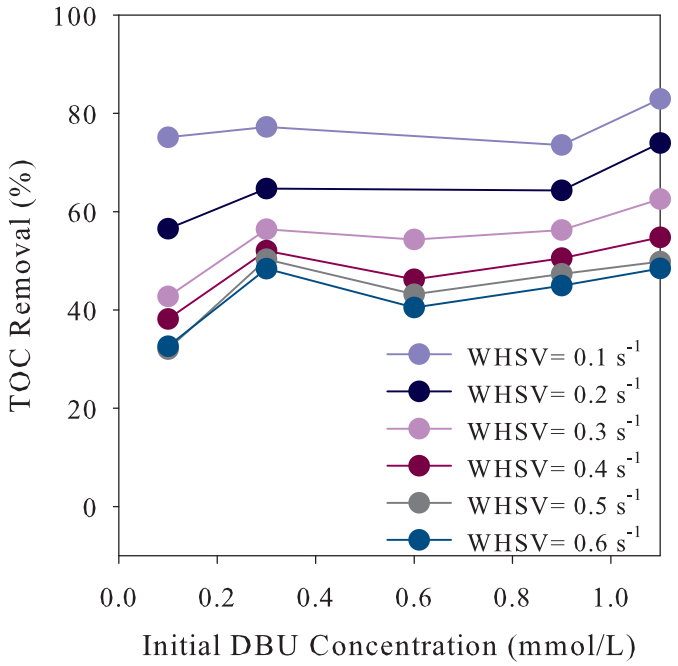

Figure 4.21: Effect of Initial DBU Concentration on the CSCWO over *CuO*

4.3.3.4 Effect of Initial Oxygen Concentration on the CSCWO of DBU over *CuO*

An examination of the effect of the initial concentration of oxygen in the reaction was carried out at 673 K and 23.0 MPa, meanwhile the concentration of DBU was held constant at 0.3 mmol/L. The oxygen was varied from a SR of 0.5 to 12 and its influence is shown in Figure 4.22. Increasing concentration of oxygen improved the reaction conversion, however the addition of a

stoichiometric ratio higher than 2 only improved the reaction by a maximum of 15% of TOC removal. The effect of oxygen was unnoticed at higher oxygen concentrations. When the space velocity was 0.1 s^{-1}, it did not seem to have an effect on the TOC removal above at a SR of 2.

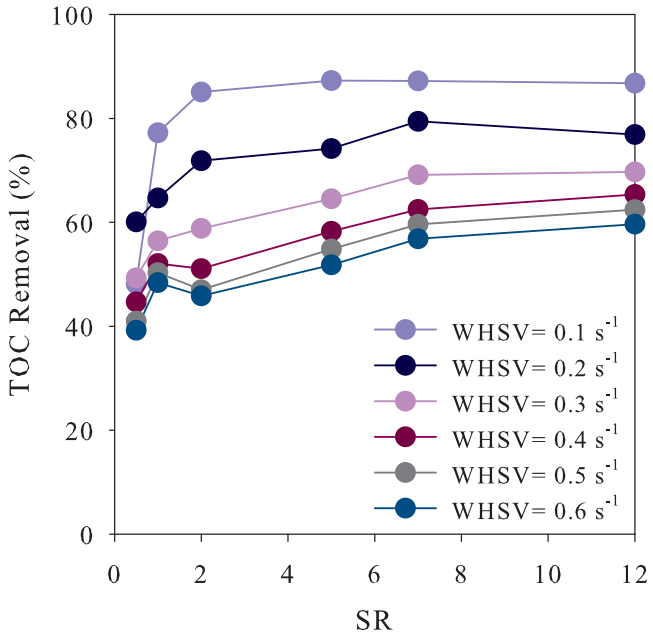

Figure 4.22: Effect of Initial Oxygen Concentration on the CSCWO of DBU over *CuO*

4.3.4 Kinetics of the Reaction

The kinetics of the catalytic oxidation were represented by the power-law kinetic model assuming a pseudo-homogeneous reaction. The reaction rate constant and reaction orders (kinetic parameters) were obtained by applying the integral method of analysis by assuming an ideal tubular reactor model. The experimental data of the CSCWO of DBU at 673 K and 23.0 MPa were used to fit the reactor model (Equation 4.8) and obtain the kinetic parameters (a thorough description of the fitting of the experimental data is given in Appendix B). The best fitting is given by the following rate expression in terms of TOC content:

$$\mathscr{R}_{TOC} = 1.5780 \pm 0.2681 \; C_{TOC}^{1.0811 \pm 0.2503} \; C_{O_2}^{0.1608 \pm 0.1113} \tag{4.33}$$

A parity plot of the experimental and predicted fraction is given in Figure 4.23. Around 0.5 of reacted fraction, the model tends to underpredict the fraction of the experimental TOC.

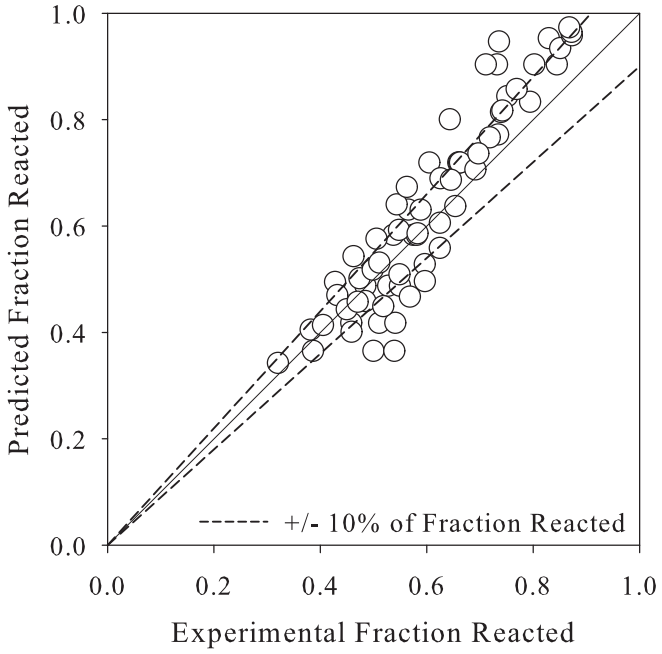

Figure 4.23: Comparison of Predicted and Experimental Fraction of TOC Reacted over CuO

On the other hand, above a fraction of approximately 0.7, the reaction rate overestimated the fraction reacted of TOC. These should be taken into account if the kinetic data taken are used for future scaling up of the reactor. This also could be a consequence that the reaction rate proposed was not appropriate. To confirm that the reaction was not limited by the presence of internal gradients, the criterion proposed by Bischoff [280] was evaluated for the experimental values (Section 4.2.3.2). The values varied from 0.42 to 0.93 which satisfies the criterion, even when the reaction proceeded faster with a high initial concentration of oxygen in the stream.

If it is assumed that the temperature dependence of the reaction rate follows the Arrhenius equation, the final expression of the reaction rate as a function of temperature and the concentration of the reactants is given by:

$$\mathscr{R}_{TOC} = 3.3972\text{x}10^{6}\pm1.3857\text{x}10^{7}\exp\left(-\frac{83.5823 \pm 25.8577}{RT}\right) C_{TOC}^{1.0811\pm0.2503} C_{O_2}^{0.1608\pm0.1113} \quad (4.34)$$

The parameters fitted have confidence limits of 95% and the oxidation reaction over CuO could be well assumed to proceed by a reaction order of 1.

4.3.5 Product Identification

A series of experiments were carried out at temperatures ranging from 673 to 773 K at 23.0 MPa. The initial concentration of DBU was maintained constant at 1.1 mmol/L and a SR of 1. The space velocities during the experiments were 0.1, 0.35 and 0.6 s^{-1} and liquid and gaseous samples were taken for further analysis. GC-MS could not identify organic compounds in the liquid phase because their low concentration levels of them in the stream were not enough to be detected. Moreover, nitrogen oxides in the gas phase were not detected, nevertheless their concentration could be under the lower detection limit of the GC. The solutions analysed after the reaction had a pH of 7 to 8 which had reduced from an initial basic pH between 10.7 to 11.9. Figure 4.24 shows a distribution of the carbon and nitrogen as a fraction of the initial concentration values for a space velocity of 0.35 s^{-1}. The major fraction of carbon was encountered as carbon dioxide. The organic carbon was reduced as the temperature rose, while the content of inorganic carbon and carbon monoxide was almost unchanged. One important fact is that whereas the catalyst promoted the elimination of the organic carbon, it did not promote complete oxidation of it.

Nitrogen was present mainly in the form of ammonium and nitrate ions. Ammonium ion concentration only slightly decreased up to temperatures of 773 K, however the nitrate ion formation was not favoured at this temperature. Nitrite ion was produced in small quantities and it did not rely on the temperature of the reactor. Copper oxide neither prevented the formation of ammonia as ammonium ion nor improved its elimination. As was mentioned previously, CuO promoted the oxidation of ammonia at low temperatures, however its catalytic properties at supercritical conditions of water did not show the same effect.

4.3.6 Catalyst Activity

The catalyst activity was investigated by oxidising a stream of DBU with a concentration of 0.3 mmol/L and SR of oxygen to DBU of 1. Operating conditions selected were 673 K and 23.0 MPa. The activity of the catalyst was measured according to the amount of TOC that was being removed in the reaction. A constant space velocity of 0.1 s^{-1} was maintained during the 8 hour experimental run. The profile of TOC content against time is plotted in Figure 4.25. The removal of TOC decreased to around 10% within 1 hour of operation and after, it was reduced only slightly until the end of the experiment. Samples were analysed by ICP-OES showing the

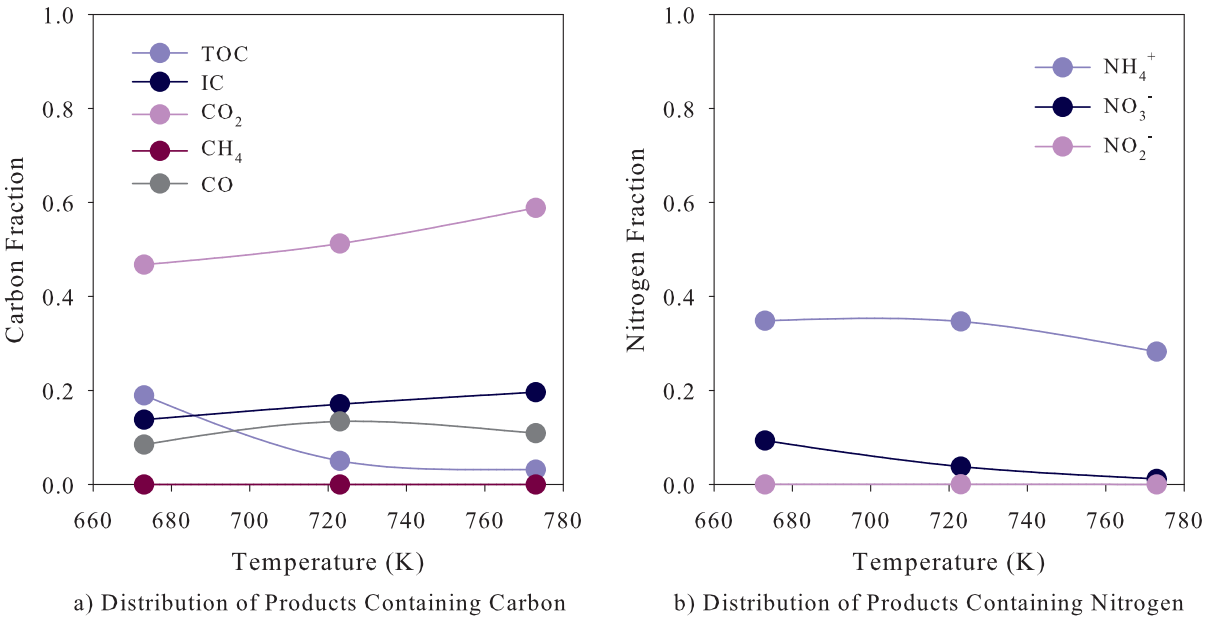

Figure 4.24: Carbon and Nitrogen Fractions for the CSCWO of DBU over CuO

presence of copper in aqueous samples at a maximum concentration of 0.164 ppm. Consequently, the loss in the activity is due in part to the reduction of the concentration of the active metal on the surface of the catalyst.

In addition, part of the surface area of the catalyst was reduced from 204 to about 81 m^2/g. Adsorption and desorption analysis carried out by DVS showed this change in the catalyst surface area, although the same reversible adsorption-desorption mechanism was present in the catalyst, the changes in the catalyst surface influenced the water intake during the analysis (see Appendix D for details). The XRD analyses have showed that there were structural changes to the crystalline materials in the spent catalyst (for details refer to Appendix E). The X-ray diffraction pattern indicated some residues of the SiO_2, which was used as a packing of the catalyst. The CuO oxide structured remained without significant changes, however the transformation to Cu_2O has been reported at supercritical conditions [288]. The Al_2O_3 used as support was present in the form of bohemite which it a more stable structure under oxidation reaction conditions.

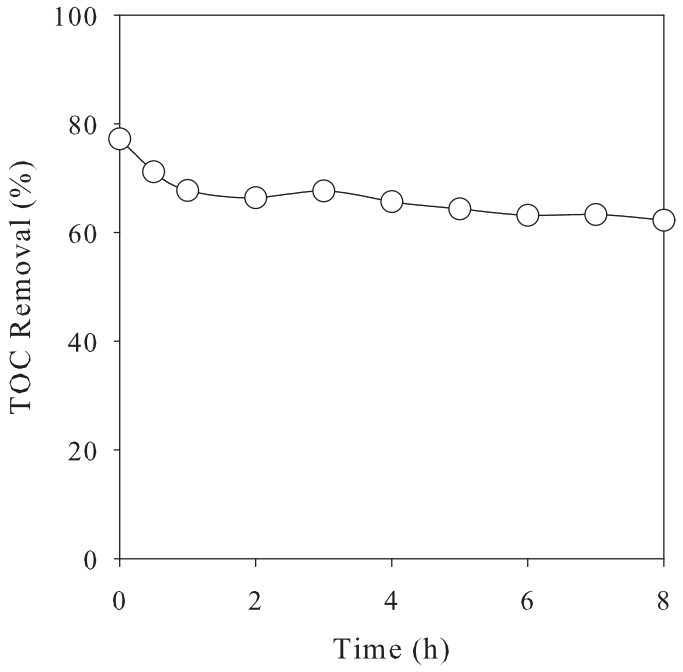

Figure 4.25: Catalyst Stability under CSCWO of DBU over CuO

4.4 CSCWO of DBU over MnO_2/CuO Catalyst

MnO_2 or manganese based catalysts have been widely used for the oxidation of organic compounds in supercritical water [200, 206, 207, 215, 216, 288, 292]. However, a MnO_2/CuO mixed catalyst has been demonstrated to be among the most effective [193, 204, 208]. Although, the research has been mainly focused on the oxidation of phenol in presence of manganese dioxide, Ding et al. [216] have also investigated its effect in the oxidation of ammonia. While both oxides have been demonstrated to perform under CSCWO of several organic compounds, CuO has also the property to contribute to the oxidation of NH_3.

4.4.1 Evaluation of External and Internal Concentration Gradients

A detailed description of the experimental test to evaluate the concentration gradients during the catalytic reaction are given in Section 4.1.3.2. A maximum pressure drop of 0.35 MPa and a maximum fluctuation of ±0.35 MPa assured isobaric operation. The isothermal behaviour of the reactor was also assumed because of a small variation of 2 K.

4.4.1.1 Interphase Concentration Gradients

The external concentration gradients were studied based on the removal of the TOC from the stream. A catalyst particle size of 212-250 μm was used during the experiments. The weights of the catalyst studied were 0.1, 0.2, 0.4 and 0.5 g, which were diluted with SiO_2 to maintain isothermal operation (particle size of 212-250 μm). The concentration of DBU was maintained at 0.3 mmol/L which is equivalent to 2.7 mmol of TOC/L at reaction conditions. Oxygen was supplied to maintain a SR of 1 and the temperature and pressure were fixed at 673 K and 23.0 MPa. During the experiments the flow rate of the reacting mixture was varied to allow space velocities ranging from 0.2 to 0.6 s^{-1}. Figure 4.26 presents the findings from the evaluation of the external gradients concentrations. It was concluded that above a catalyst weight of 0.4 g the change in the TOC removal was minimal and thus the absence of these gradients was confirmed.

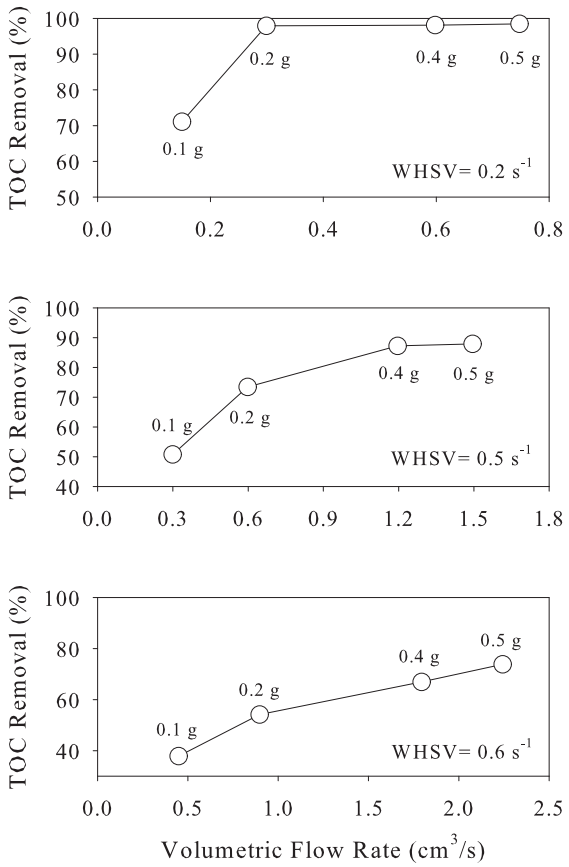

Figure 4.26: External Concentration Gradients of DBU on MnO_2/CuO Catalyst

4.4.1.2 Intraphase Concentration Gradients

Internal concentration gradients were evaluated by varying the particle size of the catalyst as shown in Table 4.9, and again the TOC content was followed to investigate the influence of internal concentration gradients. The catalyst amount employed was 0.4 g which assured the absence of external concentration gradients. The operating conditions during the study were held constant at 673 K and 23.0 MPa. The concentration of DBU was maintained at 0.3 mmol/L (2.7 mmol of TOC/L) and oxygen was supplied to give a SR of 1. The results of the study are illustrated in Figure 4.27.

Table 4.9: Particle Sizes for Evaluation of Internal Concentration Gradients

Experiment	Particle Size Range, μm	Average Particle Size, μm
1	212–250	231.0
2	150–212	181.0
3	63–106	84.5
4	45–63	54.0

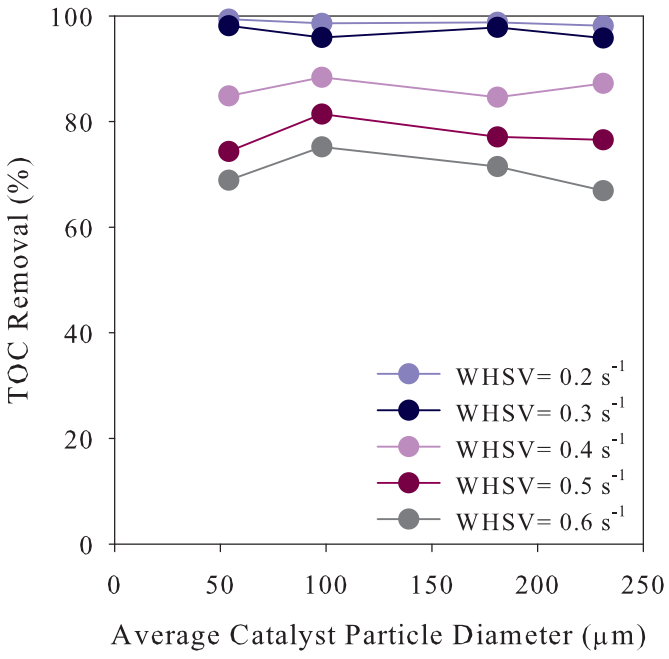

Figure 4.27: Internal Concentration Gradients of DBU on MnO_2/CuO

The change in the TOC removal was minimal as the particle size was varied from 231.0 to 54.0 μm, although there were slight intermittent changes in the intermediate particle sizes, those changes were practically the same for the whole particle at different space velocities. Thus it was assumed that the reaction was in pure chemical kinetic control. Nevertheless, the Bischoff criterion will be evaluated to confirm this finding [280] (see Section 4.4.3.1).

4.4.2 Reproducibility Tests and the Effect of Key Operating Conditions

DBU was not detected in the effluent of the reactor and therefore TOC content was followed as an indicator of the efficiency of the reaction. Table 4.10 summarises the experimental conditions studied and shows the details of the catalytic bed.

Table 4.10: Experimental Conditions of CSCWO of DBU over MnO_2/CuO

Parameter	Interval Studied
Temperature Range, K	673-773
Pressure Range, MPa	23.0-30.0
Initial DBU Concentration Range, mmol/L	0.1-1.1
Initial Concentration of Oxygen Range (SR)	0.5-12
Catalyst weight, g	0.4±0.0001
Catalyst particle size, μm	45-63
SiO_2 particle size, μm	212-250
Bed length, cm	8.2±0.1
Dilution factor catalyst to SiO_2, v:v	1:3

4.4.2.1 Reproducibility Tests

Reproducibility tests were performed to evaluate the experimental error during the catalytic study over the MnO_2/CuO mixed catalyst. During this test a total of five experiments were carried out at 673 K and 23.0 MPa. The initial concentration of DBU and oxygen remained constant at 0.3 mmol/L and SR of 1, respectively. The effluent of the reactor was sampled at space velocities ranging from 0.2 to 0.7 s^{-1}. For each space velocity the TOC removal was

averaged from the samples collected and its standard deviation was calculated. Table 4.11 shows the results and Figure 4.28 illustrates the average removal of TOC with error bars of ±1 of their standard deviation. A maximum standard deviation of 3 % was obtained at the highest space velocity, and consequently flow rate. When the flow rate increased its control became less accurate.

Table 4.11: Reproducibility Tests of CSCWO of DBU over MnO_2/CuO

$WHSV$, s^{-1}	Average TOC Removal, %	Std. Dev. of TOC Removal, %
0.2	99.24	0.15
0.3	95.00	2.74
0.4	81.84	2.72
0.5	72.82	2.85
0.6	67.68	2.88
0.7	61.62	2.92

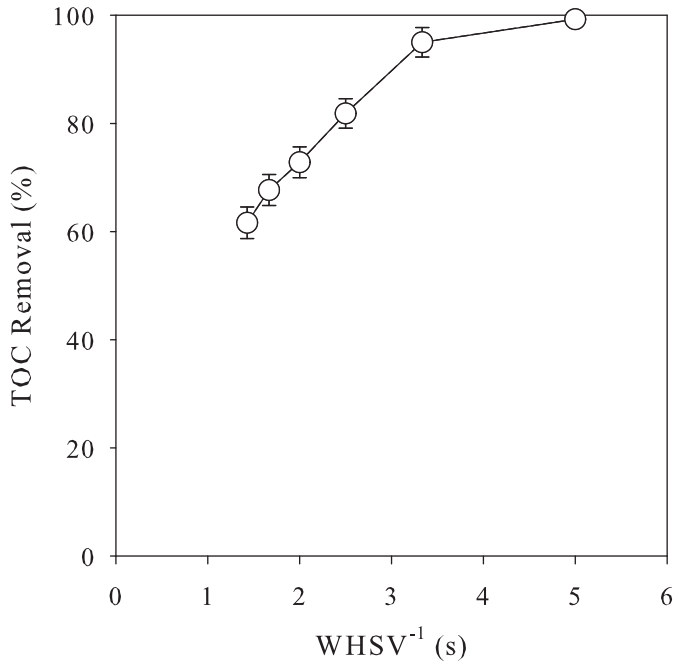

Figure 4.28: Reproducibility Tests of CSCWO of DBU over MnO_2/CuO

4.4.2.2 Effect of Temperature on the CSCWO of DBU over MnO_2/CuO

The effect of temperature on the removal of TOC was studied at 23.0 MPa by varying the temperature from 673 to 773 K. The initial concentration of DBU was maintained constant at 0.3 mmol/L with an initial oxygen concentration equal to the stoichiometric value (SR=1). The effect of temperature was studied at space velocities that ranged from 0.2 to 0.7 s^{-1}. Samples were taken at different space velocities for TOC content analysis. Figure 4.29 illustrates the effect of temperature in the removal of TOC. The temperature did not have any effect at $WHSV = 0.2$ s^{-1}, where the reaction approached completion. Higher space velocities revealed that the temperature positively influenced the reaction. The catalytic reaction showed that the TOC content of the stream can be reduced to a value of 99.2% when the experiment took place at 673 K and $WHSV = 0.2$ s^{-1}. The addition of the MnO_2/CuO catalyst improved the TOC removal.

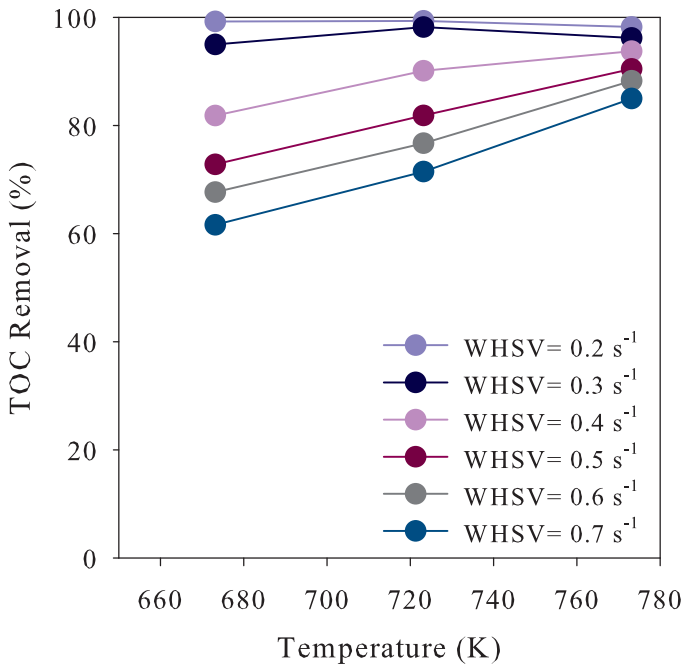

Figure 4.29: Effect of Temperature on the CSCWO of DBU over MnO_2/CuO

4.4.2.3 Effect of Pressure on the CSCWO of DBU over MnO_2/CuO

A series of experiments were performed to observe the effect of pressure during the CSCWO of DBU. The pressure was varied from 23.0 to 30.0 MPa at a constant temperature of 673 K.

For the experiments the concentration of DBU was kept constant at a value of 0.3 mmol/L and the oxygen was present at a SR of 1. Samples were taken at space velocities from 0.2 to 0.7 s^{-1}. Figure 4.30 displays the effect of pressure in the CSCWO of DBU. At space velocities of 0.3 s^{-1} and lower, the pressure did not affect the removal of TOC. The removal of TOC in the reaction improved when the pressure increased at space velocities from 0.4 to 0.7 s^{-1} and the most efficient removal was obtained when the pressure reached 30.0 MPa. However, the removal improved slightly when the system pressure was increased from 23.0 to 28.0 MPa. Although, the reaction proved to be pressure dependent; the study has shown that high TOC efficiencies could be obtained at pressures close to the water critical pressure.

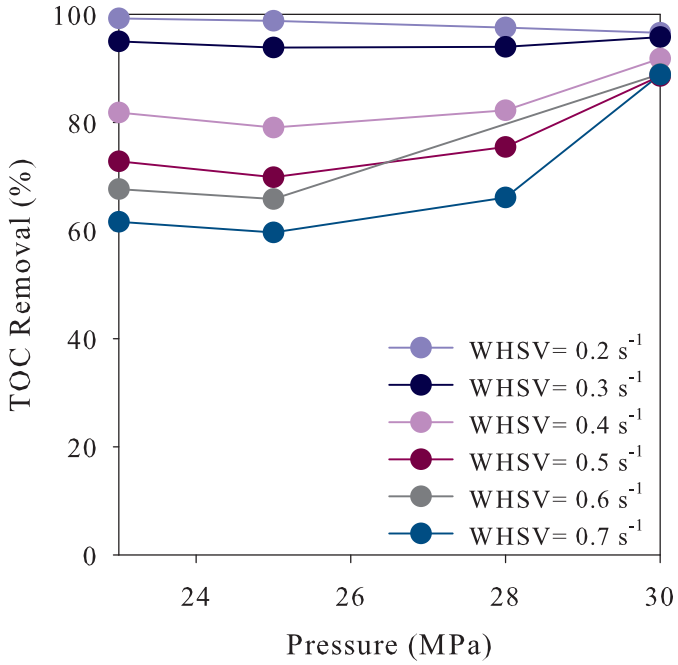

Figure 4.30: Effect of Pressure on the CSCWO of DBU over MnO_2/CuO

4.4.2.4 Effect of Initial DBU Concentration on CSCWO over MnO_2/CuO

The effect of the initial DBU concentration on the oxidation reaction was studied at 673 K and 23.0 MPa. For the experimental study the initial concentration of DBU was varied from 0.1 to 1.1 mmol/L and for each case the oxygen was fed to meet a SR of 1. A plot of the effect of the initial DBU concentration on TOC removal appears in Figure 4.31. At space velocities of 0.2 and 0.3 s^{-1} the concentration of DBU did not affect the removal of TOC because the reaction rate

was fast enough that became concentration independent. However, at higher space velocities an increase in DBU concentration improved the removal of TOC. Consequently, an increase in the reactant concentration favoured the reaction. Similar findings have been also reported for the oxidation phenol over MnO_2 catalyst [206].

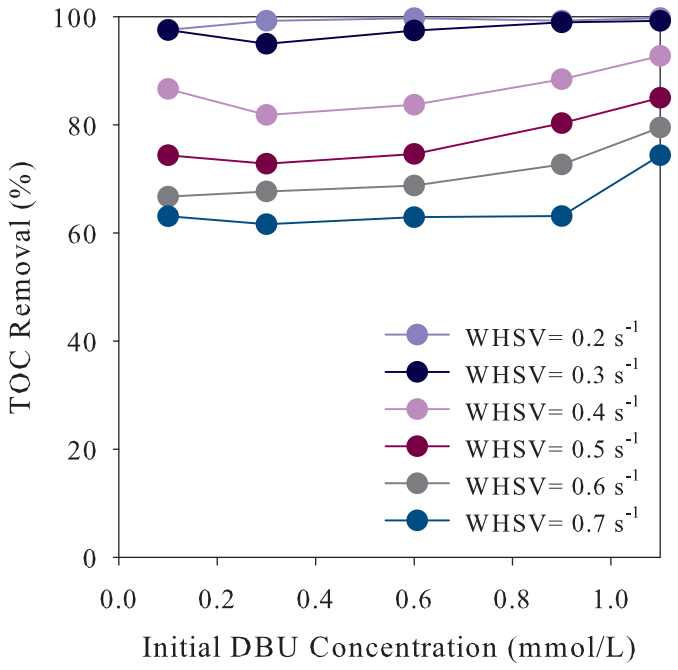

Figure 4.31: Effect of Initial DBU Concentration on the CSCWO over MnO_2/CuO

4.4.2.5 Effect of Initial Oxygen Concentration on the CSCWO of DBU over MnO_2/CuO

The influence of the concentration of oxygen in the catalytic reaction was studied at 673 K and 23.0 MPa. While the concentration of DBU remained constant at a value of 0.3 mmol/L, the concentration of oxygen was varied from a SR of 0.5 to 12. Figure 4.32 shows the results of the experiments performed. The removal of TOC was independent of the oxygen present in the stream at a space velocity of 0.2 s^{-1}. An increase in SR of oxygen improved the elimination of TOC when higher space velocities were adopted. The improvement in the TOC was considerable when the SR was varied from 0.5 to 5 and shows a strong dependence of the reaction on the oxygen concentration. Above a SR 5 the influence of oxygen was minimal. The effect of oxygen in CSCWO over MnO_2/CuO followed the same trend found by Yu and Savage [206].

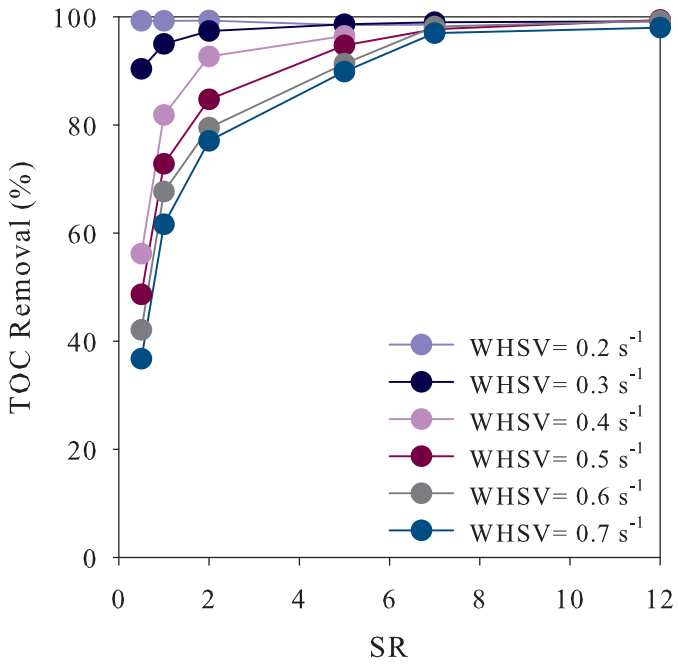

Figure 4.32: Effect of Initial Oxygen Concentration on the CSCWO of DBU over MnO_2/CuO

4.4.3 Kinetics of the Reaction

The kinetics of the reaction were assumed to follow the power-law kinetic model, and by discarding the external and internal concentration gradients, a pseudo-homogeneous reaction is assumed to take place. The kinetic parameters were obtained by fitting the experimental data into the ideal tubular reactor model coupled to a power-law reaction rate (Equation 4.8). The fitting of the kinetic parameters was done by following the integral method of analysis (A thorough description of the fitting is given in Appendix B). The experimental data used for the fitting of the kinetic parameters correspond to those obtained at 673 K and 23.0 MPa. The best fitting obtained can be presented by:

$$\mathscr{R}_{TOC} = 4.6312 \pm 1.0369\, C_{TOC}^{0.7535\pm0.2124}\, C_{O_2}^{0.2962\pm0.1317} \tag{4.35}$$

A parity plot of the experimental fraction of TOC predicted and experimental is shown in Figure 5.19. According to the results the reaction rate model predicted properly the removal of TOC where almost all experimental points lay within the $\pm 10\%$ conversion line.

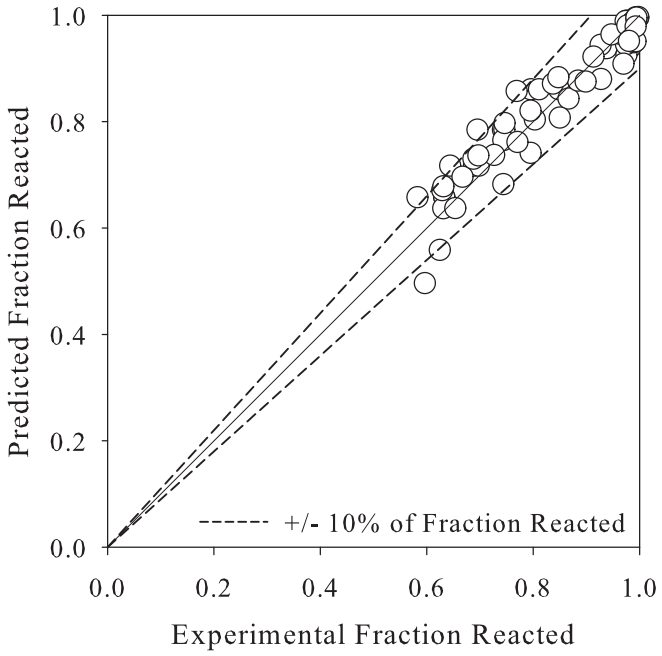

Figure 4.33: Comparison of Predicted and Experimental Fraction of TOC Reacted over MnO_2/CuO

4.4.3.1 The Criterion of Pore Diffusion in Chemical Reactions

Because the experimental assessment of the absence of internal concentration gradients was not conclusive (discussed in Section 4.2.3.2), in the case of reactions which proceed fast, it is important to estimate if the reaction was influenced by pore diffusion. For this the experimental data were taken to solve Equation 4.15 and estimate the criterion of diffusion. The results gave a Bischoff criteria that ranged between 1.92 and 12.95, indicating that the reaction was influenced by internal concentration gradients. Consequently, the reaction rate shown in Equation 4.35 must include the effect of the diffusion process through the evaluation of the effectiveness factor. Based on an excess of oxygen concentration, because the SR was calculated as a function of the initial DBU concentration, and to simplify the solution of the calculation of the effectiveness factor a reaction order of 1 was assumed. The resultant expression can be given as shown in Equation 4.28. Once the effectiveness factor is evaluated it will be incorporated into Equation 4.27 (reactor model) and then used to calculate the new kinetic parameters in the absence of the diffusion effects.

This led to the best fitting of the experimental data for the oxidation of DBU in terms of the TOC content with confidence limits of 95% is shown in the following equation:

$$\mathscr{R}_{TOC} = 4.5991 \pm 0.2557\, C_{TOC}^{0.6972\pm0.0484}\, C_{O_2}^{0.4398\pm0.0426} \tag{4.36}$$

Equation 4.36 differs from 4.35 mainly on the reaction order of the oxygen which has been augmented by the inclusion of the effectiveness factor to account for the phenomenon intrapartcle diffusion. By using the experimental data at different temperatures and assuming that the reaction could be represented by the Arrhenius equation, the dependence of the reaction rate on temperature is given by calculating the Arrhenius parameters:

$$\mathscr{R}_{TOC} = 4.6698\text{x}10^5 \pm 2.4282\text{x}10^5 \exp\left(-\frac{63.9696 \pm 3.1115}{RT}\right) C_{TOC}^{0.6972\pm0.0484}\, C_{O_2}^{0.4398\pm0.0426} \tag{4.37}$$

The parameters obtained were calculated within a confidence limit of 95% and are expressed in terms of the volumetric properties of the reacting mixture and where the activation energy is given in kJ/kmol.

4.4.4 Product Identification

The distribution of carbon and nitrogen of the CSCWO over the mixed MnO_2/CuO catalyst was studied at a temperature interval of 673 to 773 K at a constant pressure of 23.0 MPa. The initial concentration of DBU was kept at 1.1 mmol/L and the oxygen was fed at a SR of 1. The oxidation reaction was studied at space velocities of 0.2, 0.4 and 0.7 s^{-1}. Although, the total organic carbon content was detected, its low concentration values did not allow to identify some individual products by GC-MS. The initial pH of the reactant solution was from 10.7 to 11.9 which dropped to a pH of 6.6 to 7.2 after the reaction. In Figure 4.34 the carbon and nitrogen fraction distribution of the products are given as a function of temperature at space velocity of 0.4 s^{-1}. The main carbon product of the reaction was carbon dioxide which increased with reaction temperature, however carbon monoxide and inorganic carbon (in the form of carbonates and bicarbonates) concentration did not change in the reaction. The carbon monoxide and the carbonates are incomplete reaction products during the oxidation of carbon that produced carbon dioxide as final product.

In the case of the distribution of nitrogen only inorganic products in the liquid stream were identified. Nitrogen oxides were not detected in the gas stream. The reaction produced a high amount of the ammonium ion, although the concentration of nitrates and nitrites were low. This suggests that the ammonium ion was formed from ammonia formation during the reaction, and as a consequence of the aqueous media was very stable and was hardly oxidised to molecular nitrogen, this explains the low values of nitrates and nitrites in the reaction. In the Figure 4.34b, the production of ammonium ion diminished at 723 K which is likely to be a consequence of the ammonia equilibrium reaction being displaced at this temperature. It can therefore be concluded that the mixed catalyst of MnO_2/CuO was not very selective for the complete oxidation of the ammonia produced during the reaction.

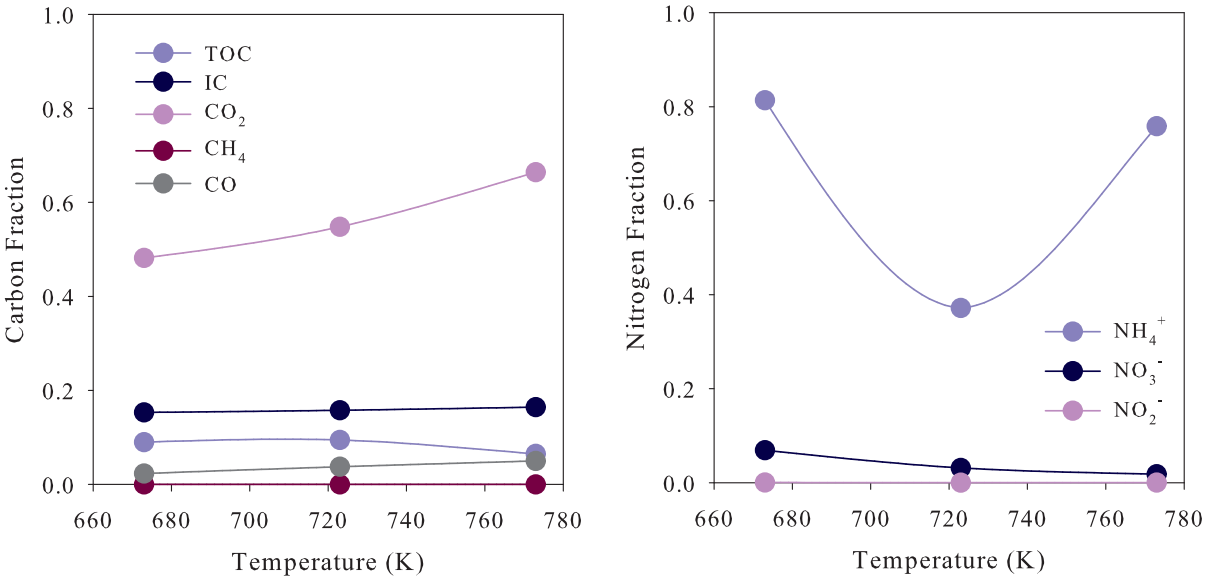

a) Distribution of Products Containing Carbon

b) Distribution of Products Containing Nitrogen

Figure 4.34: Carbon and Nitrogen Fraction for the CSCWO of DBU over MnO_2/CuO

4.4.5 Catalyst Activity

Under severe operating conditions catalysts are likely to deactivate due to the thermal and mechanical stress at which they are exposed, especially in the presence of an oxidative and corrosive atmosphere. A test carried out at 673 K and 23.0 MPa was used to investigate the activity of the catalyst. During the experiment a constant space velocity of 0.2 s^{-1} was maintained. The

reacting mixture contained an initial concentration of 0.3 mmol of DBU/L and oxygen was supplied at a SR of 1. The test was performed for 8 hours and samples were taken regularly for subsequent analysis. Figure 4.35 shows the activity of the catalyst measured by the amount of the TOC removed during the experiment. The removal of TOC dropped to around 13.5% during the first hour of experiment; after the first hour of operation, the catalyst maintained almost a constant activity. Residues of copper and manganese in the effluent of the reactor were detected at a maximum concentration of 0.043 ppm of copper and 0.045 ppm of manganese. The loss of the metals was probably due to the poor mechanical properties because of the lack of a support for the catalyst.

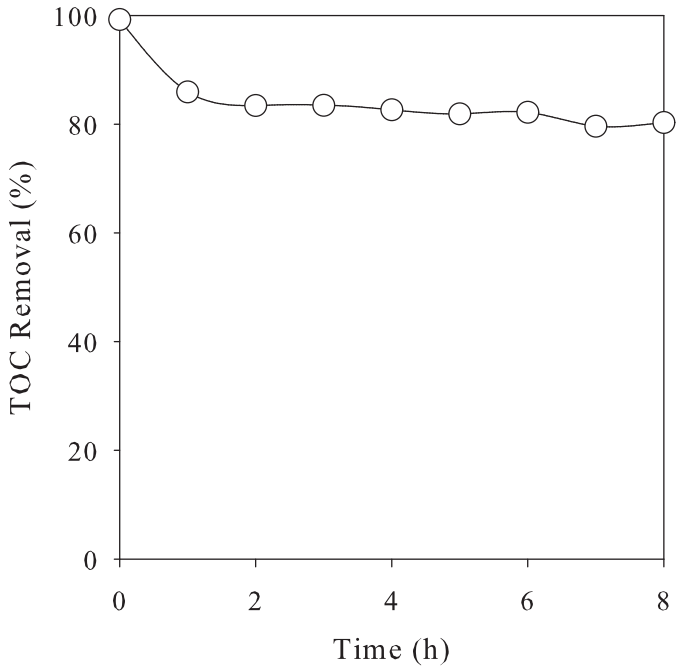

Figure 4.35: Catalyst Stability under CSCWO of DBU over MnO_2/CuO

In addition, analysis carried out by DVS showed that the catalyst surface area was reduced from 195 to around 63 m^2/g, which also explains the loss in the activity of the catalyst. Analysis by DVS demonstrated that the adsorption-desorption mechanism over the mixed catalyst was different than the Pt and CuO supported catalyst (refer to Appendix D for details in the difference between water intake mechanisms). The mechanism was observed to be the same in the fresh and spent catalyst, however the spent catalyst showed a lower water intake which indicated a surface structure change.

XRD analysis has shown changes in the structure of the catalyst; the fresh catalyst was an amorphous material, however the spent catalyst showed changes due to the presence of crystalline structures (see Appendix E). The catalyst has an amorphous MnO_2/CuO chemical structure and the X-ray diffraction identified a crystalline structure in which the oxidation state of manganese (Mn^{2-}) has changed to form Mn_2O_3. This phase is the most stable phase of the manganese oxides and has been reported by other research studies after being subjected to the catalytic oxidation of MnO_2 in supercritical water [289]. Also Cu_2O has been identified from the transformation of the copper in the process. Another structure, which is a mixed oxide ($CuMn_2O_4$) was formed during the reaction.

4.5 Summary of Findings

It has been demonstrated experimentally that hydrogen peroxide is completely decomposed to produce oxygen and water in the preheating section. This fact proved that the oxidation reaction can be attributed only to the presence of oxygen in the reactor rather than hydrogen peroxide. It has also been demonstrated that the packing material did not promote the oxidation.

CSCWO of DBU was carried out over Pt, CuO and MnO_2/CuO catalyst. Only traces of DBU were identified in the effluent of the reactor, and consequently the reaction was followed by the change in the TOC content of the samples. The presence of external and internal concentration gradients have been also experimentally assessed. External concentration gradients were not present at the reaction conditions studied. However, internal concentration gradients existed when the reaction took place over Pt and MnO_2/CuO mixed catalysts. Although, the particle size was reduced to avoid the presence of the internal concentration gradient by facilitating the transport of the reagents within the catalytic particles, the reaction is fast enough that the transport of the reactants controlled the heterogeneous reaction.

A series of experiments were performed to evaluate the reproducibility of the experiments and thus the experimental error. The experimental error obtained tended to be higher as the flow rate was increased. This is a consequence of a reduction in the ability to accurately control the system pressure at high flow rates. HPLC pumps were used to vary the space velocity and pressurise the system.

The effect of temperature, pressure, initial concentration of DBU and oxygen on the catalytic

oxidation reaction were studied. Temperature was the main controlling variable of the process; operation at high temperature led to almost complete elimination of TOC at temperatures of 773 K. CSCWO reduced the severity and improved the efficiency of the process compared with a non-catalytic reaction where the TOC content was not reduced at temperature of 873 K [167].

The effect of pressure did not follow a clear trend among the catalysts. In the case of the reaction over Pt, the increment of the system pressure hindered the elimination of the TOC. For the two other catalysts studied, the pressure effect on the TOC removal was smaller and on the contrary favored its elimination. The contribution of pressure in the reaction is minimal and it could be overlooked for design purposes. This is on the basis that the efficiency of the process was maintained at the lowest value of pressure studied.

The reaction was not limited by the initial content of DBU in the stream; a higher concentration of reactants in the reacting mixture favoured the reaction. However, the amount of oxygen supplied above a stoichiometric values of 5 only slightly increased the TOC removal. The effect of oxygen concentration was appreciable when the oxygen was increased from a SR of 0.5 to 1 which made the reaction proceed faster.

Catalytic reactions are often chosen to be represented by adsorption or desorption reaction models of the Langmuir-Hinshelwood-Hougen-Watson type (LHHW). In the present chapter, these models were not used due to the lack of information of the precise mechanism of the reaction. In addition, because unreacted DBU could not be detected in the stream, only the TOC content was employed for the purpose of determining the kinetics of the reaction. Albeit, some LHHW reaction models have been proposed for the catalytic oxidation at supercritical conditions of organic compounds [204, 205, 207, 208, 216, 217, 218], there are uncertainties of the precise mechanism followed by the reaction and thus were not considered.

The kinetics of the reaction were represented by the means of a power-law kinetic model. As the reaction was heterogeneous, the model was considered as pseudo-homogeneous. The integral method of analysis was adopted to fit the experimental data into the continuity equation of a plug flow reactor. The power-law represented adequately the experimental data, nonetheless the evaluation of the criterion proposed by Bischoff to the individual reactions showed that those over Pt and MnO_2/CuO were affected by intraphase concentration gradients. During the experiments some considerations were carried out to avoid the presence of internal concentration gradients, but

the nature of the reaction did not allow operation in a zone where the kinetic reaction dominates the phenomenon. Consequently, the reaction rate model was modified by incorporating the effectiveness factor to account for the mechanism of diffusion within the catalytic particles. Table 4.12 shows a summary of the kinetic parameters obtained after fitting the experimental data. The reaction order with respect to the TOC concentration varied in all reaction rate models and the highest value was obtained for the reaction over Pt. For the case of oxygen concentration, the values were smaller than those for the TOC. The effect of oxygen in the reaction over Pt and CuO were similar, however the order over MnO_2/CuO was around three times larger.

Table 4.12: Kinetic Parameters of the CSCWO of DBU

Kinetic Parameter	Pt	CuO	MnO_2/CuO
Reaction Order of C_{TOC}	1.3730	1.0811	0.6972
Reaction Order of C_{O_2}	0.1544	0.1608	0.4398
Activation Energy, kJ/mol	109.5381	85.5823	63.9696

In order to compare the activity of the catalyst, the reaction rates over individual catalysts were used to produce a plot of predicted TOC removal against $WHSV^{-1}$ at 673 and 773 K. The pressure was held constant at 23.0 MPa, meanwhile the DBU initial concentration was 0.3 mmol/L and a SR of oxygen of 1. Figure 4.36 depicts the results of the calculations performed. At 673 K and $WHSV^{-1} = 0.1$ s, the TOC removal was 61% for Pt, 9% for CuO and 26% for the MnO_2/CuO (Figure 4.36a). An increment in temperature produced more efficient reactions; at 773 K and $WHSV^{-1} = 0.1$ s the TOC removed was around 95% for the Pt catalyst. A similar trend was found for the reaction over CuO and MnO_2/CuO where the removal rose to 26% and 55%, respectively (Figure 4.36b). According to the results of the present study the catalyst activity was found to be of the order $Pt > MnO_2/CuO > CuO$.

Besides the elimination of TOC from the stream, the catalysts were compared by the intermediates produced during the reaction, which were mainly inorganic carbon and nitrogen species. Pt again produced the less amount of carbon intermediates, which in the liquid phase were in the form of CO_3^{2-} and HCO_3^- species. Carbon in the outlet gas stream occurred mainly in the form of CO_2, nevertheless traces of CO and CH_4 appeared at 773 K. The transition metal oxides produced a higher amount of inorganic carbon, which was independent of the operating

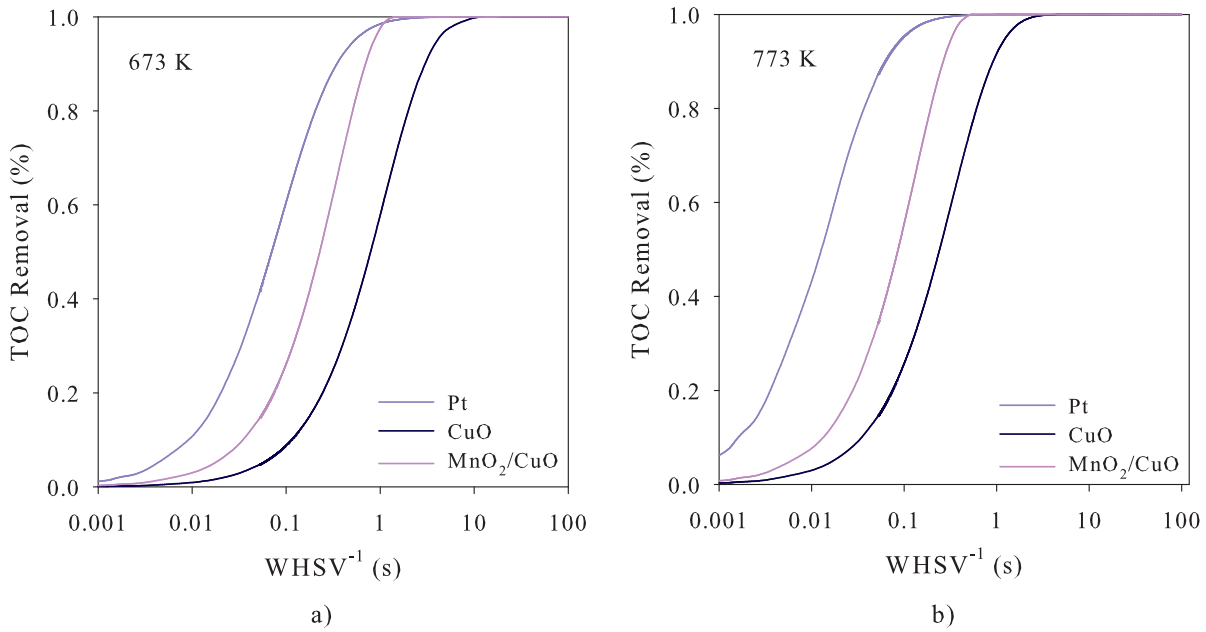

Figure 4.36: Catalyst Comparison for the CSCWO of DBU

temperature. They also produced a higher concentration of CO in the gas stream than Pt. The production of CO was lower over the MnO_2/CuO, which in this case saw an increase at higher reaction temperature. CSCWO over Pt, CuO and MnO_2/CuO showed that CO_2 production was the most favoured carbon species.

The oxidation of nitrogen represented another complex mechanism because of the intermediates identified during the reaction. It has been pointed out (supported by a developed detailed kinetic reaction mechanism) that ammonia is one of the main products of oxidation of nitrogen-containing organic compounds in supercritical water. However, ammonia formation pathways are not completely understood in SCW [175]. Cocero et al. [182] have experimentally demonstrated the occurrence of ammonia formation as an intermediate during the SCWO of several nitrogen containing organic streams.

Ammonia oxidation in supercritical water has been the centre of different studies because of the difficulty to achieve its complete conversion to N_2. An early study by Killilea et al. [293] revealed the production of inorganic nitrogen species such as nitrates and nitrites ions (dissociation products from mineral acids) and proved that NO_x formation was not favoured in SCWO. The study also suggested that NO_x^- ions were present as intermediates before they

reacted to produce N_2 and N_2O. The low favoured production of NO_x and the presence of NO_x^- ions has been confirmed from another experimental study of the oxidation of different nitrogen-containing organic compounds [182]. A set of reactions have been proposed for the ammonia reaction mechanism as follows [293]:

$$2N_2 + O_2 \longleftrightarrow 2N_2O \tag{4.38}$$

$$4NH_3 + 3O_2 \longleftrightarrow 2N_2 + 6H_2O \tag{4.39}$$

$$2N_2 + 2H_2O + 5O_2 \longleftrightarrow 4HNO_3 \tag{4.40}$$

$$2N_2 + 2H_2O + 3O_2 \longleftrightarrow 4HNO_2 \tag{4.41}$$

Dell'Orco et al. [168] suggested that ammonia oxidises through a more complex reaction involving an ionic and free radical mechanism. They also argued that the NO_x were formed, but they further reacted to produce the observed products of N_2 and N_2O.

Although their work was mainly on non-catalytic reaction their findings could be extrapolated to explain the presence of the nitrogen species in the products of the reaction. According to Ding et al. [216] catalytic oxidation of ammonia in supercritical water has been demonstrated as an efficient alternative to alleviate the operating condition required. During their experiments NO_2^- has been detected at low concentration levels. Oxidation of ammonia in subcritical conditions has proved the presence of nitrites as products of the reaction, and it has been suggested that NO_2^- participated in the conversion to N_2 [294, 285], which explains the smaller proportion of the species compared to NO_3^-. Because both ions are intermediates, their concentration in the outlet stream will indicate the degree of conversion of ammonia in the reaction.

The reaction performed over Pt produced less nitrogen containing intermediates. NH_4^+ and NO_2^- concentrations were small compared to NO_3^-, which also explained the change in the pH of the solution. The concentration of nitrates were reduced with temperature although the production of NH_4^+ was favoured at high temperature, which suggests that Equations 4.39 and 4.40 predominated at such conditions.

CuO catalyst did not effectively remove the ammonia produced during the reaction even at high temperature. The amount of NH_4^+ produced did not appreciably change during the reaction, which explained the low content of nitrates and nitrites in the reaction, and thus the alkaline pH. Although CuO has been demonstrated to produce a high selectivity towards N_2, the presence of a high concentration of water in the system shifts the reaction towards a different mechanism. Here Equation 4.40 is shifted to the right hand side and nitric acid production is favoured over the nitrogen production [295]. This does not occur in the gas phase reactions [290, 296].

The MnO_2/CuO produced also a high concentration of incomplete nitrogen oxidation species. This showed that although a faster reaction was obtained over this catalyst, in terms of organic carbon oxidation, it was not very effective for the oxidation of ammonia. Thus Pt has been demonstrated to be the most effective of the catalysts for both carbon and nitrogen oxidation.

The activity of the catalysts during each reaction fell from their initial values around the first hour of operation. This was especially observed for the CuO and MnO_2/CuO catalysts, nevertheless their activities were maintained until the end of the tests. DVS, ICP-OES and XRD analyses have confirmed changes in the structure of the catalyst and loss of active metal contributed to the deactivation. Three factors have been found to be responsible for the loss of activity:

1. Reduction of the surface area of the catalyst.
2. Leaching of the active metal.
3. Changes in the morphology of the catalyst.
4. Changes in the oxidation state of metals.

Catalyst transformations occurred due to the instability of the metals and oxide metals at supercritical conditions where predominant species such as $AlO(OH)$, Mn_2O_3 and Cu_2O were found in the spent catalyst. These new structures would have exhibited a good activity during the process although the slow leaching of the active metals would have also contributed in lower the activity of the catalysts.

Chapter 5

CSCWO of Quinoline

Owing to the difficulty of the destruction of nitrogen containing heterocyclic compounds, in this chapter is presented a study of the destruction of quinoline by catalytic supercritical water oxidation. Quinoline (see Figure 5.1) is a non-biodegradable organic compound which require operating conditions higher than 823 K and 25.0 MPa to be efficiently removed by non-catalytic SCWO [260]. It is believed that in the presence of a catalyst these conditions can be lowered.

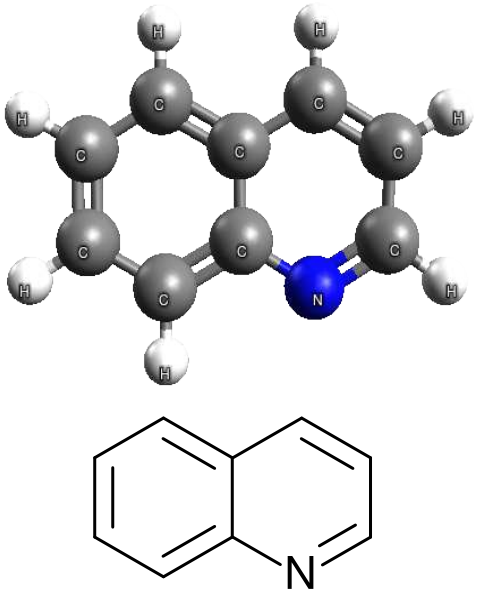

Figure 5.1: Chemical Structure of Quinoline

In the pharmaceutical industry, quinoline is part of the structure of many antiseptics and antibiotics, though it is also used to produce dyes, herbicides and paints. It is a mutagen agent which also attacks the human respiratory system; continuous exposure causes liver damage and can create allergic responses [297, 298].

The stoichiometric reaction that represents the complete oxidation of quinoline is given by

$$2C_9H_7N + 21.5O_2 \longrightarrow 18CO_2 + 7H_2O + N_2 \tag{5.1}$$

From the reaction the stoichiometric ratio (SR) of oxygen to quinoline is defined as the amount of oxygen required to completely oxidised the quinoline present in the stream based on the initial concentration of quinoline as defined by:

$$\text{SR} = \frac{v_Q C_{O_2\,0}}{v_{O_2} C_{Q_0}} \tag{5.2}$$

Where v_Q is the stoichiometric coefficient of quinoline, v_{O_2} is the stoichiometric coefficient of oxygen, $C_{O_2\,0}$ is the initial concentration of oxygen and C_{Q_0} is the initial concentration of quinoline. The efficiency of the process is given in terms of the remaining organic compound and TOC according to

$$Removal_{TOC} = \frac{C_{TOC_0} - C_{TOC}}{C_{TOC_0}}(100) \tag{5.3}$$

$$Removal_Q = \frac{C_{Q_0} - C_Q}{C_{Q_0}}(100) \tag{5.4}$$

Where C_{TOC_0} and C_{TOC} are the initial and final concentration of the total organic content, respectively and C_Q is the concentration of quinoline.

5.1 CSCWO of Quinoline over Pt Catalyst

It has been demonstrated in previous CSCWO studies that nitrogen-containing organic compounds can be efficiently eliminated by using a platinum catalyst [214, 215]. Precious metals like platinum are expensive, however they have been shown to lead to fast reactions. Aki and Abraham [299] have demonstrated that by promoting faster reactions than the non-catalytic process, the overall CSCWO could be cost effective compared with some other aqueous wastewater treatment processes.

5.1.1 Evaluation of the External and Internal Concentration Gradients

The presence of external (interphase) and internal (intraphase) concentration gradients were experimentally assessed according to the procedures described in Chapter 4 [250, 267]. The tests

were performed to evaluate whether during the chemical reaction the presence of concentration gradients has any influence on the experimental data.

5.1.1.1 Interphase Concentration Gradients

The evaluation of external concentration gradients were studied at 673 K and 23.0 MPa. During the experiments the initial concentration of quinoline was kept constant and oxygen was fed at a SR of 1. In order to accomplish an operation regime in which the conversion is independent of the superficial velocity (flow rate) at the same space velocity ($WHSV$, a ratio of volumetric flow rate to weight of catalyst); tests were performed with different amounts of catalyst which were weighed and placed in the reactor. Five experiments were performed with catalyst weights of 0.08, 0.16, 0.24, 0.32 and 0.40 g, and to maintain a constant space velocity for each of them the volumetric flow rate of the reacting mixture was varied proportionally. In the tests, a catalyst particle size of 355-425 μm was selected; the catalyst was diluted with sand (v:v, 4:1) with a particle size of 212-250 μm. Samples were taken at space velocities of 0.3, 0.5, 0.7 and 0.9 s^{-1}. Figure 5.2 depicts the findings. The results show that the lowest conversion was obtained for a catalyst weight of 0.04 g at 0.7 and 0.9 s^{-1}. Above a catalyst weight of 0.08 g, there was just a slight change in the conversion when the flow rate was increased at constant $WHSV$. To summarize, by using amounts of catalyst higher than 0.08 g, it can be assured that interphase concentration gradients will not be present.

5.1.1.2 Intraphase Concentration Gradients

To assess internal concentration gradients a series of tests were performed using different particle sizes. The catalyst particle sizes employed during the study are presented in Table 5.1. The reagent concentrations of 0.3 mmol of quinoline/L and oxygen were introduced into the mixing chamber to give a SR of 1. For the experiments a total of 0.24 g of catalyst was diluted with sand with a particle size of 212−250 μm and packed into the tubular reactor. The operating conditions were held constant at 673 K and 23.0 MPa. Samples were taken at space velocities from 0.3 to 1.3 s^{-1} and the plot of removal in terms of the TOC against the particle size is shown in Figure 5.3. At spaces velocities higher than 0.3 s^{-1}, the removal of TOC increased considerably up to average catalyst particle sizes of 98 μm. At smaller particles sizes the conversion did

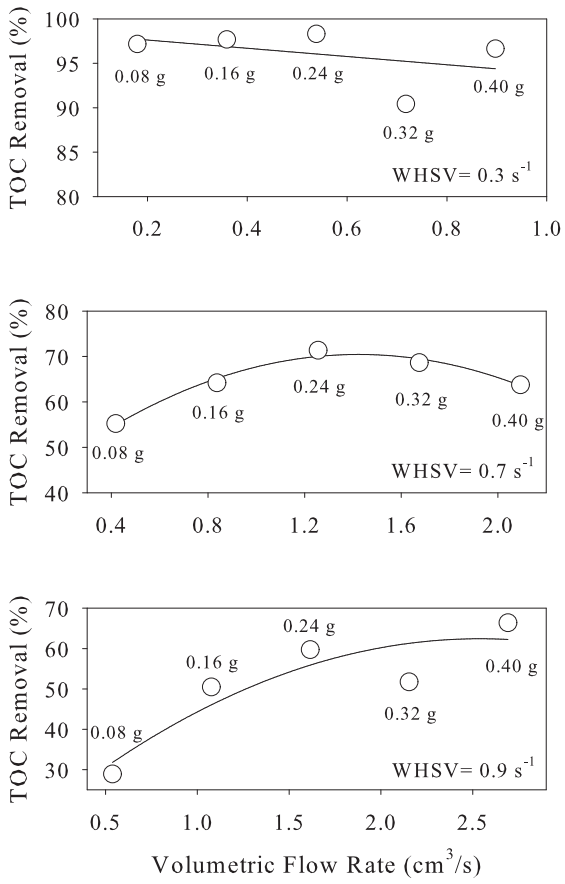

Figure 5.2: External Concentration Gradients of Quinoline on *Pt*

not change considerably, nevertheless there was still uncertainty about disregarding the internal concentration gradients. This will be assessed by the calculation of the criterion proposed by Bischoff [280] in Section 5.1.3.

Table 5.1: Catalyst particle sizes for Evaluation of Internal Concentration Gradients over *Pt*

Experiment	Particle Size Range, μm	Average Particle Size, μm
1	355−425	390.0
2	250−300	231.0
3	150−212	181.0
4	90−106	98.0
5	45−63	54.0

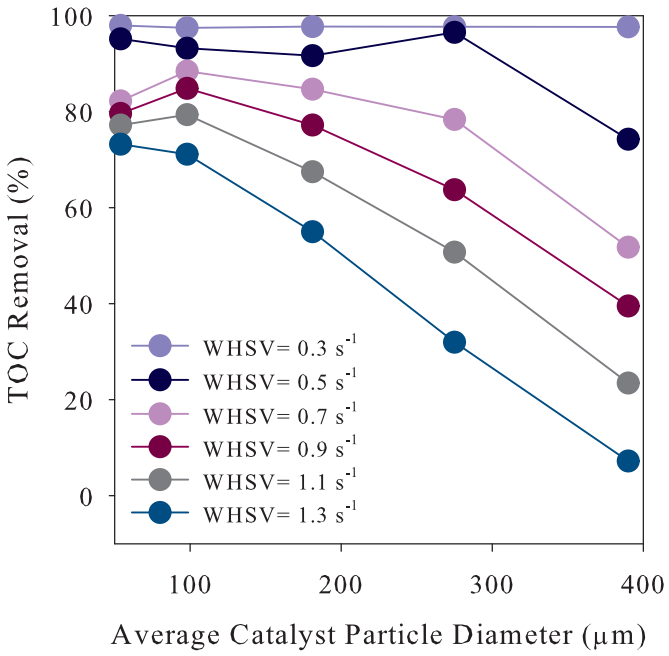

Figure 5.3: Internal Concentration Gradients of Quinoline on *Pt*

5.1.2 Reproducibility Tests and Effect of Key Operating Conditions

Once the effects of interphase and intraphase concentration gradients have been evaluated, the appropriate weight and particle size of catalyst were conveniently selected not only to avoid mass transfer limitations in the reaction but also to allow an isothermal and isobaric reactor operation. A series of experiments were planned to assess, firstly the experimental error and later to study the effect of the temperature, pressure, initial concentration of quinoline and oxygen over the catalytic reaction. Table 5.2 condensates the experimental conditions studied and provides information of the catalytic bed.

5.1.2.1 Reproducibility Tests

A series of five experiments were carried out to evaluate the experimental error during the catalytic study. During each test the temperature and pressure were kept constant at 673 K and 23.0 MPa, respectively. The reacting mixture had a concentration of quinoline of 0.3 mmol/L and oxygen was supplied at a SR of 1. Samples were taken at space velocities ranging from 0.3 to 1.3 s^{-1}, and subsequently analysed by TOC and HPLC. The maximum variation of temperature

Table 5.2: Experimental Conditions of CSCWO of Quinoline over Pt

Parameter	Interval Studied
Temperature Range, K	653-773
Pressure Range, MPa	23.0-30.0
Initial Quinoline Concentration Range, mmol/L	0.2-0.6
Initial Concentration of Oxygen Range (SR)	0.5-10
Catalyst weight, g	0.24±0.0001
Catalyst particle size, μm	45-63
SiO_2 particle size, μm	212-250
Bed length, cm	7.5±0.1
Dilution factor catalyst to SiO_2, v:v	4:1

and pressure in the reactor were ±1 K and ±0.35 MPa. Moreover, the maximum pressure drop measured of the system was 0.3 MPa. Consequently, the reactor was considered to operate in an isobaric and isothermal regime. The latter was also assured because despite the oxidation reaction being highly exothermic, the dilution of the catalyst with inter material (sand) and the low concentration of reagents avoided the presence of hot spots in the catalytic bed [250, 267]. After the analysis the average removal of quinoline and TOC content and its standard deviation was calculated for the five samples taken at each space velocity, and the results obtained are presented in Table 5.3. The results are also shown in Figure 5.4, where the error bars represent ±1 standard deviation of the average value calculated.

The reaction was fast at space velocities of 0.3 s^{-1} where the removal in terms of TOC and quinoline reached values close to 99%. The overlapping of both curves indicate that production of intermediates was minimised. TOC is related to the production of intermediates and is based on that if conversion was due to only the remaining quinoline, the removal of TOC and quinoline would be equal. It was also noticed that the experimental error tended to increase at higher space velocities where the control of pressure for a given flow rate was less accurate.

Table 5.3: Reproducibility Tests of CSCWO of Quinoline over Pt

$WHSV$, s^{-1}	Average TOC Removal, %	Std. Dev. TOC Removal, %	Average Quinoline Removal, %	Std. Dev. Quinoline Removal, %
0.3	99.09	0.34	99.13	0.27
0.5	98.84	0.85	98.18	0.95
0.7	94.54	4.26	93.45	2.70
0.9	86.88	5.55	87.15	3.91
1.1	79.01	7.73	79.62	8.11
1.3	67.82	9.23	69.33	10.69

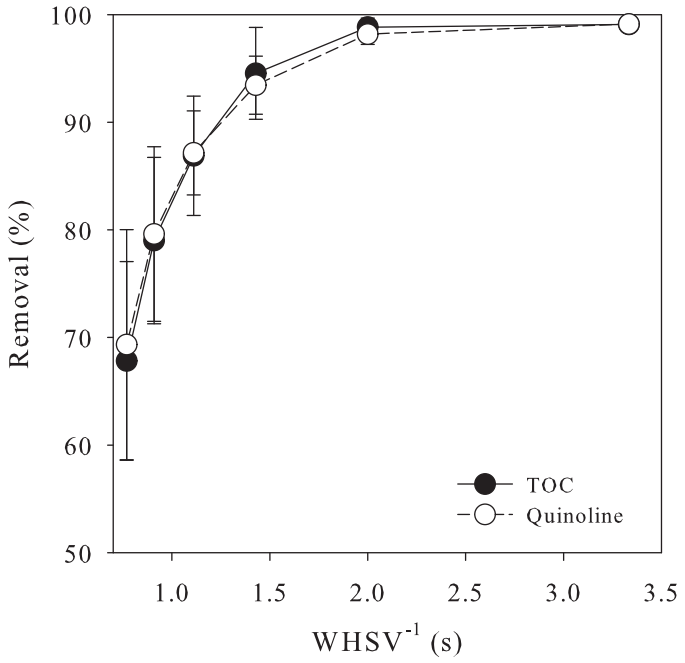

Figure 5.4: Reproducibility Tests of CSCWO of Quinoline over Pt

5.1.2.2 Effect of Temperature on the CSCWO of Quinoline over Pt

For this purpose a series of experiments were undertaken at the isobaric condition of 23.0 MPa, while the temperature was varied 653 to 773 K. The reactants were fed to the reactor at a concentration of 0.3 mmol of quinoline/L and oxygen at a SR of 1. The influence of temperature

on the reaction is depicted in Figure 5.5 where the efficiency is given in terms of TOC and quinoline removal.[1] The effect of temperature was negligible at $WHSV = 0.3$ s^{-1} where the reaction was near completion. Higher space velocities showed that the content of TOC and quinoline were reduced as the temperature was increased. However, the influence of temperature on the reaction was lowered considerably greater than 748 K when the removal of TOC and quinoline were narrowed to a small region where they almost did not depend on the space velocity. At 773 K, the removal in terms of both parameters became constant and completely independent of the space velocity. Furthermore, intermediates formation was reduced as the temperature in the system was increased. Consequently, it was shown that the removal of quinoline and TOC was efficient at temperatures close to the critical point of water where the energy consumption of the process was low.

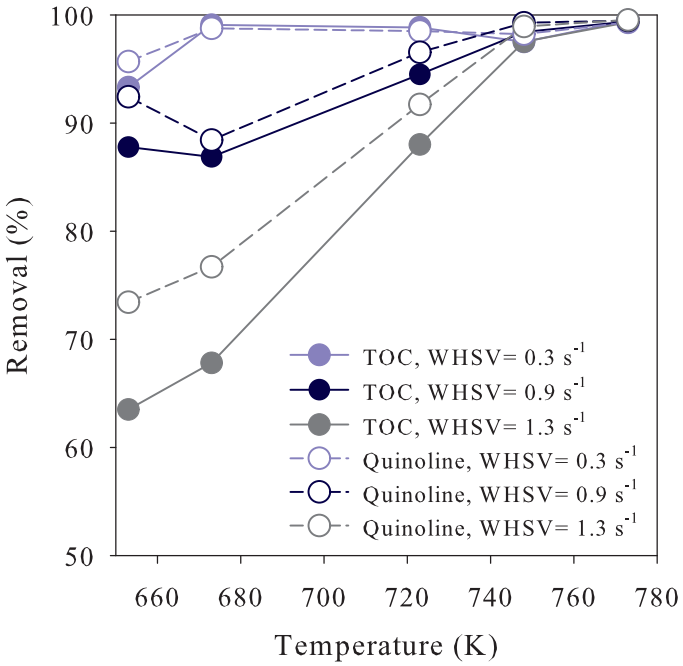

Figure 5.5: Effect of Temperature in the CSCWO of Quinoline over *Pt*

[1] Although a total of 6 space velocities were studied in this and subsequent sections, for clarity in the presentation of experimental results only those at 0.3, 0.9 and 1.3 s^{-1} were plotted.

5.1.2.3 Effect of Pressure on the CSCWO of Quinoline over *Pt*

The reliance of the removal of TOC and quinoline on the system pressure was studied by varying this parameter from 23.0 to 30.0 MPa at a constant temperature of 673 K. The concentration of quinoline and oxygen were held at 0.3 mmol of quinoline/L and a SR of oxygen of 1. In these experiments the reacting mixture density increased from 133.76 kg/m^3 at 23.0 MPa to 240.0 kg/m^3 at 30.0 MPa. The concentration of the reactants were accordingly adjusted because the density change of the reacting mixture. The effect of pressure on the the removal of quinoline and TOC is shown in Figure 5.6. When space velocities higher than 0.3 s^{-1} were used, the elimination of TOC was slightly decreased by the system pressure, whereas it did not have an appreciable influence on the quinoline removal. The quinoline values decreased slightly when the pressure reached 30.0 MPa.

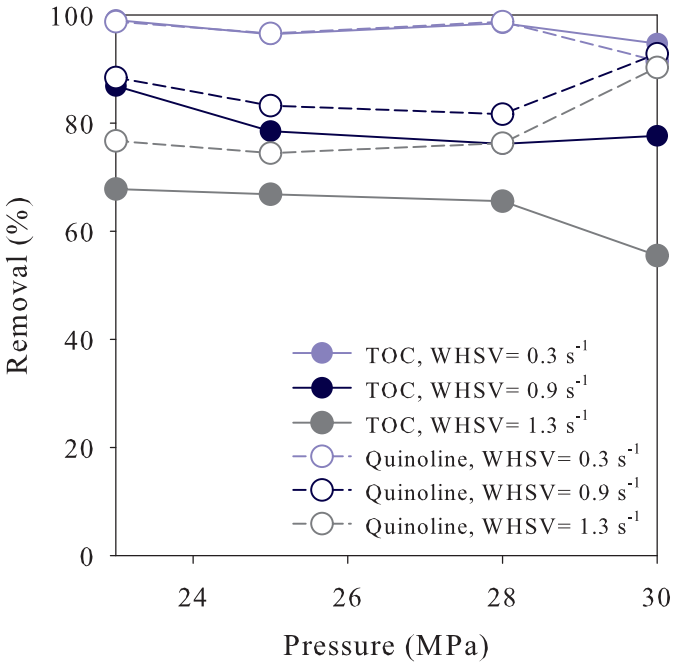

Figure 5.6: Effect of Pressure in the CSCWO of Quinoline over *Pt*

5.1.2.4 Effect of Initial Quinoline Concentration on CSCWO over *Pt*

Quinoline and TOC removal dependence on the initial quinoline concentration was performed at 673 K and 23.0 MPa. For this purpose the initial concentration of quinoline in the inlet stream was varied from 0.2 to 0.6 mmol/L, in each experiment the oxygen met a SR of 1. The space

velocity was varied from 0.3 to 1.3 s^{-1} and samples were taken for analysis. Figure 5.7 shows that the removal of quinoline and TOC was affected to a minor extent by the increment of the initial concentration of quinoline from 0.2 to 0.3 mmol/L at 0.9 and 1.3 s^{-1}. Above 0.3 mmol/L of quinoline the removal of TOC or quinoline remained unchanged. The production of intermediates were also unaffected by the increment of the concentration of the organic compound. Both TOC and quinoline removal followed the same trend and remained at the same distance apart. It is important to notice that at $WHSV = 0.3$ s^{-1} there was almost not production of intermediates and quinoline was oxidised almost completely.

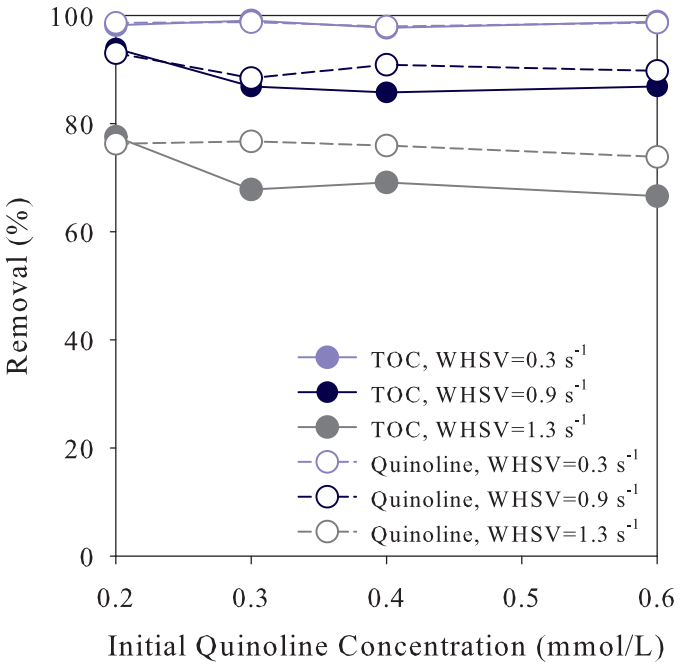

Figure 5.7: Effect of Initial Quinoline Concentration in the CSCWO over *Pt*

5.1.2.5 Effect of Initial Oxygen Concentration on the CSCWO of Quinoline over *Pt*

The behaviour of the reaction under the presence of different oxygen concentration was studied by varying the oxygen supplied from a concentration lower than the minimum required for the complete oxidation of quinoline (SR=0.5) to a high excess of oxygen (SR=10). The quinoline was supplied at a constant concentration of 0.3 mmol/L during each experiment and the operating conditions were maintained at 673 K and 23.0 MPa. The results of the effect of oxygen

concentration in the reaction is shown in Figure 5.8. At $WHSV = 0.3\ s^{-1}$ and in the presence of oxygen concentration lower than the minimum required, the elimination of TOC and quinoline was close to 98%. At higher space velocities by increasing the concentration of oxygen to a SR of 1, the elimination of TOC and quinoline increased approximately of 40%, which showed the strong dependence of the reaction on the oxygen concentration. However, the influence of oxygen was lowered when higher concentration other than SR of 1 were used. Because the gap between the TOC and quinoline removal curves at $WHSV = 1.3\ s^{-1}$ were unchanged, oxygen did not improve the break down of the intermediates formed in the reaction. Nonetheless, their elimination was highly reduced by the presence of the Pt catalyst at lower space velocities.

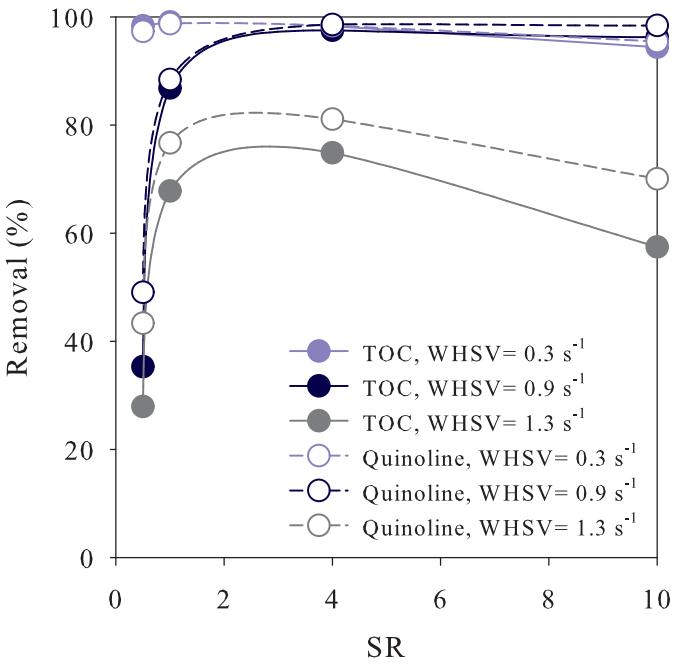

Figure 5.8: Effect of Initial Oxygen Concentration in the CSCWO of Quinoline over Pt

5.1.3 Kinetics of the Reaction

The experimental data obtained at 673 K and 23.0 MPa were fitted into the continuity equation of an ideal tubular reactor coupled to the power law reaction rate model by assuming a pseudo-homogeneous reaction [273]. The best fitting parameters obtained after solving the minimisation routines are shown in the following expression for the reaction rate of quinoline oxidation over Pt catalyst with confidence limits of 95% on the regression of the parameters (details of the fitting

of the experimental data are given in Appendix B):

$$\mathscr{R}_Q = 15.9295 \pm 10.0917\, C_Q^{1.0217\pm0.1978}\, C_{O_2}^{-0.0423\pm0.0778} \tag{5.5}$$

Figure 5.9 shows a plot of the comparison of the experimental data with those calculated by the fitted reaction rate. The model gives good agreement with the experimental data and only two points lie outside the line of ±10%. This demonstrates that relatively simple reaction rate models can be employed in the fitting of the heterogeneous catalytic reactions when no information of the precise reaction mechanism is available. This avoids the assumption of typical heterogeneous adsorption-desorption reaction mechanisms like LHHW.

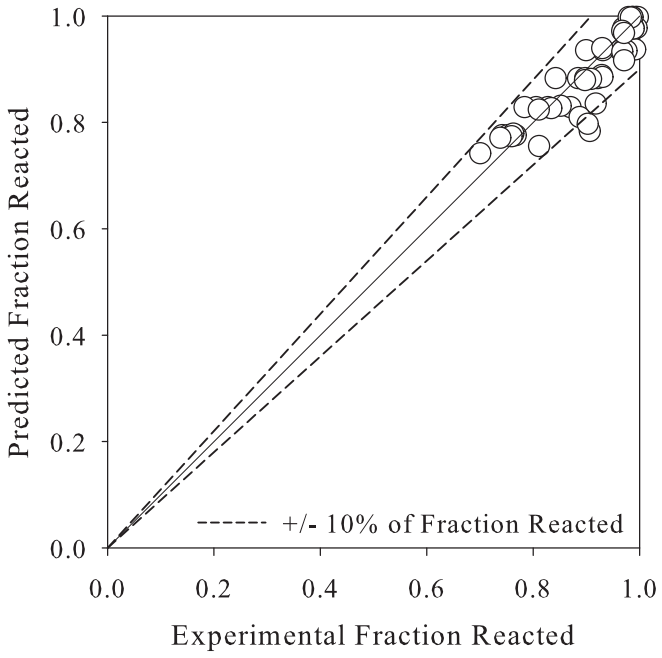

Figure 5.9: Comparison of Predicted and Experimental Fraction of Quinoline Reacted over Pt

As the oxidation reactions over Pt were fast, it is important to corroborate the absence of internal concentration gradients. As it was explained in Chapter 4, the evaluation can be done through the calculation of the criteria proposed by Bischoff [280]:

$$\frac{\mathscr{R}_{i_{Obs}} d_p^2 g(C_{i_{Obs}})}{2\mathscr{D}_{i_{Eff}} C_{i_0} \int_{X_{i_{Obs}}}^{1} g(X_i) dX_i} < 1 \tag{5.6}$$

Based on the equation proposed by Woerlee [136], the molecular diffusivity of quinoline ($\mathscr{D}_{i_m}$) in supercritical water at 673 K and 23.0 MPa was calculated to be 1.17953x10^{-7} m^2/s and from it the effective diffusivity ($\mathscr{D}_{i_{Eff}}$) was calculated to be 7.47037x10^{-9} m^2/s from Equation 5.7.

$$\mathscr{D}_{i_{Eff}} = \frac{\epsilon}{\tau}\mathscr{D}_{i_m} \tag{5.7}$$

Where the voidage of the catalytic bed (ϵ) is 0.38[2] and the tortuosity factor (τ) was assumed to be 6 [281]. The effective diffusivity was thus used to compute the criteria proposed by Bischoff. The values ranged between 5.0 and 6.6 showing that the internal diffusion of reactants was significant to affect the calculation of the kinetic parameters. Consequently, the kinetic parameters found were obtained in a region where diffusion prevailed over the kinetics of the reaction.

Consequently, the fitting of the experimental data was modified to account for the diffusion effect by the calculation of the Thiele modulus and the effectiveness factor coupled into the continuity equation of a tubular reactor, which in normalized parameters is given as [281, 282, 283]:

$$\frac{dv_Q}{dz} = \frac{\eta\, k\, C_Q^a\, C_{O_2}^b L}{u_S C_{Q_0}} \tag{5.8}$$

A thorough description of the solution of the previous equation is given in Chapter 4. Some simplifications were made in order to calculate the effectiveness factor. It depends on the calculation of the Thiele modulus which relies on the reaction rate obtained in Equation 5.5. The term $C_{O_2}^{-0.0423}$ is almost constant and close to unity for all experimental data, and the reaction order of quinoline was also assumed as unity and consequently:

$$\mathscr{R}_Q = k\, C_Q^a\, C_{O_2}^b = (k\, C_{O_2}^b) C_Q = k'' C_Q \tag{5.9}$$

The equation to calculate the normalised Thiele modulus by assuming a spherical geometry of the catalytic particle ($\phi_S = 3\phi_L$) and discarding the external mass transfer concentration gradients (the concentration in the bulk is that available at the surface of the catalyst, $C_i = C_{i_S}$), when the reaction order respect to quinoline (n) is 1, the equation for the calculation of the normalised Thiele modulus can be simplified as:

[2] This value was taken from Aki and Abraham [215] for a very similar particle size and shape.

$$\phi_L = L_p\sqrt{(n+1)\frac{kC_{i_S}^{n-1}}{2\mathscr{D}_{Eff}}} = L_p\sqrt{\frac{k}{\mathscr{D}_{Eff}}} \tag{5.10}$$

Once the Thiele modulus is calculated, the effectiveness factor expression becomes the well-know expression [279]:

$$\eta = \frac{\tanh(3\phi_L)}{3\phi_L} = \frac{\tanh\phi_S}{\phi_S} \tag{5.11}$$

By including the calculation of the effectiveness factor in the routines for the fitting of experimental data, a new set of kinetic parameters was calculated:

$$\mathscr{R}_Q = 14.3140 \pm 2.3636\, C_Q^{0.8511\pm0.0725}\, C_{O_2}^{-0.0175\pm0.0338} \tag{5.12}$$

The kinetic parameters were calculated within a confidence interval of 95% and in this case the reaction rate was not influence by the presence of internal concentration gradients. By comparing Equations 5.5 and 5.12, accounting for the effect of diffusion in the reaction, the order respect to quinoline and oxygen was affected. If the dependency of the reaction rate on temperature is assumed to follow the Arrhenius equation (by fitting the experimental data at different temperatures) a new equation was produced:

$$\mathscr{R}_Q = 1.5105\text{x}10^7 \pm 4.5369\text{x}10^7 \exp\left(-\frac{77.2406 \pm 18.9943}{RT}\right) C_Q^{0.8511\pm0.0725}\, C_{O_2}^{-0.0175\pm0.0338} \tag{5.13}$$

This equation also used a confidence limits interval of 95% on the calculation of the frequency factor and the activation energy. The activation energy is given in kJ/mol of quinoline reacted and the frequency factor has the same units as the kinetic constant.

5.1.4 Product Identification

A series of experiments were performed to evaluate the efficiency of the catalyst measured in terms of the final products of the reaction. For this purpose the pressure of the system was held constant at 23.0 MPa and the temperature was varied from 673 to 773 K. The initial concentration of quinoline in the experiments was fixed at 0.6 mmol/L and the oxygen supplied was at a SR of 1 in each experiment samples were taken at space velocities of 0.3, 0.8 and 1.3 s^{-1}.

The tests were designed to follow the main carbon and nitrogen products in the gas and liquid effluent. However, a detailed speciation of the residual organic products in the liquid phase could not be carried out due to the low concentration of the remaining compounds. Two species were followed during the reaction instead; those containing carbon and nitrogen. Figure 5.10 shows the results of the analysis of both fractions at $WHSV = 1.3$ s^{-1}.

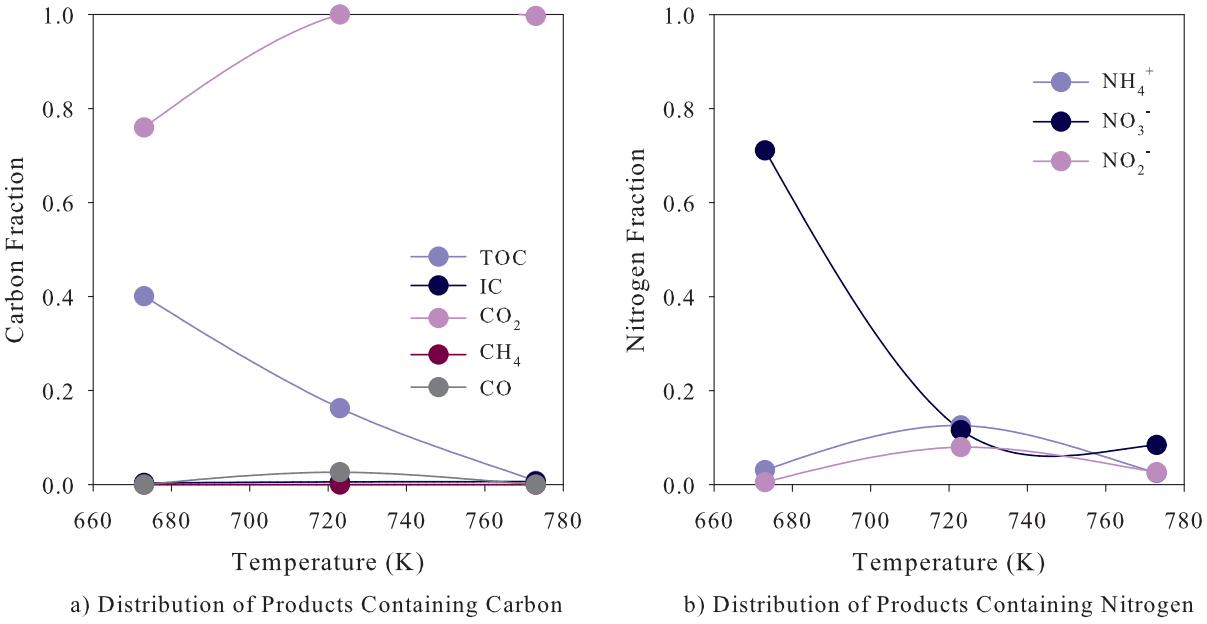

Figure 5.10: Carbon and Nitrogen Fraction for the CSCWO of Quinoline over Pt

Gaseous products were not found dissolved in the liquid effluent. The principal carbon product of the reaction was CO_2, however traces of some unreacted quinoline and some other by-products containing carbon were found (see Figure 5.10a). The TOC content was efficiently eliminated as soon as the temperature was increased. Only traces of carbon monoxide were found in the gas phase at 723 K and inorganic carbon content in the liquid effluent at 723 and 773 K. This proved that the Pt catalyst efficiently oxidised the carbon present in the stream by converting it mainly to CO_2.

Regarding nitrogen species, it was evident that the main intermediate of the reaction was ammonia in the form of the ammonium ion. In aqueous oxidation reactions involving molecules containing nitrogen, it is common that products such as ammonia are present, which are extremely difficult to oxidise [144]. Ammonia oxidation in aqueous media produced NO_3^- and

NO_2^- ions as intermediates which were also found in the liquid effluent in this work. Nevertheless, the NO_3^- ion was favoured rather than the NO_2^- ion at the operating conditions studied; nitrate ions were removed as the temperature approached 773 K (Figure 5.10b). Consequently, the elimination of ammonia was efficient over the Pt catalyst.

The NO_3^- and NO_2^- ions and those produced as intermediates from the oxidation of carbon (CO_3^{2-} and HCO_3^-) were responsible for the change in the pH of the final solution. The initial pH of the solution prior the reaction had a value around 8.0, which then was lowered after the reaction to values ranged between 2.5 and 5.5.

It also important to indicate that adsorption of the some chemical species on the Pt catalyst was detected. This was concluded by following the total fraction of carbon present as products in the outlet stream (see Figure 5.10a) and the mass balances carried out around carbon. The adsorption of the products could be related also to the lost of the activity of the catalyts provided that active sites on the surface of the catalyst were blocked.

5.1.5 Catalyst Activity

The activity of the catalyst was measured in terms of the change of TOC and quinoline removal over a continuous operation of 8 h. For this test a mixture containing 0.3 mmol of quinoline/L and oxygen at a SR of 1 was pumped through the catalytic reactor. The operating conditions were maintained at 673 K, 23.0 MPa and $WHSV = 0.3$ s^{-1}. The TOC and quinoline residual content was plotted in Figure 5.11. The results show a strong deactivation of the catalyst within the first hour of operation, where the catalyst reduced its activity by around 20% based on the removal of quinoline and TOC. After approximately 6 hours of operation the catalyst deactivation did not change. The TOC removal was however affected; at the beginning of the experiment the difference between the TOC and quinoline eliminated was marginal. As the test proceeded, the gap between both curves grew showing a reduction in the TOC eliminated. Although, the ICP analysis did not revealed that deactivation was due to any loss of the active metal, the lower detection limit suggested that it might have lost part of the metal from the system at a concentration that could not be detected.

DVS analysis provides information that occurs on the surface of the catalyst. A change in the surface was detected by plotting the adsorption and desorption isotherms of the fresh and

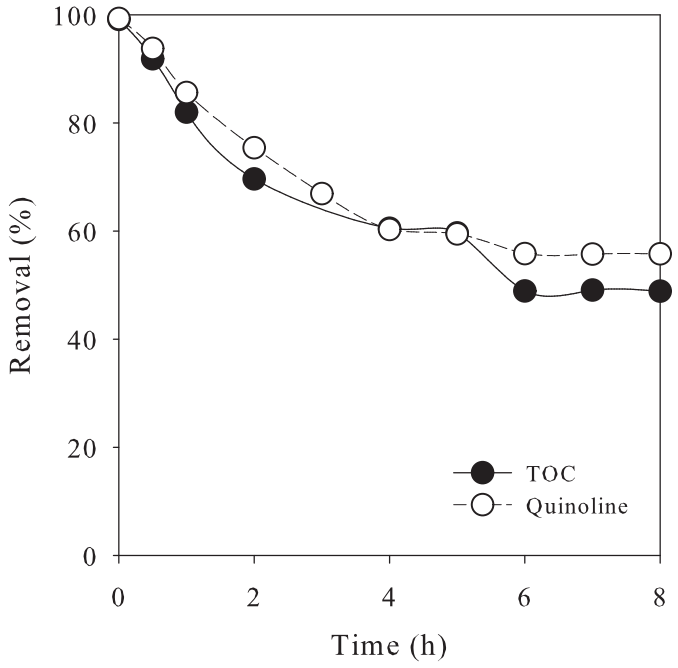

Figure 5.11: Catalyst Stability under CSCWO of Quinoline over Pt

spent catalyst. Although the isotherms of the catalyst had the same shape the amount of water being adsorbed by the spent catalyst was smaller when compared to the clean catalyst. This fact indicates undoubtedly a physical change in the catalyst surface. This finding was corroborated by analysing the catalyst surface area which decreased from 122.2 to 73.4 m^2/g indicating that the reduction of active surface contributed to the loss of the activity. In addition, the XRD showed an amorphous pattern of the catalyst which was not modified after the reaction. No crystalline structures of Pt were found, the peaks shown on the diffraction pattern were due to SiO_2 that was used as a packing material (see Appendix D for plots of the isotherms produced from DVS and Appendix E for XRD patterns). The catalyst activity decreased appreciably within the 6 hours of operation, after which the physical and chemical changes on the catalyst were minimised and it reached a continuous activity.

5.2 CSCWO of Quinoline over CuO Catalyst

Three experiments of quinoline oxidation in supercritical water were performed over a CuO catalyst. The operating conditions were 673 K, 23.0 MPa, initial concentration of quinoline of

0.3 mmol/L and oxygen was supplied to a SR of 1. The weight of the catalyst and particle size range used during the experiments were 0.5 g and 45-63 μm, respectively. Space velocities were varied between 0.1 to 0.3 s^{-1}. Nevertheless, the TOC content of the stream did not show any change and adsorption of the reactants on the surface of the catalyst was observed. After the reaction, a sample of the catalyst was taken and analyzed by DVS and XRD analysis to investigate the deactivation (see Appendix D for plots of the isotherms produced from DVS and Appendix E for XRD patterns).

The DVS analysis showed a change on the surface of the spent catalyst. Although, the shape of the adsorption and desorption isotherms were basically the same showing a complete reversible process the amount of water being adsorbed by the spent catalyst was considerably lower suggesting at least a physical change in the catalyst. The surface area of the catalyst was reduced from 204 to 76.9 m^2/g. Moreover, the catalyst suffered a chemical transformation in its structure. The fresh catalyst did not present any crystalline structure, however in the spent catalyst the amorphous structure of Al_2O_3 was affected and a crystalline structure of bohemite ($AlO(OH)$) appeared on the XRD pattern of the catalyst. Bohemite has been commonly reported as a stable structure produced from alumina supported catalyst of the reaction [288, 289]. On the contrary, the CuO did not seem to be affected during the experiments but a new crystalline phase of CuO (tenorite) was detected. Therefore, it was observed that the deactivation of the catalyst was a complex process where chemical and physical changes contributed to the reduction of the catalyst activity.

5.3 CSCWO of Quinoline over MnO_2/CuO Catalyst[3]

MnO_2/CuO catalyst has been demonstrated to be effective for the oxidation of the organic compounds and thus it was selected as a suitable catalyst for the oxidation of quinoline [193].

5.3.1 Evaluation of the External and Internal Concentration Gradients

The presence of external (interphase) and internal (intraphase) concentration gradients were experimentally assessed to evaluate their effect on the reaction. Both tests were carried out

[3] **Parts of this Section were published in a special issue of the Industrial and Engineering Chemistry Research [300]**

following common procedures which rely on the evaluation of conversion dependency on the former to the superficial velocity, and the latter to the particle size [250, 267].

5.3.1.1 Interphase Concentration Gradients.

A series of experiments were performed at a pressure of 23.0 MPa and temperature of 673 K. For the experiments the quinoline concentration was maintained at 0.3 mmol/L with a SR of oxygen at 1. Catalyst particle size was 212-250 μm and the amounts of catalyst in the reactor were 0.6, 0.8, 1.0 and 1.2 g. The flow rate will therefore proportionally increase to keep a constant space velocity. For the test space velocities of 0.04 and 0.125 s^{-1} were selected to investigate whether there is a change in the removal caused by the increment of the flow rate of the reacting mixture. Figure 5.12 illustrates the effect of the flow rate at the 3 different space velocities studied. At $WHSV = 0.04$ s^{-1} the conversion was kept constant and thus it was independent of the flow rate of the reacting mixture. At 0.125 s^{-1} there is a slight increment in conversion, however it was considered that the change was not significant enough to have any influence in the reaction. Oshima et al. [207] have also shown the absence of interphase concentration gradients at almost the same reaction conditions; however in their study the organic compound studied was phenol.

5.3.1.2 Intraphase Concentration Gradients

Once the external concentration gradients have now been discarded, the next step was to quantify the effect of the particle size on the removal of TOC. The operating pressure and temperature and reactants concentration were the same as for the evaluation of external concentration gradients. For these experiments 1.0 g of catalyst was placed in the reactor and the range of catalyst sizes used are shown in Table 5.4. The effects of the particle sizes on the conversion are shown in Figure 5.13. At any given space velocity and particle size the removal was unchanged, and consequently, the intraphase concentration gradients were also discarded.

After external and internal concentration gradients were assessed and discarded, it was concluded that the system was under chemical kinetic control. The kinetic parameters evaluated will not therefore be affected by any concentration gradient and thus it can be considered as a pseudo-homogeneous model.

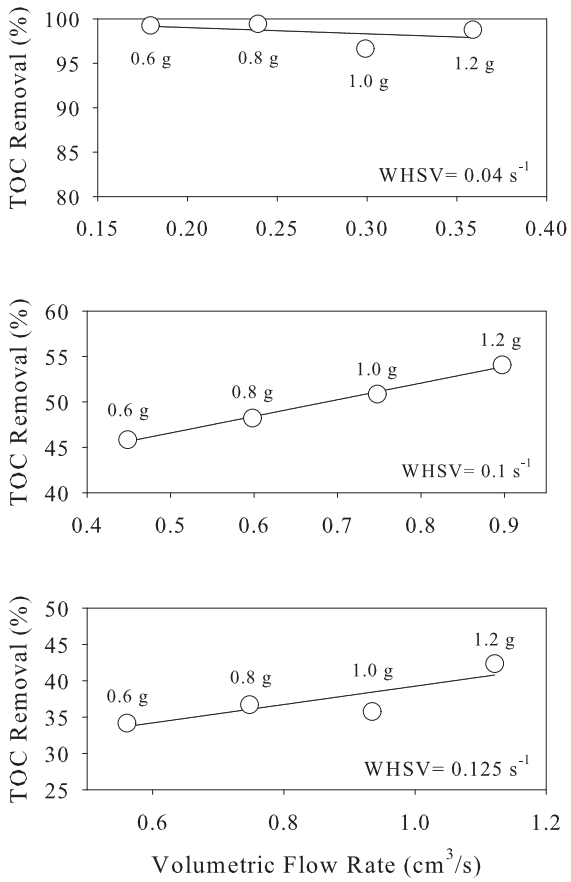

Figure 5.12: External Concentration Gradients of Quinoline on MnO_2/CuO

Table 5.4: Particle sizes for Evaluation of Internal Concentration Gradients over MnO_2/CuO

Experiment	Particle Size Range, μm	Average Particle Size, μm
1	212−250	231.0
2	150−212	181.0
3	45−63	54.0

5.3.2 Reproducibility Tests and Effect of Key Operating Conditions

Although, oxidation reactions are highly exothermic, isothermal operation was assumed based on the low concentration of quinoline in the feed stream and also because water removes the heat generated by the oxidation reaction. Moreover, the dilution of the catalyst with inert material

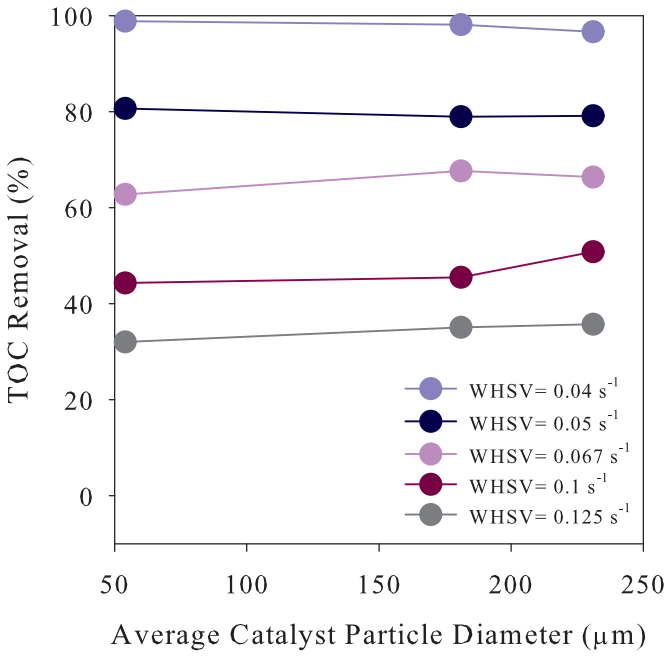

Figure 5.13: Internal Concentration Gradients of Quinoline on MnO_2/CuO

assures an even distribution of the temperature along the reactor and prevents the presence of hot-spots in the catalytic bed [250]. In support of this, the fluctuation of temperature was ±1 K and pressure varied by ±0.3 MPa, with a maximum pressure drop in the system of ±0.3 MPa, and consequently isobaric conditions were assumed. Previous research work on the hydrolysis of quinoline in our group conducted by Pinto [260] has demonstrated that quinoline was not decomposed at temperatures below 753K and only less than 1.2% was removed at 773K. A trend that was different for the hydrolysis of DBU conducted by Ashraf [167]. Thus the effect of the hydrolysis reaction of quinoline was negligible and it assures that only the oxidation reaction is responsible for its removal. Catalytic supercritical water oxidation experiments were carried out to observe the effect of the process variables; temperature, pressure, concentration of oxygen and initial concentration of quinoline (a summary of the operating conditions studied and the details of the reactor shown in Table 5.5). The quinoline concentration range studied mimics the values found in pharmaceutical waste water streams.

Table 5.5: Experimental Conditions of CSCWO of Quinoline over MnO_2/CuO

Parameter	Interval Studied
Temperature Range, K	673-773
Pressure Range, MPa	23.0-30.0
Initial Quinoline Concentration Range, mmol/L	0.1-0.6
Initial Concentration of Oxygen Range (SR)	0.5-10
Catalyst weight, g	1.0±0.0001
Catalyst particle size, μm	45-63
SiO_2 particle size, μm	212-250
Bed length, cm	9.0±0.1
Dilution factor catalyst to SiO_2, v:v	1:1

5.3.2.1 Reproducibility Tests

Tests were performed to evaluate the experimental error during the catalytic study. A series of five experiments were carried out under the same operating conditions of 23.0 MPa and 673 K, using a concentration of quinoline of 0.3 mmol/L and a SR of 1. During each experiment samples were taken at $1/WHSV$ of 8, 10, 15, 20 and 25 s. The average and standard deviation of the removal in terms of TOC and quinoline were calculated from the 5 samples obtained at each residence time (Table 5.6). The results of the reproducibility tests are shown in Figure 5.14. The maximum values of standard deviation were 5.7 and 4.8% of removal in terms of TOC and quinoline removal, respectively. The values provide an estimate of the reliability of the experimental results. An interesting result is that as the reaction proceeds towards higher spatial times values of removal in terms of TOC and quinoline were very close to each other and indistinguishable. TOC removal was associated with the production of intermediates during the reaction. If the remaining TOC value depended solely on the remaining quinoline in the outlet stream both removal values would be equal. However, if any by-product is present the TOC removal value will be lower than quinoline value. The reaction proceeds slower than other similar nitrogen-containing organic compounds previously studied and this shows that quinoline has a higher stability [214, 301].

Table 5.6: Reproducibility Tests of CSCWO of Quinoline over MnO_2/CuO

$WHSV$, s^{-1}	Average TOC Removal, %	Std. Dev. TOC Removal, %	Average Quinoline Removal, %	Std. Dev. Quinoline Removal, %
0.04	98.84	0.59	97.20	0.81
0.05	83.47	5.71	86.18	4.81
0.0667	62.77	3.35	69.64	4.73
0.1	44.32	2.57	55.24	3.35
0.125	32.03	3.53	47.04	0.65

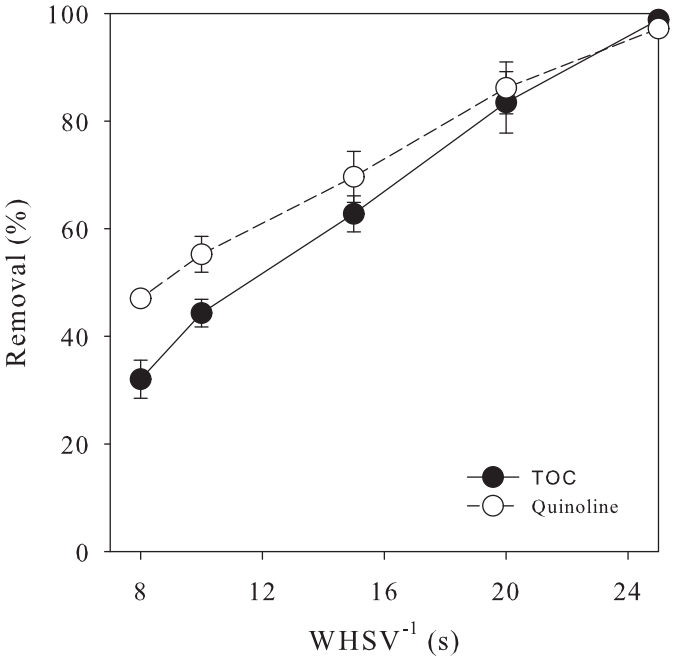

Figure 5.14: Reproducibility Tests of CSCWO of Quinoline over MnO_2/CuO

5.3.2.2 Effect of Temperature on the CSCWO of Quinoline over MnO_2/CuO

Quinoline has been the subject of study in previous work and it was shown that it was hardly oxidised under non-catalytic conditions under temperatures of 773 K [297]. The addition of a catalyst aims to lower the severity of the reaction mainly its temperature and therefore the energy consumption and to improve the oxidised product. Temperature has been proven to be the main

controlling variable of the reaction; essentially the higher the temperature, the more effective the oxidation reaction is in terms of the removal of the organic compound and the production of intermediates. However, the severity of the reaction can accelerate the corrosion of the reactor. Therefore, the inclusion of a catalyst is envisaged as a means to diminish the thermal stress as well.

A series of experiments were performed at 23.0 MPa, with an initial quinoline concentration of 0.3 mmol/L and an oxygen stoichiometric ratio of 1. The temperature was varied from 673 to 773 K and liquid samples were taken and analyzed. Figure 5.15 shows the effect of temperature at different space velocities.[4] The reaction proceeded nearly to completion at $WHSV = 0.04$ s^{-1}, and the temperature did not have any effect on the removal of TOC and quinoline. At the lowest temperature value studied (673 K) the removal reached a value close to 99% for TOC and 98% for quinoline. The closeness of the values indicated that the catalyst also lowered the production of any intermediates. As the temperature increased at higher $WHSV$ than 0.04 s^{-1}, the conversion was higher as the temperature increased.

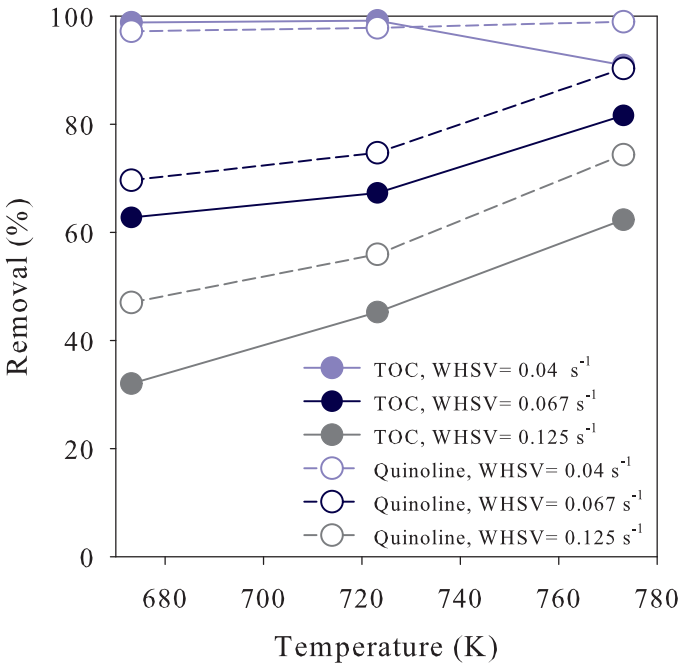

Figure 5.15: Effect of Temperature in the CSCWO of Quinoline over MnO_2/CuO

[4]For clarity in the presentation of experimental results, only three space velocities were plotted in this and subsequent parts of the section, however a total of five were studied.

5.3.2.3 Effect of Pressure on the CSCWO of Quinoline over MnO_2/CuO

During the experiments the temperature was maintained at 673 K and the concentration of quinoline was 0.3 mmol/L with an oxygen stoichiometric ratio of 1. The density of the reacting mixture varied from 133.8 to 357.1 kg/m^3 by adjusting the pressure from 23.0 to 30.0 MPa. The results are depicted in Figure 5.16. A $WHSV = 0.04$ s^{-1} allowed the reaction to near completion and the effect of pressure was largely unnoticed. Higher space velocities showed clearly the dependency on pressure. As the pressure increased the amount of remaining TOC and quinoline decreased. When the pressure rose from 23.0 to 30.0 MPa at a constant space velocity of 0.125 s^{-1}; the removal improved by 34% for TOC and 42% for quinoline. It is said that the solvation power of supercritical fluids is intimately related to their density and that density can be adjusted to improve reaction rates at supercritical conditions [14]. In addition, the TOC and quinoline removal values maintained the same trend by keeping a constant distance from each other, which showed that pressure did not affect the production of by-products.

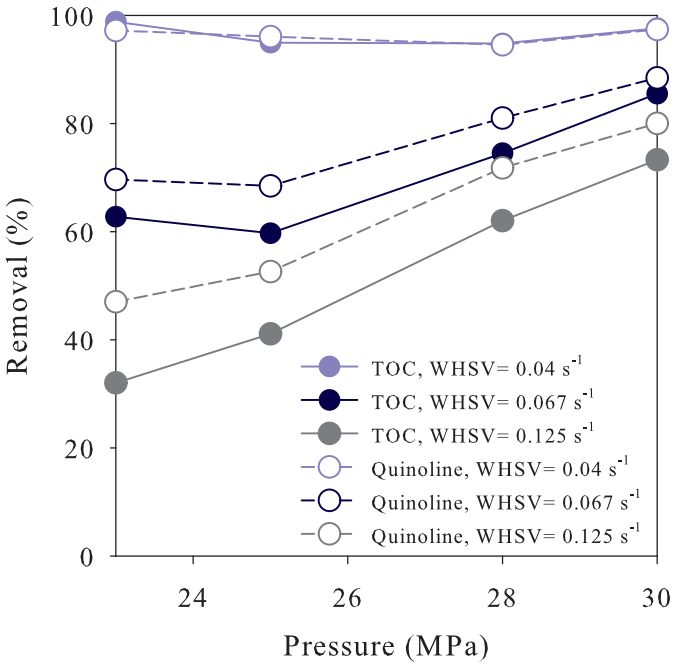

Figure 5.16: Effect of Pressure in the CSCWO of Quinoline over MnO_2/CuO

5.3.2.4 Effect of Initial Quinoline Concentration on CSCWO over MnO_2/CuO

The oxidation reaction was evaluated in terms of the amount of quinoline concentration that can be efficiently oxidised. For this purpose the concentration of quinoline was varied from 0.1 to 0.6 mmol/L and oxygen was supplied to a stoichiometric ratio of 1 in each case. The pressure of the system was 23.0 MPa and the temperature was 673 K. Figure 5.17 presents the findings of the experiments. In general higher concentrations of the quinoline led to an improvement in the removal. For example, an inlet concentration of 0.6 mmol/L (approximately 600 ppm of quinoline at atmospheric conditions) reduced its TOC content to 99% at a $WHSV = 0.04$ s^{-1}. The reaction was therefore able to cope with higher concentrations of quinoline more efficiently without affecting the reactor performance. At space velocity of 0.04 s^{-1}, the effect was barely noticeable above a concentration of 0.2 mmol/L; higher concentrations brought the reaction close to completion and just traces of both TOC and quinoline were found in the stream. The effect of concentration in a tubular fixed bed reactor has been previously studied by Krajnc and Levec [217], where they also proved that higher concentration of the acetic acid (the organic compound studied) promoted faster reaction rates.

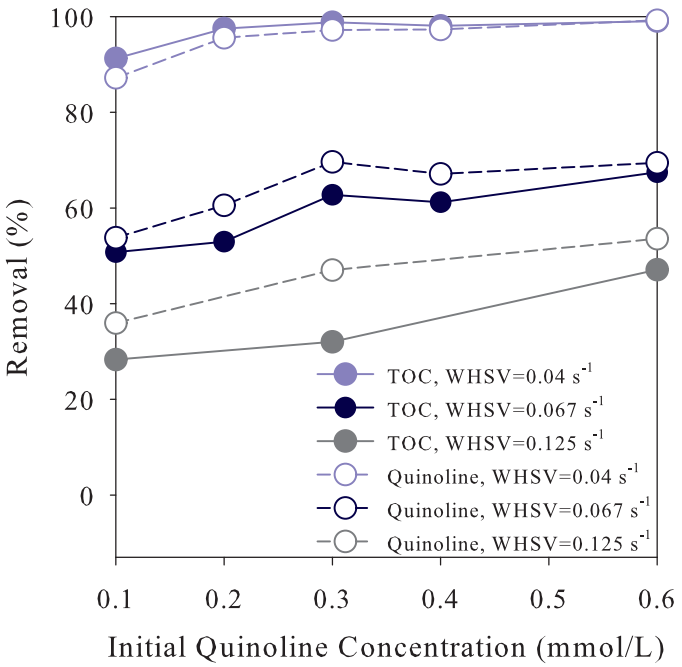

Figure 5.17: Effect of Initial Quinoline Concentration in the CSCWO over MnO_2/CuO

5.3.2.5 Effect of Initial Oxygen Concentration on the CSCWO of Quinoline over MnO_2/CuO

The stoichiometric ratio of oxygen to quinoline was evaluated from 0.5 to 10 according to Equation 5.2. Meanwhile the quinoline concentration was kept constant at 0.3 mmol/L. The pressure and the temperature of the system was maintained at 23.0 MPa and 673 K, respectively. The oxygen concentration rapidly improved the removal of the organic compound in the outlet stream when it was increased from 0.5 to 4.0 (Figure 5.18). Above a SR of 4 the elimination was not significantly improved. However, the concentration of oxygen did have an effect on the amount of TOC produced. Above SR 2 the values of TOC and quinoline removal tend to overlap, which indicates elimination values close to each other. Consequently, an excess of oxygen can be introduced as an additional parameter to control (to some extent) the oxidation reaction and the elimination of the intermediates.

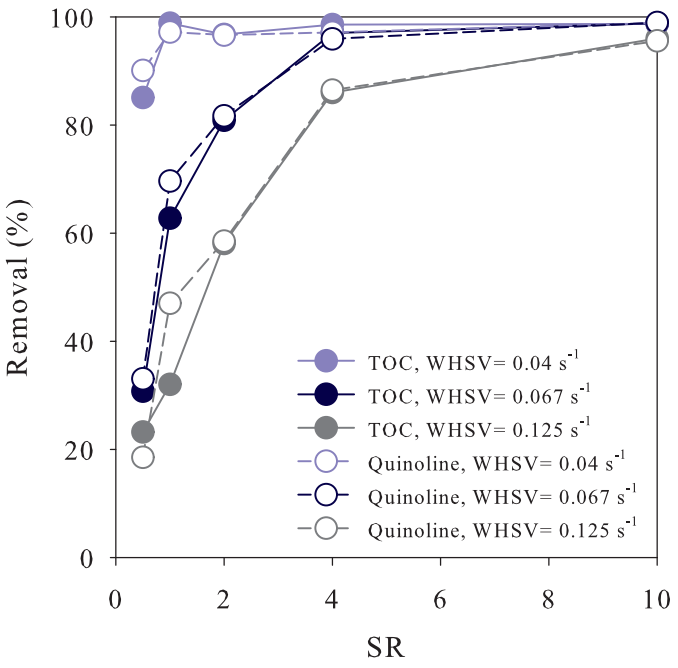

Figure 5.18: Effect of Initial Oxygen Concentration in the CSCWO of Quinoline over MnO_2/CuO

5.3.3 Kinetics of the Reaction

The fitting of experimental data were performed using the integral analysis method proposed by Froment and Hosten [273] (a detailed description of the fitting of experimental data is given in Appendix C). In this analysis the experimental data were fitted to the continuity equation of a tubular reactor. The best fitting values that were found after solving the minimisation with a confidence level of 95% are shown in the following equation. The equation expresses the reaction rate of quinoline in the reactor according to:

$$\mathscr{R}_Q = 0.2280 \pm 0.1233\, C_Q^{0.4277\pm0.2292}\, C_{O_2}^{0.2375\pm0.0865} \tag{5.14}$$

Figure 5.19 shows a comparison of the fraction reacted between the experimental data set and those values found using the fitted reaction rate. In most of the cases, the values lie within a ±10% of the fraction of quinoline reacted, showing a good agreement of the power-law kinetic model with the predicted experimental values. Pinto et al., [147] have reported reaction orders for the non-catalytic oxidation of quinoline and it is interesting to compare how the reaction rate changes with respect to the heterogeneous reaction. The reaction orders reported in their study were 0.8 with respect to quinoline and 0.3 with respect to oxygen. The values presented in this study showed smaller reaction orders, although the difference with respect to oxygen was minimal. The reaction rate showed a similar dependency on oxygen concentration although the influence of quinoline was lowered in the catalytic reaction. The non-integer values of the reaction orders for both scenarios reflects the complexity of the process, which goes beyond the simple interaction of quinoline and oxygen (as shown in Equation 5.1) and implies the occurrence of side reactions [230].

The dependency of temperature on the reaction can be represented, as it commonly is assumed by the Arrhenius equation by fitting the experimental data at different temperatures. A new form of Equation 5.14 can therefore be obtained:

$$\mathscr{R}_Q = 47.9015 \pm 886.9099 \exp\left(-\frac{28.7631 \pm 114.0256}{RT}\right) C_Q^{0.4277\pm0.2292}\, C_{O_2}^{0.2375\pm0.0865} \tag{5.15}$$

where the parameters that best fit the experimental data are calculated within confidence intervals of 95%. It is common to find reactions with high frequency factor values provided they

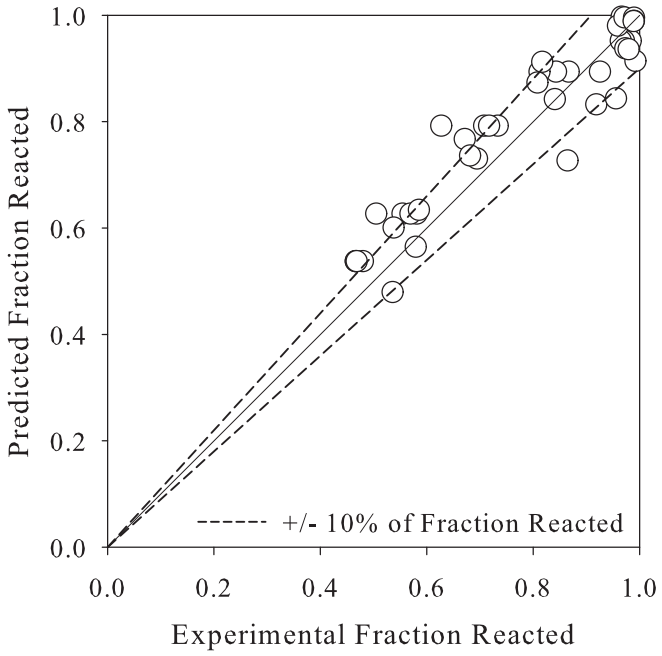

Figure 5.19: Comparison of Predicted and Experimental Fraction of Quinoline Reacted over MnO_2/CuO

in some sense represent the collision occurring in a certain chemical reaction. Nevertheless, the slow course of the reaction gave a small value in this case. Another explanation comes from the point that chemical reaction performed at supercritical conditions do not behave in the same way as gas phase reactions. The anomalous behaviour of reactions carried out above the critical point has been pointed out previously [219]. The wide confidence limits in the Arrhenius parameters could indicate that this equation might not be appropriate for the calculation of the parameters but it is certainly a reasonable good approximation in absence of any other information.

5.3.4 Product Identification

The aim of a complete oxidation is the production of final products such as CO_2, and therefore it is commonly used to follow the completeness of the reaction. Consequently, a series of experiments were performed to identify the products of the reaction. The pressure in the experiments were maintained at 23.0 MPa and the temperature was varied from 673 to 773 K. The initial concentration of quinoline in the stream to be treated was kept constant at 0.3 mmol/L with an oxygen concentration that met a SR of 1. Meanwhile, samples were taken at space velocities of

0.04, 0.067 and 0.125 s^{-1}.

Figure 5.20 presents the carbon and nitrogen fractions at $WHSV = 0.04$ s^{-1}. A more detailed evaluation of the organic compounds could not be done due to the low concentration of the organics in the samples taken. Consequently, speciation in terms of carbon was done by analysing the TOC and IC in the liquid together with the gas phase, where CO_2, CO and CH_4 were analysed. It was found that CO_2 was the main chemical structure containing carbon, while no other gases were present in the gas phase (see Figure 5.20a). Regarding the liquid, the TOC content was rapidly eliminated as the reaction proceeded towards a higher temperature, but there was almost no production of IC during the reaction.

Figure 5.20b depicts the distribution of nitrogen products in the liquid effluent. Only traces of ammonium and nitrite ions appeared in the sample, nonetheless the production of nitrate ions were favoured by the catalyst. The set of reactions that oxidise ammonia in an aqueous media are reversible which could explain the reduction of nitrate content at 723 K, however the equilibrium was rapidly switched at 673 and 773 K. Therefore, the catalyst proved to be effective for the oxidation of the ammonia produced during the reaction but it was not selective towards N_2.

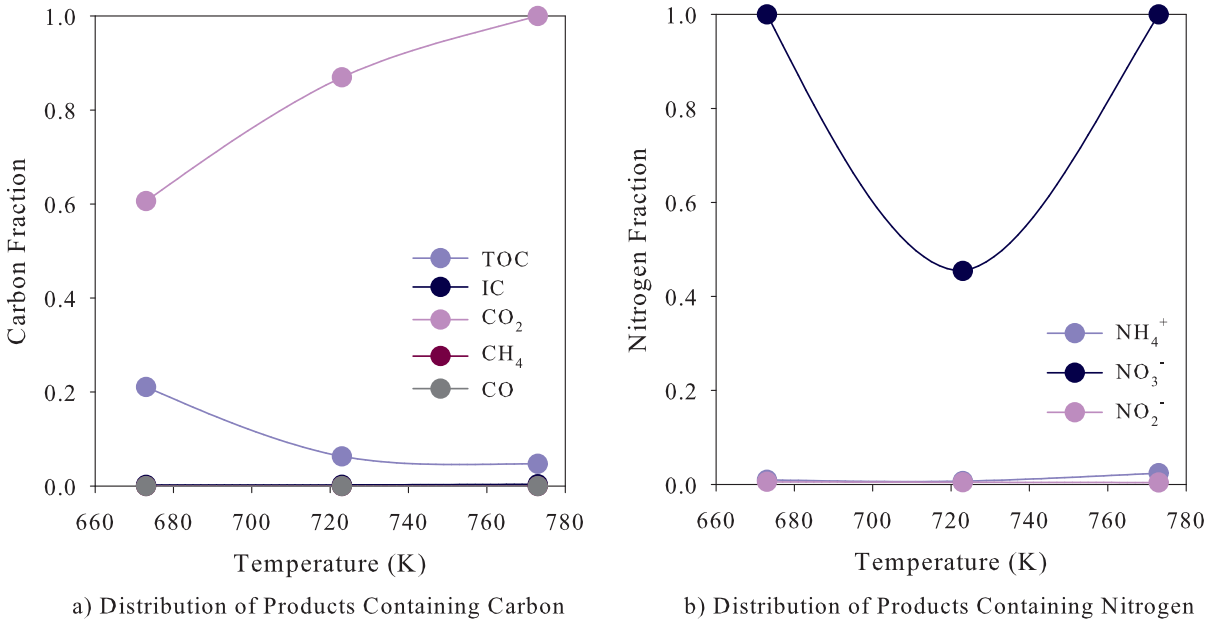

a) Distribution of Products Containing Carbon

b) Distribution of Products Containing Nitrogen

Figure 5.20: Carbon and Nitrogen Fraction for the CSCWO of Quinoline over MnO_2/CuO at $WHSV$ =0.04 s^{-1}

Higher initial concentrations of quinoline than 0.3 mmol/L lead to a fast deactivation of catalyst that interfered with the chemical reaction. Even at the initial concentration of the organic compound studied, carbon mass balances carried out showed that quinoline or some of the products of the reaction were adsorbed on the catalyst surface. This could explain the loss of activity of the catalyst when higher concentrations of quinoline were treated for longer periods of the experiment.

The initial pH of the sample of approximately 8.0 decreased to values that ranged between 2.8 to 6.5, this is a consequence of the production of mainly NO_3^- which was found as product of the dissociation of nitric acid. However, in minor degree some other inorganic and organic compounds could be responsible for this change such as nitrous acid or some carboxylic acids.

5.3.5 Catalyst Activity

An experiment was performed to evaluate the activity of the catalyst at supercritical conditions. In the test a solution of 0.3 mmol/L of quinoline was pumped through the reactor at $WHSV = 0.04$ s^{-1}. The stoichiometric ratio of oxygen was maintained at 1 and the operation conditions were 23.0 MPa and 673 K. The liquid stream was sampled to monitor the stability of the catalyst in terms of TOC and quinoline removal. The catalyst deactivation was considerably within 0.5 h of operation and after 1.0 h, the removal of TOC and quinoline was reduced by 25 and 20% respectively, from its initial value (Figure 5.14) and the production of intermediates occurred. After this time the activity of the catalyst was slightly affected until the end of the experiment. A similar finding was reported by Yu and Savage [204] for the oxidation of phenol. The loss of catalyst activity can be a consequence of the transformation of the amorphous structure of both oxides under supercritical conditions, which were less active [288, 292]. In addition, it is worth mentioning that the unsupported catalyst mix used here lacks the advantageous properties of a catalyst support; mainly the resistance to any thermal or mechanical shock. At supercritical operating conditions these factors are prevalent and they are likely to lessen the catalyst life-time. However, it is very promising that catalyst formulations based on MnO_2 and CuO can be successfully exploited as alternatives to reduce the severity of the process and to be used for a wider range of organic compounds.

It was identified by ICP analysis that part of the deactivation process is due to leaching

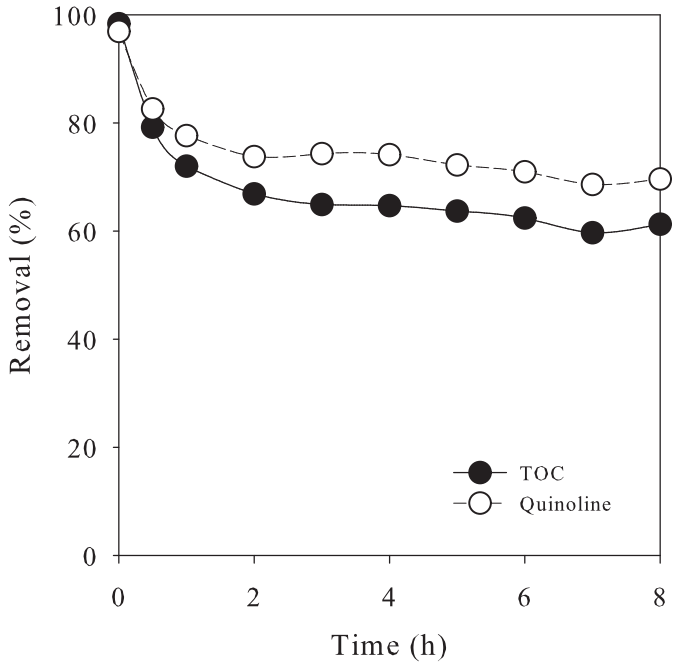

Figure 5.21: Catalyst Stability under CSCWO of Quinoline over MnO_2/CuO

during the reaction. Manganese and copper have been identified in a maximum concentration of 0.118 and 0.044 ppm, respectively. The effect of leaching at this condition was a consequence of the poor mechanical resistance of the catalyst and the change to a strong acidic pH of the reacting caused by product formation. The DVS analysis also demonstrated that although the shape of the adsorption and desorption curves were the same for fresh and spent catalyst, the water adsorbed by the spent catalyst was about a third of the amount of water adsorbed by the fresh catalyst (for details refer to Appendix D). DVS analysis confirmed that in part, it was a consequence of the reduction in the catalyst surface area. DVS measurements detected that the fresh catalyst was reduced from 195.0 to 70.4 m^2/g.

The XRD pattern of the fresh catalyst showed a complete amorphous structure. On the contrary, the spent catalyst suffered changes that showed the appearance of crystalline structures (see Appendix E for XRD patterns). Although the MnO_2 seemed to be preserved albeit in a different phase, the diffraction pattern also showed the appearance of Cu_2O and $Cu_{1.5}Mn_{1.5}O_4$. The Cu_2O (less active) has been reported as one of the chemical species that are transformed from CuO [288]. The aggregate composed of copper and manganese oxides has also been detected as one of the species which are produced from mixed catalyst oxides [289]. The presence of silica

in the pattern was a consequence of the packing material used during the experimental work.

5.4 A Note on the Reaction Mechanisms in CSCWO

Some authors have proposed that more traditional reaction rates for heterogeneous reactions that comprise adsorption and desorption steps of chemical species could be more appropriate to explain the CSCWO reaction. The reaction models proposed are in majority the type of Langmuir-Hinshelwood-Hougen-Watson (LHHW), although a Mars-van Krevelen mechanism has also been proposed [204, 205]. Three LHHW reaction rate models were also explored to fit the experimental data. The LHHW reaction models were taken from previous research works; the first one assumes adsorption of reactants on different catalyst sites, the second presumes adsorption of the species on the same site and the last model comprises adsorption of one of the species on a site and then a dissociative adsorption of the second species on a different site [206, 207, 218]. However, the kinetic data in the present work were better represented by the power-law kinetic model. This fact has been pointed out before when Aki and Abraham [215] could not justify the use of any LHHW models with their experimental data, arguing that there is no clear evidence of the precise mechanism of the CSCWO. Additionally, Krajnc and Levec [217] compared the power-law and LHHW reaction rates and concluded that, although both represented appropriately their experimental results, due to the uncertainty generated by the mechanistic approach, they recommended the use of power-law kinetic models instead. This is supported by the fact that different reaction mechanisms have been proposed for the catalytic oxidation of phenol at the same reaction conditions [206, 207]. CSCWO could be better explained in terms of elementary reaction mechanisms that can be used to gain insight into the reaction process. Nonetheless, only non-catalytic reactions have been modelled by this approach at operating conditions that allow the assumption that water only acts as a collision partner and disregard any other type of molecular interaction. Although the models have identified the importance of the production of free radicals during the reaction, they were not able to accurately predict either product distribution or reagent disappearance [233, 235]. This suggests that the reaction indeed could be more complex and the presence of a side mechanism could be expected [20]. Hayashi et al. [245] have supported the presence of an alternative mechanism by studying the oxidation of phenol at sub- and supercritical conditions. They proposed that the presence of the ionic mechanism

was more favorable at subcritical conditions as a consequence of the considerable difference in the ion product of water. This mechanism could partially be responsible for the appearance of some reaction products. Studies of oxidation in water and carbon dioxide have showed that gas phase reactions adapted to supercritical conditions did not show any difference in conversion rates over these solvents, nevertheless the presence of small amounts of water in the CO_2 system lead to small differences in the conversion of oxygen and CO production. Besides, it is also postulated the appearance of non-free radical intermediates [302, 303]. In addition, any models should also take into account the solute-solvent interactions present in supercritical fluids [25]. Thus a simpler model that could account for more complex reaction steps, like the power-law model, is preferred for its practicality [304].

5.5 Summary of Findings

The complete oxidation reaction of quinoline over Pt, CuO and MnO_2/CuO was studied. CuO catalyst was not active for the oxidation of quinoline in SCW as there was not a reduction on the TOC content of the stream being treated. Pt on the other hand was the most active catalyst for the reaction. A series of experiments were performed to evaluate the presence of external and internal concentration gradients, the reproducibility, the effect of the operating conditions and the kinetic parameters (Arrhenius parameters and reaction orders). The reaction was followed by analysing the remaining TOC and quinoline in the samples taken. A complementary set of samples identified the main carbon and nitrogen species produced during the reaction and to investigate the catalyst deactivation.

External and internal concentration gradients were evaluated experimentally and it was concluded that they were present when the reaction took place over the platinum catalyst. Although the amount of catalyst used during the experiments was chosen appropriately and the particle size reduced to a minimum; if the chemical reaction is fast enough, the process of transfer of reactants from the bulk to the catalyst and products in the opposite direction become the controlling step of the reaction (see Section 4.1.3). Consequently, the kinetic parameters should be calculated by including the effect of mass transport together with the chemical reaction. On the contrary, over the MnO_2/CuO mixed catalyst the chemical reaction occurred slower than the transport of reagents and products, and therefore the reaction was the limiting step.

The reproducibility of the experiments was assessed by calculating the experimental error as a standard deviation. The error increased as the HPLC pumps were adjusted to higher flow rates. The error is a consequence of the lack of control of the pressure and therefore flow rate in the experimental rig. Nevertheless, the experimental error was small enough to obtain a reliable set of experimental data. It is worth to point out that the experimental error should not be extrapolated outside the set of experiments from it was calculated; instead it helps to support the reliability of the experimental data.

Temperature was the main controlling variable of the process and it can be used to control the effectiveness of the reaction. In the case of Pt catalyst a removal higher than 92% was achieved in terms of TOC and quinoline content at 653 K and $WHSV = 0.3$ s^{-1}, which reached almost complete oxidation when the temperature was increased by 20 degrees. The temperature also had an important effect when the reaction took place over the MnO_2/CuO mixed catalyst. At $WHSV = 0.04$ s^{-1} and 673 K the removal of TOC and quinoline was also close to 99%. Figure 5.22 shows a comparative plot of the removal of quinoline performed at 23.0 MPa with an initial quinoline concentration of 0.3 mmol/L and an oxygen feed of SR= 1. The figure was obtained by Equations 5.13 and 5.15. At 673 K and $WHSV^{-1} = 0.1$ s (Figure 5.22a), the removal of quinoline had a value of 78% over the Pt catalyst while it only reached a value of 5% over MnO_2/CuO. At the same residence time and 773 K the removal over Pt increased to 100%, meanwhile over the mixed metallic oxide catalyst increased to 6.1% (Figure 5.22b). Consequently, the complete removal of quinoline over Pt occurred considerably faster than over MnO_2/CuO.

The effect of pressure on the reaction had a different effect on Pt than MnO_2/CuO. In the case of Pt the pressure decreased the removal of TOC and improved the removal of quinoline. The removal of intermediates (which can be measured by the TOC content) in the case of Pt catalyst were lowered by the increment of the system pressure. However, the removal of quinoline and TOC over MnO_2/CuO were both increased by an increase in pressure.

The initial concentration of quinoline in the stream also had a different effect for both catalysts. When the reaction took place over Pt, the removal of TOC and quinoline exhibited a small drop when the concentration was varied from 0.2 to 0.3 mmol/L. At higher initial quinoline concentrations the removal levelled off. In the case of the MnO_2/CuO catalyst the removal of

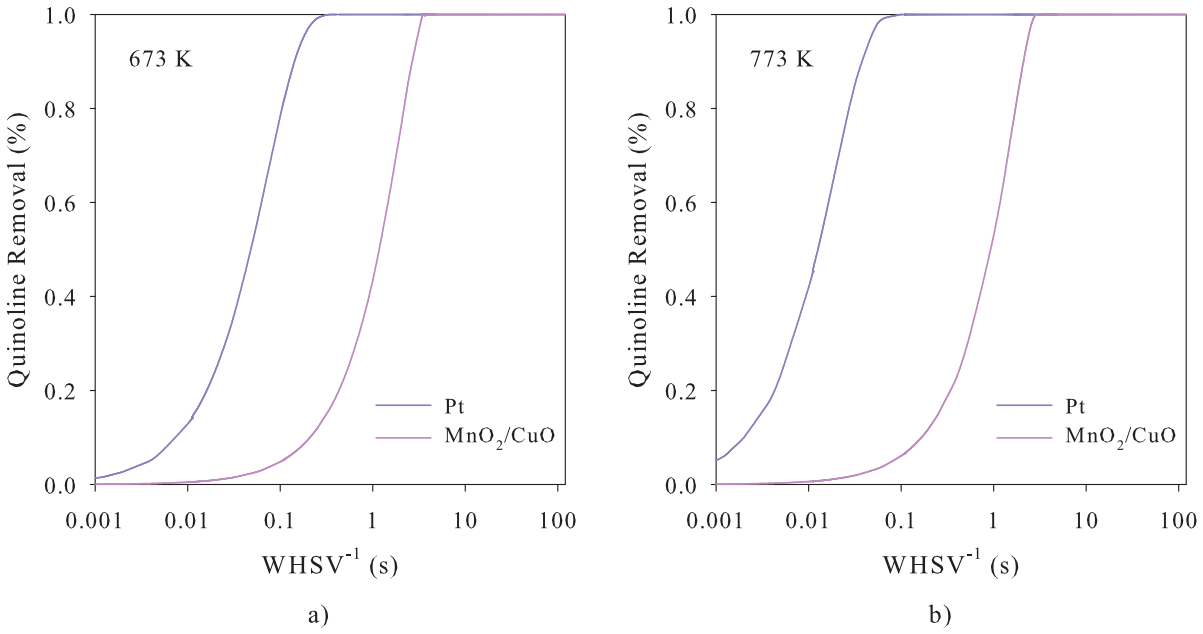

Figure 5.22: Catalyst Comparison for the CSCWO of Quinoline

quinoline and TOC was favoured as the initial concentration of quinoline was increased. This proved that the system performance was not very sensitive to changes in the initial concentration of quinoline.

The oxygen concentration improved the removal of both TOC and quinoline on the reaction, but its effects reached a maximum at a SR equal to 4. Above this value it only had a small effect or even lowered the removal of quinoline and TOC. The oxygen concentration can also be used to reduce the production of intermediates. The removal (in percentage) lines of quinoline and TOC tended to overlap when the oxygen concentration was higher than the stoichiometric value; this was seen for the reaction that took place over MnO_2/CuO mixed catalyst, but the opposite trend was witnessed for the Pt catalyst.

A power-law kinetic model was proposed to represent the removal of quinoline over both catalysts. The reaction over Pt catalyst was limited by the transport of reagents, which was concluded from evaluating the criteria proposed by Bischoff. The calculation of the Thiele modulus in order to obtain the effectiveness factor was therefore necessary to establish the intrinsic chemical kinetic parameters. Because information about the reaction mechanism is lacking in the literature several reaction rate models were used to fit the experimental data. The

power-law kinetic model was most suited to represent the removal of quinoline. Table 5.7 shows the reaction order and the activation energy calculated from the experimental data. The reaction orders obtained with respect to quinoline and oxygen were different for both catalysts. However, they did follow the same trend with the reaction order with respect to quinoline being higher than oxygen. Although the reaction order with respect to oxygen had a negative value in the reaction over Pt. The activation energy showed a value three times higher over the Pt catalyst.

Table 5.7: Kinetic Parameters for the CSCWO of Quinoline

Kinetic Parameter	Pt	MnO_2/CuO
Reaction Order of C_Q	0.8511	0.4277
Reaction Order of C_{O_2}	-0.0175	0.2375
Activation Energy, kJ/mol	77.2406	28.7631

A detailed identification of the by-products could not be done due to the low concentration in the samples taken. It was found that CO_2 was the main product of the reaction over both catalysts, while only traces of other gases were identified. This fact showed that the catalysts largely caused the complete oxidation of the organic carbon present in the molecule. Moreover, both catalysts avoided the production of ammonia (identified as ammonium ion) commonly found in aqueous oxidation of nitrogen-containing organic compounds. MnO_2/CuO produced a large amount of nitrates, which are intermediates in the complete oxidation of the nitrogen atom in the molecule. Meanwhile, Pt produced a very efficient removal of nitrates at a temperature of 723 K in comparison to lower temperatures where the amount of nitrates decreased considerably.

The adsorption of reagents on the surface of the catalyst were detected which would have contributed to the loss of activity of the CuO catalyst. Both catalysts demonstrated different adsorption and desorption isotherms but in both cases were completely irreversible processes. The catalysts post-reaction suffered changes to their structure when they were compared to fresh samples. A structural transformation of the MnO_2/CuO catalyst was confirmed by the XRD pattern showing the aggregation and growth of different crystals in the catalyst [305], although this could not be explicitly confirmed in the Pt catalyst. The loss of catalyst activity was also due to reduction on the surface of catalysts. It was also proved although the deactivation took place within a few hours of the experiment, the catalyst reached a stable structure that allowed

a constant activity. Furthermore, manganese and copper were detected by ICP analysis of the stream exiting the reactor. The leaching was a consequence of the poor mechanical structure of the catalyst and the corrosive atmosphere under which the reaction took place.

The mechanism for which the oxidation of organic compounds in supercritical fluids has been thoroughly discussed. Several typical reaction models, which involve steps of adsorption and desorption, such as LHHW and power-law have been used to fit the experimental data. The comparison of the models is based on the residual value of the function being optimised, which relates the difference between the experimental and predicted values calculated from the proposed model. In conclusion, the power-law reaction rate best fitted the experimental data. Detailed mechanisms based on elementary reaction models have been proposed for the oxidation of organic compounds in supercritical water. Nonetheless, such models were adapted from gas phase combustion reactions where four important effects are neglected: the effect of water as solvent in the system, the extrapolation of the model to a high pressure zone, the occurrence of an ionic mechanism that simultaneously takes place, and in the case of this research, an heterogeneous system.

After the experimental study carried out to catalytically oxidize both nitrogen-containing organic compounds over three catalyst a summary of findings is presented in Table 5.8. Oxidation occurred faster in reactions with DBU than quinoline and it was concluded that chemical structure influenced the rate at which molecules are being oxidized. The aromatic ring present in the quinoline structure was more stable and thus higher residence time within the reactor was required to allow that interactions between reactants and catalyst produces a less stable molecule. Once the reaction started, it proceed without a high production of intermediates. This demonstrated that aromatics rings were more difficult to oxidise. On the contrary, DBU molecule was highly unstable in spite of the ring structures and only traces of it were detected in some experiments. The fact of the poor stability was also of importance because DBU produced a high amount of intermediates which were not completely oxidized. As it was mentioned in Chapter 4, DBU can be completely hydrolyzed in supercritical water but the TOC content of the stream was unchanged. As the molecule is degraded lower molecular weight molecules are produced which it can be the case carboxylic acids or ammonia. These are recalcitrant to the reaction and became important to evaluate the efficiency of the process. Also, in Table 5.8 the

performance of the catalysts was evaluated in terms of the production of carbon and nitrogen containing by-products and catalyst stability. Pt catalyst promoted the fastest oxidation rate and reduced the production of carbon and nitrogen containing by-products. However, it was the most unstable at supercritical conditions according to the reduction in the elimination of TOC and organic compound at the beginning and the end of the test. It was demonstrated that at least for this catalyst, the loss of surface of the catalyst was responsible for the reduction of its stability. Although the MnO_2/CuO and CuO catalyst maintained an acceptable oxidation of carbon and nitrogen containing intermediates, the rate of oxidation was lower than the Pt catalyst. From both of them, it was demonstrated that MnO_2/CuO exhibited the lowest rate of deactivation. The deactivation observed was due to chemical and physical changes on the catalyst surface but the structures found after the process were active and stable after the stability test.

Table 5.8: Comparison of the Catalyst Performance for DBU and Quinoline

Parameter Evaluated	DBU	Quinoline
Rate of oxidation	$Pt>MnO_2/CuO>CuO$	$Pt>MnO_2/CuO$
Lowest production of carbon-containing intermediates	$Pt>MnO_2/CuO>CuO$	$MnO_2/CuO>Pt$
Lowest production of nitrogen-containing intermediates	$Pt>CuO>MnO_2/CuO$	$Pt>MnO_2/CuO$
Catalyst performance under SCWO conditions	$MnO_2/CuO>CuO>Pt$	$MnO_2/CuO>Pt$

Chapter 6

Optimal Modelling and Experimentation in CSCWO

In Chapters 4 and 5 the kinetics of the catalytic reaction were obtained from experimental data by assuming a certain reaction rate model that best fitted the data. The experimental data however, were fitted into different reaction models, typically those which, in the sense of the chemical kinetics, could represent the phenomenon at least with a basic understanding of the reaction occurring (stoichiometric equation) by the principle of mass action [306]. Nevertheless, this approach not necessarily assured that the reaction was indeed described by this practical and convenient assumption. For the case of heterogeneous reactions, other *suitable* reaction mechanisms based on the adsorption and desorption steps have been also investigated (Langmuir-Hinshelwood-Hougen-Watson (LHHW) and Mars van Krevelen). These mechanisms, besides giving more information about the reaction mechanism by not overlooking the inherent mechanism of heterogeneous catalytic reactions [307], do not necessarily indicate a better representation of the reaction. If the mechanism of the reaction happens to be more complex or different than is assumed, the kinetic and adsorption constants only served as mere fitting parameters of the experimental data, and consequently, they lack of any physical meaning; a greater number of parameters would give a better computational fit for a given set of experimental data. In addition, in the case of reactions at supercritical conditions the fitted values obtained from the reaction rate (adsorption constants) cannot be compared to any experimental data because those are rarely available for the organic compound studied. It has been demonstrated by rigorous computer calculations (Appendix B), that at least the use of LHHW reaction rate models do not necessarily mean a better representation of the experimental data. In spite of its simplicity and theoretical background (compared with adsorption-desorption models), the power-law reaction rate model could be extended to applications like those presented in this

research. A power-law reaction rate does not represent a true mechanism of the reaction, instead it would rather be seen as a summary of a set of reactions occurring (e.g. stoichiometric equation)[1]. In the field of investigating reaction kinetics, until now this work has covered one of the parameters that could influence the acquisition of kinetic data. According to Cutler et al. [308], the source of error in chemical kinetic data are due to errors in the assumption of the reaction model, experimental error, and the selection of the reactor model.

A second type of error has been assessed experimentally by performing reproducibility tests of the experimentation and establishing a set of operating conditions that could accomplish the adoption of an isothermic, isobaric and isochoric reactor operation. Nonetheless, the reactor model is often omitted as source of error in obtaining the reaction rate models. It was not intended to say that the assumption of a tubular approach was poor, instead it has rather given ground to support its selection and add some guidelines for the design of a better reactor for catalytic and non-catalytic SCWO, and consequently kinetic calculations.

First of all, the scale at which experimental data are taken have a direct impact on the chemical kinetic data produced. It is advisable that in the design stage of a fixed-bed chemical reactor, two factors that give dimensions to the reactor should be followed to minimise the deviation of a plug-flow operation [250]:

$$\frac{d_R}{d_p} > 10 \tag{6.1}$$

$$\frac{L}{d_p} > 50 \tag{6.2}$$

Where d_R is the reactor diameter, d_p is the diameter of the catalytic particle and L is the length of the reactor. Both factors would assume an ideal plug-flow operation because the length of the reactor and minimum diameter strongly influence its performance. At industrial scale both are commonly achieved, however in the laboratory this is not the case because of the limitations of the laboratory equipment. Consequently, microreactors like the one used in this research could produce certain limitations when compared to ideal reactors. Nevertheless, microreactors are preferred because at operating conditions above the thermodynamic critical point of water,

[1] By this it is assumed that the kinetics of the reaction have been represented by a pseudohomogeneous model in which there is no information of any interaction between the fluid and the packing material. Strictly speaking this is not appropriate for fluid-solid catalytic reactions but in absence of an exact mechanism for the reaction, this was followed as the most reasonable approach.

they are economical, have easy operation, have simple construction and are safer because of the small amount of materials involved. The design of a microreactor is an aspect previously reviewed by Silverstein and Shinnar [309] where they exposed key aspects, such as the back-mixing and mass transfer effects as preventing the use of microreactors for scaling-up purposes because the unrealistic kinetics obtained from them. The latter, however is often evaluated from experimentation by varying the amount of catalyst and the particle size in the reactor, which are related as interphase and intraphase concentration gradients respectively [250, 267]. The backmixing limitation occurs in the case when the pressure drop is significant enough to create fluctuations in the concentration of the reacting mixture or by limitations in the flow rate, and thus, the superficial velocity of the fluid. The degree of dispersion in a fixed-bed reactor deviates it from its plug-flow operation and causes reduction in the conversion or selectivity and therefore produces unreliable kinetic parameters. In order to estimate the degree of dispersion in the reactor, the residence time theory has been extensively applied [310]. Nonetheless, measurements of the degree of dispersion are not always possible, as for example in supercritical water. Most common tracer techniques involve salts or other organic compounds that are quantified analytically. In supercritical water salts are poorly soluble and the stability of the organic compounds are compromised by the operating conditions. These common assumptions avoid the evaluation of the real reactor operation which greatly simplifies the mathematical model used.

6.1 The Isothermal Fixed-bed Reactor Model

Two general balances can describe the operation of a tubular reactor: mass and energy. When an isothermal operation has been reached the amount of heat generated or absorbed is considered as null and the reactor operation is given only in terms of mass balance. Consider a reactor of radius R and length L as represented by Figure 6.1 (since the geometry of reactor is cylindrical these coordinates are preferred, though it also can be transformed to other coordinates):

Considering the differential elements in the radial and axial direction (dr and dx), a shell mass balance of the tubular fixed-bed catalytic reactor carried out in cylindrical coordinates by assuming a constant fluid density is given by

$$u_S \frac{\partial C_i}{\partial x} = D_L \frac{\partial^2 C_i}{\partial x^2} + D_R \left[\frac{1}{r} \frac{\partial C_i}{\partial r} + \frac{\partial^2 C_i}{\partial r^2} \right] + \varepsilon \mathscr{R}_i - \frac{\partial C_i}{\partial t} \tag{6.3}$$

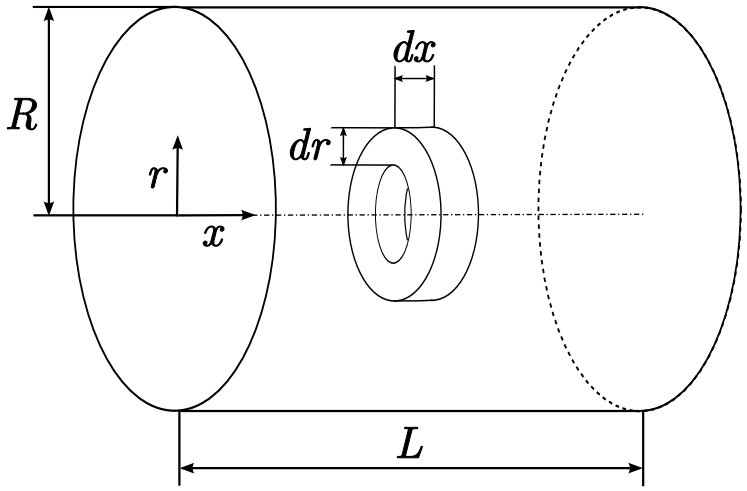

Figure 6.1: Shell Balance of a Tubular Reactor

Where x (length) and r (radius) define a point inside the reactor, u_S the superficial velocity along x and D_L and D_R are the dispersion in axial (longitudinal) and in radial (transverse) position, respectively (a detailed mathematical treatment to arrive to the conservation equation presented above can be found elsewhere [230]).

6.1.1 One Dimensional Models for Isothermal Fixed-bed Reactors

A first simplification of the reactor is given when a steady state operation is reached and the accumulation term $\frac{\partial C_i}{\partial t}$ is set to zero. Further simplifications can be done by assuming that the degree of dispersion in axial and radial positions are negligible and thus an ideal tubular reactor flowing in plug-flow operation was satisfied, consequently Equation 6.3 can be transformed to

$$u_S \frac{\partial C_i}{\partial x} = \mathscr{R}_i \qquad \text{or} \qquad u_S \frac{dC_i}{dx} = \mathscr{R}_i \tag{6.4}$$

Note that the void fraction was ignored and the reaction rate is given in terms of the volumetric properties and not to any catalyst property. This equation is known as one dimensional model of tubular reactor. Written in this manner Equation 6.4 seems unfamiliar, albeit a few mathematical manipulations can be done by identifying that:

$$F_i = C_i u_S (\frac{\pi d_R^2}{4}) \qquad \text{and} \qquad V_R = (\frac{\pi d_R^2}{4}) L \tag{6.5}$$

and thus a more familiar expression is derived from Equation 6.4:

$$\frac{dF_i}{dV_R} = \mathscr{R}_i \tag{6.6}$$

This equation resembles the one proposed by Froment and Hosten [273] used in the fitting of the experimental data by substitution of the weight of the catalyst by $W = \rho_B V_R$ (where ρ_B is the density of the bed). This model is often used to represent the operation of a catalytic reactor because it is easier to integrate. This model is only an approximation that can be used to study the response of the system to changes in the process operating conditions or catalyst size and to obtain information about reaction kinetics. A simple correction to Equation 6.4 is obtained by adding the diffusive term and obtain the one dimensional axial dispersion model [311]:

$$u_S \frac{dC_i}{dx} = D_L \frac{d^2 C_i}{dx} + \mathscr{R}_i \tag{6.7}$$

This reactor model has been perhaps one of the most useful mathematical expressions to study the real behaviour of chemical reactors. Attributed to Danckwerts [312] by his pioneering work on continuous flow-systems and recently reviewed by Nauman [313], the convective-diffusive axial or axial dispersion model has been for many years the ground for the understanding the mixing phenomena that occurs in chemical reactors and it has helped to settle the two performance boundaries of performance of any real continuous flow reactor. These boundaries lie between a continuous stirred tank (maximum mixedness) and plug flow reactor (minimum segregation) [314]. However, the solution of the axial dispersion model represents a mathematical *particularity* imposed by set of the boundary conditions involved, whose solution involves an iterative procedure [315, 316, 317]. Much work has been discussed and published about the boundary conditions and their significance in the solution of the axial dispersion model but Danckwerts' boundary conditions (closed type) are the most commonly applied [313][2].

From its formulation the axial dispersion model can be applied to evaluate the packed-bed tubular reactor performance. This is because in this type of reactor the velocity in the interstices originated by the packing is higher than the superficial velocity which gives importance to the back-mixing of the reacting mixture, a fact that remains unimportant in conventional laminar-flow reactors [319]. A solution of this reactor model satisfies the boundary conditions proposed by Danckwerts or the closed type model:

[2] See Bischoff [318] for a comprehensive discussion on the boundary conditions.

$$C_{i_0} = C_i - \frac{D_L}{u_S}\frac{dC_i}{dx} \qquad \text{at the inlet,} \qquad x = +0 \tag{6.8}$$

$$\frac{dC_i}{dx} = 0 \qquad \text{at the outlet,} \qquad x = L \tag{6.9}$$

If the first boundary condition is carefully analysed, the model predicts a change of reactant concentration created by the dispersion coefficient, which is the main difference from initial value problem (IVP) where the initial concentration at position $x = +0$ are the same. By convenience the initial concentration of i and length of reactor are used to yield a dimensionless equation when:

$$v_i = \frac{C_i}{C_{i0}}; \qquad z = \frac{x}{L} \tag{6.10}$$

Thus the axial dispersion model is given by the following expression:

$$\frac{dv_i}{dz} = \frac{D_L}{u_S L}\frac{d^2 v_i}{dz^2} + \frac{\mathscr{R}_i L}{C_{i0} u_S} \tag{6.11}$$

When conversion data (X_i) are given, Equation 6.11 can be modified by making $dv_i = -dX_i$ which yields to

$$\frac{d^2 v_i}{dz^2} = N'_{Pe,L}\left(\frac{dv_i}{dx} + \frac{\mathscr{R}_i L}{C_{i0} u_S}\right) \tag{6.12}$$

A dimensional number known as the Peclet number is defined as $N'_{Pe,L} = \dfrac{D_L}{u_S L}$. The boundary conditions were also scaled and given in terms of conversion to produce:

$$\frac{dv_i}{dz} = N'_{Pe,L} v_i \qquad \text{at the inlet,} \qquad z = +0 \tag{6.13}$$

$$\frac{dv_i}{dz} = 0 \qquad \text{at the outlet,} \qquad z = 1 \tag{6.14}$$

The numerical integration of the differential equation imposes a boundary value problem (BVP) where its solution must satisfy the two-point boundary conditions set. The solution of the ordinary differential equation requires a different integration procedure than common IVP's. For BVP a common approach is to implement numerical routines known as shooting methods

[320], however the method chosen for the integration of the differential equation was collocation [321]. The collocation method is based on the interpolation of the sample points by a function which is usually a polynomial (which has the form $P_n(x) = c_0 + c_1x + c_2x + \cdots + c_nx$) that best approximates the solution of the differential equation within the range of integration. The method searches for the value of the coefficients of the polynomial that minimises the difference between the true solution of the differential equation and the polynomial. Thus for a certain number of collocation points, and consequently an equal number of coefficients, the aim is to find the values of these constants in the polynomial that produce an exact solution of the differential equation. As it is common for the polynomials the larger number of collocation points the closer it would be from the true solution of the differential equation. In the case of the axial dispersion model two of the collocation points are already determined by the boundary conditions of the equation. If the collocation points are equidistant the interpolating polynomial resembles a finite difference method because both methods are based on representing the function studied as an expansion of a Taylor series [321, 322].

A MATLAB® (The MathWorks, Inc.) code was written to solve the axial dispersion model which implements a finite difference algorithm for the integration. Because the integration routine only allows the solution of first-order differential equations a substitution of the term of conversion of the form $y_1 = v_i$ and $y_2 = dv_i/dz = v_i\prime$ produced a simplified set of first-order differential equations:

$$y_1' = y_2 \tag{6.15}$$

$$y_2' = N_{Pe,L}\left[y_2 + \frac{\mathscr{R}_i L}{C_{i0}u_S}\right] \tag{6.16}$$

Figure 6.2 provides a comparison of the reaction rate of quinoline over MnO_2/CuO catalyst for the two types of one dimensional reactor model. The operating conditions chosen were 673 K and 23.0 MPa, while the initial concentration of reagents were 0.3 and 3.225 mmol/L of quinoline and oxygen, respectively. As seen from the figure the outlet conversion of quinoline predicted by both models was very close. However, the initial boundary condition imposes a different behaviour at the entrance of the reactor. The plug flow assumes that the concentration at the inlet ($z = 0$) remained unchanged due to the initial value solved (assumption of no conversion

until this point). On the other hand, the axial dispersion model showed a change of the quinoline concentration caused by the degree dispersion of the flow just after the inlet ($z = +0$). The Peclet number was calculated from a correlation proposed by Foumeny and Chowdhry [323]; the value close to 2 indicates a high dispersion at the entrance ($D_L \to \infty$), and so in this limit the model behaves closer to a continuous stirred tank. The N_{Re} based on the superficial velocity was 334, however the values of Reynolds number based on interstitial velocity are considerably higher which allow the assumption of an axial dispersion model.

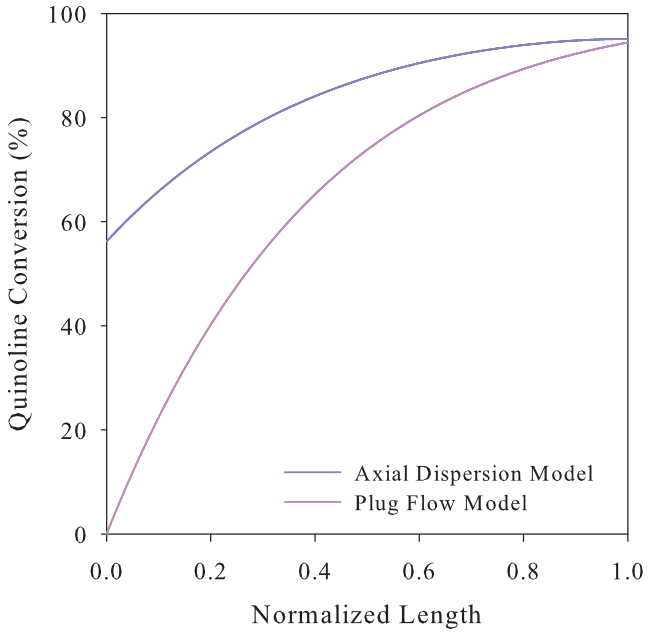

Figure 6.2: Reactor Model Comparison for N_{Pe_L} =1.92 and $u_S = 1.44\ cm/s$

There are two important factors, one operational and the other mathematical to notice from the solution of the BVP. The first one is to calculate the axial Peclet number, which is not an easy task considering that the correlations to calculate it are functions of the Schmidt and Reynolds numbers. The calculation of these dimensionless numbers incidentally depend on the physicochemical properties of the reacting mixture, data that are not always available for chemical substances at supercritical conditions. Moreover, the mathematical relationship to compute the Peclet number are obtained from experimental data of liquids and gases. The latter point is because the numerical solution of BVP generates more than one solution, nevertheless careful scrutiny of the solution will give the most sensible answer.

It is important to notice the fact that the evaluation of the Peclet numbers in non-reactive packed-bed systems to assess the absence of dispersion in either longitudinal or radial is not appropriate. It is evident (as pointed out by Wakao et al. [324]), that dispersion coefficients are strongly influenced by the reaction taking place in the fluid-solid heterogeneous reaction or even in homogeneous reactions [308].

A criteria that involves the hydrodynamics and reaction influence of this type was formulated by Mears [277, 325] and it is useful to estimate the absence of axial dispersion as given by:

$$\frac{L}{d_p} > \frac{20\,n}{N_{Pe,L}}\,\ln\left(\frac{C_{i_0}}{C_{i_f}}\right) \tag{6.17}$$

Where C_{i_0} and C_{i_f} are the initial and final concentrations of the species i in the reaction and n is the reaction order. For the case of fluid-solid catalytic reactions in supercritical water, data of dispersion are scarce and thus assumptions were made in order to calculate Peclet numbers. In this criteria, it is clearly shown that as the conversion increases, the backmixing is avoided in a longer reactor.

An interesting point that is worth considering is that the performance of the reactor could be affected by its design. As it was originally proposed by Langmuir, the assumption of the initial boundary condition assumes a degree of dispersion which was explained by the author as if a porous disc was place in the entrance of the reactor; a shared design characteristic with this experimental reactor [313]. Thus the dispersion created by the flow of the mixture in the microchannels of the porous disc could have affected the conversion of the reagents before they even were in contact with the catalyst surface. However, it goes beyond the scope of this work and it would be considered as a future research topic.

Another valid point by choosing the axial dispersion model is that the radial dispersion can be neglected for a small ratio of column diameter to length and large fluid velocity. By this, it is the diffusion term could still have significance in the specific case of CSCWO reactions, but a more traditional approach to model a packed-bed catalytic tubular reactor has been proposed to study its performance.

6.1.2 Two Dimensional Model for Isothermal Fixed-bed Reactors

Until now, a brief mathematical description of the most studied models was presented based on the importance of the model selected for representing the experimental data. Once the reactor model has been selected to study a certain reaction, it is typically assumed in most cases to be an ideal reactor. Deviation from the ideal behaviour are very common i. e. constraints in the design, unknown behaviour of the reaction, limitations in the experimental equipment and operating conditions and safety regulations. In spite of all these limitations, the ideal reactor is still chosen to study the reaction rate. In other words it is necessary to evaluate the *appropriateness* of a reactor model to represent a certain reaction. It is not intended to assess the different reactor models at fitting the experimental data, instead it is rather to assess how far is the assumption of a ideal reactor from the real behaviour of the experimental reactor.

A more complete representation of the reactor is given if the accumulation term in Equation 6.3 is null and then chemical reactor is represented by the two dimensional convective diffusive model of the form (note that the void fraction ε, indicates a reaction occurring in an heterogeneous system):

$$u_S \frac{\partial C_i}{\partial x} = D_L \frac{\partial^2 C_i}{\partial x^2} + D_R \left[\frac{1}{r} \frac{\partial C_i}{\partial r} + \frac{\partial^2 C_i}{\partial r^2} \right] + \varepsilon \mathscr{R}_i \tag{6.18}$$

The dispersion coefficients are an indication of the degree of the mixing phenomena that take place inside the vessel and characterise the performance of the reactor. It is well documented that the dispersion is intimately related to the conversion in a chemical reactor while the fluid moves along the fixed-bed [278]. The degree of dispersion of the fluid in an inert packed-bed is a consequence of the diffusive and convective forces in the interstices, and which consequently, are complexly related to the system geometry, packing and fluid physicochemical properties [326]. In the field of reactor design the dispersion coefficients are presented as a dimensionless number that relates the axial convection to axial and radial diffusive transport known as Peclet numbers:

$$N_{Pe,L} = \frac{u_S d_p}{D_L} \tag{6.19}$$

$$N_{Pe,R} = \frac{u_S d_p}{D_R} \tag{6.20}$$

At high Reynolds numbers the axial and radial Peclet numbers tend to values of 2 and 10-12, meanwhile when $u_S \to \infty$, the values become 2 and 12, respectively [230, 326]. As $u_S \to 0$, the dispersion will depend solely on the molecular diffusion (microscopic scale). On the other hand, as the velocity increases the contribution of the convective force becomes noticeable. So far, a complete description of the reactor model has been done by incorporating the longitudinal and transverse dispersion terms. Nevertheless, the two dimensional model could also be simplified by assuming that term of dispersion in the axial direction could be neglected and Equation 6.18 yields to:

$$u_S \frac{\partial C_i}{\partial x} = D_R \left[\frac{1}{r} \frac{\partial C_i}{\partial r} + \frac{\partial^2 C_i}{\partial r^2} \right] + \varepsilon \mathscr{R}_i \tag{6.21}$$

This assumes a premixed feed stream with axial symmetry (an assumption which is done in the case of a fixed-bed), where the axial transport by molecular and turbulent diffusion is neglected [271][3]. At high Reynolds numbers, the main mechanism of the transverse dispersion is due to the deflections of the fluid path as it flows downstream (macroscopic scale). The flow does not reach the superficial velocity where the longitudinal coefficients largely contribute. Moreover, an extrapolation made from tubular reactors points out that the radial dispersion coefficient are all alike by assuming either a flat flow profile or averaging the coefficient from a varying velocity profile [327, 328]. The D_L term represents the backmixing process in the system that imposes an additional transfer mechanism that effectively increases the concentration of the reagent in the effluent and lowers the conversion. In gas phase, the overall effect of dispersion becomes significant for the case of short beds and when high conversion values are attained, which are rarely encountered in commercial-scale reactors. On the other hand, it is in laboratory units when this could be critical especially in microreactors.

The addition of the axial diffusive term (Equation 6.18) posed a more complex solution because the boundary conditions taken and the non-linear dependence of concentration. The model in Equation 6.21 has been shown to give an acceptable representation of the reaction in fixed-bed catalytic reactor of different reactions [329, 330, 331]. Consequently, the term of axial

[3]The velocity profile inside a packed bed is complex and it is often assumed to be flat, albeit the superficial velocity near the wall is different from the rest of the tube because the voidage near the wall of the tube is higher. Consequently, the zone of the vessel in which the fluid velocity is high is restricted to that area where the porosity is also high; which does not extend more than a particle diameter from the wall and thus the assumption of a flat profile is sensibly accurate [326].

diffusion does not contribute appreciably during the reaction [311].

Based on the previous discussion and the hydrodynamics of the system studied, Equation 6.21 was the most suited representation for the catalytic reactor. The solution of the partial differential equation is given by three boundary conditions one in the axial direction $C_i(r,0) = C_{i_0}$, given at the inlet and having an initial value of concentration (C_{i_0}) and two other in the radial position which are set at the centerline ($r = 0$) and the wall ($r = R$) where $\dfrac{\partial C_i}{\partial r} = 0$. Because of simplicity Equation 6.21 has been transformed into dimensionless parameters by taking

$$v_i = \frac{C_i}{C_{i\,0}}; \qquad y = \frac{r}{R}; \qquad z = \frac{x}{L} \tag{6.22}$$

Furthermore, by changing the data of conversion instead of concentration that is $dv_i = d(C_i/C_{i\,0}) = -dX_i$, as a result a new equation is produced:

$$\frac{\partial v_i}{\partial z} = \frac{D_R L}{u_S R^2}\left[\frac{1}{y}\frac{\partial v_i}{\partial y} + \frac{\partial^2 v_i}{\partial y^2}\right] + \frac{\varepsilon L \mathscr{R}_i}{u_S C_{i\,0}} \tag{6.23}$$

which is analogous to Equation 6.21 in dimensionless form and where the contribution of the axial diffusive term is unimportant. Equation 6.23 has been solved numerically by the method of lines (MOL). The MOL discretises only the radial direction and solves the remaining axial position analytically. (A thorough description of the MOL applied to the solution of the partial differential equation represented by Equation 6.23 is given in Appendix C).

Additionally as the catalytic bed was diluted the reaction rate has to be modified and a new form of the reaction rate yields to

$$\mathscr{R}_i^{\dagger} = \frac{\varepsilon \mathscr{R}_i}{1+\varphi} \tag{6.24}$$

Where φ is the dilution factor of the bed, in this form the reaction rate is written in terms of the interstitial volume [332]. The main difference is that in this way the model is not considered as a pseudo-homogeneous, a convention usually taken in the case of a plug-flow model, where the kinetic constant and the space velocity are independent of the dilution. When the catalyst is diluted with inert solids, the bed length is also increased and therefore approximates the performance to a plug flow operation. This also can be equally achieved by increasing the amount of catalyst and keeping a constant space velocity [250].

Nevertheless, in isothermal operation the set of ordinary differential equations is self simplified and each line created (by MOL) resembles a plug-flow reactor model. This can be seen from the concentration profile in Figure 6.3 a and c and Figure 6.3 b and d where the three lines plotted (at centerline, middle and wall) are overlapped.

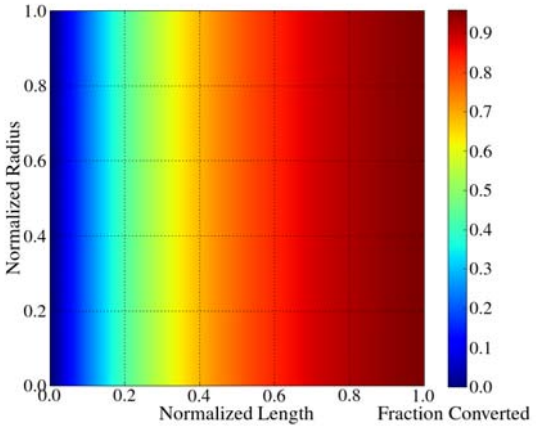

(a) Concentration in three lines $u_S = 0.5\ cm/s$

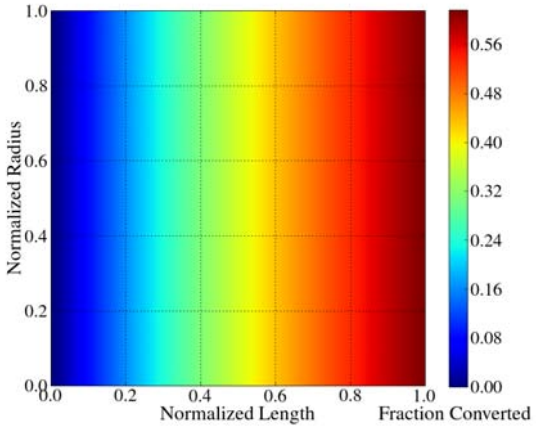

(b) Concentration in three lines $u_S = 1.5\ cm/s$

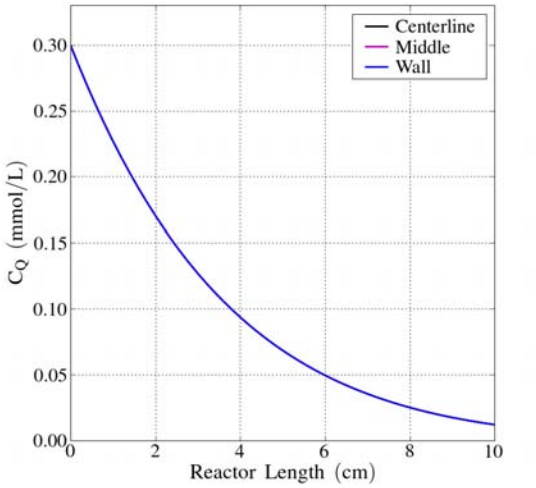

(c) Concentration in three lines $u_S = 0.5\ cm/s$

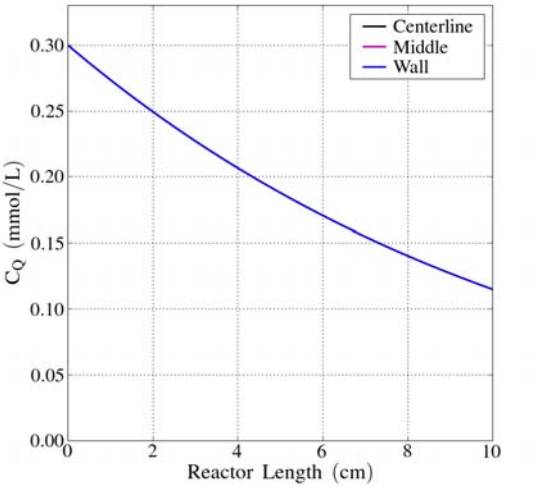

(d) Concentration in three lines $u_S = 1.5\ cm/s$

Figure 6.3: Concentration Calculated by the MOL Method

These results were a consequence of carefully adopted operating conditions in order to avoid abrupt changes in temperature along the catalytic bed which would generate a more complicated problem. However, Equation 6.23 can give a better reactor representation when it is coupled

to an energy balance. In industrial reactors temperature changes occur constantly, at least for SCWO, because inlet concentration changes are common and it moves the operation to a non-isothermal zone where both equations (mass and energy balances) become vital to predict unstable operation regimes [333].

6.2 Application of Inverse Methods in Investigating Reaction Kinetics

The intention of this final section is to establish the mathematical grounds of the procedures in Chapter 4 and 5 for computing the kinetics of the reaction with the aim of establishing some guidelines for better data acquisition (experimental design) and results computation. The importance of the common sources of error in the development of reaction kinetics have been previously discussed however, there are always factors that are overlooked and that could be improved, but unfortunately cannot always be implemented.

These factors basically arise from the experience in collecting and performing the fitting of experimental data. It is a common approach (at least at experimental level), especially in the case of novel process, to study the influence of the main operating conditions over its performance. The traditional way to understand the influence of the variables in the process is by keeping one of them stationary while the remaining ones are varied in the ranges of interest to the experimenter. This is however a mere empirical approach that is commonly accepted yet not completely convincing. The reality is that although the number of experimental data might be generous not all of them possess significant information required to build up a reliable kinetic model. Consequently, the modelling of any steady or transient operation not only relies on its governing equations but also on the quality of the data used to produce such a model.

Fitting experimental kinetic data to a basic problem in question is known as an inverse problem. In this case certain measurements of the system were obtained at operating conditions and the task is to find those parameters in the model that best minimise the difference between the experimental data and those predicted by the model. To understand this it is necessary to study the typical formulation of a forward problem. Conventionally, a forward problem at least in the sense of chemical kinetics in vector notation is given by:

$$m = f(p : \beta) \tag{6.25}$$

where a set of the kinetics parameters (p) and operational parameters (β) is used to predict a set of measurements of the system (m) [334]. On the other hand, an inverse problem is posed as:

$$p = f^{-1}(m : \beta) \tag{6.26}$$

This is of course a non-trivial problem and its solution will depend if the problem is well defined (well-posed) [335]. In many cases data are overdetermined (the number of measurements is greater than the number of parameters) and again the problem requires the modification of the traditionally inverse function.

Zimmerman and Rees [336] have stressed the importance of optimal modelling and experimentation based specifically on the application of the inverse methods. Inverse methods can also be developed and implemented not only to estimate kinetic parameters, but also for example, for the calculation of the physicochemical properties of the substances when there are not data available [337, 338]. This trend is common in supercritical fluids or to identify zones of optimal performance of irreversible and reversible reactions limited by mass transfer effects [339, 340] or even in reaction-separation systems [341]. Although only the application related with reaction engineering field was disclosed through this thesis, the idea of combining inverse methods can be extended to different research areas in different disciplines of knowledge [342]. Incorporating inverse methods gives a novel approach to obtain more reliable and useful information from experimental work by identifying which experiments provide the most qualitative information in order to construct better models to represent chemical processes.

Conclusions

Based on the results obtained for the non-catalytic hydrolysis of glycerol in supercritical water and the catalytic supercritical water oxidation of nitrogen-containing organic compounds carried out in a tubular reactor, it is concluded that:

- Hydrolysis in supercritical water can be used to produce alternative fuels from industrial waste. Fuels such as hydrogen and methane were produced from the pyrolysis of glycerol in supercritical water (see Section 1.2.2.1).
- Temperature and pressure played an important roll in the production of hydrogen and methane from the decomposition of glycerol in supercritical water. Hydrogen and methane production was favoured at a temperature of 873 K and pressure of 25.0 MPa.
- The prediction of the physicochemical properties of water was important especially near its critical point. Errors in the prediction of fluid properties can lead to inadequate design of the equipment. A specific equation of the state IAPWS 95 was implemented for the prediction of the properties of water at supercritical conditions.
- Complete decomposition of hydrogen peroxide to oxygen and water was verified experimentally in the preheating section.
- It was experimentally demonstrated that the catalytic supercritical water oxidation process oxidised faster and produced less intermediates than the non-catalytic process.
- Operating conditions, such as temperature, pressure and space velocities time were lower in the catalytic process than the non-catalytic reaction.
- The chemical structure of the organic compound had an effect on the operating conditions required for its oxidation. Organic compounds containing aromatic rings were more stable (i. e. quinoline) and thus required higher temperature and lower space velocities for their oxidation than less stable molecules (DBU).

- Absence of external concentration gradients was evaluated experimentally for all catalysts.
- Fast reactions were influenced by intraphase concentration gradients as calculated from the Bischoff criterion. Reaction rates for DBU on Pt and MnO_2/CuO catalysts and quinoline on Pt catalyst were affected by the internal concentration gradient effect through the calculation of the effectiveness factor.
- Reproducibility tests were performed to establish the reliability of experimental data with maximum 10% of experimental error.
- Temperature was the main controlling variable of the catalytic oxidation reaction in supercritical water. An operation temperature near to the critical temperature of water (653 K) produced almost complete removal of the nitrogen-containing organic compounds and the total organic content.
- The effect of pressure on the oxidation depended on the catalyst over which the reaction took place. However, the effect of increasing the system pressure did not prove to enhance considerably the removal of the organic compound. Pressure operation near the critical pressure of water (23.0 MPa) was sufficient to eliminate a considerable amount of the organic compound being oxidised.
- Increasing the initial concentration of the organic compound did not affect the removal of the organic compound and total organic carbon content.
- An increment of initial oxygen concentration above a stoichiometric ratio of 2 produced only a small improvement to both organic compound and total organic carbon content removal.
- It was demonstrated by rigorous computer calculations that reaction rate models such as LHHW did not necessary provide a better representation of the experimental data. Power-law reaction rate models provided the smallest difference between experimental data and the data predicted by the model. This indicated that reaction rate models that include adsorption steps were not appropriate for the experimental data produced during this research.

- The activity of the catalysts studied during the present research was in the order of $Pt > MnO_2/CuO > CuO$.
- The main carbon product of the oxidation reactions in supercritical water were CO_2.
- NH_4^+, NO_3^- and NO_2^- were identified as the main nitrogen containing species in the liquid effluent.
- Among the catalysts tested, Pt on alumina gave the highest reaction rates, the highest selectivity towards the production of CO_2 and minimum production of products containing nitrogen in the liquid effluent.
- MnO_2/CuO mixed catalyst had a high selectivity towards CO_2, but it allowed the production of nitrogen-containing products.
- The adsorption and desorption isotherms of water in the fresh and spent catalysts showed that both process were reversible and did not affect the catalytic surface.
- Catalysts suffered a considerable loss of activity after a few hours of constant operation. Physical and chemical changes on the surface of the catalyst originated by the operating conditions and the oxidant atmosphere were responsible for the reduction of the catalyst activity.
- A considerable reduction in the surface area between fresh and spent catalyst was present for the catalysts studied.
- Isotherms calculated for the fresh and spent catalysts showed that although the same mechanism of adsorption-desorption was present, the amount of water adsorbed by the fresh catalyst was higher compared to the spent catalyst.
- It was demonstrated by carbon mass balance calculations the adsorption of some chemical species on the catalyst surface.
- The leaching of metals was detected in the liquid effluent for reactions that took place over MnO_2/CuO and CuO catalysts.

- X-ray diffraction patterns did not provide evidence of any change to Pt catalysts after the reaction. This indicates that operation above the critical point of water and the oxidising atmosphere of the reaction had no effect on the catalyst.

- MnO_2/CuO and CuO spent catalyst studies by X-ray diffraction showed the appearance of crystalline structures when compared to the fresh catalyst where only amorphous phases where detected. Al_2O_3 used for the catalyst support in the copper oxide catalysts was transformed to a more stable structure of $AlO(OH)$. The amorphous metal oxides were also transformed to crystalline structures, such as CuO for the copper oxide catalyst. The amorphous MnO_2/CuO catalyst was transformed to crystalline structures such as Mn_2O_3, CuO_2, MnO_2 and mixed metallic oxides of the form $Mn_XCu_YO_Z$.

- The reactor was considered to operate as a plug flow reactor. Although some other modes of operation were studied, the one dimensional convective model was the most convenient representation of the experimental reactor.

- When experimental data are required to produce a kinetic model of the reaction studied it is more convenient to apply inverse methodologies to identify what data would provide the most useful information, and thus establish a more reliable mathematical modelling of the phenomenon being studied.

Future Work

During the research some areas were identified that are worthy of further study to provide more evidence to support the development of the process at industrial scale as an available technology for the destruction of organic compounds:

- The physical and chemical properties to the catalyst surface led to a decrease in catalyst efficiency during the reaction. It would therefore be of interest to explore other catalytic materials that could maintain activity through longer periods of operation. These materials should not change their active phase during reactions unless the activity is maintained. Resistant support materials should be also explored as alumina suffered changes to its chemical structure. Platinum on silica could be an interesting catalyst because of its resistance to thermal stress.

- Novel catalytic reactor designs should also be studied to attain higher efficiencies in terms of the removal of the organic compounds, as well as a means to deal with real feedstocks where the salt content could limit the application of the process.

- Two stage operations have been envisaged as alternatives to increase the productivity of the process. For the case of supercritical water oxidation, an operation that involves a non-catalytic stage follows by a catalytic process can eliminate high concentrations of any contaminants (which are easily oxidised) during the first step leaving the second process for recalcitrant by-products and molecules hard to oxidise. In this way, the energy input for the first process is integrated in to the second stage.

- It has been demonstrated that processes involving supercritical water can also be used to convert residues such as glycerol to useful alternative fuels, e.g. hydrogen and lighter hydrocarbons. The process that is a non-catalytic pyrolysis in an aqueous media produces small amounts of solid carbonaceous residues and other water soluble molecules that can be efficiently and easily destroyed by the addition of the oxygen in a subsequent stage.

- The modelling of the reactor was done by assuming the simplest mathematical expression (for convenience in the mathematical calculations) which is the plug flow reactor model. Because the design of the catalytic reactor implies a high turbulence zone at the entrance an extension of the one dimensional reactor that includes the convective and diffusive terms would be enough to improve the mathematical representation of the reactor.

- So far, the implementations of detailed kinetic mechanisms that have been extrapolated from the combustion of organic compounds have been produced good results in the prediction of product distributions for supercritical water oxidation. There is however, no information about their application to heterogeneous catalytic systems. A kinetic study of heterogeneous catalytic reactions will help to understand how the reactions proceed above the critical point of water and to establish how water influences the reaction.

- The catalyst performance in terms of selectivity changed above the critical point of water. Catalysts used during the research project were expected to increase the oxidation of ammonia, nevertheless in aqueous reactions the equilibrium that is responsible for the production of molecular nitrogen was displaced, which led to a high concentration of intermediates such as nitrates. Consequently, it is necessary to have a better understanding of the reactions that take place in the oxidation of nitrogen by catalytic supercritical water oxidation. The effect of pressure that was overlooked during the present research project should be considered.

- The aim of the research was to establish a basic understanding of catalytic oxidation in supercritical water of nitrogen-containing organic compounds. Any future research should consider the identification and quantification in detail of the products and the remaining by-products in order to build a proper reaction mechanism. It has been assumed that the mechanism responsible for the oxidation of the organic compounds has been a free radical, nevertheless the addition of a large amount water and operating conditions above the critical point make it appropriate to consider a parallel ionic reaction mechanism.

Bibliography

[1] P. G. Jessop; W. Leitner. *Chemical synthesis using supercritical fluids.* Wiley-VCH, Weinheim, 1999.

[2] P. Kritzer; E. Dinjus. An assessment of supercritical water oxidation (SCWO). Existing problems, possible solutions and new reactor concepts. *Chemical Engineering Journal*, 83:207–214, 2001.

[3] W. Wagner; A. Pruß. The IAPWS formulation 1995 for the thermodynamic properties of ordinary water substance for general and scientific use. *Journal of Physical and Chemical Reference Data*, 31:387–535, 2002.

[4] J. S. Haselow; S. J. Han; R. A. Greenkorn; K. C. Chao. Equations of state for supercritical extraction. In *ACS Symposium Series*, pages 156–178, U. S. A., 1986. American Chemical Society.

[5] F. Gaspar; T. Lu; G. A. Leeke. Effect of flowrate on the extraction of volatile concentrates and resinoid compounds from Origanum virens using compressed CO_2. *Journal of Essential Oil Research*, 17:89–93, 2005.

[6] G. A. Leeke; F. Gaspar. Comparison between compressed CO_2 extraction and hydrodistillation of essential oils. *Journal of Essential Oil Research*, 16:64–68, 2004.

[7] J. D. Seader; E. J. Henley. *Separation Process Principles.* John Wiley and Sons, Inc., New York, 1998.

[8] J. F. Brennecke; C. A. Eckert. Phase equilibria for supercritical fluid process design. *AIChE Journal*, 35:1409–1427, 1989.

[9] G. A. Leeke; R. C. Santos; B. Al-Duri; J. P. K. Seville; C. J. Smith; C. K. Y. Lee; I. F. McConvey. Continuous-flow Suzuki-Miyaura reaction in supercritical carbon dioxide. *Organic Process Research and Development*, 11:144–148, 2007.

[10] E. Reverchon; I. De Marco. Supercritical fluid extraction and fractionation of natural matter. *Journal of Supercritical Fluids*, 38:146–166, 2006.

[11] E. Reverchon; R. Adami. Nanomaterials and supercritical fluids. *Journal of Supercritical Fluids*, 37:1–22, 2006.

[12] W. H. Hauntal. Advances with supercritical fluids [review]. *Chemosphere*, 43:123–135, 2001.

[13] A. S. Teja; C. A. Eckert. Commentary on supercritical fluids: Research and applications. *Industrial and Engineering Chemistry Research*, 39:4442–4444, 2000.

[14] C. A. Eckert; K. Chandler. Tuning fluids solvents for chemical reactions. *Journal of Supercritical Fluids*, 13:187–195, 1998.

[15] B. Subramaniam; M. A. McHugh. Reactions in supercritical fluids - A review. *Industrial Engineering Chemistry Process Design and Development*, 25:1–12, 1986.

[16] P. E. Savage; S. Gopalan; T. I. Mizan; E. E. Brock. Reactions at supercritical conditions: Applications and fundamentals. *AIChE Journal*, 1995(7):1723–1778, 1995.

[17] A. Baiker. Supercritical fluids in heterogeneous catalysis. *Chemical Reviews*, 99:453–473, 1999.

[18] P. G. Jessop; T. Ikariya; R. Noyori. Homogeneous catalysis in supercritical fluids. *Chemical Reviews*, 99:475–493, 1999.

[19] A. Kruse; E. Dinjus. Hot compressed water as a reaction medium and reactant. Properties and synthesis reactions. *Journal of Supercritical Fluids*, 39:362–380, 2007.

[20] W. Bühler; E. Dinjus; H. J. Ederer; A. Kruse; C. Mas. Ionic reactions and pyrolysis of glycerol as competing reaction pathways in near- and supercritical water. *Journal of Supercritical Fluids*, 22:37–53, 2002.

[21] J. V. Sengers; B. Kamgar-Parsi. Representative equations for the viscosity of water substance. *Journal of Physical and Chemical Reference Data*, 13:601–609, 1984.

[22] V. I. Anikeev; A. Yermakova; V. A. Semikolenov; M. Goto. Effect of supercritical water density on the rate constant of aliphatic nitrocompounds decomposition. *Journal of Supercritical Fluids*, 33:243–246, 2005.

[23] D. P. Fernández; A. R. H. Goodwin; E. W. Lemmon. A formulation for the static permitivity of water and steam at temperatures from 238 K to 873 K at pressures up to 1200 MPa, including derivatives and Debye-Huckel coefficients. *Journal of Physical and Chemical Reference Data*, 26:1125–1166, 1997.

[24] N. Akiya; P. E. Savage. Roles of water for chemical reactions in high-temperature water. *Chemical Reviews*, 102:2725–2750, 2002.

[25] A. Kruse; E. Dinjus. Hot compressed water as a reaction medium and reactant 2. Degradation reactions. *Journal of Supercritical Fluids*, 41:361–379, 2007.

[26] H. Schmieder; J. Abeln. Supercritical water oxidation: State of the art. *Chemical Engineering and Technology*, 22:903–908, 1999.

[27] D. Bröll; C. Kaul; A. Krämer; P. Krammer; T. Richter; M. Jung; H. Vogel; P. Zehner. Chemistry in supercritical water. *Angewandte Chemie International Edition*, 38:2998–3014, 1999.

[28] J. Fraga-Dubreuil; M. Poliakoff. Organic reactions in high-temperature and supercritical water. *Pure and Applied Chemistry*, 78:1971–1982, 2006.

[29] R. L. Holliday; B. Y. M. Jong; J. W. Kolis. Organic synthesis in subcritical water. Oxidation of alkyl aromatics. *Journal of Supercritical Fluids*, 12:255–260, 1998.

[30] P. Krammer; S. Mittelstädt; H. Vogel. Investigating the synthesis potential in supercritical water. *Chemical Engineering and Technology*, 22:126–130, 1999.

[31] X. Xu; C. P. De Almeida; M. J. Antal. Mechanism and kinetics of the acid-catalyzed formation of ethene and diethyl ether from ethanol in supercritical water. *Industrial and Engineering Chemistry Research*, 30:1478–1485, 1991.

[32] R. Narayan; M. J. Antal. Influence of pressure on the acid-catalyzed rate constant for 1-propanol dehydration in supercritical water. *Journal of American Chemical Society*, 112:1927–1931, 1990.

[33] S. Ramayya; A. Brittain; C. DeAlmeida; W. Mok; M. J. Antal. Acid-catalysed dehydration of alcohols in supercritical water. *Fuel*, 66:1364–1371, 1987.

[34] R. C. Crittendon; E. J. Parsons. Transformations of cyclohexane derivatives in supercritical water. *Organometallics*, 13:2587–2591, 1994.

[35] Y. Nagai; S. Morooka; N. Matubayasi; M. Nakahara. Mechanisms and kinetics of acetaldehyde reaction in supercritical water: noncatalytic disproportionation, condensation, and decarbonylation. *Journal of Physical Chemistry A*, 108:11635–11643, 2004.

[36] W. S.-L. Mok; M. J. Antal. Formation of acrylic acid from lactic acid in supercritical water. *Journal of Organic Chemistry*, 54:4596–4602, 1989.

[37] Y. Harano; H. Sato; F. Hirata. A theoretical study on a Diels-Alder reaction in ambient and supercritical water: viewing solvent effects through frontier orbitals. *Chemical Physics*, 258:151–161, 2000.

[38] Y. Ikushima; K. Hatakeda; O. Sato; T. Yokoyama; M. Arai. Noncatalytic organic synthesis using supercritical water: The peculiarity near the critical point. *Angewandte Chemie International Edition*, 38:2910–2914, 1999.

[39] Y. Ikushima; K. Hatakeda; O. Sato; T. Yokoyama; M. Arai. Acceleration of synthetic organic reactions using supercritical water: Noncatalytic Beckmann and pinacol rearrangements. *Journal of American Chemical Society*, 122:1908–1918, 2000.

[40] J. Ancheyta; M. J. Angeles; M. J. Macías; G. Marroquín; R. Morales. Changes in apparent reaction order and activation energy in the hydrodesulfurization of real feedstocks. *Energy and Fuels*, 16:189–193, 2002.

[41] K. Arai; T. Adschiri; M. Watanabe. Hydrogenation of hydrocarbons through partial oxidation in supercritical water. *Industrial and Engineering Chemistry Research*, 39:4697–4701, 2000.

[42] H. R. Holgate; J. C. Meyer; J. W. Tester. Glucose hydrolysis and oxidation in supercritical water. *AIChE Journal*, 41:637–648, 1995.

[43] Y. Izumizaki; K. C. Park; Y. Tachibana; H. Tomiyasu; Y. Fujii. Organic decomposition in supercritical water by an aid of ruthenium (IV) oxide as a catalyst-exploitation of biomass resources for hydrogen production. *Progress in Nuclear Energy*, 47:544–552, 2005.

[44] L. Calvo; D. Vallejo. Formation of organic acids during the hydrolysis and oxidation of several wates in sub- and supercritical water. *Industrial and Engineering Chemistry Research*, 41:6503–6509, 2002.

[45] A. Demirbas. *Biodiesel*. Springer-Verlag London Limited, London, U.K., 2008.

[46] T. Hirai; N. Ikenaga; T. Miyake; T. Suzuki. Production of hydrogen by steam reforming of glycerin on ruthenium catalyst. *Energy and Fuels*, 19:1761–1762, 2005.

[47] X. Xu; Y. Matsumura; J. Stenberg; M. J. Antal. Carbon-catalyzed gasification of organic feedstocks in supercritical water. *Industrial and Engineering Chemistry Research*, 35:2522–2430, 1996.

[48] J. Ginsburg; H. I. de Lasa. Catalytic gasification of biomass in a CREC fluidized riser simulator. *International Journal of Chemical Reactor Engineering*, 3:1–18, 2005.

[49] J. W. Shabaker; R. R. Davda; G. W. Huber; R. D. Cortright; J. A. Dumesic. Aqueous-phase reforming of methanol and ethylenglycol over alumina-supported platinum catalysts. *Journal of Catalysis*, 215:344–352, 2003.

[50] S. Hayashi; H. Hatano; Z. Suzuki. Production of hydrogen by thermochemical decomposition. Patent EP1001002, CT of Coal Utilization Japan; Agency Ind Science Techn; Hatano Hiroyuki; Suzuki Zenso, 1999.

[51] D. Bröll; A. Krämer; H. Vogel; H. Fueß. Heterogeneously catalyzed partial oxidation in supercritical water. *Chemical Engineering and Technology*, 24:142–146, 2001.

[52] D. Bröll; A. Krämer. Heterogeneously catalyzed partial oxidation of methane in supercritical water. *Chemical Engineering and Technology*, 26:733–737, 2003.

[53] A. M. Gaffney; J. A. Sofranko. Oxidation of olefin to glycol. Patent US5210336, Arco Tech Chem, 1993.

[54] H. Kawanami; K. Hatada; Y. Ikushima. Method for producing organic compounds by using high-temperature and high-pressure water. Patent JP2004099545, Nat. Inst. of Adv. Ind. and Technol., 2004.

[55] P. E. Savage; J. B. Dunn; J. Yu. Recent advances in catalytic oxidation in supercritical water. *Combustion Science and Technology*, 178:443–465, 2006.

[56] P.-Q. Yuan; Z.-M. Cheng; W.-L. Jiang; R. Zhang; W.-K. Yuan. Catalytic desulfurization of residual oil through partial oxidation in supercritical water. *Journal of Supercritical Fluids*, 35:70–75, 2005.

[57] P.-Q. Yuan; Z.-M. Cheng; X.-Y. Zhang; W.-K. Yuan. Catalytic denitrogenation of hydrocarbons through partial oxidation in supercritical water. *Fuel*, 85:367–373, 2006.

[58] G. T. Hong; M. H. Spritzer. Supercritical water partial oxidation. In *The 2002 U.S.DOE Hydrogen Program Review*, 2002.

[59] N. W. Johanson; M. H. Spritzer; G. T. Hong; W. S. Rickman. Supercritical water partial oxidation. In *The 2001 DOE Hydrogen Program Review*, 2001.

[60] T. Richter; H. Vogel. The partial oxidation of isobutene in sub- and supercritical water. *Chemical Engineering and Technology*, 26:688–690, 2003.

[61] T. Richter; H. Vogel. The partial oxidation of cyclohexane in supercritical water. *Chemical Engineering and Technology*, 25:265–268, 2002.

[62] M. Watanabe; H. Inomata; M. Osada; T. Sato; T. Adschiri; K. Arai. Catalytic effects of NaOH and ZrO_2 for partial oxidative gasification of n-hexadecane and lignin in supercritical water. *Fuel*, 82:545–552, 2003.

[63] H. E. Barner; C. Y. Huang; T. Johnson; G. Jacobs; M. A. Martch; W. R. Killilea. Supercritical water oxidation: An emerging technology. *Journal of Hazardous Materials*, 31:1–17, 1992.

[64] European Commission (DG Environment). Water Note 8. Pollution: Reducing dangerous chemicals in Europe's waters, December, 2008.

[65] European Commission (DG Environment). Water Note 9. Integrating water policy: Linking all EU water legislation within a single framework, December, 2008.

[66] The European Parliament and of the Council. Directive 2008/105/ec of The European Parliament and of the Council of 16 december 2008 on environmental quality standards in the field of water policy, amending and subsequently repealing Council Directives 82/176/eec, 83/513/eec, 84/156/eec, 84/491/eec, 86/280/eec and amending directive 2000/60/ec of the european parliament and of the council, December, 2008.

[67] Foundation for Water Research. European Union legislation on wastewater treatment and nutrients removal, 2005.

[68] B. Veriansyah; J.-D. Kim. Supercritical water oxidation for the destruction of toxic organic wateswaters: A review. *Journal of Environmental Sciences*, 19:513–522, 2007.

[69] A. K. Chowdhury; W. C. Copa. Wet air oxiation of toxic and hazardous organics in industrial wastewater. *Industrial Chemical Engineering*, 28:3–10, 1986.

[70] D. Kodra; V. Balakotaiah. Autothermal oxidation of dilute aqueous wastes under supercritical conditions. *Industrial Engineering Chemistry Research*, 33:575–578, 1994.

[71] P. E. Savage. Organic chemical reactions in supercritical water. *Chemical Reviews*, 99:603–621, 1999.

[72] J. W. Griffith; D. H. Raymond. The first commercial supercritical water oxidation sludge processing plant. *Waste Management*, 22:453–459, 2002.

[73] M. Svanträm; M. Fröling; M. Olofsson; M. Lundin. Environmental assessment of supercritical water oxidation and other sewage sludge handling options. *Waste Management and Research*, 23:356–366, 2005.

[74] M. Svanträm; M. Fröling; M. Modell; W. A. Peters; J. Tester. Environmental assessment of supercritical water oxidation of sewage sludge. *Resources, Conservation and Recycling*, 41:321–338, 2004.

[75] M. S. Spencer. *Catalyst Handbook*, chapter Fundamentals Principles, pages 17–84. Manson Publishing Ltd, London, England, 1996.

[76] M. Modell. Processing methods for the oxidation of organics in supercritical water. Patent WO 81/03169, Modar Inc., 1981.

[77] J. B. Joshi; Y. T. Shah; S. J. Parulekar. Engineering aspects of the treatment of aqueous waste streams. *Industrial Chemical Engineering*, 37:3–37, 1985.

[78] J. B. Johnston; R. E. Hannah; V. L Cunningham; B. P. Daggy; F. J. Sturm; R. M. Kelly. Destruction of pharmaceutical and biopharmaceutical wastes by the modar supercritical water oxidation process. *Biotechnology*, 6:1423–1427, 1988.

[79] G. C. Jin. Technological process of treating oil-containing sludge with supercritical water oxidation. Patent CN101066828, Daqing Petroleum College, 2007.

[80] B. Dahlblom; J. Dahlin; M. E. Larsson; E. Mattsson; A. Sundkvist; A. Almqvist. Process for recovery inorganic material from deinking sludge. Patent EP1352123, B. Dahlblom; J. Dahlin; M. E. Larsson; E. Mattsson; A. Sundkvist; A. Almqvist, 2004.

[81] T. Shimada; A. Noguchi; K. Aoki. Cleaning disposal method for spent nuclear fuel shear material. Patent JP2001174584, Mitsubushi Heavy Ind Ltd, Advance Reactor Technology Co., 2001.

[82] M. Oonobu; A. Suzuki. Method and apparatus for oxidation of incinerator fly ash with supercritical water. Patent JP20002023999, Organo KK, 2000.

[83] X.-Y. Chen; X.Q. Dong; M.-H. Zhang. Study on catalytic supercritical water oxidation of coke plant waste water. *Journal of Chemical Engineering of Chinese Universities*, 21:1065–1071, 2007.

[84] V. I. Anikeev; N. S. Belobrov; R. N. Piterkin; R. Sh. Prosvirnin; L. S. Zvolsky; P. E. Mikenin; A. Yermakova. Results of testing the plant for supercritical water oxidation of nitroglycerin and diethylene glycol dinitrate. *Industrial and Engineering Chemistry Research*, 45:7977–7981, 2006.

[85] P. J. Crooker; K. S. Ahluwalia; Z. Fan; J. Prince. Operating results from supercritical water oxidation plants. *Industrial and Engineering Chemistry Research*, 39:4865–4870, 2000.

[86] A. Honchi; M. Makaide; I. Okochi; H. Hida; H. Yamashita; T. Fukushima. Waste plastic recycling systems. Patent JP11080745, Hitachi Ltd, 1999.

[87] O. Kakimoto; T. Aida. Oxidation method for alkanes or cycloalkanes. Patent JP2007008903, Idemitsu Kosan; Univ Kinki, 2007.

[88] H. Obuse; Y. Hatake. Method and equipment for treating water-soluble polymer-containing waste liquid. Patent JP2004097997, Kurita Water Ind Ltd; Komatsu MFG Co Ltd, 2004.

[89] H. Kako; M. Wakita. Method and equipment for treating human waste and/or sludge in septic tank. Patent JP2002273482, Kurita Water Ind Ltd; Komatsu MFG Co Ltd; Gen Atomics Inc., 2002.

[90] M. Wakita. Method and equipment for processing foodstuff waste. Patent JP2004105855, Kurita Water Ind Ltd; Komatsu MFG Co Ltd; Gen Atomics Inc, 2004.

[91] B. Veriansyah; J.-D. Kim; Y.-W. Lee. Simultaneous recovery of chromium and destruction of organics from LCD manufacturing process wastewater by supercritical water oxidation. *Journal of Cleaner Production*, 15:972–978, 2007.

[92] M. Kudo; M. Kikuchi; S. Shimizu; H. Inomata. Method of recovery inorganic matter parts from electronic parts using supercritical water. Patent JP2002233847, Asaka Riken Kogyo KK, 2002.

[93] S. Collard; A. Gidner; B. Harrison; L. Stenmark. Precious metal recovery from organics-precious metal compositions with supercritical water reactant. Patent EP1294955, S. Collard; A. Gidner; B. Harrison; L. Stenmark, 2003.

[94] Supercritical Fluids International. AquaCritox Process. http://www.scfi.eu/, March 2008.

[95] G. H. Lee; K. Yamamoto. Combined process of pyrolysis and oxidation of organic matter using supercritical water. Patent KR20010069798, G. H. Lee; K. Yamamoto, 2001.

[96] M. D. Bermejo; M. J. Cocero. Supercritical water oxidation: A technical review. *AIChE Journal*, 52:3933–3951, 2006.

[97] P. A. Marrone; M. Hodes; K. A. Smith; J. W. Tester. Salt precipitation and scale control in supercritical water oxidation-part B: commercial/full-scale applications. *Journal of Supecritical Fluids*, 29:289–312, 2004.

[98] K. Sugawara. Ni based alloy having excellent corrosion resistance to inorganic acid-containing supercritical water environment. Patent JP2003201532, Mitsubishi Materials Corp., 2003.

[99] G. T. Hong. Ceramic coating systems for water oxidation environments. Patent US5545337, Modar Inc., 1996.

[100] M. D. Bermejo; F. Fdez-Polanco; M. J. Cocero. Experimental study of operational parameters of a transpiring wall reactor for supercritical water oxidation. *Journal of Supercritical Fluids*, 39:70–79, 2006.

[101] L. D. Bond; C. C. Mills; P. Whiting; S. L. Koutz; D. A. Hazlebec. K. W. Downey. Method and apparatus to remove inorganics scale from a supercritical water oxidation reactor. Patent US6056883, Abitibi Consolidated Inc., 2000.

[102] Y. Hatake. Method for discharging salt from reaction vessel in hydrothermal reaction apparatus and hydrothermal reaction apparatus. Patent JP2004033952, Komatsu MFG Co Ltd; Kurita Water Ind Ltd; Gen Atomics Inc, 2004.

[103] F. Martinez de la Ossa; E. Nebot; J. R. Portela; J. Sanchez. System and method for hydrothermal oxidation of water-insoluble organic residues. Patent EP1834928, University of Cadiz, 2007.

[104] S. Pilz; M. Veeh; K. Rebstock. Process and device for supercritical wet oxidation. Patent US20022113024, S. Pilz; M. Veeh; K. Rebstock, 2002.

[105] M. Miyake; K. Suzuki. Hydrothermal reaction treatment apparatus. Patent JP2004033975, Komatsu MFG Co Ltd; Kurita Water Ind Ltd; Gen Atomics Inc., 2004.

[106] M. Hodes; P. A. Marrone; G. T. Hong; K. A. Smith; J. W. Tester. Salt precipitation and scale control in supercritical water oxidation-part A: fundamentals and research. *Journal of Supercritical Fluids*, 29:265–288, 2004.

[107] J. R. Hyde; P. Licence; D. Carter; M. Poliakoff. Continuous catalytic reactions in supercritical fluids. *Applied Catalysis A: General*, 222:119–131, 2001.

[108] M. J. Cocero; J. L. Martínez. Cool wall reactor for supercritical water oxidation modelling and operation results. *Journal of Supercritical Fluids*, 31:41–55, 2004.

[109] R. N. McBrayer; J. M. Eller; J. E. Deaton. Turbulent flow cold-wall reactor. Patent US5552039, RPC Waste Management Services, 1996.

[110] T. Miyabayashi. Method for controlling reaction temperature and supecritical water oxidation device. Patent JP11300198, Hitachi Plant Eng and Constr Co., 1999.

[111] T. G. McGuinness. Supercritical oxidation reactor. Patent US5384051, T. G. McGuinness, 1995.

[112] H. H. Mueggenburg; D. C. Rousar; M. F. Young. Supercritical water oxidation reactor with wall conduits for boundary flow control. Patent US5387398A, Aerojet General Corporation, 1995.

[113] G. W. Nauflett; R. E. Farncomb; M. L. Kumar. Supercritical water oxidation reactor with a corrosion-resistant lining. Patent US5461648, US Army, 1995.

[114] Turbosystems Engineering Inc. Transpiring wall reactor. http://www.turbosynthesis.com/, 2002.

[115] G. T. Hong; W. R. Killilea; T. B. Thomason. Methods for solid separation in a wet oxidation type process. Patent US4822497, Modar Inc., 1989.

[116] L. Li; E. F. Glyona. Apparatus for reverse-injection wet oxidation. Patent US5421998, University of Texas, 1995.

[117] L. Stenmark; A. Gid; K. Carlsson; G. Wass. Reactor and method for supercritical water oxidation. Patent EP1812353, Chematur Eng AB, 2007.

[118] A. Gidner. Method and system for supercritical water oxidation of a stream containing oxidizable material. Patent EP1812352, Chematur Eng AB, 2007.

[119] C. Joussot-Dubien; G. Didier; H.-A. Turé. Methods for oxidizing materials in supercritical water. Patent US2004011746, Commisariat a l'Energie Atomique, 2005.

[120] H. E. Barner; C.-Y. Huang; W. R. Killilea; G. T. Hong. Supercritical water oxidation with overhead effluent quenching. Patent US5200093, Lummus Crest Inc; Modar Inc., 1992.

[121] K. Yamamoto; F. Takashi; K. Fukushi; Y. Oshima. In situ catalyst for supercritical water oxidation and supercritical water oxidation method and device using the catalyst. Patent JP2005087927, K. Yamamoto; F. Takashi; K. Fukushi; Y. Oshima, 2005.

[122] R. Gupta; P. Muthukumaran. Supercritical water oxidation with reduced corrosion and enhaced oxidation rate. Patent WO0196247, Univ. of Auburn; R. Gupta; P. Muthukumaran, 2001.

[123] V. I. Anikeev; N. S. Belobrov; A. Yermakova; P. E. Mikenin; R. N. Piterkin; R. S. Prosvirnin. Method of performing oxidation reactions of organic compounds. Patent RU2309009, Boreskova Inst Kataliza Sibir, 2007.

[124] B. K. Cho; G. H. Choi; G. Y. Hwang; H. C. Lee; S. G. Lee; Y. P. Lee; I. U. Na. Supercritical oxidation reactor having reinforced corrosion-resistance for increasing the cooling efficiency of reaction-completed water. Patent KR20040097441, Korea Institute Science Technology, 2004.

[125] H. H. Mueggenburg; D. C. Rousar; M. F. Young. Injector for SCWO reactor. Patent US5804066, Aerojet General Co., 1997.

[126] Y. S. Wei; R. J. Sadus. Equations of state for the calculation of fluid-phase equilibria. *AIChE Journal*, 46:169–196, 2000.

[127] J. O. Valderrama. The state of the cubic equations of state. *Industrial and Engineering Chemistry Research*, 42:1603–1618, 2003.

[128] J. J. Martin. Cubic equations of state-which? *Industrial and Engineering Chemistry Fundamentals*, 18:81–97, 1977.

[129] L. Haar; J. S. Gallagher; G. S. Kell. *NBS/NRS Steam tables*. Hemisphere Publishing Corp., New York, 1984.

[130] D. Y. Peng; D. B. Robinson. A new two-constant equation of state. *Industrial and Engineering Chemistry Fundamentals*, 15:59–64, 1976.

[131] G. Soave. Equilibrium constants from a modified redlich-kwong equation of state. *Chemical Engineering Science*, 27:1197–1203, 1972.

[132] A. Yermakova; V. I. Anikeev. Thermodynamic calculations in modeling of multiphase process and reactors. *Industrial and Engineering Chemistry Research*, 39:1453–1472, 2000.

[133] M. D. Bermejo; A. Martin; M. J. Cocero. Application of the Anderko-Pitzer EoS to the calculation of thermodynamical properties of systems involved in the supercritical water oxidation process. *Journal of Supercritical Fluids*, 42:27–35, 2007.

[134] National Institute of Standards and Technology. NIST Chemistry Webbook. http://webbook.nist.gov/chemistry/, March 2008.

[135] W. J. Lamb; G. A. Hoffman; J. Jonas. Self-diffusion in compressed supercritical water. *Journal of Chemical Physics*, 74:6875–6880, 1981.

[136] G. F. Woerlee. Expression for the viscosity and diffusivity product applicable for supercritical fluids. *Industrial and Engineering Chemistry Research*, 40:465–469, 2001.

[137] W. L. Marshall; E. U. Franck. Ion product of water substance, 0-1000°C, 1-10000 bars - New international formulation and its background. *Journal of Physical and Chemical Reference Data*, 10:295–304, 1981.

[138] L. D. Sortland; J. M. Prausnitz. The solvent effect in chemical equilibria of high-pressure, gas-phase reactions. *Chemical Engineering Science*, 20:847–850, 1965.

[139] J. T. Henrikson; P. E. Savage. Water-density effects on phenol oxidation in supercritical water. *AIChE Journal*, 49:718–726, 2003.

[140] P. W. Atkins. *Physical Chemistry.* Oxford University Press, Oxford, United Kingdom, 1994.

[141] R. G. Gilbert; S. C. Smith. *Theory of Unimolecular and Recombination Reactions.* Blackwell Scientific Publications, Oxford, United Kingdom, 1990.

[142] S. K. Upadhyay. *Chemical Kinetics and Reaction Dynamics.* Springer and Anamaya Publishers, New Delhi, India, 2006.

[143] R. K. Helling; J. W. Tester. Oxidation of simple compounds and mixtures in supercritical water: carbon monoxide, ammonia, and ethanol. *Environmental Science Techonology*, 22(22):1319–1324, 1988.

[144] P. A. Webley; J. W. Tester; H. R. Holgate. Oxidation kinetics of ammonia and ammonia-methanol mixtures in supercritical water in the temperature range 530-700°C at 246 bar. *Industrial Engineering Chemistry Research*, 30:1745–1754, 1991.

[145] M. Goto; D. Shiramizu; A. Kodama; T. Hirose. Kinetic analysis for ammonia decomposition in supercritical water oxidation of sewage sludge. *Industrial and Engineering Chemistry Research*, 38:4500–4503, 1999.

[146] N. Segond; Y. Matsumura; K. Yamamoto. Determination of ammonia oxidation rate in sub- and supercritical water. *Industrial and Engineering Chemistry Research*, 41:6020–6027, 2002.

[147] L. D. S. Pinto; L. M. Freitas dos Santos; R. C. D. Santos; B. Al-Duri. Supercritical water oxidation of quinoline in a continuous plug flow reactor - part 2: kinetics. *Journal of Chemical Technology and Biotechnology*, 81:919–926, 2006.

[148] H. R. Holgate; P. A. Webley; J. W. Tester. Carbon monoxide oxidation in supercritical water: The effects of heat transfer and the water-gas shift reaction on observed kinetics. *Energy and Fuels*, 6:586–597, 1992.

[149] R. K. Helling; J. W. Tester. Oxidation kinetics of carbon monoxide in supercritical water. *Energy and Fuels*, 1:417–423, 1987.

[150] J. M. Ploeger; A. C. Madlinger; J. W. Tester. Revised global kinetics measurements of ammonia oxidation in supercritical water. *Industrial and Engineering Chemistry Research*, 45:6842–6845, 2006.

[151] F. Vogel; J. L. DiNaro; P. A. Marrone; S. F. Rice; P. A. Webley; W. A. Peters; K. A. Smith; J. W. Tester. Critical review of kinetic data for the oxidation of methanol in supercritical water. *Journal of Supercritical Fluids*, 34:249–286, 2005.

[152] G. Anitescu; Z. Zhang; L. L. Tavlarides. A kinetic study of methanol oxidation in supercritical water. *Industrial and Engineering Chemistry Research*, 38:2231–2237, 1999.

[153] S. F. Rice; R. R. Steeper. Oxidation rates of common organic compounds in supercritical water. *Journal of Hazardous Materials*, 59:261–278, 1998.

[154] E. E. Brock; Y. Oshima; P. E. Savage; J. R. Barker. Kinetics and mechanism of methanol oxidation in supercritical water. *Journal of Physics and Chemistry*, 100:15834–15842, 1996.

[155] J. Schanzenbächer; J. D. Taylor; J. Tester. Ethanol oxidation and hydrolysis in supercritical water. *Journal of Supercritical Fluids*, 22:139–147, 2002.

[156] S. P. Maharrey; D. R. Miller. Quartz capillary microreactor for studies of oxidation in supercritical water. *AIChE Journal*, 47:1203–1211, 2001.

[157] Z. Y. Ding; M. A. Frish; L. Li; E. F. Glyona. Catalytic oxidation in supercritical water. *Industrial Engineering Chemistry Research*, 35:3257–3279, 1996.

[158] P. E. Savage; M. A. Smith. Kinetics of acetic acid oxidation in supercritical water. *Environmental Science and Technology*, 29:216–221, 1995.

[159] J. C. Meyer; P. A. Marrone; J. W. Tester. Acetic acid oxidation and hydrolysis in supercritical water. *AIChE Journal*, 41:2108–2121, 1995.

[160] A. Yermakova; P. E. Mikenin; V. I. Anikeev. Phenol oxidation in supercritical water in a well-stirred continuous reactor. *Theorical Foundations of Chemical Engineering*, 40:168–174, 2006.

[161] M. Krajnc; J. Levec. On the kinetics of phenol oxidation in supercritical water. *AIChE Journal*, 42:1977–1984, 1996.

[162] J. T. Henrikson; Z. Chen; P. E. Savage. Inhibition and acceleration of phenol oxidation by supercritical water. *Industrial and Engineering Chemistry Research*, 42:6303–6309, 2003.

[163] J. R. Portela; E. Nebot; E. Martínez de la Ossa. Kinetic comparison between subcritical and supercritical water oxidation of phenol. *Chemical Engineering Journal*, 81:287–299, 2001.

[164] M. Koo; W. K. Lee; C. H. Lee. New reactor system for supercritical water oxidation and its application on phenol destruction. *Chemical Engineering Science*, 52:1201–1214, 1997.

[165] S. Gopalan; P. E. Savage. A reaction network model for phenol oxidation in supercritical water. *AIChE Journal*, 41:1864–1873, 1995.

[166] T. D. Thornton; P. E. Savage. Phenol oxidation in supercritical water. *Journal of Supercritical Fluids*, 3:240–248, 1990.

[167] N. H. Ashraf-Ball. *The Treatment of a Toxic Nitrogenous-Containing Organic Compound by Supercritical Water Oxidation and Wet Air Oxidation Processes: Operating Conditions and Reaction Kinetics.* PhD thesis, University of Birmingham, 2005.

[168] P. C. Dell'Orco; E. F. Glyona; S. J. Buelow. Reactions of nitrate salts with ammonia in supercritical water. *Industrial and Engineering Chemistry Research*, 36:2547–2557, 1997.

[169] G. Zhang; I. Hua. Supercritical water oxidation of nitrobenzene. *Industrial and Engineering Chemistry Research*, 42:285–289, 2003.

[170] B. Veriansyah; J.-D. Kim; J.-C. Lee; Y.-W. Lee. OPA oxidation rates in supercritical water. *Journal of Hazardous Materials*, B124:119–124, 2005.

[171] B. Veriansyah; J.-D. Kim; J-C. Lee. Supercritical water oxidation of thiodiglycol. *Industrial and Engineering Chemistry Research*, 44:9014–9019, 2005.

[172] C. J. Martino; P. E. Savage. Supercritical water oxidation kinetics, products, and pathways for CH_3- and CHO-substituted phenols. *Industrial and Engineering Chemistry Research*, 36:1391–1400, 1997.

[173] C. J. Martino; P. E. Savage. Thermal decomposition of substituted phenols in supercritical water. *Industrial and Engineering Chemistry Research*, 36:1385–1390, 1997.

[174] H.-C. Lee; J.-H. In; K.-Y. Hwang; C.-H. Lee. Decomposition of ethylenediaminetetraacetic acid by supercritical water oxidation. *Industrial and Engineering Chemistry Research*, 43:3223–3227, 2004.

[175] K. M. Benjamin; P. E. Savage. Supercritical water oxidation of methylamine. *Industrial and Engineering Chemistry Research*, 44:5318–5324, 2005.

[176] J. L. DiNaro; J. W. Tester; J. B. Howard; K. C. Swallow. Experimental measurements of benzene oxidation in supercritical water. *AIChE Journal*, 46:2274–2284, 2000.

[177] Z. Y. Ding. *Catalytic supercritical water oxidation.* PhD thesis, The University of Tulsa, 1995.

[178] L. Jin; Z. Ding; M. A. Abraham. Catalytic supercritical water oxidation of 1,4-dichlorobenzene. *Chemical Engineering Science*, 47:2659–2664, 1992.

[179] P. A. Sullivan; J. W. Tester. Methylphosphonic acid oxidation kinetics in supercritical water. *AIChE Journal*, 50:673–683, 2004.

[180] F. Jin; J. Cao; A. Kishita; H. Enomoto; T. Moriya. Oxidation reaction of high molecular weight dicarboxylic acid in sub- and supercritical water. *Journal of Supercritical Fluids*, 44:331–340, 2008.

[181] F. Jin; T. Moriya; H. Enomoto. Oxidation reaction of high molecular weight carboxylic acids in supercritical water. *Environmental Science and Technology*, 37:3220–3231, 2003.

[182] M. J. Cocero; E. Alonso; R. Torio; D. Vallelado; F. Fdz-Polanco. Supercritical water oxidation in a pilot plant of nitrogenous compounds: 2-propanol mixtures in the temperature range 500-750°C. *Industrial and Engineering Chemistry Research*, 39:3707–3716, 2000.

[183] T. Oe; H. Suzugaki; I. Naruse; A. T. Quintain; H. Daimon; K. Fujie. Role of methanol in supercritical water oxidation of ammonia. *Industrial and Engineering Chemistry Research*, 46:3566–3573, 2007.

[184] B. D. Phenix; J. L. DiNaro; J. W. Tester; J. B. Howard; K. A. Smith. The effects of mixing and oxidant choice on laboratory - scale measurements of supercritical water oxidation kinetics. *Industrial Engineering Chemistry Research*, 41:624–631, 2002.

[185] Z. Fang; S. Xu; I. S. Butler; R. L. Smith; J. A. Koziński. Destruction of decachlorobiphenyl using supercritical water oxidation. *Energy and Fuels*, 18:1257–1265, 2004.

[186] S.-J. Chang; Y.-C. Liu. Degradation mechanism of 2,4,6-trinitrotoluene in supercritical water oxidation. *Journal of Environmental Sciences*, 19:1430–1435, 2007.

[187] K. Hatakeda; Y. Ikushima; T. Aizawa; N. Saito. Supercritical water oxidation of polychlorinated biphenyls using hydrogen peroxide. *Chemical Engineering Science*, 54:3079–3084, 1999.

[188] T. Wang; B. Xiang; J. Liu; Z. Shen. Supercritical water oxidation of sulfide. *Environmental Science and Technology*, 37:1955–1961, 2003.

[189] G. Anitescu; V. Munteanu; L. L. Tavlarides. Co-oxidation effects of methanol and benzene decomposition of 4-chlorobiphenyl in supercritical water. *Journal of Supercritical Fluids*, 33:139–147, 2005.

[190] D.-S. Lee; E. F. Glyona; L. Li. Efficiency of H_2O_2 and O_2 in supercritical water oxidation of 2,4-dichlorophenol and acetic acid. *Journal of Supercritical Fluids*, 3:249–255, 1990.

[191] K.-C. Chang; L. Li; E. F. Gloyna. Supercritical water oxidation of acetic acid by potassium permanganate. *Journal of Hazardous Materials*, 33:51–62, 1993.

[192] J. Kronholm; P. Jyske; ML. Riekkola. Oxidation efficiencies of potassium persulfate and hydrogen peroxide in pressurized hot water with and without preheteaing. *Industrial Engineering Chemistry Research*, 39:2207–2213, 2000.

[193] X. Zhang; P. E. Savage. Fast catalytic oxidation of phenol in supercritical water. *Catalysis Today*, 40:333–342, 1998.

[194] J. J. Spivey. Complete catalytic oxidation of volatile organics. *Industrial Engineering Chemistry Research*, 26:2165–2180, 1987.

[195] R. K. Grasselli. Fundamental principles of selective heterogeneous oxidation catalysis. *Topics in catalysis*, 21:79–88, 2002.

[196] K.-S. Lin; H. P. Wang; Y. W. Yang. Supercritical water oxidation of 2-chlorophenol effected by Li^+ and CuO/Zeolites. *Chemosphere*, 39:1385–1396, 1999.

[197] X. H. Qi; Y. Y. Zhuang; Y. C. Yuan; W. X. Gu. Decomposition of aniline in supercritical water. *Journal of Hazardous Materials*, B90:51–62, 2002.

[198] A. M. Gizir; A. A. Clifford; K. D. Bartle. The catalytic role of the transition metal salts on supercritical water oxidation of phenol and chlorophenols in a titanium reactor. *Reaction Kinetics and Catalysis Letters*, 78:175–182, 2003.

[199] I. Arslan-Alaton; J. L. Ferry. $H_4SiW_{12}O_{40}$-catalyzed oxidation of nitrobenzene in supercritical water: kinetic and mechanistic aspects. *Applied Catalysis B: Environmental*, 38:283–293, 2002.

[200] Z.-Y. Ding; S. N. V. K. Aki; M. A. Abraham. Catalytic supercritical water oxidation: phenol conversion and product selectivity. *Environmental Science Technology*, 29:2748–2753, 1995.

[201] T. Nunoura; G. Lee; Y. Matsumura; K. Yamamoto. Reaction engineering model for supercritical water oxidation of phenol catalyzed by activated carbon. *Industrial and Engineering Chemistry Research*, 42:3522–3531, 2003.

[202] T. Nunoura; G. H. Lee; Y. Matsumura; K. Yamamoto. Modeling of supercritical water oxidation of phenol catalyzed by activated carbon. *Chemical Engineering Science*, 57:3061–3071, 2002.

[203] Y. Matsumura; T. Urase; K. Yamamoto; T. Nunora. Carbon catalyzed supercritical water oxidation of phenol. *Journal of Supercritical Fluids*, 22:149–156, 2002.

[204] J. Yu; P. E. Savage. Phenol oxidation over CuO/Al_2O_3 in supercritical water. *Applied Catalysis B: Environmental*, 28:275–288, 2000.

[205] J. Yu; P. E. Savage. Kinetics of catalytic supercritical water oxidation of phenol over TiO_2. *Environmental Science Technology*, 34:3191–3198, 2000.

[206] J. Yu; P. E. Savage. Catalytic oxidation of phenol over MnO_2 in supercritical water. *Industrial Engineering Chemistry Research*, 38:3793–3801, 1999.

[207] Y. Oshima; K. Tomita; S. Koda. Kinetics of the catalytic oxidation of phenol over manganese oxide in supercritical water. *Industrial and Engineering Chemistry Research*, 38:4183–4188, 1999.

[208] P. E. Savage. Heterogeneous catalysis in supercritical water. *Catalysis Today*, 62:167–173, 2000.

[209] M. Krajnc; J. Levec. Catalytic oxidation of toxic organics in supercritical water. *Applied Catalysis B: Environmental*, 3:L101–L107, 1994.

[210] S. N. V. K. Aki; Z.-Y. Ding; M. A. Abraham. Catalytic supercritical water oxidation: stability of Cr_2O_3 catalyst. *AIChE Journal*, 42:1995–2004, 1996.

[211] X. Chen; X. Dong; M. Zhang. Application of MnO_x/TiO_2-Al_2O_3 catalyst to supercritical water oxidation. *Shiyou Huagong/Petrochemical Technology*, 36:659–663, 2007.

[212] S.-H. Lee; K. C. Park; T. Mahiko; K. Sekizawa; Y. Izumizaki; H. Tomiyasu. Supercritical water oxidation of polychlorinated biphenyls based on redox reactions promoted by nitrite and nitrite salts. *Journal of Supercritical Fluids*, 39:54–62, 2006.

[213] L. Jin; Y. T. Shah; M. A. Martin; M. A. Abraham. The effect of supercritical water on the catalytic oxidation of 1,4-dichlorobenzene. *Journal of the Supercritical Fluids*, 3:233–239, 1990.

[214] S. N. Aki; M. A. Abraham. Catalytic supercritical water oxidation of pyridine: kinetic and mass transfer. *Chemical Engineering Science*, 54:3533–3542, 1999.

[215] S. N. Aki; M. A. Abraham. Catalytic supercritical water oxidation of pyridine: Comparison of catalyst. *Industrial and Engineering Chemistry Research*, 38:358–367, 1999.

[216] Z. Y. Ding; L. Li; D. Wade; E. F. Glyona. Supercritical water oxidation of NH_3 over a MnO_2/CeO_2 catalyst. *Industrial and Engineering Chemistry Research*, 37:1707–1716, 1998.

[217] M. Krajnc; J. Levec. The role of catalyst in supercritical water oxidation of acetic acid. *Applied Catalysis B: Environmental*, 13:93–103, 1997.

[218] M. Krajnc; J. Levec. Oxidation of phenol over transition-metal oxide catalyst in supercritical water. *Industrial and Engineering Chemistry Research*, 36:3439–3445, 1997.

[219] R. B. Snyder; C. A. Eckert. Chemical kinetics at a critical point. *AIChE Journal*, 19:1126–1133, 1973.

[220] H. Tiltscher; H. Hofmann. Trends in high pressure chemical reaction engineering. *Chemical Engineering Science*, 42:959–977, 1987.

[221] C. A. Eckert. Molecular thermodynamics of chemical reactions. *Industrial and Engineering Chemistry*, 59:20–32, 1967.

[222] C. A. Eckert. High pressure kinetics in solution. *Annual Review of Physical Chemistry*, 23:239–264, 1972.

[223] K. J. Laidler; M. C. King. The development of the transition state-theory. *The Journal of Physical Chemistry*, 87:2657–2664, 1983.

[224] D. G. Truhlar; W. L. Hase; J. T. Hynes. Current status of the transition-state theory. *The Journal of Physical Chemistry*, 87:2664–2682, 1983.

[225] C. A. Eckert; C. K. Hsieh; J. R. McCabe. Molecular thermodynamics for chemical reaction design. *AIChE Journal*, 20:20–36, 1974.

[226] S. Saim; B. Subramaniam. Chemical reaction equilibrium at supercritical conditions. *Chemical Engineering Science*, 43:1837–1841, 1988.

[227] V. Anikeev; A. Yermakova; M. Goto. Decomposition and oxidation of aliphatic nitro compounds in supercritical water. *Industrial and Engineering Chemistry Reasearch*, 43:8141–8147, 2004.

[228] T. Asano; W. J. Le Noble. Activation and reaction volumes in solution. *Chemical Reviews*, 78:407–489, 1978.

[229] C. A. Eckert; B. L. Knutson. Molecular charisma in supercritical fluids. *Fluid Phase Equilibria*, 83:93–100, 1993.

[230] C. G. Hill. *An Introduction to Chemical Engineering Kinetics and Reactor Design.* John Wiley and Sons Inc., New York, 1977.

[231] R. J. Kee; F. M. Rupley; J. A. Miller; M. E. Coltrin; J. F. Grcar; E. Meeks; H. K. Moffat; A. E. Lutz; G. Dixon-Lewis; M. D. Smooke; J. Warnatz; G. H. Evans; R. S. Larson; R. E. Mitchell; L. R. Petzold; W. C. Reynolds; M. Caracotsios; W. E. Stewart; P. Glarborg;

C. Wang; C. L. McLellan; O. Adigun; W. G. Houf; C. P. Chou; S. F. Miller; P. Ho; P. D. Young; D. J. Young. *CHEMKIN Release 4.0.2.* Reaction Design, California, 2005.

[232] A. M. Dean; J. W. Bozelli; E. R. Ritter. CHEMACT: A computer code to estimate rate constants for chemical-activated reactions. *Combustion Science and Technology*, 80:63–85, 1991.

[233] J. L. DiNaro; J. B. Howard; W. H. Green; J. W. Tester; J. W. Bozzelli. Elementary reaction mechanism for benzene oxidation in supercritical water. *Journal of Physics and Chemistry A*, 104:10576–10586, 2000.

[234] H. R. Holgate; J. W. Tester. Oxidation of hydrogen and carbon monoxide is sub- and supercritical water: Reaction kinetics, pathways, and water-density effects. 1. Experimental Results. *The Journal of Physical Chemistry*, 98:800–809, 1994.

[235] H. R. Holgate; J. W. Tester. Oxidation of hydrogen and carbon monoxide in sub- and supercritical water: Reaction kinetics, pathways and water-density effects. 2. Elementary reaction modeling. *The Journal of Physical Chemistry*, 98:810–822, 1994.

[236] E. E. Brock; P. E. Savage. Detailed chemical kinetics model for supercritical water oxidation of C_1 and H_2. *AIChE Journal*, 41:1874–1888, 1995.

[237] M. K. Alkam; V. M. Pai; P. B. Butler; W. J. Pitz. Methanol and hydrogen oxidation kinetics in water at supercritical states. *Combustion and Flame*, 106:110–130, 1996.

[238] B. D. Phenix; J. L. DiNaro; M. A. Tatang; J. W. Tester; J. B. Howard; G. J. Mcrae. Incorporation of parametric uncertainty into complex kinetics mechanisms: application to hydrogen oxidation in supercritical water. *Combustion and Flame*, 112:132–146, 1998.

[239] P. E. Savage; J. Yu; N. Stylski; E. E. Brock. Kinetics and mechanism of methane oxidation in supercritical water. *Journal of Supercritical Fluids*, 12:141–153, 1998.

[240] E. E. Brock; P. E. Savage; J. R. Barker. A reduced mechanism for methanol oxidation in supercritical water. *Chemical Engineering Science*, 53:857–867, 1998.

[241] H. Li; Y. Oshima. Elementary mechanism of methylamine oxidation in supercritical water. *Industrial and Engineering Chemistry Research*, 44:8756–8764, 2005.

[242] R. Hayashi; M. Onishi; M. Sugiyama; S. Koda; Y. Oshima. Kinetic analysis on alcohol concentration and mixture effect in supercritical water oxidation of methanol and ethanol by elementary reaction model. *Journal of Supercritical Fluids*, 40:74–83, 2007.

[243] J. M. Ploeger; P. A. Bielenberg; R. P. Lachance; J. W. Tester. Co-oxidation of methylphosphoric acid and ethanol in supercritical water I: Experimental results. *Journal of Supercritical Fluids*, 39:233–238, 2006.

[244] J. M. Ploeger; W. H. Green; J. W. Tester. Co-oxidation of methylphosphoric acid and ethanol in supercritical water II: Elementary reaction model. *Journal of Supercritical Fluids*, 39:239–245, 2006.

[245] R. Hayashi; K. Ohkuma; K. Tonokura; Y. Oshima. Contribution of ionic reactions to sub- and subcritical water oxidation of phenol. *Journal of Chemical Engineering of Japan*, 40:556–564, 2007.

[246] R. C. Reid; J. M. Prausnitz; B. E. Poiling. *The Properties of Gases and Liquids*. McGraw-Hill, New York, 1987.

[247] S. I. Sandler. *Chemical Engineering Thermodynamics*. John Wiley and Sons, Inc., New York, 1999.

[248] M. Benedict; G. B. Webb; L. C. Rubin. An empirical equation for thermodynamic properties of light hydrocarbons and their mixtures. *Journal of Chemical Physics*, 8:334–345, 1940.

[249] W. C. Edmister; J. Vairogs; A. J. Klekers. A generalized B-W-R equation of state. *AIChE Journal*, 14:479–482, 1968.

[250] C. Perego; S. Peratello. Experimental methods in catalytic kinetics. *Catalysis Today*, 52:133–145, 1999.

[251] J. M. Winterbottom; M. B. King. *Reactor Design for Chemical Engineers*. Stanley Thornes (Publishers) Ltd, United Kingdom, 1999.

[252] British Standards. Hydrogen peroxide. Standard BS 6376 : Part 2 : 1984, BS, United Kindgdom, 1984.

[253] Shimadzu Corporation. *Instruction Manual Total Organic Carbon Analyzer Model TOC-5050A*. Shimadzu Corporation, Kyoto, Japan, 2001.

[254] Merck KGaA. *Manual Spectroquant Nova 60*. Merck KGaA, Darmstadt, Germany, 2001.

[255] F. Thielmann; D. Burnett. Isotherm types and adsorption mechanisms of solvents on pharmaceutical excipients. Technical report, Surface Measurement Systems Ltd., London, UK, 2006.

[256] D. Burnett; F. Thielmann. Organic solvent sorption using a dynamic vapour sorption instrument-An overview. Technical report, Surface Measurement Systems Ltd., London, UK, 2006.

[257] F. Thielmann. Hysteresis effects in vapour sorption. Technical report, Surface Measurement Systems Ltd., London, UK, 2006.

[258] S. Brunauer; P. H. Emmett; E. Teller. Adsorption of gases in multimolecular layers. *Journal of the American Chemical Society*, 60:309–319, 1938.

[259] D. R. Williams; C. L. Levoguer. Measuring BET surface areas using organic probe molecules. Technical report, Surface Measurement Systems Ltd., London, UK, 2006.

[260] L. D. S. Pinto. *Supercritical water oxidation of nitrogen-containing organic compounds: Process operating conditions and reaction kinetics*. PhD thesis, University of Birmingham, 2004.

[261] P. Davies; R. T. Donald; N. H. Harbord. *Catalyst Handbook*, chapter Catalytic Oxidations, pages 469–518. Manson Publishing Ltd, London, England, 1996.

[262] L. Gang. *Catalytic Oxidation of Ammonia to Nitrogen*. PhD thesis, Technische Universiteit Eindhoven, 2002.

[263] M. H. Al-Dahhan; Y. Wu; M. P. Dudukovic. Reproducible technique for packing laboratory-scale trickle-bed reactors with a mixture of catalyst and fines. *Industrial and Engineering Chemistry Research*, 34:741–747, 1995.

[264] T.-J. Park; J. S. Lim; Y.-W. Lee; S.-H. Kim. Catalytic supercritical water oxidation of wastewater from terephtalic acid manufacturing process. *The Journal of Supercritical Fluids*, 26:201–213, 2003.

[265] M. Morbidelli; A. Varma. Parametric sensitivity and runaway in tubular reactors. *AIChE Journal*, 28:705–713, 1982.

[266] G. Astarita. *Mass Transfer with Chemical Reaction.* Elsevier Publishing Company, Amsterdam, 1967.

[267] F. M. Dautzenberg. Ten guidelines for catalyst testing. In S. A. Bradley; M. J. Galhuso; R. J. Bertolacini, editor, *Characterization and Catalyst Development: An Interactive Approach*, volume 411 of *ACS Symposium Series*, pages 99–119, Washington, D.C, 1989. American Chemical Society.

[268] P. Trambouze; H. Van Landeghem; J. P. Wauquier. *Chemical Reactors.* Gulf Publishing Company, Houston., 1988.

[269] G. G. Long; L. D. Freedman; G. O. Doak. *Encyclopedia of Chemical Technology*, chapter Bismuth Compounds, pages 246–270. John Wiley and Sons Inc., United States of America, 1997.

[270] H. Ulrich. *Encyclopedia of Chemical Technology*, chapter Urethane Polymers. John Wiley and Sons Inc., United States of America, 1997.

[271] R. B. Bird; W. E. Stewart; E. N. Lightfoot. *Transport Phenomema.* John Wiley and Sons, Inc, New York, 2002.

[272] P. G. Debenedetti; R. C. Reid. Diffusion and mass transfer in supercritical fluids. *AIChE Journal*, 32:2034–2046, 1986.

[273] G. F. Froment; L. Hosten. *Catalytic Kinetics Modelling*, volume 2 of *Catalysis Science and Techonolgy*, chapter 3, pages 97–170. Springer-Verlag, Berlin, 1981.

[274] H. P. Langtangen. *Python Scripting for Computational Science.* Springer-Verlag, Berlin, 2008.

[275] E. Jones; T. Oliphant; P. Peterson; J. Millman; R. Kern; S. van der Walt; J. D. Hunter; F. Perez; O. Certik; S. Kitterman and development team. Scipy: Open source scientific tools for Python. Electronic, February 2008.

[276] B. G. Olivier; J. M. Rohwer; J.-H. S. Hofmeyr. Modelling cellular processes with Python and Scipy. *Molecular Biology Reports*, 29:249–254, 2002.

[277] D. E. Mears. Tests for transport limitations in experimental catalytic reactors. *Industrial Engineering Chemistry Process Design and Development*, 10(4):541–547, 1971.

[278] N. Wakao; S. Kaguei. *Heat and Mass Transfer in Packed Beds.* Gordon and Breach, Science Publishers, Inc., New York, 1982.

[279] H. S. Fogler. *Elements of Chemical Reaction Engineering.* Prentice Hall, New Jersey, 2006.

[280] K. B. Bischoff. An extension of the general criterion for importance of pore difussion with chemical reactions. *Chemical Engineering Science*, 22:525–530, 1967.

[281] C. N. Satterfield. *Mass Transfer in Heterogeneous Catalysis.* Massachusetts Institutte of Technology Press, Cambridge, Massachussets, 1970.

[282] E. W. Thiele. Relation between catalytic activity and size of particles. *Industrial and Engineering Chemistry*, 31:916–920, 1939.

[283] K. B. Bischoff. Effectiveness factors for general reaction rate forms. *AIChE Journal*, 11:351–355, 1965.

[284] R. Aris. On the shape factors for irregular particles-I. *Chemical Engineering Science*, 6:262–268, 1957.

[285] D. K. Lee. Mechanism and kinetics of the catalytic oxidation of aqueous ammonia to molecular nitrogen. *Environmental Science Technology*, 37:5745–5749, 2003.

[286] M. Schubert; J. W. Regler; F. Vogel. Continuous salt precipitation and separation from supercritical water. Part 1: Type 1 salts. *Journal of Supercritical Fluids*, In press, 2009.

[287] M. Schubert; J. W. Regler; F. Vogel. Continuous salt precipitation and separation from supercritical water. Part 2. Type 2 salts and mixtures of two salts. *Journal of Supercritical Fluids*, In press, 2009.

[288] J. Yu; P. E. Savage. Catalyst activity, stability, and transformations during oxidation in supercritical water. *Applied Catalysis B: Environmental*, 31:123–132, 2001.

[289] A. Martin; U. Armbruster; M. Schneider; J. Radnik; M.-M. Pohl. Structural transformation of an alumina-supported mno_2-cuo oxidation catalyst by hydrothermal impact of sub- and supercritical water. *Journal of Materials Chemistry*, 12:639–645, 2002.

[290] Lu Gang; J. van Grondelle; B. G. Anderson; R. A. van Santen. Selective low temperature NH_3 oxidation to N_2 on copper-based catalysts. *Journal of Catalysis*, 186:100–109, 1999.

[291] K. M. Dooley; F. C. Knopf. Oxidation catalysis in a supercritical fluid medium. *Industrial and Engineering Chemistry*, 26:1910–1916, 1987.

[292] K. Tomita; Y. Oshima. Stability of manganese oxide in catalytic supercritical water oxidation of phenol. *Industrial and Engineering Chemistry Research*, 43:7740–7743, 2004.

[293] G. T. Hong W. R. Killilea, K. C. Swallow. The fate of nitrogen in supercritical-water oxidation. *The Journal of Supercritical Fluids*, 5:72–78, 1992.

[294] C.-M. Hung; J.-C. Lou; C.-H. Lin. Removal of ammonia solutions used in catalytic wet oxidation processes. *Chemosphere*, 52:989–995, 2003.

[295] G. Yablonsky; A. K. Ray. Equilibrium and optimum: How to kill two birds with one stone? *International Journal of Chemical Reaction Engineering*, 6:1–13, 2008.

[296] L. Gang; B. G. Anderson; J. van Grondelle; R. A. van Santen. NH_3 oxidation to nitrogen and water at low temperatures using supported transition metal catalyst. *Catalysis Today*, 61:179–185, 2000.

[297] L. D. S. Pinto; L. M. Freitas dos Santos; B. Al-Duri; R. C. D. Santos. Supercritical water oxidation of quinoline in a continuous plug flow reactor - part 1: effect of key operating parameters. *Journal of Chemical Technology and Biotechnology*, 81:912–918, 2006.

[298] A. R. Nicolaescu; O. Wiest; P. V. Kamat. Mechanistic pathways of the hydroxyl radical reactions of quinoline. 1. Identification, distributions, and yields of hydroxylated radicals. *Journal of Physical Chemistry A*, 109:2822–2828, 2005.

[299] S. N. V. K. Aki; M. A. Abraham. An economic evaluation of catalytic supercritical water oxidation: Comparison with alternative waste treatment technologies. *Environmental Progress*, 17:246–255, 1998.

[300] M. J. Angeles-Hernandez; G. A. Leeke; R. C. D. Santos. Catalytic supercritical water oxidation for the destruction of quinoline over MnO_2/CuO mixed catalyst. *Industrial and Engineering Chemistry Research*, 48:1208–1214, 2009.

[301] M. J. Angeles; A. H. Al-Marzouqui; B. Al-Duri; R. C. D. Santos. Catalytic supercritical water oxidation for the destruction of DBU. In *I Iberoamerican Conference on Supercritical Fluids, ProSCiba*, Iguassu Falls, Brasil, April 2007.

[302] A. Kruse; H. Schmieder. Supercritical water oxidation in water and carbon dioxide. *Environmental Progress*, 17:243–239, 1998.

[303] A. Kruse; H. Ederer; C. Mas; H. Schmieder. *Supercritical Fluids*, chapter Kinetics Studies of the Oxidation in Supercritical Water and Carbon Dioxide, pages 439–450. Kluwer Academic Publishers, 2000.

[304] O. Levenspiel. Chemical reaction engineering. *Industrial and Engineering Chemistry Research*, 38:4140–4143, 1999.

[305] P. Trambouze; H. Van Landeghem; J. P. Wauquier. *Chemical Reactors*. Gulf Publishing Company, Houston, 1988.

[306] C. D. Holland; R. G. Anthony. *Fundamentals of Chemical Reaction Engineering*. McGraw-Hill, New York, 1989.

[307] P. O. Mchedlov-Petrossyan; G. A. Khomenko; W. B. Zimmerman. Nearly irreversible, fast heterogeneous reactions in premixed flow. *Chemical Engineering Science*, 58:3005–30023, 2003.

[308] A. H. Cutler; M. J. Antal; M. Jones. A critical evaluation of the pluf-flow idealization of tubular-flow reactor data. *Industrial and Engineering Chemistry Research*, 27:691–697, 1988.

[309] J. Silverstein; R. Shinnar. Design of fixed bed catalytic microreactors. *Industrial Engineering Chemistry Process Design and Development*, 14:127–137, 1975.

[310] O. Levenspiel. *Chemical Reaction Engineering.* John Wiley & Sons, Inc., New York, USA, 1999.

[311] E. B. Nauman. *Chemical Reactor Design, Optimization, and Scaleup.* McGraw-Hill, 2001.

[312] P. V. Danckwerts. Continous flow systems. Distribution of residence times. *Chemical Engineering Science*, 2:1–13, 1953.

[313] E. B. Nauman. Residence time theory. *Industrial and Engineering Chemistry Research*, 47:3752–3766, 2008.

[314] T. H. Zwietering. The degree of mixing in continuous flow systems. *Chemical Engineering Science*, 11:1–15, 1959.

[315] G. F. Froment; K. B. Bischoff. *Chemical Reactor Analysis and Design.* John Wiley & Sons, Inc., New York, 1979.

[316] L. A. Belfiore. *Transport Phenomena for Chemical Reactor Design.* John Wiley & Sons, Inc., New Jersey, 2003.

[317] P. Andrigo; R. Bagatin; G. Pagani. Fixed bed reactors. *Catalysis Today*, 52:197–221, 1999.

[318] K. B. Bischoff. A note on boundary conditions for flow reactors. *Chemical Engineering Science*, 16:131–133, 1961.

[319] E. B. Nauman; A. Nigam. On axial difussion in laminar-flow reactors. *Industrial and Engineering Chemistry Research*, 44:5031–5035, 2005.

[320] W. H. Press; S. A. Teukolsky; W. T. Vetterling; B. P. Flannery. *Numerical Recipes. The Art of Scientific Computer.* Cambridge University Press, Cambridge, 2007.

[321] A. Constantinides. *Applied Numerical Methods with Personal Computers.* McGraw-Hill International Editions, New York, 1987.

[322] M. E. Davis. *Numerical Methods and Modelling for Chemical Engineers.* John Wiley and Sons, Inc., New York, 1984.

[323] E.A. Foumeny; M.A. Chowdhury. Dynamics of fixed-bed reactors in terms of mass dispersion. *Catalysis Today*, 20:501–514, 1994.

[324] N. Wakao; S. Kaguei; H. Nagai. Effective diffusion coeffiecients for fluid species reacting with first order kinetics in packed bed reactors and discussion on evaluation of catalyst effectiveness factors. *Chemical Engineering Science*, 33:183–187, 1978.

[325] D. E. Mears. On the criteria for axial dispersion in nonisothermal packed-bed catalytic reactors. *Industrial and Engineering Chemistry Fundamentals*, 15:20–23, 1976.

[326] J. M. P. Q. Delgado. A critical review on dispersion in packed beds. *Heat Mass Transfer*, 42:279–310, 2006.

[327] K. B. Bischoff; O. Levenspiel. Fluid dispersion-generalization and comparison of mathematical models - I Generalization methods. *Chemical Engineering Science*, 17:245–255, 1962.

[328] K. B. Bischoff; O. Levenspiel. Fluid dispersion-generalization and comparison of mathematical models - II Comparison of models. *Chemical Engineering Science*, 17:257–264, 1962.

[329] G. F. Froment. Design of fixed-bed catalytic reactors based on effective transport models. *Chemical Engineering Science*, 17:849–859, 1962.

[330] G. F. Froment. Fixed bed catalytic reactors. *Industrial and Engineering Chemistry*, 59:18–27, 1967.

[331] J. J. Carberry; D. White. On the role of transport phenomena in catalytic reactor behaviour. *Industrial and Engineering Chemistry*, 61:27–35, 1969.

[332] D. E. Mears. Diagnostic criteria for heat transport limitations in fixed bed reactors. *Journal of Catalysis*, 20:127–131, 1971.

[333] A. Varma; M. Morbidelli; H. Wu. *Parametric Sensitivity in Chemical Systems*. Cambridge Series in Chemical Engineering. Cambridge University Press, Cambridge, 1999.

[334] W. B. Zimmerman; P. O. Mchedlov-Petrossyan; G. A. Khomenko. Mass transfer limited heterogeneous reaction: Part I: Parametric sensitivity and inverse methods. *Chemical Engineering Science*, In preparation.

[335] E. Isaacson; H. B. Keller. *Analysis of Numerical Methods*. Dover Publications, Inc., New York, 1994.

[336] W. B. Zimmerman; J. M. Rees. Optimal modelling and experimentation for the improved sustainability of microfluidic chemical technology design. *Chemical Engineering Research and Design*, In press, 2009.

[337] K. B. Deshpande; W. B. Zimmerman. Experimental study of mass transfer limited reaction-Part I: Use of fibre optic spectrometry to infer asymmetric mass transfer coefficients. *Chemical Engineering Science*, 60:2879–2893, 2005.

[338] K. B. Deshpande; W. B. Zimmerman. Experimental study of mass transfer limited reaction-Part II: Existence of cross-over phenomenon. *Chemical Engineering Science*, 60:4147–4156, 2005.

[339] W. B. Zimmerman; P. O. Mechedlov-Petrossyan; G. A. Khomenko. Non-equilibrium effects on fast reactions in a heterogeneous batch reactor. *Chemical Engineering Science*, 60:3013–3028, 2005.

[340] P. O. Mchedlov-Petrossyan; W. B. Zimmerman; G. A. Khomenko. Fast binary reactions in a heterogeneous catalytic batch reactor. *Chemical Engineering Science*, 58:2691–2703, 2003.

[341] W. B. Zimmerman; P. O. Mchedlov-Petrossyan; G. A. Khomenko. Effects of transport and phase equilibrium on fast, nearly irreversible reactive extraction. *Chemical Enginnering Science*, 62:1770–1782, 2007.

[342] W. B. J. Zimmerman. *Multiphysics Modelling with Finite Element Methods*. World Scientific, New Yersey, 2006.

[343] American Society for Testing and Materials. Standard practice for preparation, standardization, and storage of standard and reagent solution for chemical analysis. Standard E 200 - 97, ASTM, 100 Barr Harbor Drive, West Conshohocken, PA, United States, 2001.

[344] J. Lambert; A. Holderness; F. Sherwood-Taylor. *The Essential of Volumetric Analysis.* Heinemann Educational Books Ltd, London, 1961.

[345] P. H. Borcherds. Python: a language for computational physics. *Computer Physics Communications*, 177:199–201, 2007.

[346] T. E. Oliphant. Python for scientific computing. *Computing in Science and Engineering*, 9:10–20, 2007.

[347] P. F. Dubois. Python: Batteries included. *Computing in Science and Engineering*, 9:7–9, 2007.

[348] M. J. D. Powell. An efficient method for finding the minimum of a function of several variables without calculating derivatives. *The Computer Journal*, 7:155–162, 1964.

[349] S. Kirkpatrick; C. D. Gelatt; M. P. Vecchi. Optimization by simulated annealing. *Science*, 220:671–680, 1983.

[350] N. Metropolis; A. W. Rosenbluth; M. N. Rosenbluth; A. H. Teller; E. Teller. Equations of state calculations by fast computing machines. *The Journal of Chemical Physics*, 21:1087–1092, 1953.

[351] G. Buzzi-Ferraris. Planning experiments and kinetic analysis. *Catalysis Today*, 52:125–132, 1999.

[352] J.J. Carberry. *Chemical and Catalytic Reaction Engineering.* Dover Publications, Inc., Mineola, New York, 2001.

[353] O. C. Zienkiewicz; R. L. Taylor; J. Z. Zhu. *The Finite Element Method: Its Basis and Fundamentals.* Elsevier Butterworth-Heinemann, Burlington, Massachussets, 6th edition, 2005.

[354] A. Constantinides; N. Mostoufi. *Numerical Methods for Chemical Engineers with MATLAB Applications.* Prentice Hall PTR, New Yersey, 1999.

[355] M. N. O. Sadiku; C. N. Obiozor. A simple introduction to the method of lines. *International Journal of Electrical Engineering Education*, 37:282–296, 2000.

[356] B. N. Hewakandamby. *Interfacial Dynamics driven by Marangoni stresses on a slowly moving liquid film.* PhD thesis, University of Sheffield, Sheffield, United Kingdom, 2002.

[357] A. C. Hindmarsh. *Scientific Computing*, volume 1 of *IMACS Transactions on Scientific Computing*, chapter ODEPACK, A Systematized Collection of ODE Solvers, pages 55–64. North-Holland Publishing Co., Amsterdam, Netherlands, 1983.

[358] R. Krishnan; A. C. Hindmarsh. Description and use of LSODE, the Livermore solver for ordinary differential equations. Technical Report UCRL-ID-113855, Lawrence Livermore National Laboratory, Livermore, California, 1993.

Appendix A

Preparation and Standardization of the $KMnO_4$ Solution

The normality of the potassium permanganate solution is given by:

$$\mathrm{N}_{KMnO_4} = \frac{\mathrm{g}\ KMnO_4}{(\mathrm{EW}\ KMnO_4)(1\ \mathrm{L})} \tag{A.1}$$

To prepare 1 L of a solution 0.1 N of the potassium permanganate is necessary to weight 3.16 g of potassium permanganate and then dissolve it in 1 L of distillate water. However, an accurately solution of potassium permanganate cannot be made up directly from the solid because this may be reduced by organic matter from the atmosphere and so rendered impure; further, organic matter present in the water in which the salt is dissolved may reduce it. So, it is desirable to make up a solution slightly stronger.

1. Weight 3.25 g of potassium permanganate.
2. Dissolve the potassium permanganate in 100 mL of distillate water.
3. Transferred into a 1 L measuring flask.
4. Dissolve the solution until the mark and shake.
5. Store in a dark place.

A.1 Standardization of the Potassium Permanganate by Ferrous Ammonium Salt

Due to its poor stability of potassium permanganate, it is strongly recommended to standardize it weekly [343]. Although, there are several methods to standardize potassium permanganate, the oxidation of a ferrous salt by potassium permanganate is a method often used to test the concentration of potassium permanganate and it is expressed as [344]:

$$10FeSO_4 + 2KMnO_4 + 8H_2SO_4 \longrightarrow 5Fe_2(SO_4)_3 + K_2SO_4 + 2MnSO_4 + 8H_2O \tag{A.2}$$

According to the reaction, 10 mol of ferrous sulphate salt accept 5 atoms of oxygen available from the potassium permanganate then the equivalent weight of this salt is:

$$\text{EW } FeSO_4 = \frac{10(\text{MW}_{FeSO_4})}{10} = 151.913 \text{ geq} \tag{A.3}$$

Ferrous sulphate crystals ($FeSO_4 \cdot 7H_2O$) cannot be used for standardization because they are rendered impure by efflorescence and by atmospheric oxidation to form a brown basic sulphate as a result of a reaction of the type:

$$12FeSO_4 + 3O_2 + 6H_2O \longrightarrow 4\,[Fe(OH)_3Fe_2(SO_4)_3] \tag{A.4}$$

The salt, ferrous ammonium sulphate ($FeSO_4(NH_4) \cdot 2SO_4 \cdot 6H_2O$) is free from these disadvantages and can be obtained in high state of purity. (It is prepared by dissolving ferrous and ammonium sulphates in the calculated quantities in hot water containing sulfuric acid and allowing the solution to crystallize). In solution, it breaks into ferrous ions, sulphate ions and ammonium ions. Only the former reagent reacts with the permanganate.

To standardize the potassium permanganate the next procedure was followed:

1. Take 10 or 15 mL of the acidic solution of ferrous ammonium sulphate with a measuring pipette.
2. Add 3 mL of H_2SO_4 2 N.
3. Titrate with the solution 0.1 N of potassium permanganate until the first permanent pink coloration.

4. Repeat twice

Thus the normality of $KMnO_4$ is calculated by:

$$\mathrm{N}_{KMnO_4} = \frac{(\mathrm{mL}\ FeSO_4)(\mathrm{N}_{FeSO_4})}{\mathrm{Average\ mL}\ KMnO_4} \tag{A.5}$$

A.2 Primary Standard Preparation ($FeSO_4$)

The normality of the ferrous sulphate solution is given by:

$$\mathrm{N}\ FeSO_4 = \frac{(\mathrm{g}\ FeSO_4)}{(\mathrm{EW}\ FeSO_4)(1\ \mathrm{L})} \tag{A.6}$$

The solution of the ferrous ammonium sulphate is prepared as follows:

1. Weight 7.84 g of ferrous ammonium sulphate (the salt contains 3.037 g of ferrous sulphate).
2. Add 12 ml of H_2SO_4 2 N (which has been boiled previously to remove the oxygen dissolved.
3. Add water slowly and dissolve completely with 100 mL of distillate water.
4. Transferred into a 200 mL measuring flask.
5. Add water until the mark and shake.
6. Store in a dark place.

Appendix B

Fitting of the Experimental Data

The fitting of experimental data could be included into a branch of numerical analysis known as minimization, which is also a part of an extensive mathematical area known as optimization. The general minimization problem is stated as a single function (f) which depends on one or more independent variables and it is necessary to find those values where f takes a minimum value. This value could be either a local minimum (a value which could be found in the proximity) or a global minimum (which addresses the lowest function value) which could be hidden among several other local minimum points, and thus it represents a more difficult problem to solve. Let us imagine that our objective function is represented as in Figure B.1. The points f_1, f_2, f_3 and f_4 represent minimum points of the function, albeit only f_3 represents the global minimum of the function. Consequently, the selection of the appropriate minimization method relies on the type of problem to be solved and it cannot necessarily be extended beyond this particular problem. There is no general algorithm that can be applied for a problem and it is strongly recommended to apply more than one method for the solution of a specific problem.

The definition of the objective or cost function also plays an important roll for the correct statement of the problem and the probability to obtain sensible results. The objective function measures quantitatively the *goodness* of the system being analyzed. For the case of fitting experimental data, it shows the *goodness* of the model to represent a particular phenomenon. In other words, if we have a vector of data (y_{exp}) that is the result from a certain experiment, therefore it is crucial to know how well they are represented by a certain model (y_{model}). The model is a function of known parameters found during the experimentation and unknown parameters that will be calculated. The aim is to calculate those unknowns variables to provide the best

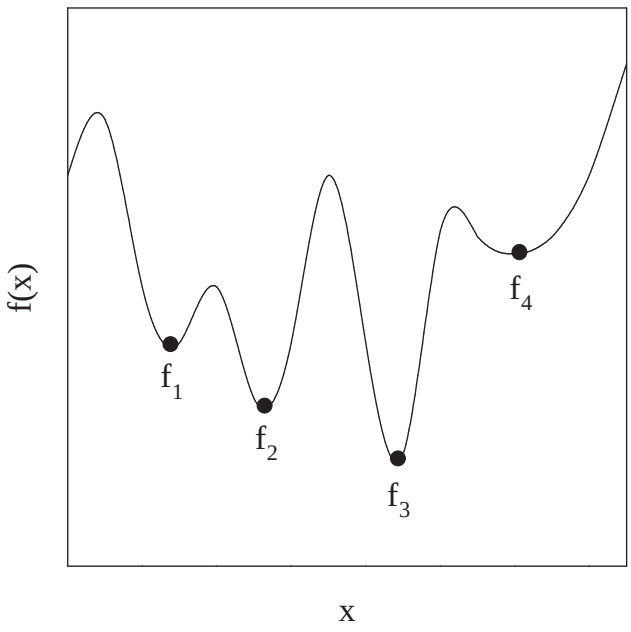

Figure B.1: Objective Function

estimation of the experimental vector such as:

$$Error = \sum_i \left(\frac{y_{i\ exp} - y_{i\ model}}{y_{i\ exp}} \right)^2 \tag{B.1}$$

The *Error* function is the objective function (f) to be minimized. Although there are specific methods to fit experimental data into specific models, many minimization routines can be easily extended to solve this problem if the appropriate objective function is defined, thus they become a very flexible and powerful tool. There are different methods already included in specialized computer optimization packages able to solve minimization problems. In this work, the solution of the minimization problem was done using the open source programming language *Python* [274, 345, 346]. *Python* is a high level programming language and it has become popular among the scientific community because its scientific libraries included in *SciPy* [275, 347]. *SciPy* provides a fair number of general purpose minimization routines and four of them were implemented for the solution of the problem: downhill simplex or Nelder-Mead algorithm, Powell's algorithm, simulated annealing and a modification of the Marquardt-Levenberg algorithm.

B.1 Numerical Algorithms

The problem faced deals with multidimensional minimization and an appropriate solution will depend on how the problem is defined. Because, the gradient of the function was not provided, thus only algorithms that require function evaluations were implemented. The downhill simplex method developed by Nelder and Mead is a good starting point for almost any kind of minimization problem. The algorithm might be slow but it is robust and it almost surely converges to a solution. Another routine implemented was Powell, which is a direction set method. Powell's method in general performs faster than the downhill simplex. The main disadvantage of simplex and Powell's algorithm is that they could converge to local minimums in the proximity of the initial vector of parameters. Consequently, minimization routines that are able to find a global extremum among local minimum become important. Minimization by simulated annealing was used for this specific purpose. The last algorithm was a modified version of the Marquardt-Levenberg algorithm, which is a specialised method for fitting experimental data and it is commonly found in scientific libraries.

B.1.1 Downhill Simplex or Nelder-Mead Algorithm

This unconstrained method requires only function evaluations and it does not compute any derivatives. It is basically the best starting point for relatively simple problems. When simplex is initialized; it takes a series of steps attempting to find a point where the function being minimized has the largest value and it turns to the opposite direction where the function has a lower value. Thus it proceeds taking larger steps in the downhill direction where a minimum (not necessarily global) is likely to be found. Once the method has found a valley floor it contracts itself taking smaller steps until it slowly descends through the valley. If the algorithm attempts to pass over the minimum value it automatically pull itself around to the best minimum reached [320].

B.1.2 Powell's Algorithm

The Powell's algorithm is the prototype of a series of methods called direction set methods. These methods involve a certain steps for updating the next set of directions in a multidimensional problem that the method is going to take. As the algorithm proceeds it generates a series of

values that either will lead to valley floor where a minimum is located or come up with some new values for the next step. When the minimization of one variable fails, it does not affect the successive minimization on the rest of the variables (the concept of non interfering directions is often denominated conjugated gradients). Once the method minimizes along a direction, the gradient of the function being minimized would be perpendicular to the function at the minimum. The method is better known as Powell's quadratically convergent method which comes from the fact of how the function is approximated. If we choose a particular point P as the origin of the system in rectangular coordinates, any function could be approximated using Taylor series as:

$$f(x) = f(P) + \sum_i \frac{\partial f}{\partial x_i} x_i + \frac{1}{2} \sum_{i,\,j} \frac{\partial^2 f}{\partial x_i x_j} x_i x_j + \cdots \tag{B.2}$$

$$f(x) \approx c - b \cdot x + \frac{1}{2} x \cdot A \cdot x \tag{B.3}$$

where

$$c \equiv f(P) \qquad b \equiv -\nabla f \mid_P \qquad [A]_{ij} \equiv \frac{\partial^2 f}{\partial x_i x_j} \mid_P \tag{B.4}$$

Then the gradient of the function is approximated by:

$$\nabla f = A \cdot x - b \tag{B.5}$$

The gradient then will change along an specific direction following

$$\delta(\nabla f) = A \cdot (\delta x) \tag{B.6}$$

Let us assume that we have moved along some direction d_1 to a minimum and the method changes to a new direction d_2. The way that the method adjusts itself to avoid that the new direction taken d_2 does not affect the minimization in the d_1 direction, is that the gradient should stay perpendicular; this condition is given by

$$0 = d_1 \cdot \delta(\nabla f) = d_1 \cdot A \cdot d_2 \tag{B.7}$$

The two vectors d_1 and d_2 are called conjugate; if the minimization is carried out the method provides a set of linearly independent conjugates. Then when Powell's method minimizes over

the line directions, it will converge to a minimum of a quadratic form like that given in Equation B.2 [320, 348].

B.1.3 Minimization by Simulated Annealing

This minimization routine is suited for finding a global minimum value of a function, when it is suspected that it lies among a series of several local minimums. One important characteristic of the method is that the space over which the objective function is minimized is discrete. The configuration of space that is being discretised is large and also the sense of direction in which some minimization methods are based looses its meaning. In its conception the method keeps an analogy with thermodynamics and specifically with mechanical statistics. Let us imagine a system of a finite number of molecules in a certain known configuration, what it would happen when the system reaches the lowest temperature possible? The molecules will eventually loose mobility and solidify and they will be arranged into a crystalline structure. This is denominated ground state and they are extremely rare to find in nature. However, this is what will happen at extreme low temperatures and thus the structures formed will have the lowest energy state possible. Nonetheless, it is not an easy task to achieve even if we can easily reach those low temperatures. If the temperature is not lowered slowly once the ground state is reached the molecules will not follow an order and the ground state will not result into the smallest energy configuration possible. The lowest energy state is only achieved by carefully annealing the structure. Structural arrangements obtained by lowering the objective function at extreme quenching from a high temperature to $T = 0$ will result into metastable structures. Distinguishing the ground state (global minimum or lowest energy state) at low temperature among those metastable structures (local minimum) forms the basis of the concept of minimization by simulated annealing [349].

This concept has been applied for computing properties of equation of state based on the interaction of individual molecules applying mechanical statistics [350]. In the algorithm a given small random displacement of any individual molecule will result in a change of the energy system (ΔE) which is computed. If $\Delta E \leq 0$ the new structure configuration is accepted and becomes in the next starting point. When $\Delta E \geq 0$ the new starting point is calculated from probability. The probability of the new configuration is given by $\mathrm{P}(\Delta E) = \exp(-\Delta E/k_B T)$,

where k_B is the Boltzmann constant. A random number is chosen in the interval $(0, 1)$ and compared with $\mathrm{P}(\Delta E)$. If $\mathrm{P}(\Delta E)$ is higher the new configuration is taken and if it is lower the initial configuration is used as the new step, thus the system is then represented by a Boltzmann distribution. If the objective function is place instead of the energy and configurations are replaced by a vector of parameters (p), the method generates a set of new parameters that will solve a given minimization problem. The physical process of the minimization problem solved by simulated annealing process will first melt the system being minimized at an effective temperature and then lower the temperature slowly until the system freezes and reaches its minimum energy value forming a well ordered structure [349].

B.1.4 Levenberg-Marquardt Algorithm

As it was mentioned earlier the finding of the best-fitting parameters can be seen as a minimization of the parameters in multidimensional space. However, there are already more efficient methods that deal with the special task of fitting the experimental data into a model; the Levenberg-Marquardt algorithm is one of them. Assuming that the experimental data are normally distributed and they can be represented by the chi-square distribution (χ^2), the method assumes that χ^2 could be approximated by a quadratic Taylor expansion then:

$$\chi^2(p) \approx \gamma - d \cdot p + \frac{1}{2} p \cdot D \cdot p \tag{B.8}$$

Which is similar to Equation B.3, where p is the vector of parameters to be minimized, d is a vector and D is a matrix of the second derivatives of the function denominated Hessian matrix. The new point in the minimization is then calculated from:

$$p_{new} = p + D^{-1} \cdot \left[-\nabla \chi^2(p) \right] \tag{B.9}$$

The main difference from the previous algorithms is that the Levenberg-Marquardt provides a direct method to calculate the Hessian matrix because χ^2 is based on a model function previously specified. The method allows a switch between calculation of the inversion of the Hessian when the function is far from the minimum to use the steepest descent method once the function approaches to its minimum. Levenberg-Marquardt works if a fairly well educated guess of the initial parameters is assumed.

B.2 An Example of the Usage of the Routines for the Fitting of Kinetic Data

In order to compare the different methods of minimization a reaction engineering problem was taken from *An Introduction to Chemical Engineering Kinetics and Reactor Design* by Hill [230] pages 50 and 51. The solution of the problem involves the calculation of the kinetic parameters of a reaction performed in a batch reactor. The reaction studied was the dehalogenation reaction of ethylene bromide when it reacts with potassium iodine in 99% of methanol (solvent) according to the reaction:

$$C_2H_4Br_2 + 3KI \longrightarrow C_2H_4 + 2KBr + KI_3 \tag{B.10}$$

The temperature of the reaction was 332.87 K and the initial concentration of the reactants were 0.1531 kmol KI/m^3 and 0.02864 kmol $C_2H_4Br_2/\mathrm{m}^3$. The fraction of $C_2H_4Br_2$ reacted versus time is given in Table B.1.

Table B.1: $C_2H_4Br_2$ Reacted

Time, (ks)	Fraction Reacted of $C_2H_4Br_2$
29.7	0.2863
40.5	0.3630
47.7	0.4099
55.8	0.4572
62.1	0.4890
72.9	0.5396
83.7	0.5795

A bimolecular power-law kinetic model is presumed to represent the reaction. The solution showed in the book supposed unity individual reaction orders and the kinetic constant was calculated from a linearization of the integrated batch reactor model. The same problem was solved by implementing the minimization methods described previously to calculate the kinetic parameters. The kinetic parameters were calculated by the minimization of the Equation B.1

coupled to a power-law kinetic model. The $y_{i\,exp}$ corresponds to the values of time given in Table B.1 and $y_{i\,model}$ is given by:

$$y_{i\,model} = \frac{dC_A}{dt} = -\mathscr{R}_A = -k\,C_A^a\,C_B^b = -k\,(C_{A_0} - C_{A_0}X_A)^a(C_{B_0} - 3C_{A_0}X_A)^b \tag{B.11}$$

Where A designates $C_2H_4Br_2$ and B the KI. The parameters k, a and b, which represent the kinetic constant and reaction orders respectively, are the parameters calculated by the routines during the minimization. During the solution Equation B.11 is integrated numerically by the routine provided in the *SciPy* mathematical library (A description of the ordinary differential equation solver is given in Appendix C). Table B.2 shows the solution obtained from the fitting of experimental data and Figure B.2 depicts a plot of the experimental data and the minimized values obtained by the numerical methods.

Table B.2: Result of the Minimization Routines

Method of Solution	Initial Vector [k, a, b]	Fitted k	Fitted a	Fitted b
Linear Solution (Book)		0.0847	1	1
Downhill simplex	[0.1, 1.5, 1.5]	0.0848	0.1858	2.5548
Powell	[0.1, 1.5, 1.5]	0.0499	0.9719	0.8010
Simulated Annealing	[0.1, 1.5, 1.5]	0.1633	0.4549	2.3613
Levenberg-Marquardt	[0.1, 1.5, 1.5]	0.1226	1.0160	1.1604

By comparing the values obtained in Table B.2 enables a preliminary conclusion to be drawn based solely on the molecularity of the reaction. It is commonly found that reaction orders have integer values and usually for bimolecular reactions they should strictly be 1 or 2. Consequently, only methods that provided reasonable orders (from the molecularity point of view of the reaction) would be considered. However, this is not completely valid because orders smaller than 1 are sometimes found and the possibility that they are higher than 2 cannot be at all discarded. Moreover, which of the above solutions would be *appropriate*. At this, point it is not only in terms of chemical kinetics that the problem has been defined, it is partially due to its mathematical statement that several solutions were found. When the objective function is being minimized the solution depends on many factors e. g. the function being minimized, initial

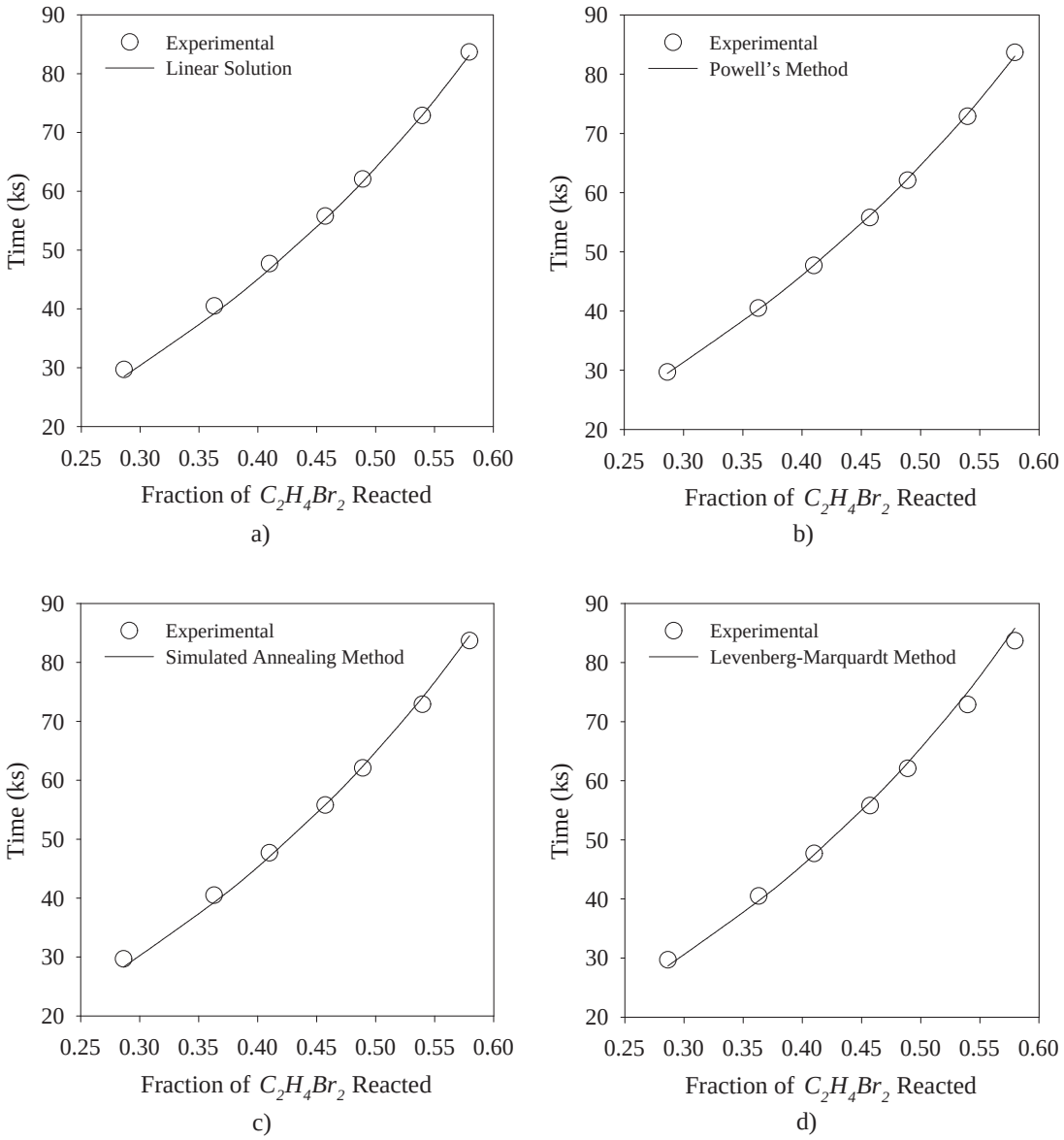

Figure B.2: Comparison of Minimization Methods

point, algorithm used, termination conditions, amongst others. Looking at the results plotted in Figure B.2 allows a *visual* inspection of the results to be made and from them the adopted final solution can be defined. Surprisingly, all routines fitted fairly well the experimental data (only 3 were plotted). So the question remains, which one would be the most *appropriate*? The answer is not easy, it is clear that any solution would be adequate but it would be more reasonable choosing among the linearization, Powell or Levenberg-Marquardt solution. It is suggested that when integral-type reactors are considered, to avoid error in the parameters estimation the

integration of the continuity reactor equation should be solved numerically and not by a linear transformation [351]. Besides, linearization methods become impractical if the reaction order must be assumed all the time, especially when a computer program can provide a faster and more accurate solution, albeit here is not the case. Now any of the remaining three would be an suitable solution. The problem illustrates that the function might indeed have several minimums as it is shown in Figure B.1 and the use of only one method for fitting the experimental data would not be sufficient to find a reliable solution. Consequently, the task to select a solution of a problem could become difficult and care must be taken to adopt any of them.

B.3 Heterogeneous Catalytic Reaction Rate Models

The fitting of experimental data were performed using the integral analysis method proposed by Froment and Hosten [273]. In the analysis, the experimental data were fitted to the continuity equation of an ideal tubular reactor:

$$\frac{dX_i}{d\left(W/F_{i_0}\right)} = \mathscr{R}_i \tag{B.12}$$

Where X_i is the fraction of the reacted species i, W is the weight of the catalyst, F_{i0} initial molar flow rate and $\mathscr{R}_i$ is the reaction rate based on the disappearance of the reactant i. The continuity equation is then subject to the initial conditions:

$$X_i\left(0\right) = X_{i_0} \qquad \text{when} \qquad W/F_{i_0} = 0 \tag{B.13}$$

The problem is to assume a suitable model for the reaction rate and compare the predicted outcome values of the proposed model to the experimental data. The reaction rate is a function of known parameters (X_i, W, F_{i0}) and unknown parameters that will be calculated by the minimization routines (fitted parameters); thus the best fitting parameters will be those which minimizes Equation B.1.

The selection of the appropriate model relies on the knowledge of the precise reaction mechanism. When it is unknown, then two approaches could be taken. The first one and most common is to use a semi-empirical reaction rate model like the power-law. The second is to

formulate the reaction rate model based on the supposition of a reaction mechanism (Langmuir-Hinshelwood-Hougen-Watson). A thorough discussion about Langmuir-Hinshelwood-Hougen-Watson (LHHW) reaction mechanisms could be found elsewhere [230, 352]. The mechanistic reaction rates are often used to represent heterogeneous catalytic reactions and include adsorption and desorption steps. Consequently, experimental data were analysed by incorporating the reaction rate proposed into the reactor continuity equation (Equation B.12). If the proposed model represents adequately the experimental set of data, there is, however not completely, a degree of certainty about how the reaction proceeds. The reaction rates proposed were based on previous work of similar reactions:

1. The power-law kinetic model of a pseudo homogeneous bimolecular reaction:

$$\mathscr{R}_i = k\, C_i^a\, C_j^b = k\, (C_{i_0} - C_{i_0} X_i)^a\, (C_{j_0} - \nu_j C_{i_0} X_i)^b \tag{B.14}$$

   where the C_{i_0} and C_{j_0} are the reactants concentration. The reaction rate constant k and the individual reaction orders a and b were fitted into the model.

2. Langmuir-Hinshelwood-Hougen-Watson (LHHW 1) [207]. This reaction rate assumes adsorption of reactants on different sites of the catalyst and then the chemical reaction. The equation takes the following expression:

$$\mathscr{R}_i = \frac{k K_i C_i K_j C_j}{(1 + K_i C_i)\,(1 + K_j C_j)} \tag{B.15}$$

   where k and the adsorption constants K_i and K_j for each species were fitted into the continuity reactor equation.

3. Langmuir-Hinshelwood-Hougen-Watson (LHHW 2) [207]. It supposes reactants adsorption on the same site of the catalyst and then the chemical reaction. The equation takes the following expression:

$$\mathscr{R}_i = \frac{k K_i C_i K_j C_j}{(1 + K_i C_i + K_j C_j)^2} \tag{B.16}$$

4. Langmuir-Hinshelwood-Hougen-Watson (LHHW 3) [206, 218]. Comprising adsorption of specie i on one type of catalyst site and dissociative adsorption of the specie j on different site and a rate-determining irreversible surface reaction between i and j. The mathematical

expression takes the following form:

$$\mathscr{R}_i = \frac{kK_iC_iK_j^{0.5}C_j^{0.5}}{(1+K_iC_i)\left(1+K_j^{0.5}C_j^{0.5}\right)} \tag{B.17}$$

5. Eley-Rideal. Where only one molecule is adsorbed and the other reacts directly without adsorbing. The proposed mechanism arises from the fact that in the CSCWO of organic compounds like those studied here, the amount of oxygen per each organic compound molecule is at leats 10 times higher. Consequently, at any given time the concentration of oxygen surpasses that of the organic compound. It is assumed that oxygen is being adsorbed before any organic compound molecule could reach any active site.

$$\mathscr{R}_i = \frac{kC_iK_jC_j}{1+K_iC_i+K_jC_j} \tag{B.18}$$

B.3.1 Fitting of the Experimental Data into a Reaction Rate Models

The experimental data set corresponds to the catalytic supercritical water oxidation of quinoline over a mixed catalyst of MnO_2/CuO at 673 K and 23.0 MPa. The elucidation of the best model and thus the best fitting of the parameters was done by testing each of the reaction rate models with a series of different initial vectors to estimate the solution. Then a comparison of the solution vectors was done to find out any trend on results together with the value of the objective function at the minimum point.

Although the models 2 to 5 are theoretically more appropriate for mechanisms present in catalytic reactions, the power-law kinetic model represented better the experimental data. Thus the use of the LHHW or Eley-Rideal reaction rate mechanisms was not justified for this set of experimental data. The best fitting values with a confidence level of 95% are shown in the following equation that expresses the reaction rate of quinoline in the reactor:

$$\mathscr{R}_Q = 0.228 \pm 0.12\, C_Q^{0.4\pm0.23}\, C_{O_2}^{0.23\pm0.09} \tag{B.19}$$

Figure B.3 shows the minimized parameters and the value reached by the objective function at each iteration obtained by the Nelder-Mead simplex algorithm. The objective function reaches a minimum once the values obtained by Equation B.19 are computed, which assures that the minimization reached a solution, this was also obtained by the Powell's and Levenberg-Marquardt

methods. The minimization by simulated annealing confirmed that the minimum point also is a global minimum of the function.

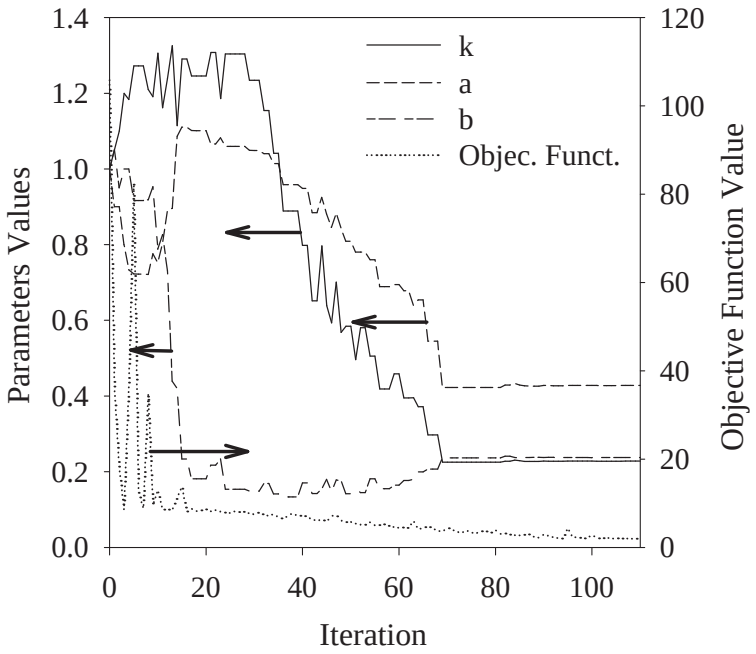

Figure B.3: Objective Function and Minimized Kinetic Parameters by Simplex Algorithm

The sensitivity of the calculated parameters over the objective function was also investigated. The reaction orders showed the strongest influence on the objective function. Figure B.4 depicts the value of the objective function at different values of the reaction orders obtained by the Nelder-Mead simplex algorithm. As it is shown from the graph, the objective function value depended strongly on the reaction order respect to quinoline concentration (C_Q). It had a minimum when the reaction order respect to quinoline had a positive value lower than unity. On the other hand, the reaction order value of oxygen did not have a noticeable change on the objective function at constant reaction orders respect to quinoline higher than 0. At this point the reaction order of oxygen could adopt a value in the range of 0 to 2 without appreciable affecting the value of the function being minimized.

The non-integer values of the reaction orders of both reagents reflects that the reaction is more complex than it is shown by the stoichiometric equation and suggests that the oxidation goes beyond the simple interaction of quinoline and oxygen and implies the occurrence of side reactions [230]. Another point worth to discuss are the confidence limits on the fitted parameters.

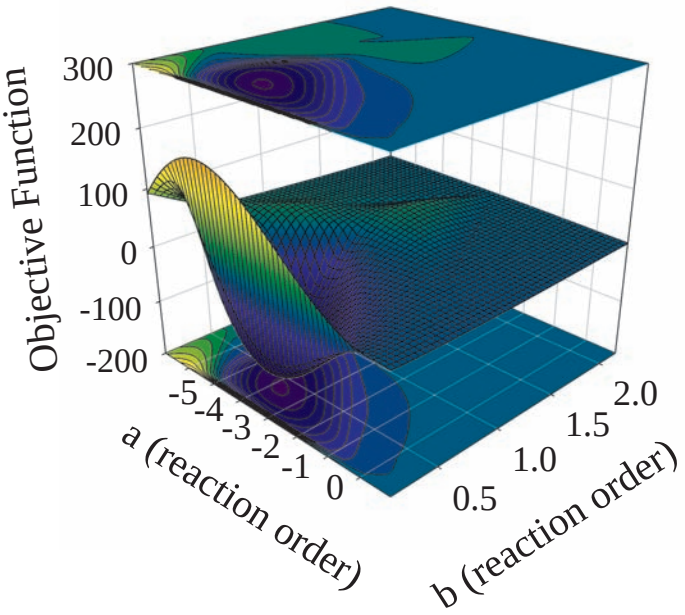

Figure B.4: Variation of Objective Function and Minimized Reaction Orders

The wide confidence limits observed indicates changes in the reaction orders due to reactants concentration. This fact was proven by calculating the reagents reaction orders for individual set of experiments. Figure B.5 shows a comparison of the fitting provided by the global kinetic model (Equation B.19) and the individual fitting of each experimental data set for different quinoline to oxygen concentrations. Concentration of reactants are given in mmol/L at reaction conditions. Table B.3 summarizes the values of the fitted kinetic parameters.

When the initial concentration of oxygen ($C_{O_{20}}$) increased the fraction of quinoline reacted augmented considerably and there was a steep change in the gradient of the curve when it tended to 1. This effect was compensated by increasing the reaction order of oxygen in the reaction rate, which it was observed when initial concentration of oxygen varied from 6.45 to 32.5 mmol/L at constant quinoline initial concentration (C_{Q_0}) of 0.3 mmol/L. A similar finding occurred when quinoline concentration was varied keeping a constant ratio of quinoline to oxygen. These findings support the assumption of a complex reaction mechanism.

The model agreed with the experimental data and it confirms that relatively simple reaction rate model as power-law could be used to represent complex process, although the understanding

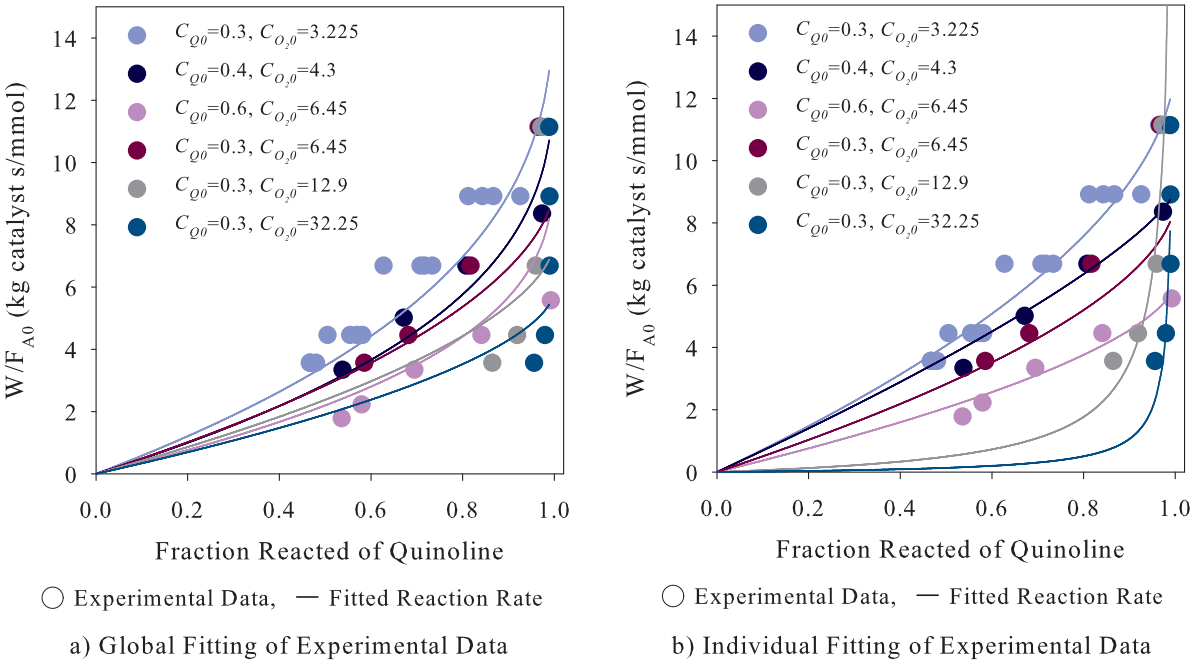

Figure B.5: Global and Individual Fitting of the Experimental Data

of the reaction mechanism still lies hidden in the kinetic parameters. These models are useful when preliminary studies are carried out to investigate the feasibility of the process rather than assume that the reaction undergoes a certain mechanism.

Table B.3: Implementation of the Simplex Routine for Each Experimental Run

C_{Q_0}, mmol/L	$C_{O_{20}}$, mmol/L	$[k,\ a,\ b]$
0.3	3.225	[0.2365, 0.4439, 0.0242]
0.4	4.3	[0.1153, 0.0496, 0.1951]
0.6	6.45	[0.3706, 0.4442, −0.0374]
0.3	6.45	[0.2167, 0.7174, 0.5235]
0.3	12.9	[1.0868, 1.6796, 1.0166]
0.3	32.5	[0.1305, 1.8822, 1.7941]

Appendix C

Packed-bed Tubular Reactor Continuity Equation

The mathematical model that describes the material balance of a steady state operation in a tubular packed-bed reactor written in cylindrical coordinates is given by [352] (refer to Figure C.1):

$$u_S \frac{\partial C_i}{\partial x} = D_R \left[\frac{1}{r} \frac{\partial C_i}{\partial r} + \frac{\partial^2 C_i}{\partial r^2} \right] + \varepsilon \mathscr{R}_i \tag{C.1}$$

Where i is referred to as the reacting species, u_S as the superficial velocity, D_R as the dispersion coefficient in the radial direction, ε as the void fraction and $\mathscr{R}_i$ is the reaction rate.

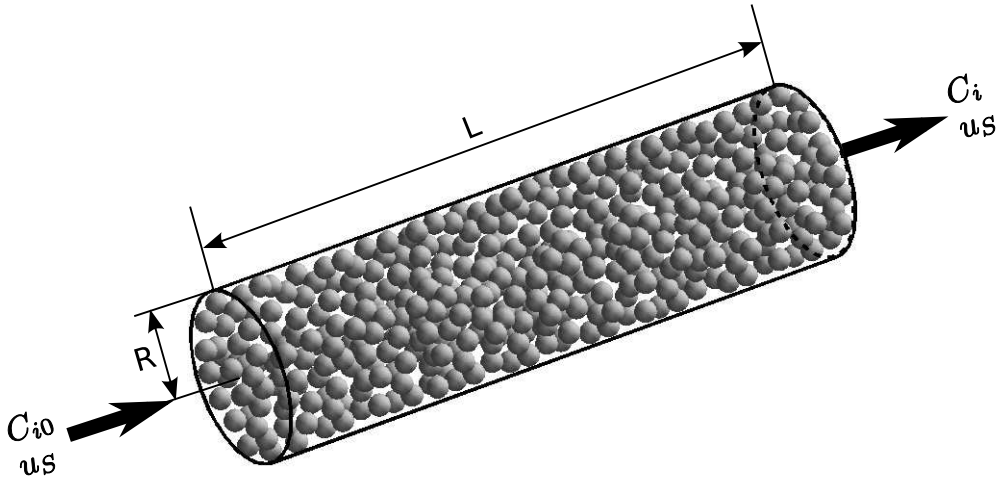

Figure C.1: Fixed Bed Tubular Reactor

In the model the velocity profile is considered as constant along the axial position except near the wall. This means that the reactor is not an ideal plug flow, where concentration gradients

in radial positions are negligible. Instead, Equation (C.1) is able to account for those variations in concentration along the reactor cross section. The continuity equation obeys three boundary conditions, one in axial and two in radial position. The boundary condition in the axial position for the concentration of i at the inlet is:

$$C_i(r,0) = C_{i0} \tag{C.2}$$

This assumes that reagents are premixed before enteringing the reactor. Meanwhile the boundary condition in the radial axis are:

$$\frac{\partial C_i}{\partial r} = 0 \qquad \text{at the wall,} \qquad r = R \tag{C.3}$$

$$\frac{\partial C_i}{\partial r} = 0 \qquad \text{at the centerline,} \qquad r = 0 \tag{C.4}$$

Which can be also for convenience expressed in dimensionless units, for this the concentration and the two characteristic lengths are scaled:

$$v_i = \frac{C_i}{C_{i\,0}}; \qquad y = \frac{r}{R}; \qquad z = \frac{x}{L} \tag{C.5}$$

Then the equation is transformed as:

$$u_S \frac{C_{i\,0}}{L}\frac{\partial v_i}{\partial z} = D_R \left[\frac{1}{r}\frac{C_{i\,0}}{R}\frac{\partial v_i}{\partial y} + \frac{C_{i\,0}}{R^2}\frac{\partial^2 v_i}{\partial y^2}\right] + \varepsilon \mathscr{R}_i \tag{C.6}$$

Rearranging:

$$\frac{\partial v_i}{\partial z} = \frac{D_R L}{u_S R^2}\left[\frac{1}{y}\frac{\partial v_i}{\partial y} + \frac{\partial^2 v_i}{\partial y^2}\right] + \frac{\varepsilon L \mathscr{R}_i}{u_S C_{i\,0}} \tag{C.7}$$

C.1 Method of Lines Applied to the Solution of a Packed-bed Tubular Reactor Continuity Equation

This partial differential equation (PDE) that represent a packed-bed reactor (Equation C.1) has a canonical form of a parabolic equation. Although, the solution of PDE could be done by several methods (e. g. finite differences, finite element method or finite volume method [353]), this type

of PDE can also be solved by a procedure known as the method of lines (MOL) [311, 323] which produces stable solutions for parabolic PDE [354]. The MOL is regarded as a special numerical method (or rather a semianalytical method) which discretises a given differential equation in one or two dimensions while using analytical solution in the remaining direction. It combines the advantages of finite differences and analytical methods which offers [355, 356]:

1. Computational efficiency. Because it is a semianalytical method the algorithm is simple and compact, which yields accurate results and less computational effort than pure finite difference methods.

2. Numerical stability. When the dimensions are separated during the discretisation, it is easier to establish stability and convergence of the problem.

3. Compact programming code. By using a well documented and reliable ordinary differential equations (ODE) solvers, the code can be substantially reduced.

In this method the PDE is converted into a set of ordinary differential equations by discretising only the radial axis using finite differences and leaving the axial axis unchanged (see Figure C.2). For example, a central difference for a first derivative can be calculated as:

$$\frac{\partial v_i}{\partial y} \approx \frac{v_i(y+\Delta y, x) - v_i(y-\Delta y, x)}{2\Delta y} \tag{C.8}$$

And for a second derivative the equation is given by:

$$\frac{\partial^2 v_i}{\partial y^2} \approx \frac{v_i(y+\Delta y, x) - 2v_i(y, x) + v_i(y-\Delta y, x)}{\Delta y^2} \tag{C.9}$$

In the limit where $\Delta y \to 0$, Equations (C.8) and (C.9) result in a good approximation for the first and second derivatives. Both equations are substituted into the governing PDE and thus Equation (C.7) is then transformed as:

$$\frac{\partial v_i}{\partial z} = \mathscr{K}_1 v_i(y+\Delta y, z) + \mathscr{K}_2 v_i(y, z) + \mathscr{K}_3 v_i(y-\Delta y, z) + \frac{\varepsilon L \mathscr{R}_i}{u_S C_{i0}} \tag{C.10}$$

where:

$$\mathscr{K}_1 = \frac{D_R L}{R^2 u_S}\left[\frac{1}{2y\Delta y} + \frac{1}{\Delta y^2}\right]; \qquad \mathscr{K}_2 = \frac{D_R L}{R^2 u_S}\left[-\frac{2}{\Delta y^2}\right]$$

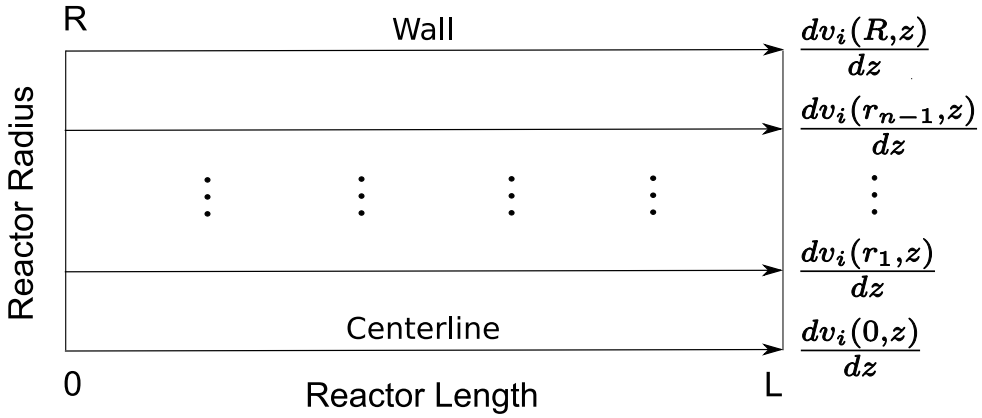

Figure C.2: Discretisation of MOL in a Tubular Reactor

$$\mathscr{K}_3 = \frac{D_R L}{R^2 u_S}\left[\frac{1}{\Delta y^2} - \frac{1}{2y\Delta y}\right] \tag{C.11}$$

When the radial axis is discretised Equation (C.10) can be written in terms of the increments along the radius of the reactor, for $j = 1, \ldots, n-1$,

$$\frac{dv_i(j,z)}{dz} = \mathscr{K}_1(j)v_i(j+1,z) + \mathscr{K}_2(j)v_i(j,z) + \mathscr{K}_3(j)v_i(j-1,z) + \frac{\varepsilon L \mathscr{R}_i}{u_S C_{i0}} \tag{C.12}$$

Now the concentrations along the reactor are given by a set of ordinary differential equations. However, the set needs to be modified to account for the boundary conditions at the centerline and the wall. Two additional ODE are needed to satisfy the boundary conditions. In the case of the centerline when $\partial v/\partial y = 0$ at $y = 0$, Equation (C.7) becomes indeterminate because:

$$\lim_{y\to 0} \quad \frac{1}{y} = \infty \tag{C.13}$$

Using l'Hôpital's rule, a special form of the equation is derived when:

$$\frac{\dfrac{\partial}{\partial y}\left(\dfrac{\partial v_i}{\partial y}\right)}{\dfrac{\partial}{\partial y}(y)} = \frac{\partial^2 v}{\partial y^2} \tag{C.14}$$

Then Equation (C.7) at the centerline is transformed to give:

$$\frac{\partial v_i}{\partial z} = \frac{D_R L}{u_S R^2}\left[2\frac{\partial^2 v_i}{\partial y^2}\right] + \frac{\varepsilon L \mathscr{R}_i}{u_S C_{i\,0}} \tag{C.15}$$

Applying the boundary condition at the centerline $\partial v_i/\partial y = 0$ to Equation (C.8), the symmetry condition at the centerline is obtained where $v_i(y + \Delta y, z) = v_i(y - \Delta y, z)$, using the boundary condition on Equation (C.9), we obtain:

$$\frac{\partial^2 v_i}{\partial y^2} \approx \frac{2[v_i(y + \Delta y, x) + v_i(y, x)]}{\Delta y^2} \tag{C.16}$$

Which is substituted into Equation (C.15) to give:

$$\frac{dv_i(0, z)}{dz} = \mathscr{K}_4(0)v_i(1, z) + \mathscr{K}_5(0)v_i(0, z) + \frac{\varepsilon L \mathscr{R}_i}{u_S C_{i0}} \tag{C.17}$$

where:

$$\mathscr{K}_4 = \frac{D_R L}{R^2 u_S}\left[\frac{4}{\Delta y^2}\right]; \qquad \mathscr{K}_5 = \frac{D_R L}{R^2 u_S}\left[-\frac{4}{\Delta y^2}\right] \tag{C.18}$$

On the other hand, at the wall $\partial v_i/\partial y = 0$ when $y = 1$, Equation (C.7) is again modified to satisfy the boundary condition. The symmetry condition is used again into Equation (C.8) and substituted into Equation (C.7) we obtain the ODE at the wall:

$$\frac{dv_i(n, z)}{dz} = \mathscr{K}_6(n)v_i(n - 1, z) + \mathscr{K}_7(n)v_i(n, z) + \frac{\varepsilon L \mathscr{R}_i}{u_S C_{i0}} \tag{C.19}$$

where:

$$\mathscr{K}_6 = \frac{D_R L}{R^2 u_S}\left[\frac{2}{\Delta y^2}\right]; \qquad \mathscr{K}_7 = \frac{D_R L}{R^2 u_S}\left[-\frac{2}{\Delta y^2}\right] \tag{C.20}$$

The system formed by Equations (C.17), (C.12) and (C.19) are thus used to calculate the variation of the concentration along both radial and axial axis in the tubular heterogeneous catalytic reactor.

In the case where the concentration might not be uniform in the radial axis then the real concentration at any z point in the reactor will have to be calculated from considering all concentration values at that point in the reactor. The concentration of the species i at any z point is calculated from the summation of the individual molar flow rates of i at every point ($v_i(y, z)$) divided by the total flow rate using the average mixing cup concentration [311]:

$$v_{imix}(z) = \frac{\int C_{i0} v_i(y,z) u_S dA}{\int u_S dA_R} = \frac{\int C_{i0} v_i(y,z) r dr}{\int R dR} \tag{C.21}$$

For this particular case where the superficial velocity is assumed as constant Equation (C.21) can be written in terms of the radius:

$$v_{imix}(z) = \frac{\int C_{i0} v_i(y,z) r dr}{\int R dR} = \frac{2\int C_{i0} v_i(y,z) r dr}{R^2} \tag{C.22}$$

If data of conversion are given instead of concentration the Equation (C.7) can be easily transformed recognising that $dv_i = d(C_i/C_{i0}) = -dX_i$ where X_i is the conversion or fraction reacted of the species i. Then equation (C.7) is transformed to give:

$$\frac{\partial v_i}{\partial z} = \frac{D_R L}{u_S R^2}\left[\frac{1}{y}\frac{\partial v_i}{\partial y} + \frac{\partial^2 v_i}{\partial y^2}\right] - \frac{\varepsilon L \mathscr{R}_i}{u_S C_{i0}} \tag{C.23}$$

The only difference with Equation (C.7) is the negative sign in the last term on the right hand side of the equation and all terms derived from this must be affected. It is worth to point out that the usual sign convention for the reaction rate ($\mathscr{R}_i$) is followed.

C.2 The Ordinary Differential Equation (ODE) Solver

For the numerical solution of ODE systems, it is important to identify the type of problem being solved, which will define the approach followed for the solution of the problem, in other words identify the *stiffness* of the ODE system. The *stiffness* can be roughly defined as the presence of one or more fast decays processes in time. ODE systems are then classified as *stiff* and *nonstiff*, the former type being a more challenging numerically speaking task. From the various numerical methods used for solving ODE initial value problems, the Adams multistep methods (explicit and implicit) are suitable for *nonstiff* systems, meanwhile for *stiff* problems the most popular methods are based on the so-called backward differentiation (BDF) method.

Only a brief description of the methods used by the ODE solver is presented here, further information could be found elsewhere [357, 358]. First of all, consider the system $\overset{*}{y} = f(t,y)$, where y is a vector of length N, and consider a discrete time mesh t_0, t_1, ..., t_n, ... (t which

is often related as time or time-related variable; it necessarily need not be the independent variable). If a fixed step size $h = t_n - t_{n-1}$ is considered, thus discrete approximations y_n to $y(t_n)$ are constructed , with y_0 given and where $\overset{*}{y}$ will always denote $f(t_n, y_n)$.

In the case of *nonstiff* problems, the implicit Adams (or Adams-Moulton) formulas produces an approximation given by:

$$y_n = y_{n-1} + h \sum_{i=0}^{q-1} \beta_i \overset{*}{y}_{n-1} \tag{C.24}$$

Here q $(1 \leq q \leq 12)$ is the order of accuracy (if it is not mentioned the order of accuracy of the solution is $q = 12$), and the coefficients β_i depend only on the value of q. The formula is implicit in that $\beta_0 > 0$. The solution of this implicit equation is done by functional iteration:

$$y_{n_{(m+1)}} = y_{n-1} + h\,\beta_0\, f(t_n, y_{n_{(m)}}) + h \sum_{i=1}^{q-1} \beta_i \overset{*}{y}_{n-1} \tag{C.25}$$

where an initial guess (or prediction) $y_{n_{(0)}}$ is obtained from an analogous explicit formula. Both the step size h and order q are actually varied during the integration process, by use of the local errors committed in relation to a tolerance criteria. Changes in h are achieved by interpolation of the multistep data. Note that no $N \times N$ matrices are involved in this case.

For *stiff* problems, the BDF

$$y_n = \sum_{i=1}^{q} \alpha_i\, y_{n-i} + h\,\beta_0 \overset{*}{y}_n = a_n + h\,\beta_0\, f(t_n, y_n) \tag{C.26}$$

where q is again the order (in this case $1 \leq q \leq 5$), and $\beta_0 > 0$. When the problem is *stiff* functional iteration fail to converge for the step sizes of interest, because the strong dependencies of f upon y. Consequently, a modified Newton iteration is implemented:

$$-P[y_{n_{(m+1)}} - y_{n_{(m)}}] = y_{n_{(m)}} - a_n - h\,\beta_0\, f(t_n, y_{n_{(m)}}) \tag{C.27}$$

where P is an $N \times N$ matrix approximating the Jacobian of the algebraic system to be solved:

$$P \approx I - h\,\beta_0\, J, \qquad J = \frac{\partial f}{\partial y} \tag{C.28}$$

(I denotes the $N \times N$ identity matrix). The prediction value $y_{n_{(0)}}$ is obtained from an analogous explicit formula. This iteration differs from a true Newton method because the J is

evaluated periodically. J is evaluated only at predicted values $y_{n_{(0)}}$, and only where a new value appears necessary, for example a failure of a convergence criteria or another indication. The same value of P (or its LU decomposition, if used) is used over all iterations in any one step, and typically also over several time steps, until a new evaluation of J and P is required.

When the BDF method is applied to large *stiff* problems, the numerical solution of the linear system is given by:

$$P\,c = r \tag{C.29}$$

Where c is a correction vector and r is a residual vector, which take advantage of the the sparse structure in P. This is accomplished either for suitable structured LU decompositions, or through iterative linear system methods that use a given matrix structure. This becomes very useful for ODE systems that come from PDE discretisation as in the MOL.

The ODE solver also incorporates a very important and efficient characteristic that allows the routine to automatically switch between *stiff* (BDF) and *nonstiff* (Adams-Moulton) methods, which is more convenient when the nature of the problem is not known and for efficiency of the computational code.

Appendix D

Adsorption and Desorption Curves of Catalyst

D.1 CSCWO of DBU

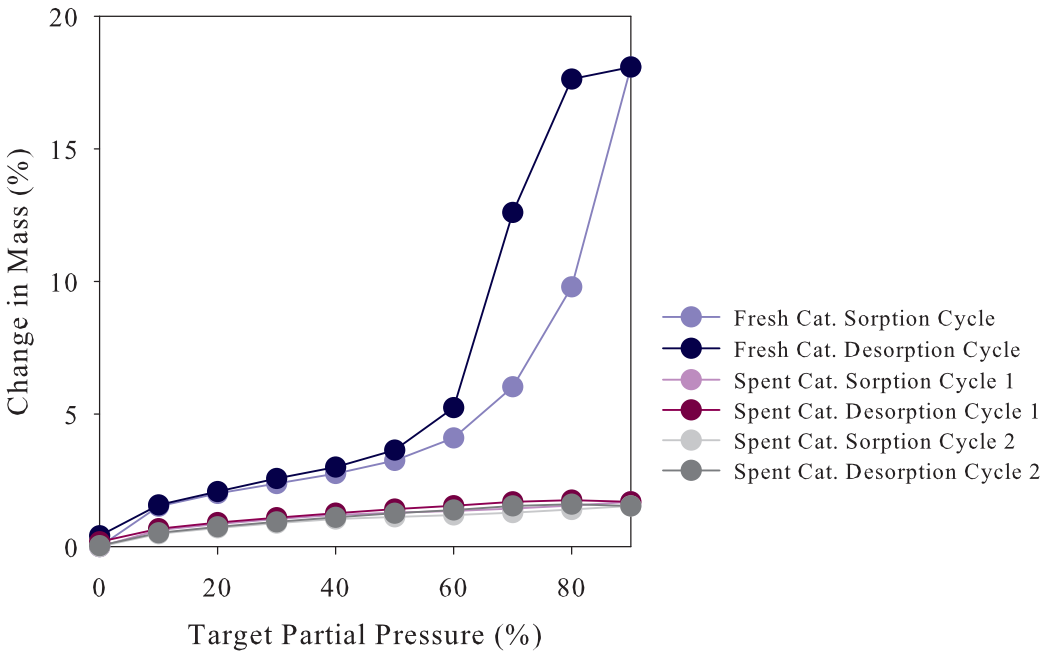

Figure D.1: Adsorption and Desorption Curves of Fresh and Spent *Pt* Catalyst

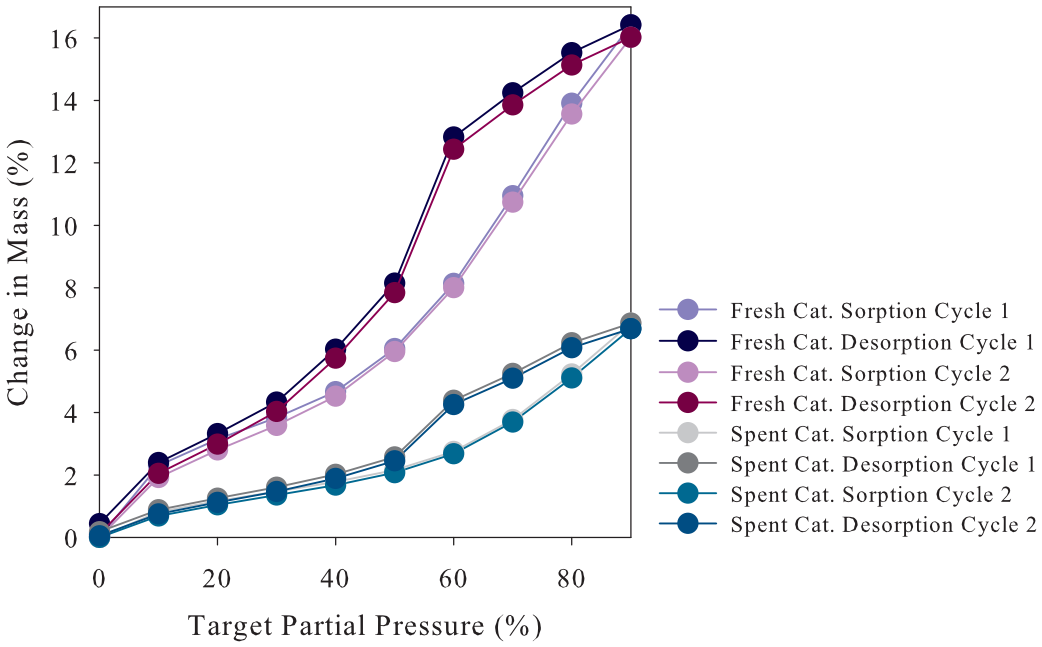

Figure D.2: Adsorption and Desorption Curves of Fresh and Spent CuO Catalyst

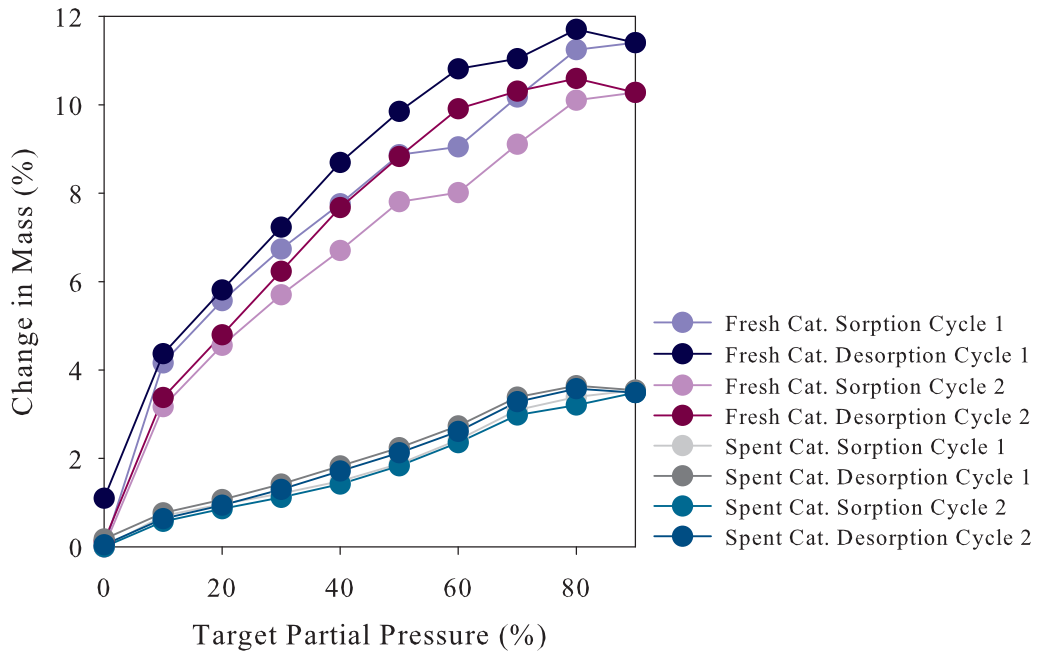

Figure D.3: Adsorption and Desorption Curves of Fresh and Spent MnO_2/CuO Catalyst

D.2 CSCWO of Quinoline

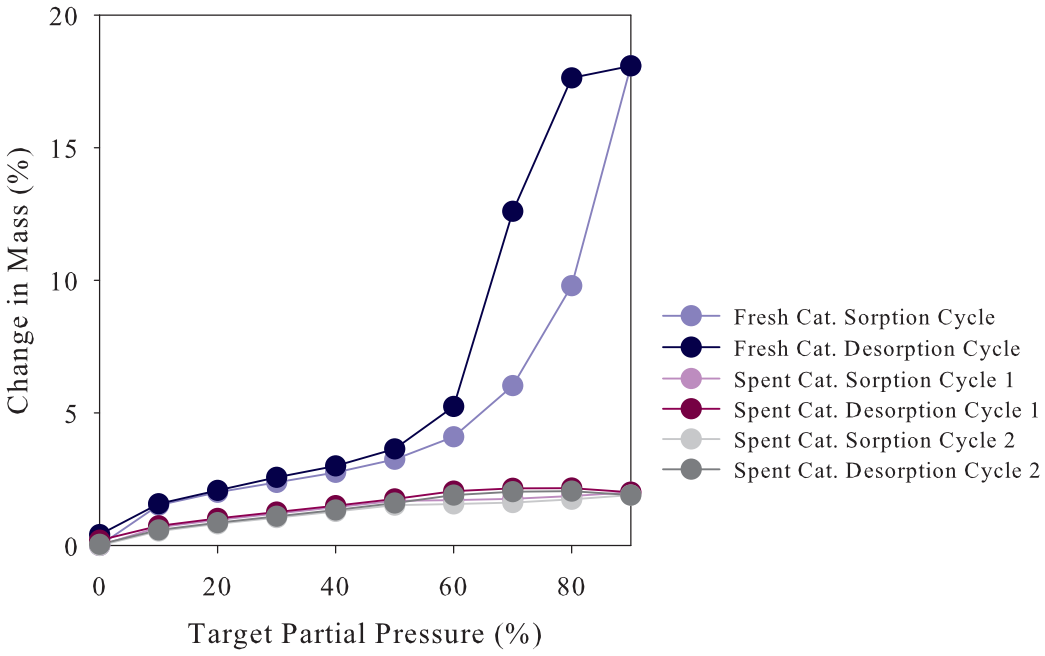

Figure D.4: Adsorption and Desorption Curves of Fresh and Spent *Pt* Catalyst

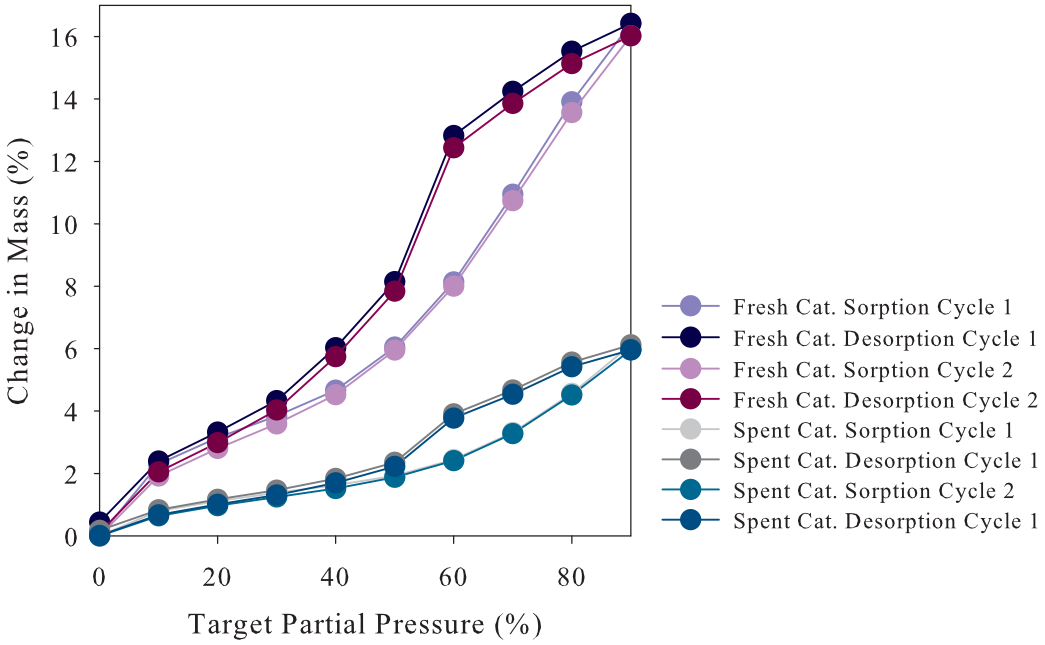

Figure D.5: Adsorption and Desorption Curves of Fresh and Spent *CuO* Catalyst

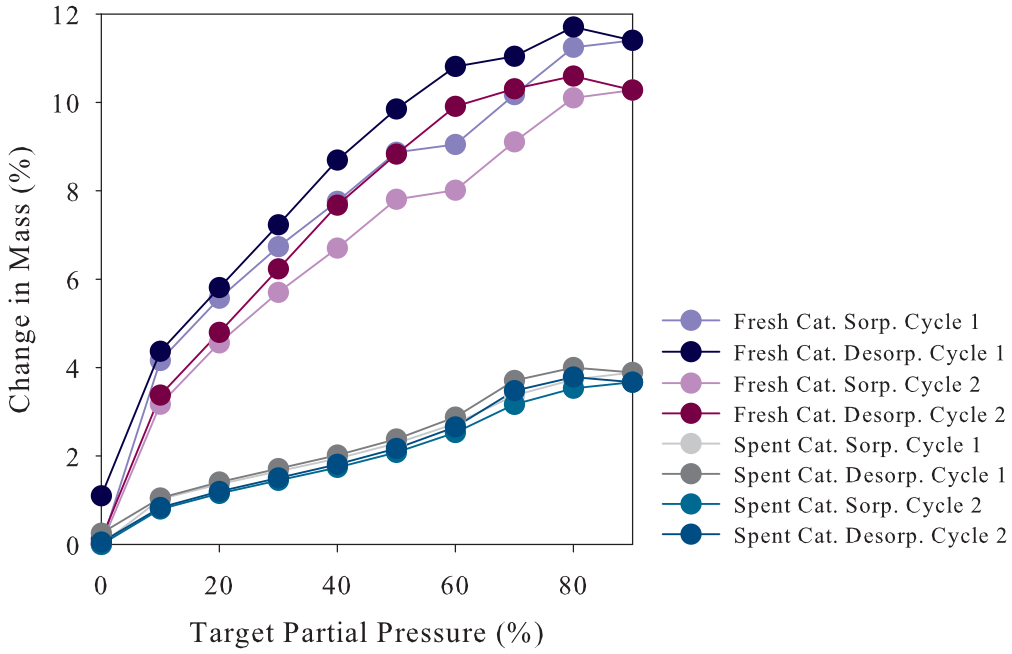

Figure D.6: Adsorption and Desorption Curves of Fresh and Spent MnO_2/CuO Catalyst

Appendix E

X-ray Diffraction Patterns of Spent and Fresh Catalysts

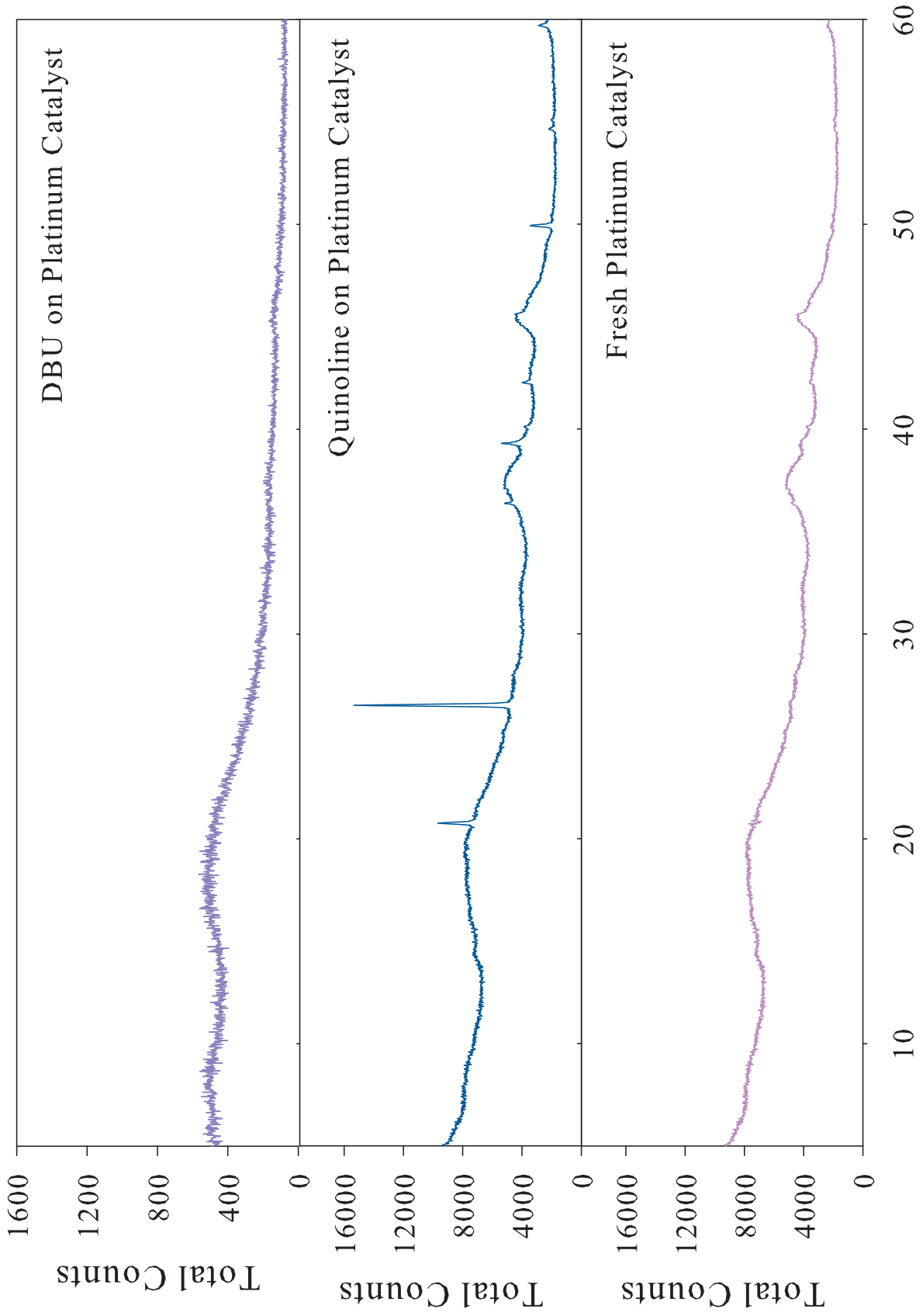

Figure E.1: X-ray Diffraction Pattern of Platinum Catalyst

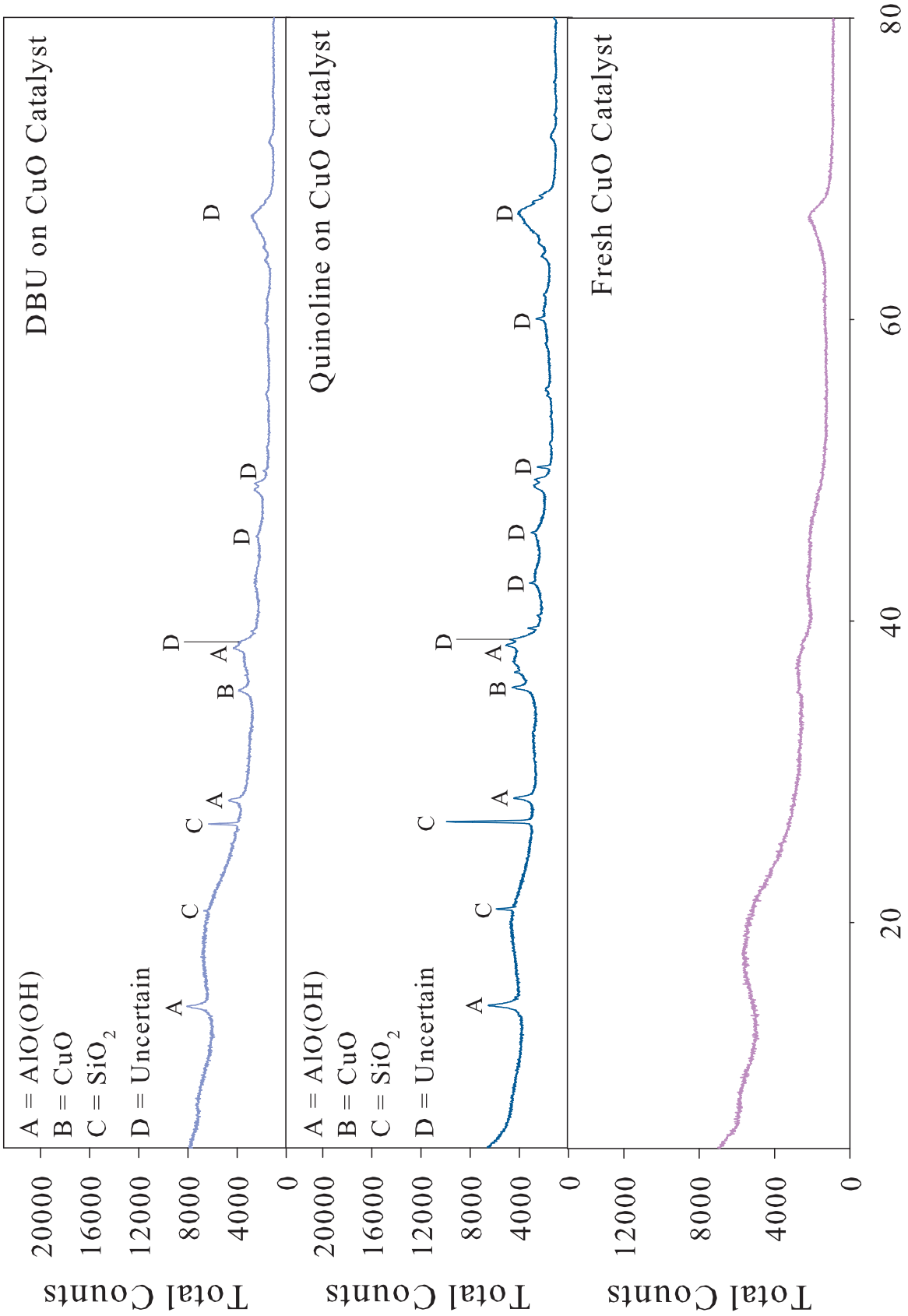

Figure E.2: X-ray Diffraction Pattern of Copper Oxide Catalyst

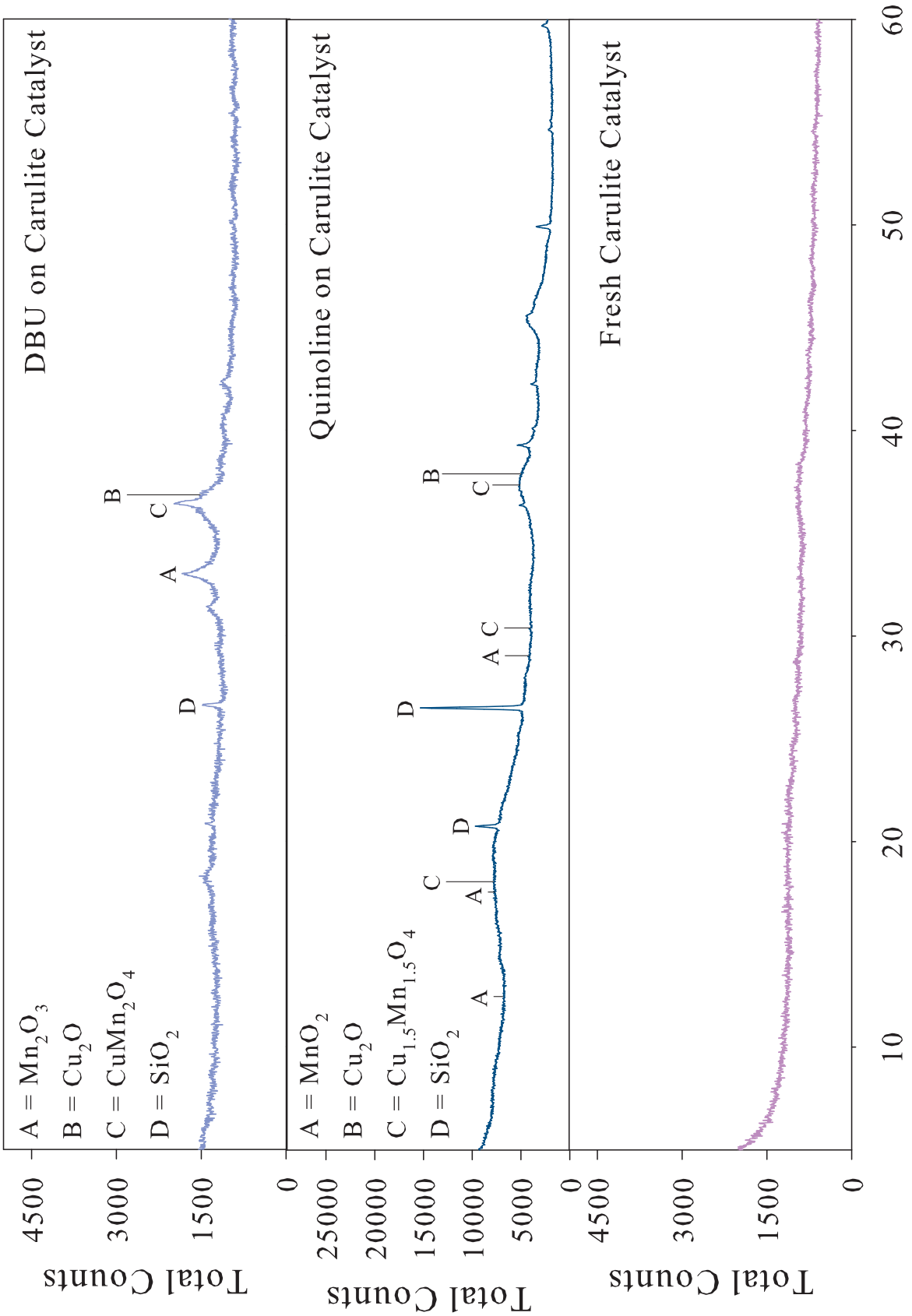

Figure E.3: X-ray Diffraction Pattern of Carulite Catalyst

Appendix F

Scanning Electron Microscopy Analysis of Catalysts

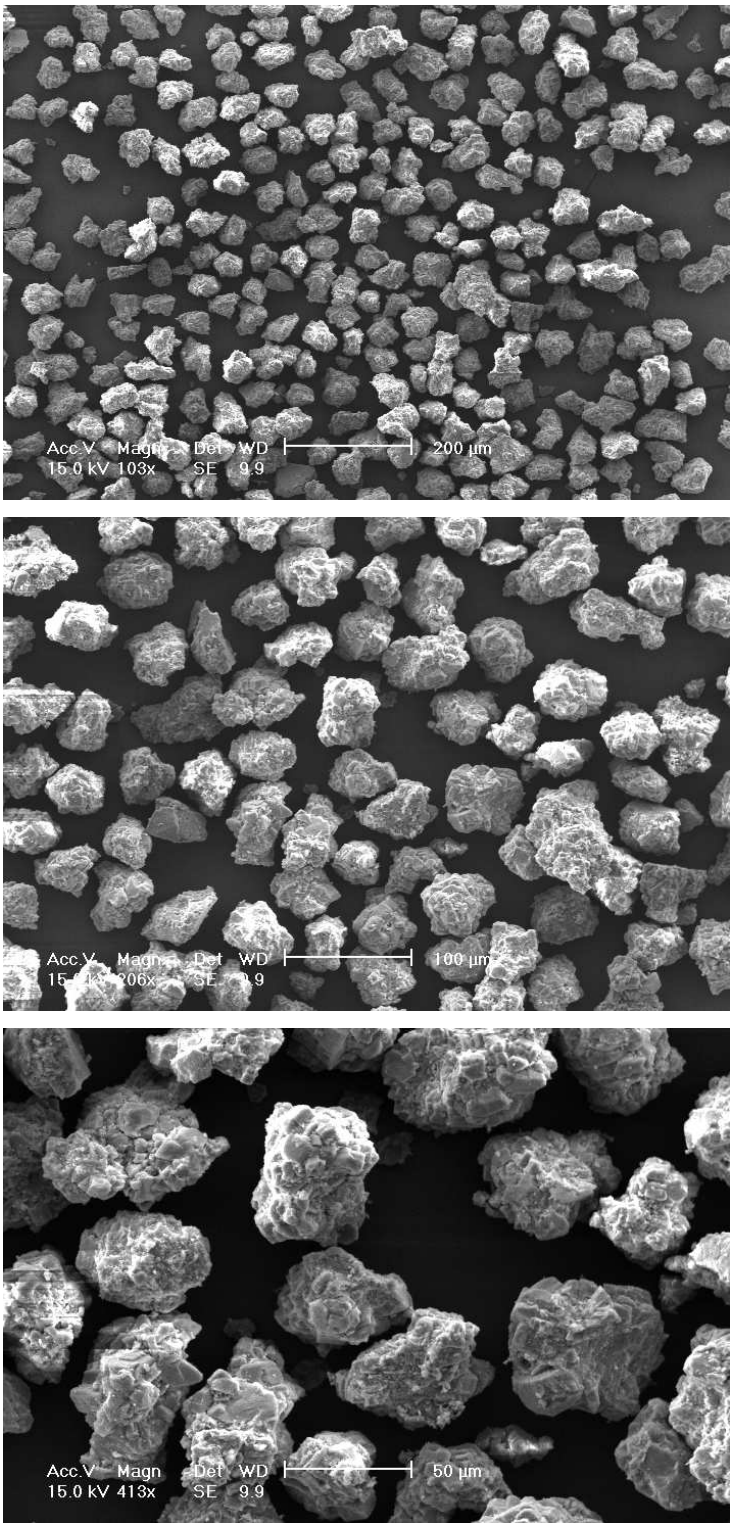

Figure F.1: Spent Catalyst of CSCWO of DBU on Platinum Catalyst after 8 hours at 23.0 MPa and 673 K

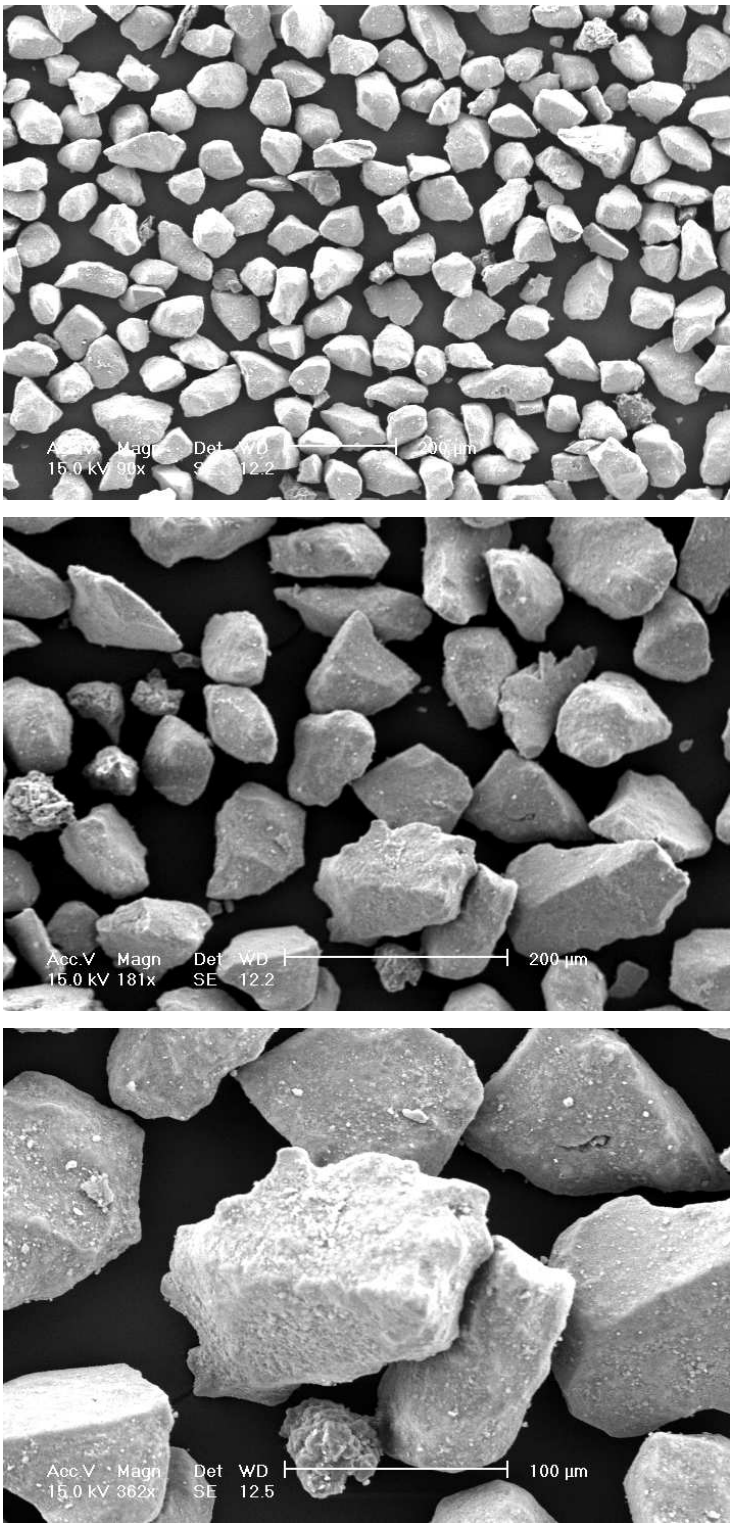

Figure F.2: Spent Catalyst of CSCWO of Quinoline on Carulite Catalyst after 8 hours at 23.0 MPa and 673 K

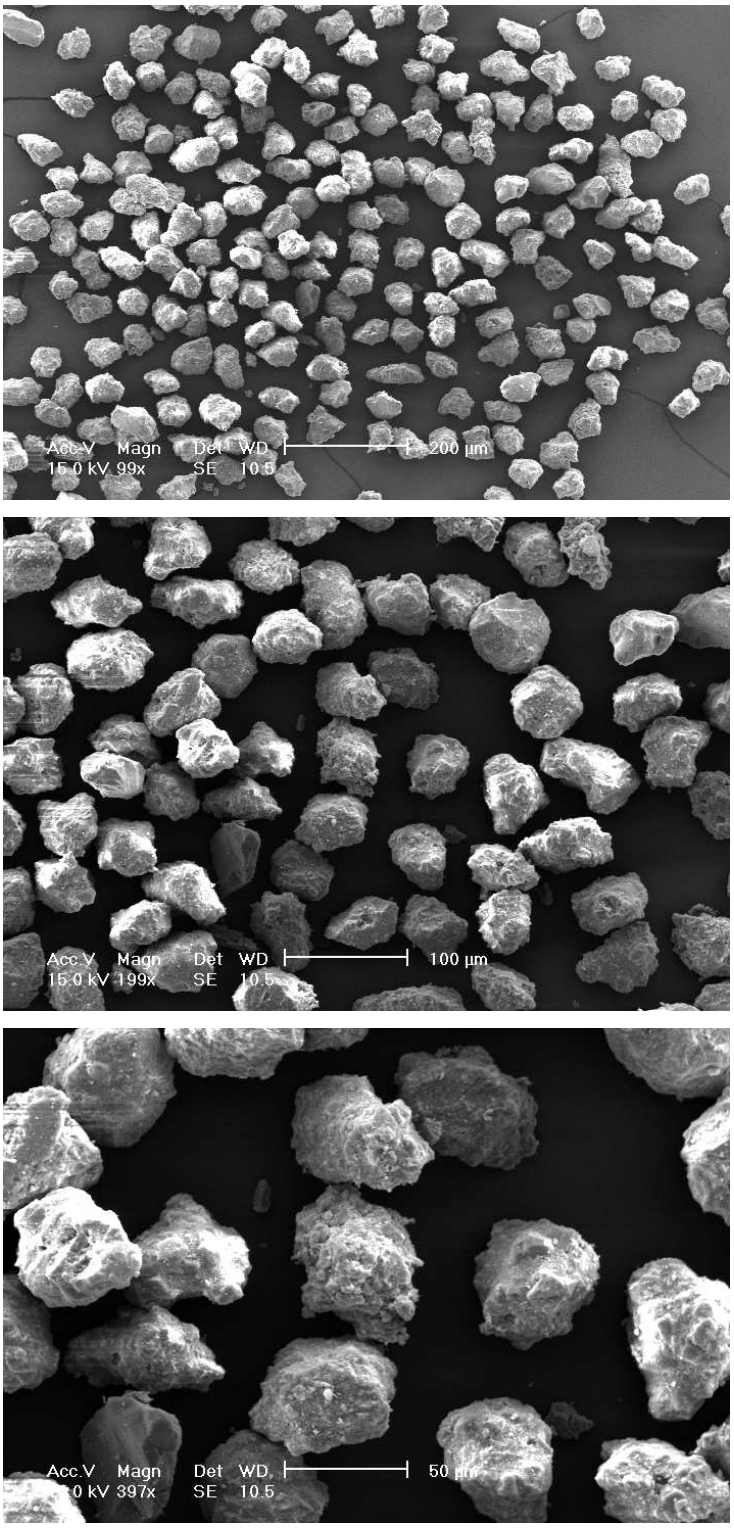

Figure F.3: Spent Catalyst of CSCWO of Quinoline on Platinum Catalyst after 8 hours at 23.0 MPa and 673 K

Appendix G

Computer Programs

G.1 Program for the Calculation of Physicochemical Properties of the Reacting Mixture and Flow Rate and Concentration of Reactants at Room Conditions (Written in *Fortran 95*)[1]

G.1.1 Main Program

```
Program   SCWO_Reactor
!!!!!!!!!!!!!!!!!!!!!!!!!!!!!!!!!!!!!!!!!!!!!!!!!!!!!!!!!!!!!!!!!!!!!!!!!!!!!!!!!!!!!!!!!!!!!!!!!!!!!!!!!!!!!!!!!!
!             The program compute the space velocity of the oxidant and organic solution                   !
!             into the SCWO reactor.  The program has 5 subroutines and 4 external functions:             !
!             1.           Compute the density of water (Water EOS)                                        !
!             2.           Compute  the density of oxygen and DBU (LK-BWR EOS)                            !
!             3.           Compute the mixing rules (LK mixing rules)                                      !
!             4.           Compute the space velocity                                                      !
!             5.           Writing results                                                                  !
!!!!!!!!!!!!!!!!!!!!!!!!!!!!!!!!!!!!!!!!!!!!!!!!!!!!!!!!!!!!!!!!!!!!!!!!!!!!!!!!!!!!!!!!!!!!!!!!!!!!!!!!!!!!!!!!!!
Implicit   None
Integer   ndata,   n   Parameter   (   n   =   3   )                        !Ternary system
Real   (   kind   =   8   )::   P,   T,   dens,   Zoxygen,   Zdbu,   WMW,   Rgas,   Voxygen,   Vdbu,   Vwater,   Vm,   Tcm,   Vcm,   omegam,   &
                   Pcm,   conoxid   ,   oexcess   ,   Vreactor   ,   visc
Real   (   kind   =   8   ),   dimension   (   n   )::   y,   ymol
Real   (   kind   =   8   ),   dimension   (   20   )::   pumpoxid,   pumporg,   spacevel,   concorg,   Rpumpoxid,   Rpumporg,   pumpwater,   &
                   Rpumpwater
Print   *,   'Enter the pressure in bar= '
Print   *,   ''
Read   *,   P
Print   *,   ''
Print   *,   'Enter the temperature in C= '
Print   *,   ''
Read   *,   T
Print   *,   ''
T   =   T   +   273.15
WMW   =   18.015268
Rgas   =   83.14   !bar cm3 / mol K
Open   (   unit   =   13   ,   file   =   'conditions.dat'   )
```

[1] Only the main program and the subroutines were included in the appendix.

```
write ( 13 ,*) T , P
close ( 13 )
!             Computation of water density at operating conditions, units kg/m3
Call Water_EOS ( P , T , dens )
!             Computation of water viscosity at oprating conditions, units Pa.s
Call WVisc ( dens , visc )
dens = dens / WMW / 1000
Vwater = 1 / dens                                              !cm3/mol
!             Computation of oxygen and dbu volume usig BWR-LK-EOS
Call BWR_LK_EOS ( P , T , Zoxygen , Zdbu )
Zoxygen * Rgas * T / P
Vdbu = Zdbu * Rgas * T / P

!             Voxygen          !cm3/mol
!             Vdbu              !cm3/mol
Call LK_MIXR ( Vwater , Voxygen , Vdbu , Vm , Tcm , Vcm , omegam , Pcm , y , ymol , oexcess )
Call Conditions ( y , ymol , pumpoxid , pumporg , Vm , spacevel , ndata , conoxid , concorg , &
                    Rpumpoxid , Rpumporg , Rpumpwater , pumpwater , Vreactor )
Call Writing_Results ( y , ymol , pumpoxid , pumporg , spacevel , ndata , conoxid , concorg , &
                    oexcess , Rpumpoxid , Rpumporg , Rpumpwater , pumpwater , Vreactor , visc )
Stop
End   Program
```

G.1.2 Subroutine for the Calculation of Density of Water (Written in *Fortran 95*)

```
Subroutine Water_EOS ( P , T , dens )
!!!!!!!!!!!!!!!!!!!!!!!!!!!!!!!!!!!!!!!!!!!!!!!!!!!!!!!!!!!!!!!!!!!!!!!!!!!!!!!!!!!!!!!!!!!!!!!!!!!!
!   This program compute the water density at supercritical conditions.  The EOS of water     !
!   is proposed by Wagner and Pruss and which is adopted for the International Association     !
!   for the Properties of Water and Steam Formulation 1995 for the Thermodynamic Properties   !
!   of Ordinary Water Substance for General and Scientific Use.  Journal of Physical and      !
!   Chemical Reference Data 31 (2), 2002, 387-535.                                             !
!!!!!!!!!!!!!!!!!!!!!!!!!!!!!!!!!!!!!!!!!!!!!!!!!!!!!!!!!!!!!!!!!!!!!!!!!!!!!!!!!!!!!!!!!!!!!!!!!!!!
Use Numerical_Libraries
Implicit None
!             Parameters specified for the Water EOS
Integer nroot , itmax
Real ( kind = 8 ):: P , T , dens , densC , tempdat , tempC , Rconst , pressdat , eps , &
errabs , errrel , eta , Func
Parameter ( nroot = 1 )
Integer , dimension ( nroot ):: info
Real ( kind = 8 ), dimension ( nroot ):: densguess
External Func
pressdat = P / 10.0
tempdat = T
Rconst = 0.46151805 !kJ kg-1 K-1
densC = 322.0
tempC = 647.096
Open ( unit = 13 , file = 'waterdata.dat' )
                   write ( 13 ,*) pressdat , tempdat
close ( 13 )
!             Data guess for density at critical point
densguess = 100.0
!             Routine definitions
eps = 1.0E - 2
```

```
eta = 1.0E - 2
errabs = 0.0
errrel = 1.0E - 12
itmax = 100.0
CALL DZREAL ( Func , errabs , errrel , eps , eta , nroot , itmax , densguess , dens , info )
Return
End Subroutine
```

G.1.3 Subroutine for the Calculation of the Viscosity of Water (Written in *Fortran 95*)

```
 Subroutine WVisc ( dens , visc )

!!!!!!!!!!!!!!!!!!!!!!!!!!!!!!!!!!!!!!!!!!!!!!!!!!!!!!!!!!!!!!!!!!!!!!!!!!!!!!!!!!!!!!!!!!!!
! This program calculates the viscosity of water based on the on the "Representative      !
! equations for the viscosity of water substance" by J. V. Sengers; B. Kamgar-Parsi         !
! Journal of Physical and Chemical Reference Data, 13, 1984, 601-609                       !
!!!!!!!!!!!!!!!!!!!!!!!!!!!!!!!!!!!!!!!!!!!!!!!!!!!!!!!!!!!!!!!!!!!!!!!!!!!!!!!!!!!!!!!!!!!!
Use Numerical_Libraries
Implicit None
Integer i , j , k , m , n
Real ( kind = 8 ):: T , P , visc , dens , redT , redP , redvisc , reddens , visc0 , visc1 , visc2
Real ( kind = 8 ), dimension ( 4 ):: consth1
Real ( kind = 8 ), dimension ( 6 , 7 ):: consth2
Open ( unit = 13 , file = 'conditions.dat' , status = 'old' )
read ( 13 ,*) T , P
close ( 13 )
redT = T / 647.226
redP = P / 221.15
reddens = dens / 317.763
Open ( unit = 13 , file = 'waterd1.dat' , status = 'old' )
          do i = 1 , 4
                    read ( 13 ,*), consth1 ( i )
          end do
close ( 13 )
Open ( unit = 13 , file = 'waterd2.dat' , status = 'old' )
          read ( 13 ,*),(( consth2 ( i , j ), j = 1 , 7 ), i = 1 , 6 )
close ( 13 )

visc0 = 0.0
do i = 1 , 4
          visc0 = visc0 + consth1 ( i )/ redT **( i - 1 )
end do
visc0 = dsqrt ( redT )/ visc0
visc1 = 0.0
do i = 1 , 6
          do j = 1 , 7
                    visc1 = visc1 + consth2 ( i , j )*( 1 / redT - 1.0 )**( i - 1 )*( reddens
- 1.0 )**( j - 1 )
          end do
end do
visc1 = reddens * visc1
visc1 = dexp ( visc1 )
visc2 = 1.0
if (( redT .gt. 0.996 .and. redT .lt. 1.01 ) .and. ( reddens .gt. 0.71 .and. reddens .lt. 1.36 )) then
          print *, 'The value of viscosity computed might be miscalculated'
end if
```

```
visc = visc0 * visc1 * visc2 * 55.071E - 6
Return
End Subroutine
```

G.1.4 Subroutine for the Calculation of the Compressibility of Oxygen and Organic Compound (Written in *Fortran 95*)

```
Subroutine BWR_LK_EOS ( P , T , Zoxygen , Zdbu )
!!!!!!!!!!!!!!!!!!!!!!!!!!!!!!!!!!!!!!!!!!!!!!!!!!!!!!!!!!!!!!!!!!!!!!!!!!!!!!!!!!!!!!!!!!!
! This program constains the generalized Benedict-Webb-Rubin EOS with the modification !
! of Lee-Kesler. The program is built to calculate the compresibility factors of !
! Oxygen and DBU. (Reid, Prausnitz and Poling. "The properties of gases and liquids"). !
! The program uses four internal functions for the calculations for the evaluation !
! of the volumes of oxygen and DBU (Two references fluids and two simple fluids). !
!!!!!!!!!!!!!!!!!!!!!!!!!!!!!!!!!!!!!!!!!!!!!!!!!!!!!!!!!!!!!!!!!!!!!!!!!!!!!!!!!!!!!!!!!!!
Use Numerical_Libraries
Implicit None
Real ( kind = 8 ):: P , T , PcO2 , TcO2 , Vrsimple , Vrref , PrO2 , TrO2 , Zsimple , Zref , &
                        Zoxygen , Zdbu , Prdbu , Trdbu , Pcdbu , Tcdbu , Vcdbu , omegaO2 , omegadbu
Integer ITMAX , NROOT Real ( kind = 8 ):: EPS , ERRABS , ERRREL , ETA
PARAMETER ( NROOT = 1 )
INTEGER , dimension ( NROOT ):: INFO
Real ( kind = 8 ), dimension ( NROOT ):: Vr , Vrguess
EXTERNAL Func1 , Func2 , Func3 , Func4
!            Critical constants for oxygen
PcO2 = 50.46
TcO2 = 154.6
PrO2 = P / PcO2
TrO2 = T / TcO2
omegaO2 = 0.025
DATA Vrguess / 3.0 /
!            Initial Values for the solutions of the subroutine
EPS = 1.0E - 10
ERRABS = 1.0E - 10
ERRREL = 1.0E - 5
ETA = 1.0E - 2
ITMAX = 1000
!            Simple Fluid Reduced Volume Solution for oxygen
CALL DZREAL ( Func1 , ERRABS , ERRREL , EPS , ETA , NROOT , ITMAX , Vrguess , Vr , INFO )
!            CALL DWRRRN ('Vr simple fluid', 1, NROOT, Vr, 1, 0)
Vrsimple = Vr ( 1 )
Zsimple = PrO2 * Vrsimple / TrO2
!            Reference Fluid Reduced Volume Solution for oxygen
CALL DZREAL ( Func2 , ERRABS , ERRREL , EPS , ETA , NROOT , ITMAX , Vrguess , Vr , INFO )
!CALL DWRRRN ('Vr reference fluid', 1, NROOT, Vr, 1, 0)
Vrref = Vr ( 1 )
Zref = PrO2 * Vrref / TrO2
Zoxygen = Zsimple +( omegaO2 / 0.3978 )*( Zref - Zsimple )
!            Critical Constants for Quinoline
Pcdbu = 46.60
Tcdbu = 782.15
Vcdbu = 469.0
Trdbu = T / Tcdbu
Prdbu = P / Pcdbu
!            Simple Fluid Reduced Volume Solution for Quinoline
DATA Vrguess / 3.0 /
```

```
CALL DZREAL ( Func3 , ERRABS , ERRREL , EPS , ETA , NROOT , ITMAX , Vrguess , Vr , INFO )
!             CALL DWRRRN ('Vr simple fluid', 1, NROOT, Vr, 1, 0)
Vrsimple = Vr ( 1 )
Zsimple = Prdbu * Vrsimple / Trdbu
!             Reference Fluid Reduced Volume Solution for DBU
CALL DZREAL ( Func4 , ERRABS , ERRREL , EPS , ETA , NROOT , ITMAX , Vrguess , Vr , INFO )
!             CALL DWRRRN ('Vr reference fluid', 1, NROOT, Vr, 1, 0)
Vrref = Vr ( 1 )
Zref = Prdbu * Vrref / Trdbu
omegadbu = 0.43100656383
Zdbu = Zsimple +( omegadbu / 0.3978 )*( Zref - Zsimple )
Return
End Subroutine
```

G.1.5 Subroutine for the Calculation of the Mixture Properties (Written in *Fortran 95*)

```
 Subroutine LK_MIXR ( Vwater, Voxygen, Vdbu, Vm, Tcm, Vcm, omegam, Pcm, y, ymol, oexcess )
!!!!!!!!!!!!!!!!!!!!!!!!!!!!!!!!!!!!!!!!!!!!!!!!!!!!!!!!!!!!!!!!!!!!!!!!!!!!!!!!!!!!!!!!!!!!!!!
!  The subroutine evaluate the mixing rules of Lee and Kesler                          !
!  (Reid, Prausnitz and Poling.  "The properties of gases and liquids")                !
!!!!!!!!!!!!!!!!!!!!!!!!!!!!!!!!!!!!!!!!!!!!!!!!!!!!!!!!!!!!!!!!!!!!!!!!!!!!!!!!!!!!!!!!!!!!!!!
Integer i , j
Real ( kind = 8 ):: Vwater , Voxygen , Vdbu , Vm , Tcm , omegam , Pcm , Vcm , ysol , oexcess
!  Ternary system
Parameter ( n = 3 )
Real ( kind = 8 ) , dimension ( n ):: y , Tci , Vci , w , Vcomp , ymol
Real ( kind = 8 ) , dimension ( n , n ):: Tc , Vc , Vmcomp
!  Properties of water
Pcwater = 220.64                                                                    !bar
Tcwater = 647.096                                                                   !K
MWwater = 18.015268
Vcwater = 1.0 /( 322 / MWwater / 1000.0 )                                           !cm3/mol
omegaw = 0.344
!  Properties of oxygen
Pc02 = 50.46                                                                        !bar
Tc02 = 154.6                                                                        !K
Vc02 = 73.4                                                                         !cm3/mol
MW02 = 31.999
omega02 = 0.025
!  Properties of Quinoline
Pcdbu = 46.60                                                                       !bar
Tcdbu = 782.15                                                                      !K
Vcdbu = 469.0                                                                       !cm3/mol
omegadbu = 0.329
Tci ( 1 )= Tcwater
Tci ( 2 )= Tc02
Tci ( 3 )= Tcdbu
Vci ( 1 )= Vcwater
Vci ( 2 )= Vc02
Vci ( 3 )= Vcdbu
w ( 1 )= omegaw
w ( 2 )= omega02
w ( 3 )= omegadbu
Vcomp ( 1 )= Vwater
Vcomp ( 2 )= Voxygen
```

```
Vcomp ( 3 )= Vdbu
do      i = 1 , n
                do j = 1 , n
                                Tc ( i , j )= DSQRT ( Tci ( i )* Tci ( j ))
                                Vc ( i , j )= 0.125 *( Vci ( i )**( 1.0 / 3.0 )+ Vci ( j )**( 1.0 / 3.0
))** 3.0
                                Vmcomp ( i , j )= 0.125 *( Vcomp ( i )**( 1.0 / 3.0 )+ Vcomp ( j )**( 1.0
/ 3.0 ))** 3.0
                end do
end do
! Entering concentration of organic inside the reactor
print *, ''
print *, 'Enter composicion of Quinoline mmol/L= '
print *, ''
read *, y ( 3 )
print *, ''
print *, 'Enter the amount of oxygen respect to stoichiometric in percent'
print *, 'according to the reaction (i.e. 100% corresponds double of stoichiometric) '
print *, ''
print *, '2 C9H7N + 43/2 O2 ---> 18 CO2 + 7 H2O + N2'
print *, ''
read *, y ( 2 )
oexcess = y ( 2 )
y ( 2 )= 43.0 / 4.0 * y ( 3 )*( 1.0 + y ( 2 )/ 100.0 )
y ( 3 )= y ( 3 )/ 1000.0                    !mol/L
y ( 2 )= y ( 2 )/ 1000.0                    !mol/L
! Computing concentration in mol fraction in 1 L
ymol ( 2 )= y ( 2 )* Voxygen
ymol ( 3 )= y ( 3 )* Vdbu
ymol ( 1 )= 1000.0 - ymol ( 2 )- ymol ( 3 )
y ( 1 )= ymol ( 1 )/ Vwater
ysol =( ymol ( 1 )+ ymol ( 2 )+ ymol ( 3 ))
ymol ( 1 )= ymol ( 1 )/ ysol
ymol ( 2 )= ymol ( 2 )/ ysol
ymol ( 3 )= ymol ( 3 )/ ysol
Tcm = 0.0
Vcm = 0.0
omegam = 0.0
Vm = 0.0
do i = 1 , n
                omegam = omegam + ymol ( i )* w ( i )
                do j = 1 , n
                                Vcm = Vcm + ymol ( i )* ymol ( j )* Vc ( i , j )
                                Vm = Vm + ymol ( i )* ymol ( j )* Vmcomp ( i , j )
                end      do
end do
do i = 1 , n
                do j = 1 , n
                                Tcm = Tcm + 1.0 /(( Vcm )** 0.25 )* ymol ( i )* ymol ( j )* Vc ( i , j
)** 0.25 * Tc ( i , j )
                end do
end do
Pcm =( 0.2905 - 0.085 * omegam )* 83.14 * Tcm / Vcm

Open ( unit = 13 , file = 'mixtureprop.dat' )
```

```
                write ( 13 ,*) Vm , Vwater , Voxygen , Vdbu , Tcm , Vcm , omegam , Pcm
Close ( 13 )
Return
End Subroutine
```

G.1.6 Subroutine for the Calculation of Concentration of Reactants and Flow Rate at Room Conditions (Written in *Fortran 95*)

```
Subroutine Conditions ( y, ymol, pumpoxid, pumporg, Vm, spacevel, ndata, conoxid, concorg, Rpumpoxid, &
                        Rpumporg, Rpumpwater, pumpwater, Vreactor )
Use Numerical_Libraries
Implicit None
Integer i , ndata
Real ( kind = 8 ):: Vreactor, conoxid, densox, MWwater, MWdbu, Vm, MWmix, MWoxygen
Real ( kind = 8 ), dimension ( 20 ):: spacevel, volflow, Mfwater, Mfoxygen, Mfdbu, water1, water2, &
                        wateroxid, pumpoxid, waterorg, concorg, pumporg, Rpumpoxid, Rpumporg, &
                        Rpumpwater, pumpwater, waterorg1, waterorg2
Real ( kind = 8 ), dimension ( 3 ):: y , ymol
Character ( len = 1 ):: resp
MWwater = 18.015268
MWdbu = 129.161
MWoxygen = 32.0
Print *, ''
Print *, 'Indicate what is the weight of catalyst in g= '
Print *, '' Read *, Vreactor
Print *, ''
Print *, ''
Print *, 'Indicate how many residence time data will be sampled= '
Print *, ''
Read *, ndata
Print *, ''
do i = 1 , ndata
        Print *, ''
        Print *, 'Enter the residence time to be analyzed (WHSV) in 1/s=' , i
        Print *, ''
        Read *, spacevel ( i )
        Print *, ''
end do
MWmix = ymol ( 1 )* MWwater + ymol ( 2 )* MWoxygen + ymol ( 3 )* MWdbu
do i = 1 , ndata
        spacevel ( i )= 1.0 / spacevel ( i )
        Volflow ( i )= Vreactor / spacevel ( i )* Vm / MWmix * 60.0
end do
99131   do i = 1 , ndata
                Mfwater ( i )= y ( 1 )* Volflow ( i )/ 1000.0
                Mfoxygen ( i )= y ( 2 )* Volflow ( i )/ 1000.0
                Mfdbu ( i )= y ( 3 )* Volflow ( i )/ 1000.0
        end do
!       Computation of the flow rates of oxygen
Print *, 'The calculation of the flow rates of oxygen at ambient conditions is based on'
Print *, 'the following reaction:'
Print *, ''
Print *, '2 H2O2 ---> 2 H2O + O2'
Print *, ''
!       According with the reaction the concentration of oxygen is based on a hydrogen peroxide
!       solution
```

```
Print  *,  ''
Print  *,  'Enter the concentration of the oxidant solution in %W= '
Print  *,  ''
Read  *,  conoxid
densox  =  0.00001  *  conoxid  **  2.0  +  0.0034  *  conoxid  +  0.9996                  !  Density of oxidant solution g/cm3
!  Volumetric flow rate of oxidant solution
!  Water from the decomposicion reaction of hydrogen peroxide
do  i  =  1  ,  ndata
                water1  (  i  )=  2.0  *  Mfoxygen  (  i  )*  MWwater
end  do

!  Water generated by the solution
do  i  =  1  ,  ndata
                water2  (  i  )=  2.0  *  Mfoxygen  (  i  )*  34.01  *(  100.0  /  conoxid  -  1.0  )
end  do
!  Total amount of water from oxidant solution
do  i  =  1  ,  ndata
                wateroxid  (  i  )=(  water1  (  i  )+  water2  (  i  ))/  MWwater                !mol/min
end  do
!  Flowrate pump oxidant
do  i  =  1  ,  ndata
  pumpoxid  (  i  )=  2.0  *  Mfoxygen  (  i  )*  34.01  *  100.0  /  conoxid  /  densox
                Rpumpoxid  (  i  )=  pumpoxid  (  i  )/  0.9234  !  Change to 10 mL head 0.9237
end  do
!              Volumetric flow rate of organic solution
do  i  =  1  ,  ndata
               waterorg  (  i  )=(  Mfwater  (  i  )-  wateroxid  (  i  ))*  MWwater  !0.998207152503702        !@20C and 1 bar, mL/min
end  do
do  i  =  1  ,  ndata
                Mfdbu  (  i  )=  Mfdbu  (  i  )*  MWdbu
end  do
do  i  =  1  ,  ndata
                waterorg1  (  i  )=  waterorg  (  i  )*  0.80
                waterorg2  (  i  )=  waterorg  (  i  )*  0.20
end  do
do  i  =  1  ,  ndata
                concorg  (  i  )=  Mfdbu  (  i  )/(  Mfdbu  (  i  )+  waterorg2  (  i  ))*  1E6       !ppm
end  do
do  i  =  1  ,  ndata
                pumpwater  (  i  )=  waterorg1  (  i  )/  0.998207152503702
                Rpumpwater  (  i  )=  pumpwater  (  i  )/  0.9054
end  do
do  i  =  1  ,  ndata
                pumporg  (  i  )=  waterorg2  (  i  )/  0.998207152503702  +  Mfdbu  (  i  )/  1.018
                Rpumporg  (  i  )=  pumporg  (  i  )/  1.0671
end  do
write  (*,  1334  )  conoxid
1334        format  (/,  1x  ,  'CONCENTRATION OF H2O2 IN OXIDANT SOLUTION='  ,  5x  ,  f10  .5  ,  2x  ,  '% W'  )
write  (*,  1337  )  concorg  (  1  )
1337        format  (  1x  ,  'CONCENTRATION OF QUINOLINE IN ORGANIC SOLUTION='  ,  5x  ,  f10  .5  ,  2x  ,  'PPM'  )
write  (*,  1335  )
1335        format  (/,  1x  ,  'SPACE VELOCITY'  ,  1x  ,  'FR OXIDANT'  ,  3x  ,  'FR ORGANIC'  ,  4x  ,  &
                                                                'FR WATER'  )
write  (*,  1338  )
1338        format  (  7x  ,  's'  ,  10x  ,  'mL/min'  ,  7x  ,  'mL/min'  ,  8x  ,  'mL/min'  )
do  i  =  1  ,  ndata
                write  (*,  1336  )  spacevel  (  i  ),  pumpoxid  (  i  ),  pumporg  (  i  ),  pumpwater  (  i  )
1336        format  (  f10  .2  ,  6x  ,  f8  .3  ,  5x  ,  f8  .3  ,  6x  ,  f8  .3  )
```

```
end do
write (*, 1339 )
1339 format (/, 1x , 'SPACE VELOCITY' , 2x , 'REAL FR OXIDANT' , 2x , 'REAL FR ORGANIC' , 2x , &
                'REAL FR WATER' )
write (*, 1340 )
1340 format ( 7x , 's' , 13x , 'mL/min' , 11x , 'mL/min' , 11x , 'mL/min' )
do i = 1 , ndata
        write (*, 1341 ) spacevel ( i ), Rpumpoxid ( i ), Rpumporg ( i ), Rpumpwater ( i )
1341 format ( f10 .2 , 9x , f8 .3 , 9x , f8 .3 , 9x , f8 .3 )
end do
print *, ''
print *, 'The results of organic concentration and flowrates are suitable for the run'
print *, 'Y/N'
print *, ''
print *, ''
read *, resp
if ( resp .eq. 'Y' .or. resp .eq. 'y' ) then
else
        goto 99131
end if
Return
End Subroutine
```

G.1.7 Subroutine for the Writing of the Conditions of the Experiment (Written in *Fortran 95*)

```
Subroutine Writing_Results ( y , ymol , pumpoxid , pumporg , spacevel , ndata , conoxid , concorg , &
        oexcess , Rpumpoxid , Rpumporg , Rpumpwater , pumpwater , Vreactor , visc )
!!!!!!!!!!!!!!!!!!!!!!!!!!!!!!!!!!!!!!!!!!!!!!!!!!!!!!!!!!!!!!!!!!!!!!!!!!!!!!!!!!!!!!!!!!
! This subroutine write the results into file results.txt for printing out.          !
!!!!!!!!!!!!!!!!!!!!!!!!!!!!!!!!!!!!!!!!!!!!!!!!!!!!!!!!!!!!!!!!!!!!!!!!!!!!!!!!!!!!!!!!!
Use Numerical_Libraries
Implicit None
Integer i , n , ndata
Real ( kind = 8 ):: T , P , conoxid , Vm , Tcm , Vcm , omegam , Pcm , Vwater , Voxygen , &
    Vdbu , oexcess , Vreactor , MWwater , MWdbu , MWoxygen , MWmix , visc
!       Ternary system
Parameter ( n = 3 )
Real ( kind = 8 ), dimension ( n ):: y , ymol
Real ( kind = 8 ), dimension ( 20 ):: pumpoxid , pumporg , spacevel , concorg , Rpumpoxid , Rpumporg , &
        pumpwater , Rpumpwater
Character ( len = 1 ):: resp
MWwater = 18.015268
MWdbu = 129.161
MWoxygen = 32.0
MWmix = ymol ( 1 )* MWwater + ymol ( 2 )* MWoxygen + ymol ( 3 )* MWdbu
Open ( unit = 13 , file = 'conditions.dat' )
        Read ( 13 ,*) T , P
Close ( 13 )
Open ( unit = 13 , file = 'mixtureprop.dat' )
        Read ( 13 ,*) Vm , Vwater , Voxygen , Vdbu , Tcm , Vcm , omegam , Pcm
Close ( 13 )
MWmix = ymol ( 1 )* MWwater + ymol ( 2 )* MWoxygen + ymol ( 3 )* MWdbu
Open ( unit = 13 , file = 'results.txt' )
write ( 13 , 1314 )
1314 format (/, 1x , 'DATE:  ' , 25x , 'EXPERIMENT NUMBER:  ' )
```

```
write ( 13 , 1315 )
1315 format (/, 1x , '----------------------------------------------------------------------' )
write ( 13 , 1316 )
1316 format (/, 1x , 'REACTION CONDITIONS' )
write ( 13 , 1516 )
1516 format ( 1x , '----------------------------------------' )
write ( 13 , 1317 ) P
1317 format (/, 1x , 'REACTION PRESSURE=' , 6x , f8 .3 , 2x , 'bar' )
write ( 13 , 1318 ) T - 273.15 , T
1318 format ( 1x , 'REACTION TEMPERATURE=' , 3x , f8 .3 , 2x , 'C' , 3x , '=' , 2x , f8 .3 , 2x ,
'K' )
write ( 13 , 1349 ) Vreactor
1349 format ( 1x , 'CATALYST WEIGHT=' , 8x , f8 .3 , 2x , 'g' )
write ( 13 , 1414 )
1414 format (/, 1x , 'MIXTURE COMPOSITIONS' )
write ( 13 , 1516 )
write ( 13 , 1340 ) oexcess
1340 format (/, 1x , 'OXYGEN IN EXCESS=' , 6x , f10 .2 , 8x , '%' )
write ( 13 , 1319 ) y ( 3 )
1319 format ( 1x , 'QUINOLINE CONCENTRATION=' , 3x , f10 .8 , 2x , 'mol/L' )
write ( 13 , 1320 ) y ( 2 )
1320 format ( 1x , 'OXYGEN CONCENTRATION=' , 6x , f10 .8 , 2x , 'mol/L' )
write ( 13 , 1321 ) y ( 1 )
1321 format ( 1x , 'WATER CONCENTRATION=' , 4x , f13 .8 , 2x , 'mol/L' )
write ( 13 , 1322 ) ymol ( 3 )
1322 format ( 1x , 'QUINOLINE MOL COMPOSITION=' , 1x , f10 .8 , 2x )
write ( 13 , 1323 ) ymol ( 2 )
1323 format ( 1x , 'OXYGEN MOL COMPOSITION=' , 4x , f10 .8 , 2x )
write ( 13 , 1324 ) ymol ( 1 )
1324 format ( 1x , 'WATER MOL COMPOSITION=' , 5x , f10 .8 , 2x )
write ( 13 , 1415 )
1415 format (/, 1x , 'VOLUMES, DENSITY AND MOLECULAR WEIGHT OF REACTING MIXTURE' )
write ( 13 , 1516 )
write ( 13 , 1325 ) Vm
1325 format (/, 1x , 'MOLAR VOLUME OF MIXTURE=' , 4x , f13 .8 , 2x , 'cm3/mol' )
write ( 13 , 1326 ) Vdbu
1326 format ( 1x , 'MOLAR VOLUME OF QUINOLINE=' , 2x , f13 .8 , 2x , 'cm3/mol' )
write ( 13 , 1327 ) Voxygen
1327 format ( 1x , 'MOLAR VOLUME OF OXYGEN=' , 5x , f13 .8 , 2x , 'cm3/mol' )
write ( 13 , 1328 ) Vwater
1328 format ( 1x , 'MOLAR VOLUME OF WATER=' , 6x , f13 .8 , 2x , 'cm3/mol' )
write ( 13 , 1420 ) 1.0 / Vm * MWmix
1420 format ( 1x , 'DENSITY OF MIXTURE=' , 9x , f13 .8 , 2x , 'g/cm3' )
write ( 13 , 1421 ) MWmix
1421 format ( 1x , 'MOLECULAR WEIGHT=' , 11x , f13 .8 )
write ( 13 , 1449 ) visc
1449 format ( 1x , 'VISCOSITY OF WATER=' , 9x , f13 .8 , 2x , 'kg/m s or Pa s' )
write ( 13 , 1416 )
1416 format (/, 1x , 'CRITICAL PROPERTIES OF REACTING MIXTURE' )
write ( 13 , 1516 )
write ( 13 , 1329 ) Pcm
1329 format (/, 1x , 'CRITICAL PRESSURE OF REACTING MIXTURE=' , 7x , f8 .4 , 3x , 'bar' )
write ( 13 , 1330 ) Tcm
1330 format ( 1x , 'CRITICAL TEMPERATURE OF REACTING MIXTURE=' , 4x , f8 .4 , 3x , 'K' )
write ( 13 , 1331 ) Vcm
1331 format ( 1x , 'CRITICAL MOLAR VOLUME OF REACTING MIXTURE=' 1x , f10 .4 , 3x , 'cm3/mol' )
write ( 13 , 1332 ) omegam
```

```
1332      format  (  1x  ,  'OMEGA CRITICAL='  ,  28x  ,  f10  .4  )
write  (  13  ,  1417  )
1417      format  (  1x  ,  '------------------------------------------------------------'  )
write  (  13  ,  1333  )
1333  format  (/,  1x  ,  'AMBIENT CONDITIONS'  )
write  (  13  ,  1516  )
write  (  13  ,  1334  )  conoxid
1334  format  (/,  1x  ,  'CONCENTRATION OF H2O2 IN OXIDANT SOLUTION='  ,  6x  ,  f10  .5  ,  2x  ,  '% W'  )
write  (  13  ,  1337  )  concorg  (  1  )
1337  format  (  1x  ,  'CONCENTRATION OF QUINOLINE IN ORGANIC SOLUTION='  ,  1x  ,  f10  .5  ,  2x  ,  'PPM'  )
write  (  13  ,  1335  )
1335  format  (/,  1x  ,  'SPACE VELOCITY'  ,  3x  ,  'WHSV'  ,  3x  ,  'FR OXIDANT'  ,  2x  ,  'FR ORGANIC'  ,  4x  ,  &
              'FR WATER'  )
write  (  13  ,  1338  )
1338  format  (  7x  ,  's'  ,  10x  ,  '1/s'  ,  6x  ,  'mL/min'  ,  6x  ,  'mL/min'  ,  8x  ,  'mL/min'  )
write  (  13  ,  1417  )
do  i  =  1  ,  ndata
write  (  13  ,  1336  )  spacevel  (  i  ),  1.0  /  spacevel  (  i  ),  pumpoxid  (  i  ),  pumporg  (  i  ),  pumpwater  (
i  )
1336  format  (  f10  .2  ,  7x  ,  f5  .2  ,  3x  ,  f8  .3  ,  4x  ,  f8  .3  ,  6x  ,  f8  .3  )
end  do
write  (  13  ,  1343  )
1343  format  (/,  1x  ,  'SPACE VELOCITY'  ,  1x  ,  &
              'REAL FR OXIDANT'  ,  1x  ,  'REAL FR ORGANIC'  ,  1x  ,  'REAL FR WATER'  )
write  (  13  ,  1345  )
1345  format  (  7x  ,  's'  ,  12x  ,  'mL/min'  ,  10x  ,  'mL/min'  ,  10x  ,  'mL/min'  )
write  (  13  ,  1417  )
do  i  =  1  ,  ndata
write  (  13  ,  1347  )  spacevel  (  i  ),  Rpumpoxid  (  i  ),  Rpumporg  (  i  ),  Rpumpwater  (  i  )
1347  format  (  f10  .2  ,  8x  ,  f8  .3  ,  8x  ,  f8  .3  ,  8x  ,  f8  .3  )
end      do
Close  (  13  )
Return
End  Subroutine
```

G.2 Program for the Fitting of the Kinetic Parameters Assuming no Concentration Gradient Limitations (Written in *Python*)

```
#!/usr/bin/python

from  scipy  import  array,  linspace,  matrix
from  numpy  import  arange
from  scipy.integrate  import  odeint
from  scipy.optimize  import  leastsq,  fmin,  fmin_powell,  anneal
import  pylab  as  pl
from  time  import  *

t1  =  time  ();  t1clock  =  clock  ()

texp  =  array  ([  3.5668469333,  4.4585586667,  6.6878380000,  8.9171173333,  11.1463966667  ])
XAexp  =  array  ([  0.4799885437,  0.5543946315,  0.7078922595,  0.8667638285,  0.9835109714  ])
CAi  =  array  ([  0.3000,  0.3000,  0.3000,  0.3000,  0.3000  ])
CBi  =  array  ([  3.2250,  3.2250,  3.2250,  3.2250,  3.2250  ])

l  =  len  (  XAexp  )
```

```
tpred = arange ( 1 , dtype = 'float32' )
print len ( texp ), len ( XAexp ), len ( CAi ), len ( CBi )

def reactor ( W_FA0 , XA , k , a , b , CA0 , CB0 ):
    rate = 1.0 / k /( CA0 *( 1.0 - XA ))** a /( CB0 - 10.75 * CA0 * XA )** b
#Power Law Reaction Rate
    return rate

def diff_eq ( XAexp , p , CAi , CBi ):
    for i in range ( 1 ):
        steps = 100
        XA = linspace ( 0 , XAexp [ i ], steps )
        k , a , b = p
        ttemp = odeint ( reactor , 0.0 , XA , args =( k , a , b , CAi [ i ],
CBi [ i ]), rtol = 1.5e-10 , atol = 1.5e-10 )
        tpred [ i ] = ttemp [ steps - 1 ]
    return tpred

def residuals ( p , texp , XAexp , CAi , CBi ):
    err = 0.5 *( texp - diff_eq ( XAexp , p , CAi , CBi ))** 2.0
    return err

def residuals2 ( p , texp , XAexp , CAi , CBi ):
    diff = 0.5 *( texp - diff_eq ( XAexp , p , CAi , CBi ))** 2.0
    err2 = sum ( diff [ 1 :])
    return err2

k = array ([ 0.001, 0.1, 0.2, 1.0, 2.0 ])
a = array ([ 0.1, 0.5, 1.0, 1.5 ])
b = array ([ 1.5, 1.0, 0.5, 0.1 ])

l2 = len ( k )
fid = open ( 'Quinoline_CaruliteGlobal3.txt' , 'w' )
for i in range ( l2 ):
    for j in range ( l2 ):
        for m in range ( l2 ):
            sol1 , output1 = leastsq ( residuals, [ k [ i ], a [ j ], b [
m ]], args =( texp , XAexp , CAi , CBi ), ftol = 1.5e-15 , xtol = 1.5e-15 )
            sol2 , fopt2 , iter2 , funcalls2 , warnflag2 = fmin ( residuals2 , [
k [ i ], a [ j ], b [ m ]], args =( texp , XAexp , CAi , CBi ), full_output = 1 )
            sol3 , fopt3 , direc3 , iter3 , funcalls3 , warnflag3 = fmin_powell
( residuals2 , [ k [ i ], a [ j ], b [ m ]], args =( texp , XAexp , CAi , CBi ), full_output =
1 )
            sol4 , Jmin4 , T4 , feval4 , iters4 , accept4 , output4 = anneal (
residuals2 , [ k [ i ], a [ j ], b [ m ]], args =( texp , XAexp , CAi , CBi ), schedule = 'fast'
, maxiter = 1000 , lower =[ 0.0 , 0.0 , 0.0 ], upper =[ 1.0 , 3.0 , 3.0 ], full_output = 1 )
        ##################Screen output#################################################
            print 'Initial Estimate' , k [ i ], a [ j ], b [ m ]
            print 'Non-linear Least Square Minimization Parameters k, a, b' , sol1 , output1
            print 'Nelder-Mead (Simplex) Minimization k, a, b' , sol2 , fopt2 , warnflag2
            print 'Powell Modification Algorithm Minimization k, a, b' , sol3 , fopt3 , warnflag3
            print 'Anneal Constrained Global Minimization' , sol4 , Jmin4 , output4
        ###############File Output#######################################################
            print >> fid , '------------------------------'
            print >> fid , 'Initial Parameters k, a, b = [' , k [ i ], ',' , a [
j ], ',' , b [ m ], ']'
```

```
                                        print >> fid , 'NLLS Parameters k, a, b = ' , sol1 , output1
                                        print >> fid , 'Simplex k, a, b = ' , sol2 , fopt2 , warnflag2
                                        print >> fid , 'Powell k, a, b = ' , sol3 , fopt3 , warnflag3
                                        print >> fid , 'Anneal Global Minimization k, a, b = ' , sol4 , Jmin4 ,
output4

fid . close ()

t2 = time (); t2clock = clock ()
print 'Iteration Finished'
print 'Initial Time' , ctime ( t1 )
print 'Final Time' , ctime ( t2 )
print 'Elapsed Time (h)' , ( t2clock - t1clock )/ 60 / 60
```

G.3 Program for the Calculation of the Criteria proposed by Bischoff for the Evaluation of the Internal Concentration Gradient Limitations (Written in *Python*)

```
#!/usr/bin/python

from scipy import array, linspace, mgrid, zeros
from numpy import arange
from scipy.integrate import odeint, romberg, quad
from numpy import *
from time import *

t1 = time (); t1clock = clock ()

texp = array ([ 0.2477273148, 0.1651515432, 0.1238636574, 0.0990909259, 0.0825757716, 0.0707792328 ])
XAexp = array ([ 0.9926811376, 0.9308936100, 0.7956939075, 0.6953389881, 0.6439222788, 0.5824943766 ])
CAi = array ([ 0.0027000000, 0.0027000000, 0.0027000000, 0.0027000000, 0.0027000000, 0.0027000000 ])
CBi = array ([ 0.0039000000, 0.0039000000, 0.0039000000, 0.0039000000, 0.0039000000, 0.0039000000 ])
CAi = CAi * 1000.0 ; CBi = CBi * 1000.0
l = len ( XAexp )
tpred = arange ( l , dtype = 'float32' )

print len ( texp ), len ( XAexp ), len ( CAi ), len ( CBi )
p = array ([ 4.63116829 , 0.75345888 , 0.29617238 ]) #Kinetic Parameters
k , a , b = p

rho = 1.1054675129                                          #Catalyst density
dp = 5.4E-5                                                 #Catalyst diameter micrometer
Deff = 8.63715E-9                                   #Effective Diffusivity m2/s
robs = zeros ( l , dtype = 'float32' )
gCobs = zeros ( l , dtype = 'float32' )
integral = zeros ( l , dtype = 'float32' )
integral2 = zeros ( l , dtype = 'float32' )
Bischoff = zeros ( l , dtype = 'float32' )
Bischoff2 = zeros ( l , dtype = 'float32' )

def rate ( X , a , b , CA0 , CB0 ):
        integ = - CA0 *( CA0 - CA0 * X )** a *( CB0 - CA0 * X )** b          #Power Law Reaction Rate
```

```
                return integ
for i in range ( l ):
                robs [ i ]= rho * k *( CAi [ i ]- CAi [ i ]* XAexp [ i ])** a *( CBi [ i ]- CAi
[ i ]* XAexp [ i ])** b
                gCobs [ i ]=( CAi [ i ]- CAi [ i ]* XAexp [ i ])** a *( CBi [ i ]- CAi [ i ]*
XAexp [ i ])** b
                integ1 = quad ( rate , 1.0 , XAexp [ i ], args =( a , b , CAi [ i ], CBi [ i ]))
                integral [ i ]= integ1 [ 0 ]
                Bischoff [ i ]= robs [ i ]* dp ** 2 * gCobs [ i ]/ 2.0 / Deff / integral [ i ]
                integral2 [ i ]= romberg ( rate , 1.0 , XAexp [ i ], args =( a , b , CAi [ i ], CBi
[ i ]))
                Bischoff2 [ i ]= robs [ i ]* dp ** 2.0 * gCobs [ i ]/ 2.0 / Deff / integral2 [ i ]

print Bischoff
print Bischoff2
t2 = time (); t2clock = clock ()

fid = open ( 'DBU_CaruliteBischoff.txt' , 'w' )
for i in range ( l ):
                print >> fid , 'XAexp' , XAexp [ i ], 'CA0' , CAi [ i ], 'CB0' , CBi [ i ],
'Criteria 1' , Bischoff [ i ], 'Criteria 2' , Bischoff2 [ i ], 'CA' , ( CAi [ i ]- CAi [ i ]* XAexp [ i
])** a , 'k*CB' , k *( CBi [ i ]- CAi [ i ]* XAexp [ i ])** b fid . close () print 'Iteration Finished'
print 'Initial Time' , ctime ( t1 ) print 'Final Time' , ctime ( t2 ) print 'Elapsed Time (h)' , ( t2clock
- t1clock )/ 60 / 60
```

G.4 Program for the Fitting of the Kinetic Parameters Assuming Concentration Gradient Limitations (Written in *Python*)

```
#!/usr/bin/python

from scipy import array, linspace, mgrid, zeros, ones
from numpy import arange, tanh
from scipy.integrate import odeint, romberg, quad,
from scipy.optimize import leastsq, fmin, fmin_powell, anneal, fsolve
from numpy import *
import pylab as pl
from time import *

t1 = time (); t1clock = clock ()

uS = array ([ 3.357086049, 5.035629073, 6.714172097, 8.392715121, 10.071258146 ])
XAexp = array ([ 0.9926811376, 0.9308936100, 0.7956939075, 0.6953389881, 0.6439222788 ])
CAi = array ([ 0.0027000000, 0.0027000000, 0.0027000000, 0.0027000000, 0.0027000000 ])
CBi = array ([ 0.0039000000, 0.0039000000, 0.0039000000, 0.0039000000, 0.0039000000 ])

CAi = CAi * 1000.0 ; CBi = CBi * 1000.0

l = len ( XAexp )

print len ( uS ), len ( XAexp ), len ( CAi ), len ( CBi )

rho = 1.1054675129                                  #Catalyst density Pt
dp = 5.4E-5                                  #Catalyst diameter micrometer [m]
```

```
Deff = 8.63715E-9                                    #Effective Diffusivity [m2/s]
L = 8.2                                             #Length of the catalytic bed [cm]
kdiff = 4.63116829                                   #k constant influenced by diffusion
k2 = zeros ( l , dtype = 'float32' )
z = ones ( l , dtype = 'float32' )
XApred = arange ( l , dtype = 'float32' )
steps = 100
v = 0.0
zdisc = linspace ( 0 , 1.0 , steps )
dvdz = zeros ( len ( zdisc ))

def reaction ( v , zdisc , uS , k , a , b , CA0 , CB0 ):
                #General Thiele Modulus for flat plate and reaction order of 1
                #k is obtained from the data influenced by diffusion  [k, a, b]= [27.0064077,  1.31501209,  0.06056691]
                knew = kdiff * rho                                  #k based on volumetric properties of the reacting mixture
                k2 = knew * ( CA0 - CA0 * v )**( 0.75345888 - 1.0 ) * ( CB0 - CA0 * v )** 0.29617238
                #For a sphere the mThiele(sphere)=3*mThiele(Flat plate)
                #References by Bishoff (1965) AIChE Journal and Aris (1957), Chem. Eng. Sci.
                mThiele = 3 * dp *( k2 / Deff )** 0.5
                #The effectiveness factor is given by
                eta = tanh ( mThiele )/ mThiele
                dvdz = eta * L * k * ( CA0 *( 1.0 - v ))** a * ( CB0 - CA0 * v )** b / uS /
CA0                                                 #Power Law Reaction Rate
                return dvdz

def diff_eq ( uS , p , CAi , CBi ):
                for i in range ( l ):
                                k , a , b = p
                                zdisc = linspace ( 0 , 1.0 , steps )
                                XAtemp = odeint ( reaction , v , zdisc , args =( uS [ i ], k , a , b ,
CAi [ i ], CBi [ i ]), rtol = 1.5e-8 , atol = 1.5e-8 )
                                XApred [ i ] = XAtemp [ steps - 1 ]
                return XApred

def residuals ( p , XAexp , uS , CAi , CBi ):
                err = (( XAexp - diff_eq ( uS , p , CAi , CBi ))/ XAexp )** 2.0
                return err

def residuals2 ( p , XAexp , uS , CAi , CBi ):
                diff = (( XAexp - diff_eq ( uS , p , CAi , CBi ))/ XAexp )** 2.0
                err2 = sum ( diff [ 1 :])
                return err2

k = array ([ 4.0 , 5.0 ])
a = array ([ 0.6 , 0.8 ])
b = array ([ 0.4 , 0.5 ])

l2 = len ( k )
fid = open ( 'DBU_CaruliteTRNormEffecFactor.txt' , 'w' )
for i in range ( l2 ):
                for j in range ( l2 ):
                                for m in range ):
                                                sol1 , output1 = leastsq ( residuals , [ k [ i ], a
[ j ], b [ m ]], args =( XAexp , uS , CAi , CBi ), ftol = 1.5e-15 , xtol =
1.5e-15 , maxfev = 2000 )
                                                sol2 , fopt2 , iter2 , funcalls2 , warnflag2 = fmin
```

```
( residuals2 , [ k [ i ], a [ j ], b [ m ]], args =( XAexp , uS , CAi , CBi
), full_output = 1 , maxfun = 2000 )
                                        sol3 , fopt3 , direc3 , iter3 , funcalls3 , warnflag3
= fmin_powell ( residuals2 , [ k [ i ], a [ j ], b [ m ]], args =( XAexp , uS ,
    CAi , CBi ), full_output = 1 , maxfun = 2000 )
                                        sol4 , Jmin4 , T4 , feval4 , iters4 , accept4 ,
output4 = anneal ( residuals2 , [ k [ i ], a [ j ], b [ m ]], args =( XAexp ,
uS , CAi , CBi ), schedule = 'fast' , maxiter = 3000 , lower =[ 3.5 , 0.5 , 0.35
], upper =[ 5.5 , 0.9 , 0.55 ], full_output = 1 )
                ###################Screen output#################################################
                                        print 'Initial Estimate' , k [ i ], a [ j ], b [ m ]
                                        print 'Non-linear Least Square Minimization Parameters k, a, b' , sol1 , output1
                                        print 'Nelder-Mead (Simplex) Minimization k, a, b' , sol2 , fopt2 , warnflag2
                                        print 'Powell Modification Algorithm Minimization k, a, b' , sol3 , fopt3 , warnflag3
                                        print 'Anneal Constrained Global Minimization' , sol4 , Jmin4 , output4
                ###############File Output#######################################################
                                        print >> fid , '------------------------------'
                                        print >> fid , 'Initial Parameters k, a, b = [' , k [ i ], ',' , a [
j ], ',' , b [ m ], ']'
                                        print >> fid , 'NLLS Parameters k, a, b = ' , sol1 , output1
                                        print >> fid , 'Simplex k, a, b = ' , sol2 , fopt2 , warnflag2
                                        print >> fid , 'Powell k, a, b = ' , sol3 , fopt3 , warnflag3
                                        print >> fid , 'Anneal Global Minimization k, a, b = ' , sol4 , Jmin4 ,
output4


fid . close ()

XApred2 = diff_eq ( uS , sol2 , CAi , CBi )

pl . figure ( figsize =( 10 , 10 ))
dot1 = ([ 0 , 1 ])
dot2 = ([ 0 , 1 ])
pl . plot ( XAexp , XApred2 , 'mo' , dot1 , dot2 , 'k-' , markersize = 14 )
pl . ylabel ( 'XA Predicted' , fontsize = 18 )
pl . xlabel ( 'XA Experimental' , fontsize = 18 )
pl . show ()


t2 = time (); t2clock = clock ()
print 'Iteration Finished'
print 'Initial Time' , ctime ( t1 )
print 'Final Time' , ctime ( t2 )
print 'Elapsed Time (h)' , ( t2clock - t1clock )/ 60 / 60
```